

May 2013

# Late Paleozoic Glaciation and Ice Sheet Collapse Over Western and Eastern Gondwana: Sedimentology and Stratigraphy of Glacial to Post- Glacial Strata in Western Argentina and Tasmania, Australia

Lindsey C. Henry

*University of Wisconsin-Milwaukee*

Follow this and additional works at: <https://dc.uwm.edu/etd>



Part of the [Geology Commons](#)

---

## Recommended Citation

Henry, Lindsey C., "Late Paleozoic Glaciation and Ice Sheet Collapse Over Western and Eastern Gondwana: Sedimentology and Stratigraphy of Glacial to Post-Glacial Strata in Western Argentina and Tasmania, Australia" (2013). *Theses and Dissertations*. 112.  
<https://dc.uwm.edu/etd/112>

This Dissertation is brought to you for free and open access by UWM Digital Commons. It has been accepted for inclusion in Theses and Dissertations by an authorized administrator of UWM Digital Commons. For more information, please contact [open-access@uwm.edu](mailto:open-access@uwm.edu).

LATE PALEOZOIC GLACIATION AND ICE SHEET COLLAPSE OVER WESTERN  
AND EASTERN GONDWANA: SEDIMENTOLOGY AND STRATIGRAPHY OF  
GLACIAL TO POST-GLACIAL STRATA IN WESTERN ARGENTINA AND  
TASMANIA, AUSTRALIA

by

Lindsey C. Henry

A Dissertation Submitted in  
Partial Fulfillment of the  
Requirements for the Degree of

Doctor of Philosophy  
in Geosciences

at

The University of Wisconsin-Milwaukee

May 2013

ABSTRACT  
LATE PALEOZOIC GLACIATION AND ICE SHEET COLLAPSE OVER WESTERN  
AND EASTERN GONDWANA: SEDIMENTOLOGY AND STRATIGRAPHY OF  
GLACIAL TO POST-GLACIAL STRATA IN WESTERN ARGENTINA AND  
TASMANIA, AUSTRALIA

by

Lindsey C. Henry

The University of Wisconsin-Milwaukee, 2013  
Under the supervision of Professors Margaret L. Fraiser and John L. Isbell

The late Paleozoic ice age (LPIA; 345-280 million years ago) provides the last complete record of a major deglaciation on a vegetated Earth, and therefore can serve as a proxy for Earth's inevitable transition out of its present glaciated state. This project analyzes climate change during and following the LPIA using two different approaches:

- 1) Detailed sedimentology analyses of five glacially-influenced formations in Argentina and Australia in order to determine the size and thermal regime of glaciers during the LPIA.
- 2) An investigation of massive volcanism along the Panthalassan margin of Gondwana as a source of CO<sub>2</sub> that may have contributed to the end of the LPIA and to two ensuing extinction events.

During the LPIA, glaciation occurred over the supercontinent Gondwana, and resulting glacial deposits are found in South America, Africa, Antarctica, India, and Australia. This project focuses on glacial and post-glacial outcrops in western Argentina and Tasmania, Australia that were deposited in western and eastern Gondwana, respectively. A study of outcrops from these two regions enables characterization and comparison of the early stages of the LPIA (when Argentina was glaciated) and when

glaciation was at its peak (when Tasmania was glaciated). Glacial and post-glacial deposits are analyzed using sedimentologic field techniques to interpret depositional events, thin section analysis to determine the micromorphology of the deposits, and mineralogical (x-ray diffraction, or XRD) and elemental (x-ray fluorescence, or XRF) analysis to differentiate sediment sources and determine the oxygenation of the environments.

Atmospheric CO<sub>2</sub> fluctuations have been linked to ice volume fluctuations during the LPIA, and CO<sub>2</sub> input from massive volcanism is considered a major driver of the Middle and Late Permian extinctions (261 and 250 million years ago, respectively). Although these events were previously considered as unrelated, volcanism along the subducting Panthalassan margin of Gondwana occurred throughout both the deglaciation of the LPIA and the Permian extinctions. Therefore, this study will also explore the hypothesis that Panthalassan margin volcanism influenced both deglaciation and the Permian extinctions. Ultimately this dissertation will improve the understanding of climate change during and following the LPIA and inform predictions for when and how Earth will experience deglaciation in the future.



© Copyright by Lindsey C. Henry, 2013  
All Rights Reserved

To my little family, Chris and Heath

## TABLE OF CONTENTS

LIST OF FIGURES .....	xiii
LIST OF TABLES .....	xx
ACKNOWLEDGEMENTS .....	xxi
Chapter 1: Introduction .....	1
The Far Field Record .....	2
The Near Field Record.....	6
Causes of Gondwana Glaciation.....	7
The Dissertation Work.....	9
Dissertation Objectives .....	11
Significance of Research .....	13
Dissertation Structure .....	14
Figures .....	18
References.....	22
Chapter 2: Carboniferous glacigenic deposits of the Protoprecordillera of west-central Argentina.....	30
Abstract.....	30
1. Introduction.....	31
2. Geologic Setting .....	32
3. Age.....	34
4. Glacigenic deposits of the Protoprecordillera.....	35
4.1. Paleovalleys .....	35
4.1.1. Agua de Jagüel.....	36
4.1.2. Quebrada de las Lajas and Quebrada Grande .....	39

4.2. Calingasta-Uspallata Basin—Hoyada Verde .....	41
4.3. Paganzo Basin—Huaco Area.....	43
4.4. Los Pozuelos Creek.....	43
4.5. Agua Hedionda Anticline.....	45
5. Ice-flow directions and ice-spreading centers .....	46
6. Postglacial transgression.....	48
7. Sequence stratigraphy .....	49
8. Conclusions.....	52
Acknowledgments .....	53
Figures .....	55
References.....	58
Chapter 3: Mid-Carboniferous deglaciation of the Protoprecordillera, Argentina recorded in the Agua de Jagüel paleovalley .....	63
Abstract.....	63
1. Introduction.....	64
2. Geologic Setting and Stratigraphy .....	67
3. Study Area and Methodology .....	70
4. Facies Analysis .....	71
4.1. Diamictite Facies .....	71
4.1.1. Diamictite Facies Description.....	71
4.1.2. Diamictite Facies Interpretation.....	73
4.2. Conglomerate and Sandstone Facies .....	76
4.2.1. Conglomerate and Sandstone Facies Description.....	76
4.2.2. Conglomerate and Sandstone Facies Interpretation.....	77

4.3. Pebbly Mudrock Facies.....	79
4.3.1. Pebbly Mudrock Facies Description.....	79
4.3.2. Pebbly Mudrock Facies Interpretation.....	80
4.4. Mudrock and Sandstone Facies .....	83
4.4.1. Mudrock and Sandstone Facies Description.....	83
4.4.2. Mudrock and Sandstone Facies Interpretation.....	84
5. X-ray Diffraction and Fluorescence Analysis .....	85
5.1. XRD results.....	86
5.2 XRF results .....	87
5.3 Discussion of x-ray results.....	87
6. Filling the Palaeovalley .....	90
6.1 Stage 1: Morainal Bank Deposition.....	90
6.2 Stage 2: Iceberg Rain-Out.....	92
6.3 Stage 3: Glacial Retreat, Shoreface Progradation.....	93
6.4 Stage 4: Transgression, Iceberg Rain-Out .....	93
7. Discussion.....	94
8. Conclusions.....	98
Acknowledgments .....	98
Tables.....	100
Figures .....	102
References.....	111
Chapter 4: The late Paleozoic El Imperial Formation, western Argentina: Glacial to post-glacial transition and stratigraphic correlations with arc-related basins in southwestern Gondwana .....	122
Abstract.....	122

1. Introduction.....	123
2. San Rafael Basin and neighboring western Gondwana basins .....	125
3. El Imperial Formation.....	128
4. Sedimentology of the El Imperial Formation .....	129
4.1. Restricted marine facies association .....	130
4.1.1. Restricted marine facies association description .....	130
4.1.2. Restricted marine facies association interpretation.....	131
4.2. Deltaic facies association .....	132
4.2.1. Deltaic facies association description .....	132
4.2.2. Deltaic facies association interpretation .....	133
4.3. Glacially-influenced facies association.....	135
4.3.1. Glacially-influenced facies association description.....	135
4.3.2. Glacially-influenced facies association interpretation .....	136
4.4. Post-glacial open marine facies association.....	138
4.4.1. Post-glacial open marine facies association description.....	138
4.4.2. Post-glacial open marine facies association interpretation .....	139
6.1. Río Blanco Basin .....	143
6.2. Calingasta–Uspallata Basin.....	145
6.3. San Rafael Basin .....	146
6.4. Tepuel Basin .....	147
7. Conclusions.....	148
Acknowledgments .....	149
Table .....	151

Figures .....	153
References .....	163
Chapter 5: Proglacial deposition and deformation in the Upper Carboniferous to Lower Permian Wynyard Formation, Tasmania: a process analysis .....	
Abstract .....	174
1. Introduction.....	175
2. Geologic setting and stratigraphy .....	178
2.1. The lower Parmeener Supergroup.....	179
2.2. Age .....	180
3. Study area and methodology.....	180
3.1. Outcrop location.....	180
3.2. Sedimentology field methods .....	181
4. Facies analysis .....	181
4.1. Massive diamictite facies association .....	181
4.1.1. Massive diamictite facies association description .....	181
4.1.2. Massive diamictite facies association interpretation.....	182
4.2. Stratified diamictite facies association.....	184
4.2.1. Stratified diamictite facies association description.....	185
4.2.2. Stratified diamictite facies association interpretation .....	187
4.3. Conglomerate and sandstone facies association .....	189
4.3.1. Conglomerate and sandstone facies association description .....	189
4.3.2. Conglomerate and sandstone facies association interpretation.....	190
4.4. Deformed mudstone and fine sandstone facies association .....	191
4.4.1. Deformed mudstone and fine sandstone description .....	192

4.4.2. Deformed mudstone and fine sandstone interpretation .....	193
4.5. Depositional environments of the Wynyard Formation.....	195
5. The Wynyard glacial record compared to nearby basins in Gondwana .....	198
6. Conclusions.....	200
Acknowledgments .....	201
Table .....	202
Figures .....	204
References.....	216
Chapter 6: Panthalassan margin volcanism: a driver of late Paleozoic deglaciation and extinction?.....	
Abstract .....	227
1. Introduction.....	228
2. Late Paleozoic Events and $p\text{CO}_2$ .....	230
3. Panthalassan Margin Volcanism.....	233
4. Choiyoi Group .....	235
5. Discussion .....	237
Acknowledgments .....	241
Figures .....	242
References.....	245
Chapter 7: A discussion of potential effects of paleotopography on glacial intervals in Argentina and Australia during the late Paleozoic ice age .....	
Abstract .....	252
1. Introduction.....	253
2. The ELA .....	259
3. Glacial II over the Protoprecordillera .....	260



4. Glacial III and subsequent glaciations in Australia .....	265
5. Conclusions.....	271
Figures .....	272

## LIST OF FIGURES

Figure 1. Gondwanan basins containing glacial deposits of the LPIA. Estimates by Powell and Li (1994) and Lawver et al. (2008) of the path of polar wander throughout the Carboniferous and Permian are illustrated. Yellow dots in the Lawver et al. (2008) polar wander path represent 10 million year time intervals. Modified from Isbell et al. (2003b). .....	18
Figure 2. Paleogeographic reconstructions of Gondwana throughout the late Paleozoic from Blakey (2008). The series of illustrations shows the docking of Laurussia with Gondwana to form Pangea in the Early Permian. ....	19
Figure 3. CO <sub>2</sub> fluctuations correlate with glacial and non-glacial intervals in the Permian. Yellow dots are from Montañez et al. (2007), red dots represent data compiled by Royer (2006), and the dashed line links the two data sets. ....	20
Figure 4. Glaciation during the LPIA occurred as alternating glacial and non-glacial intervals beginning in the Late Devonian, reaching its peak during the late Pennsylvanian – Early Permian, and ending in the Capitanian (middle Permian). ....	21
Figure 5. (A) Map showing the location of key stratigraphic sections in the Calingasta-Uspallata, Río Blanco, and Paganzo Basins (modified from Limarino et al., 2006). Sections mentioned in the text are Agua de Jagüel (AJ), Quebrada Grande (QG), Quebrada de las Lajas (QL), Hoyada Verde (HV), Los Pozuelos Creek (LPC), and the Agua Hedionda Anticline (AH). Arrows show paleo-ice-flow directions. Paleocurrent data are from Scalabrini Ortiz (1972), Andreis et al. (1975), López-Gamundí and Amos (1985), Buatois and Mángano (1994), López-Gamundí and Martínez (2000), Kneller et al. (2004), Marensi et al. (2005), Dykstra et al. (2006), and this paper. Line A–A' is the line of cross section shown in Figure 2. Inset map shows the location of the study area and the location of other basins that contain Lower Pennsylvanian glacial strata (modified from Isbell et al., 2003; Limarino and Spalletti, 2006). (B) The glacial successions in sequence 1 of the Agua de Jagüel Formation; (C) Quebrada de las Lajas, Jejenes Formation, redrafted from Dykstra et al. (2006); (D) Hoyada Verde Formation; (E) Agua Hedionda Anticline, Guandacol Formation, redrafted from Pazos (2002). All section thicknesses are in meters. ....	55
Figure 6. Cross section along transect A–A' (Fig. 1A) showing the tectonic configuration of the Calingasta-Uspallata Basin, the Protoprecordillera, and the Paganzo Basin, and the location and type of glaciers present (modified from Limarino et al., 2006). ....	56
Figure 7. Correlation chart for uppermost Mississippian, Pennsylvanian, and Lower Permian strata for sites in the Calingasta-Uspallata, Río Blanco, and Paganzo Basins mentioned in the text (units and ages are based on Taboada, 1985; López-Gamundí et al., 1994; Azcuy et al., 1999; López-Gamundí and Martínez, 2003; Limarino et al., 2005)..	56
Figure 8. Geologic map of the Agua de Jagüel area showing depositional sequences in the Pennsylvanian to Permian Agua de Jagüel Formation. Strata in the Agua de Jagüel Formation dip at up to 90°. ....	57

Figure 9. Time-space diagram summarizing the Carboniferous depositional history of the Protoprecordillera. The line of section traverses the Río Blanco Basin, Guandacol Embayment, and the Paganzo Basin (see Fig. 1A) (modified from Limarino et al., 2006).

..... 58

Figure 10. Location map of the Agua de Jagüel Formation and other formations described in the text. A. The Agua de Jagüel Formation is located 17 km northeast of the town of Uspallata, northern Mendoza, Argentina. B. Palaeogeography of the Carboniferous basins of western Argentina: the Calingasta-Uspallata, Río Blanco, and Paganzo Basins. Numbers indicate the localities mentioned in the text, 1. Agua de Jagüel Formation, 2. Tramojo Formation, 3. Hoyada Verde, 4. Huaco, and 5. Río del Peñón. A-B indicates the orientation of the cross section in Figure 2. C. Location of the Agua de Jagüel and Tramojo Formations outside the town of Uspallata..... 102

Figure 11. Cross-section of Early Permian geology through the Calingasta-Uspallata Basin, Protoprecordillera, and Paganzo Basin in western Argentina. 1. Middle Carboniferous - Permian sedimentary rocks, including the Agua de Jagüel Formation, 2. Lower Carboniferous sedimentary rocks (below the Río Blanco unconformity), 3. Pre-Carboniferous basement sedimentary rocks. After Azcuy et al. (1999) and Limarino et al. (2006)..... 102

Figure 12. Geologic map of the three sequences of the Agua de Jagüel Formation. Strata of the Agua de Jagüel Formation dip at 90°. Based on the geometry of the formation and contacts with basement rocks, the Agua de Jagüel Formation was deposited in a palaeovalley at least 700 m deep and at least 5 km wide. Modified from Henry et al. (2008)..... 103

Figure 13. Logs and interpreted depositional processes for sequence 1 of the Agua de Jagüel Formation..... 104

Figure 14. The diamictite facies association. A. Clast-rich massive diamictite B. Weakly stratified diamictite C. Thinly bedded diamictite D. Diamictite from the thick lower diamictite interval of the Agua de Jagüel Formation. Bedded Diamictite occurs just behind the person. E. Sandstone bed with sole marks, interbedded with diamictite in Log 1 F. Slumped diamictite rimmed by fine sand ..... 105

Figure 15. The conglomerate and sandstone facies association. A. Bedded conglomerate with a sandy matrix B. Interbedded conglomerate and sandstone. Jacob's staff for scale. C. Laminated sandstone D. Cross-laminated fine-grained sandstone..... 106

Figure 16. The pebbly mudrock facies association. A. Rhythmically bedded siltstone and claystone that has been deformed and folded B. Striated sandstone clast in mudrock C. Lens-shaped pods of diamictite, conglomerate, and sandstone occur within a thick pebbly mudrock interval. .... 107

Figure 17. The mudrock and sandstone facies association. A. Marl (orange rock fragments) in mudrock B. Deformed beds of fine sandstone interbedded with mudrock, overlying a thick mudrock with marl interval. Sand beds progressively extend further

south (towards the camera), indicating progradation. C. Very fine sandstone folded around siltstone. Yellow lines on Jacob's staff occur every 10 cm. D. Bulbous load structures on base of sandstone bed in mudrock E. Boudinaged sandstone in mudrock 108

Figure 18. Depositional environment of the Agua de Jagüel Formation..... 109

Figure 19. Graphic logs of the Hoyada Verde Formation and the Namurian lower member of the Tramojo Formation. The Tramojo Formation occurs as an anticline, and the two limbs of the anticline record different deglaciation successions. The Hoyada Verde and Tramojo Formations are located in the Calingasta-Uspallata Basin and occur adjacent to the Protoprecordillera (Fig. 1B)..... 110

Figure 20. Correlation diagram for uppermost Mississippian, Pennsylvanian, and Lower Permian strata for sites in the Calingasta-Uspallata, Río Blanco, and Paganzo Basins mentioned in the text (units and ages are based on Taboada, 1985; Archangelsky and Lech, 1985; Archangelsky and Archangelsky, 1987; Fernandez-Seveso and Tankard, 1995; Azcuy et al., 1999, López-Gamundí and Martínez, 2000; Gulbranson et al., 2010; Césari, personal communication)..... 111

Figure 21. Map of the San Rafael Basin and other arc-related late Paleozoic basins in western Argentina (cf. López Gamundí et al., 1994; Sato et al., 2004; Limarino and Spalletti, 2006). Selected formations are denoted as RdP = Río del Peñón, G = Guandacol, QL = Quebrada de las Lajas, QG = Quebrada Grande, HV = Hoyada Verde, AdJ = Agua del Jagüel, T = Tramojo, PdT = Pampa de Tepuel..... 153

Figure 22 . Location map for the measured section of the El Imperial Formation southwest of San Rafael, Mendoza Province, Argentina..... 154

Figure 23. Contact of glacial deposits against Devonian bedrock from the middle unit of the El Imperial Formation. Section was measured on the west side of Highway 173, ..... 155

Figure 24. Measured section of the lower and middle units of the El Imperial Formation. .... 156

Figure 25. The lower two sequences of the El Imperial Formation occur in a paleovalley with 75–100 m relief that cuts into underlying Devonian bedrock (La Horqueta Formation). The present valley, incised by the Atuel River, is excavating the paleovalley. A close-up view of the paleo-scrub is shown in Fig. 26. .... 157

Figure 26. Irregularly-shaped lenses of clast-supported conglomerate, with angular clasts derived from the underlying La Horqueta Formation, are interpreted as paleo-scrub and line the walls of the paleovalley in places. .... 158

Figure 27. Restricted marine facies association. A. Root structures in paleosol. B. Deformed mudstone. C. Orange bed is marl within mudstone. D. Climbing ripples in fine-grained sandstone. E. Internally deformed sand pod on left surrounded by deformed mudstone. Shrub in foreground is 15 cm tall for scale. .... 159

Figure 28. Deltaic facies association. A. Small-scale foresets in medium-grained sandstone. B. Gilbert delta. C. Deltaic facies association transitioning upwards into the glacial facies association (both in sequence 2). Sandstone is interbedded with siltstone in the transitional stage, a prodelta environment. D. Sequence 1, composed of the restricted marine facies association, incised by conglomerate at the base of sequence 2. .... 160

Figure 29. Glacially-influenced facies association. A. Clast rich, weakly stratified diamictite. B. Stratified diamictite stacked as imbricate slices draping underlying Devonian bedrock. Jacob staff for scale. C. Individual beds are outlined in yellow. Rose diagram shows preferred alignment of  $290^{\circ}$ – $110^{\circ}$  for clast axes (n=25) for bed surface where the Jacob staff lies. D. Climbing ripples in fine-grained sandstone. E. Internally deformed sand pod surrounded by deformed siltstone. F. Folded beds of sandstone and mudstone that slid along the substrate. G. Outsized clast in siltstone bends and deforms under- and overlying strata. .... 161

Figure 30. Post-glacial open marine facies association. A. Horizontally laminated fine-grained sandstone. B. Deformed siltstone interbedded with massive fine-grained sandstone. C. Hummocky cross-bedded fine-grained sandstone towards the top of the section. D. Wavy bedding of fine-grained sandstone and siltstone. .... 162

Figure 31. Stratigraphy and events in arc-related basins in western Argentina. Ages of events and formations are from Taboada (1985, 2010); Espejo (1993); García (1996); Azcuy et al. (1999); López Gamundí and Martínez (2000); Limarino and Spalletti (2006); Limarino et al. (2006); Strazzere et al. (2006); Gulbranson et al. (2010); Henry et al. (2010); Césari et al. (2011); and Rocha Campos et al. (2011). Carboniferous time scale is from Davydov et al. (2010); Permian time scale is from Gradstein et al. (2004). .... 163

Figure 32. Location map of Wynyard, Tasmania, where the Wynyard Formation is located, and Hellyer Gorge, where equivalent diamictites occur. Glacial distributions after Rogala et al. (2007); ice flow directions after Hand (1993). .... 204

Figure 33. Paleozoic basins of Gondwana, after Isbell et al. (2003b). Arrows show the path of polar wander during the Carboniferous and Permian according to Powell and Li (1994). .... 205

Figure 34. Major formations and corresponding ages estimated from biostratigraphy of the Lower Parmeener Supergroup of Tasmania, Australia. Modified from Reid et al. (in press). .... 206

Figure 35. Cross section of the lower Parmeener Supergroup of Tasmania, Australia. Lithostratigraphic units are assigned multiple names depending on location within the Tasmania Basin. The distribution and varying thickness of the deposits illustrates the relief of the troughs that the glaciers occupied (see Fig. 32). Modified from Clarke and Forsyth (1989). .... 207

Figure 36. Measured section of the Wynard Formation and Inglis Siltstone contact as exposed in a tributary of the River Cam, north of Hellyer Gorge and south of Wynard.

Inset photographs illustrate from bottom to top: (A) striated dropstone in stratified diamictite, near contact with fissile, structureless diamictite, (B) vertical clasts in mudstone facies of Inglis Siltstone, and (C) rhythmic laminations of siltstone, very fine grained sandstone and mudstone. Also note layers of tasmanite oil shale (t)..... 208

Figure 37. Location map and stratigraphic sections of the Wynyard Formation. Strata young to the west, so section A illustrates the oldest rocks, and section D represents the youngest rocks. The four sections are not continuous due to breaks in the shore platform. Section key also corresponds to Figures 43 and 44. .... 209

Figure 38. Massive diamictite facies association. A. Beds of massive diamictite. B. Thin fine-grained sandstone dykes in massive medium-grained sandstone overlying diamictite. .... 210

Figure 39. Stratified diamictite facies association. A. Interbedded fine sandstone and stratified diamictite in section A. Hammer for scale rests against cross-bedded sandstone. B. Lensoidal bed of stratified diamictite that shows reverse grading. C. A clump of granules and pebbles within stratified diamictite. D. Sheared interbedded stratified diamictite and sandstone in section A. E. Deformed stratified diamictite in section D. F. Bedding of stratified diamictite is outlined to show that deformation has bent beds into a concave up orientation. .... 211

Figure 40. Rotational structures, two around the same core stone, in thin section under plane light from stratified diamictite in the Wynyard Formation. .... 212

Figure 41. Conglomerate and sandstone facies association. A. Cross-bedding in sandy pebble conglomerate. Grain size fines down foresets, with pebbles grading into medium sand. B. Normally graded cobble conglomerate. Mechanical pencil near the top right of the conglomerate bed for scale. C. Massive fine- to medium-grained sandstone with pebbles that is overlain and grades laterally into sandy pebble conglomerate. Faint fissures in the massive sandstone (pointed out with arrows) are dewatering structures. 213

Figure 42. Deformed mudstone and fine sandstone facies association. A. Convolute mudstone interfingers with underlying muddy diamictite. B. Flame dewatering structures in mudstone. C. A clastic dyke of very fine sand that is internally deformed cuts through mudstone beds. D. Sandstone dropstone in mudstone. The point of view of the photograph is looking down at the top of the bed. E. Rippled fine sand. F. Fine sandstone load structures within mudstone. G. Mud volcanoes overlying mudstone beds. H. Large sand volcano (80 × 90 cm) and 30 cm dropstone that penetrates substrate occur in the same mudstone bed. .... 214

Figure 43. Interpreted depositional processes and environments for the four facies associations of the Wynyard Formation: 1. conglomerate and sandstone, 2. massive diamictite, 3. stratified diamictite, 4. deformed mudstone and fine sandstone. A buoyant meltwater plume carrying fine sand, silt, and clay rises from the glacier terminus. Facies follow the same key as Figure 37. Multiple advance and retreat cycles by the tidewater

glacier and efflux variations created the interbedding of these facies as represented in sections in Figure 37. .... 215

Figure 44. Correlation diagram for glacial and post-glacial formations in eastern Australia, Tasmania (Wynyard-Hellyer Gorge localities), Antarctica, and South Africa. Ages of formations and palynology stages are from Evans (1969), Truswell (1978), Collinson et al. (1994), Masood et al. (1994), Veevers et al. (1994), Lindström (1995), Price (1997), Askin (1998), Backhouse (1998), Briggs (1998), Claoué-Long and Korsch (2003), Fielding et al. (2008a), and Stollhofen et al. (2008). Dashed lines indicate biostratigraphic age control, and solid lines indicate radiometric age control. Colors of formations reference dominant lithology (see also Fig. 37). .... 215

Figure 45. Distribution of igneous provinces associated with the tectonically active Panthalassan margin of Gondwana. 1. Choiyoi Group, 2. Dwyka and Eccu Groups, 3. Beaufort Group, 4. Antarctic Peninsula, 5. Ellsworth Mountains, 6. Marie Byrd Land, 7. Central Transantarctic Mountains, 8. Tasmania, 9. Brook Street Arc, New Zealand, 10. Sydney, Gunnedah, and Bowen Basins and Queensland. References are cited in text. Plates reconstruction is from ~270 Ma, modified from Lawver et al. (2008). .... 242

Figure 46. Diagram of climatic, biotic, and igneous events during the Permian. Dates of igneous activity along the Panthalassan margin are from Lopatin et al., 1974; Hålbich et al., 1983; Coutinho et al., 1991; Johnson, 1991; Collinson et al., 1994; Veevers et al., 1994c; Pankhurst et al., 1998; Bangert et al., 1999; Mukasa and Dalziel, 2000; Stollhofen et al., 2000; Campbell et al., 2001; Millar et al., 2002; Price et al., 2006; Grader et al., 2008. Marine genera plots are modified from Bambach et al., 2004. For CO<sub>2</sub> fluctuations, yellow dots and dotted line are from Montañez et al. (2007), red dots represent data compiled by Royer (2006), and the dashed line links the two data sets. .... 243

Figure 47. Map showing outcrop locations of the Choiyoi Group and the inferred extent of the Choiyoi volcanism (gray), based on modern outcrops, volcaniclastic sediments, and wells, after Kay et al. (1989), Llambías et al. (1993), and López Gamundí et al. (1994). .... 244

Figure 48. Polar wander paths across Gondwana throughout the Carboniferous and Permian by Powell and Li (1994) and Lawver et al. (2008). Yellow dots in the Lawver et al. (2008) polar wander path represent 10 million year time intervals. Modified from Lawver et al. (2008) PLATES reconstruction and Isbell et al., 2010. .... 272

Figure 49. Glacial intervals of the LPIA discussed in the text based on the stratigraphic record. Ages are from Truswell (1978), Collinson et al. (1994), Isbell et al. (2003), Fielding et al. (2008a), Rocha-Campos et al. (2008), Stollhofen et al. (2008), Taboada (2010), and Gulbranson et al. (2010). Carboniferous time scale is from Davydov et al. (2010); Permian time scale is from Gradstein et al. (2004). .... 273

Figure 50. pCO<sub>2</sub> fluctuations and glacial and non-glacial intervals in the Permian. Yellow dots are from Montañez et al. (2007), red dots represent data compiled by Royer (2006), and the dashed line links the two data sets. .... 274

Figure 51. Diagram of the equilibrium line of a glacier, which separates the zone of accumulation above from the zone of ablation below. The altitude of the equilibrium line can shift with tectonic or climatic fluctuations. ....	274
Figure 52. The Protoprecordillera in west central Argentina housed glaciers in the Serpukhovian-Bashkirian (late Mississippian – early Pennsylvanian) and acted as a divide between the Río Blanco and Calingasta-Uspallata Basins to the west and the Paganzo Basin to the east until the collapse of the fold-thrust belt in the Pennsylvanian. Modified from Henry et al., 2010. ....	275
Figure 53. Cross-section showing the collapse of the Protoprecordillera in the Late Carboniferous – Early Permian and resulting loss of alpine glaciers. Modified from Henry et al., 2010. ....	276
Figure 54. Diagrams of ice extent over Australia during the P1, P2, and P3/P4 glaciations. The Kanimblan highlands provided an uplifted region where glaciers could nucleate through the Late Permian. Deposits from glaciers housed in the Kanimblan highlands were shed into the Bowen, Gunnedah, and Sydney Basins throughout the Carboniferous and Permian. After Veevers (2006), Fielding et al. (2008a, 2008c). ....	276



## LIST OF TABLES

Table 1. Facies descriptions of the lower glaciogenic sequence of the Agua de Jagüel Formation.....	97
Table 2. X-ray Diffraction Data.....	99
Table 3. X-ray Fluorescence Data.....	99
Table 4. Facies descriptions and interpretations of the lower and middle units of the El Imperial Formation. ....	149
Table 5. Facies descriptions and interpretations of the Wynyard Formation.....	200

## ACKNOWLEDGEMENTS

This project was made possible by many individuals and organizations, and I greatly appreciate their support. First I would like to thank my advisors, Dr. Margaret Fraiser and Dr. John Isbell, for their mentorship. Margaret provided thoughtful training for me in her classes and in the field, and I also greatly appreciate the collaboration and support she provided in my manuscripts and presentations. John trained me from the ground up as a sedimentologist, and I am truly grateful for the opportunities he provided to travel to Argentina and Tasmania. I am also thankful for the many publishing opportunities that John made possible and encouraged me to pursue. I have great respect for the enthusiasm shared by both Margaret and John for their work, and I am thankful that they involved me in their projects and helped impart in me a passion for these geological questions.

I am also deeply grateful for the help and input provided by Carlos Oscar Limarino of the Universidad de Buenos Aires and CONICET. His collaboration and guidance to the Namurian outcrops of west central Argentina made this project possible, and it was a pleasure and a privilege to work with him. I also had a great experience working on Tasmanian strata with Chris Fielding and Tracy Frank of the University of Nebraska-Lincoln and Eugene Domack of Hamilton College, and I appreciate their time, input, and inclusion of me in the project.

I greatly appreciate the time, effort, and influence of the members of my Ph.D. committee: Dr. Stephen Dornbos, Dr. Mark Harris, and Dr. Lindsay McHenry. Thank you for guiding me through this learning process and providing a quality education through your courses and mentorship. In this vein, I would like to thank the entire faculty

of the University of Wisconsin-Milwaukee Geosciences Department for the excellent classes and personal touch unique to our department.

The fieldwork for this project was made possible by funding from the National Science Foundation (grants ANT-0440919 and 0635537), the Geological Society of America, the Geological Society of America Coal Division, the American Association of Petroleum Geologists student grants-in-aid, the UWM Center for Latin and Caribbean Studies, the UWM Geosciences Department, and the Wisconsin Geological Society. I am also very grateful for graduate funding from the UWM Graduate School's Research Grant Initiative Program, the Graduate Student Fellowship Program, the Advanced Opportunity Program, and from the Geosciences Department.

Finally, I thank my family and friends, especially my husband, Chris Henry, for their support of me through this eight year-long endeavor!

“The ancient boulder clays of the southern continents bring us face to face with... the fiercest and longest winter of the ages.”  
Coleman, 1916, p. 186

## Chapter 1: Introduction

The geologic record of the late Paleozoic ice age (LPIA) is highly significant to the scientific community because it provides the last complete record of the transition from an icehouse to greenhouse Earth inhabited by a complex biota (Gastaldo et al., 1996). Earth is presently in an icehouse state, and understanding Earth's transition out of the LPIA will aid the scientific community in anticipating when and how Earth will return to a greenhouse state, what environmental drivers will force the transition, and how organisms will respond to such changes. During the LPIA, glaciation occurred in the southern hemisphere over Gondwana and possibly in the northern hemisphere in Siberia (Frakes, 1979; Chumakov, 1994), but the understanding of the timing, boundaries, and character of the LPIA is only fragmentary at present. The geographic and temporal extent of the glaciation is debated, as it was originally thought that one massive ice sheet covered much of the Gondwana supercontinent for 60 million years (e.g., Frakes, 1979; Veevers and Powell, 1987; Crowell, 1999; Scotese, 1999). However, ongoing research is revealing that the LPIA consisted of numerous shorter glacial intervals of 1-8 Ma duration separated by non-glacial conditions of equal duration (Dickins, 1997; López Gamundí, 1997; Visser, 1997; Isbell et al., 2003b; Fielding et al., 2008b; Gulbranson et al., 2010). This project will test the hypothesis that glaciers in western Argentina and Tasmania occurred as ice caps and small ice sheets instead of the classically interpreted supercontinental-scale ice sheet, and it explores drivers of climate change throughout the late Paleozoic.

LPIA studies can be classified as “far field,” referring to research areas that were at low latitudes during the LPIA and ‘far’ from direct glacial influence, or “near field,” in

high latitude regions that were influenced by glacial waxing and waning. When the far field and near field records were studied independently, diverging conclusions about the LPIA developed, such as the idea of a supercontinent-sized ice sheet in the absence of near field evidence. Thus, an important mission for LPIA research is to reconcile the two records in order to more fully understand issues such as eustatic fluctuations, glacial size and distribution, and biotic responses during the LPIA.

### **The Far Field Record**

A prevailing hypothesis of the LPIA is that fluctuations in Gondwanan glaciation resulted in the deposition of cyclothem in the northern hemisphere (Wanless and Shepard, 1936). While research on the northern hemisphere cyclothem (the far field record) has been ongoing for the last century, widespread exploration of the Gondwanan glacial deposits (the near field record) did not start in earnest until Frakes, Crowell, and their colleagues commenced their Gondwanan fieldwork in the 1960's (e.g., Frakes et al., 1966; Frakes and Crowell, 1969). The presentation of the glacioeustasy-cyclothem hypothesis and the easier accessibility of the field sites in the northern hemisphere in comparison to the Gondwanan glacial deposits resulted in a paradigm of LPIA glaciation extrapolated from relative sea level fluctuations inferred from the cyclothem rather than direct glacial evidence (e.g. Heckel, 1977; Ross and Ross, 1987).

Estimates of the magnitude of eustatic fluctuations during the LPIA vary widely, from 200+ m (Heckel, 1977, 1990; Ross and Ross, 1987) to as little as 50 m (Isbell et al., 2003b). Larger estimates are derived from depths of erosional surfaces and facies juxtapositions in northern-hemisphere field sites (Heckel, 1997, 1990; Soreghan and Giles, 1999). Ross and Ross (1987) generated a Carboniferous-Permian sea-level curve

with rapid (<100 ky) eustatic fluctuations of as much as 240 m from confidential stratigraphic data (proprietary to Gulf Oil Exploration and Production). The level of detail in the sea level curve and apparent corroboration with the cyclothem hypothesis resulted in this being a widely cited study. However, a recent reexamination of sea-level fluctuations by Rygel et al. (2008) using a combination of far and near field data concluded that maximum eustatic fluctuations during the LPIA were 60 – 120 m. Rygel et al. (2008) contested the findings of Ross and Ross (1987), because the high-magnitude sea level fluctuations cannot be duplicated from public access data, and in many instances the sea level curve does not correspond with now-known climatic conditions in the late Paleozoic, such as those during the mid- to late Pennsylvanian (Moscovian-Gzhelian) and the middle Permian (late Artinskian – Roadian). Both of these intervals are now considered non-glacial (Fielding et al., 2008a), but the Ross and Ross (1987) eustatic curve records sea level fluctuations of over 200 m for both of these time spans, magnitudes that are impossible without active, supercontinent-sized glacial waxing and waning.

A formula was developed by Paterson (1972) to calculate the relationship between glacier size (S) and ice volume (V):

$$\log(V) = 1.23[\log(S) - 1]$$

with the water equivalent of ice volume equal to 91.7% of V (cf. Denton et al., 1971; Crowley and Baum, 1991). Using these relationships and correcting for isostasy, Crowley and Baum (1991) determined that an ice sheet  $20.3 \times 10^6 \text{ km}^2$ , (approximately the combined area of Canada and the United States) would have to completely melt in order to produce a eustatic change of 100 m. Isbell et al. (2003b) went on to illustrate

that when applied to Gondwanan glaciation, such a glacier would cover all of Antarctica, southern and much of central Africa and extend into Australia and eastern South America. In order to produce a 200 m change in sea level, as required by the hypotheses of Heckel (1977) and Ross and Ross (1987), the responsible ice sheet would be  $34.6 \times 10^6 \text{ km}^2$  and would blanket all of southern Gondwana (Isbell et al., 2003b). Such massive ice sheets are not highly sensitive to climatic fluctuations, and could not completely grow and collapse repeatedly according to the periodicity of cyclothems (Isbell et al., 2008b; cf. DeConto and Pollard, 2003; Horton and Poulsen, 2009), especially on the timescales proposed by Ross and Ross (1987). Further, near field research on late Paleozoic Gondwanan glacial deposits suggests that glaciation occurred as multiple ice sheets and alpine glaciers, rather than one supercontinental ice sheet (cf. Dickins, 1996; 1997; Isbell et al., 2003a; 2003b; Fielding et al., 2008a; 2008b; Henry et al., 2008a, in press). Smaller ice sheets sequester much smaller volumes of water than the massive ice sheets described above, so much so that 10 ice sheets covering a total of  $33.7 \times 10^6 \text{ km}^2$  (essentially all of Gondwana) would only alter sea level by 59.1 m (Isbell et al., 2003b). These arguments are not meant to imply that glacioeustasy did not contribute to the transgressive-regressive cycles recorded in the cyclothems, but rather suggest that more sophisticated interplays of tectonics, depositional events, and glacioeustatic changes resulted in the Euramerican cyclothems than the former, simplistic hypothesis expresses.

Far field studies on biota during the LPIA, primarily focused on terrestrial plants and marine animals, have revealed how organisms responded to the onset, duration, and end of the ice age. Understanding the biotic response to Earth's transition out of the LPIA is especially instructive for how fauna and flora will respond to the inevitable



future deglaciation of Earth. Also, these studies are likely more useful for anticipating future biotic changes than conclusions drawn from Pleistocene glacial/interglacial fluctuations, because an icehouse-greenhouse transition produces more pronounced oceanographic, atmospheric, and geochemical changes than glacial/interglacial cycles. Future work is needed to determine if the transition from icehouse to greenhouse conditions in the mid-Sakmarian (Early Permian) occurred at an equivalent rate to glacial/interglacial transitions during the Pleistocene. The stratigraphic record presented herein (Chapter 5, section 5), suggests rapid climatic change at the end of the icehouse in the mid-Sakmarian, with the loss of ice sheets extending to sea level over a maximum timeframe of two million years (see Fig. 44).

The initiation of the LPIA was marked by a second-order mass extinction (Stanley and Powell, 2003), and this climatic revolution ushered in new distributions of plants and animals across the globe. The growth of glaciers changed atmospheric circulation patterns, contracting the intertropical convergence zone around the equator, so that low latitudes experienced sub-humid to ever-wet conditions (DiMichele et al., 2001; Powell, 2003). Additionally, seasonal fluctuations were more pronounced in temperate regions. These changes caused vegetational turnover, as lycopsids, pteridosperms, and tree ferns became dominant at low latitudes, and lycophytes were usurped by cordaites and seed-bearing tree ferns in the north temperate Angaran region (Gastaldo et al., 1996; DiMichele et al., 2001; Montañez et al., 2007). In response to cooling, bryozoans and brachiopods migrated to lower latitudes (Ross, 1981; Raymond et al., 1989).

Throughout the LPIA, origination and extinction rates were low, half of what they were before the onset of the ice age (Stanley and Powell, 2003; Powell, 2005).

Organisms that survived extinction at the onset of the LPIA were likely to exhibit the following characteristics: 1. they had large, stable populations; 2. they lived in a niche that was environmentally variable, so they were resilient against changing environmental conditions; 3. they lived over a large geographic area; 4. they did not exhibit stereotypical behavior, i.e., they did not behave in unique ways from other organisms, but instead employed common feeding/mating/burrowing/etc. behaviors.; 5. they were able to reproduce efficiently; and 6. they were able to migrate long distances (Hansen, 1978; Jablonski, 1986; Stanley and Powell, 2003).

As icehouse conditions collapsed at the end of the Early Permian, origination and extinction rates rebounded (Stanley and Powell, 2003; Powell, 2005). Brachiopods migrated back to pre-icehouse latitudes (Raymond et al., 1989). In the floral realm, vegetational overturn occurred once more as the climate became hotter, drier, and less seasonal. Initially, opportunistic plants grew profusely, but eventually xeromorphic plants reclaimed dominance (Gastaldo et al., 1996; DiMichele et al., 2001; Montañez et al., 2007). These types of observations can be used to predict evolutionary trends for other biota throughout the LPIA and even other periods of climate change, including biotic changes in the future.

### **The Near Field Record**

Glacial deposits in South America, Africa, Antarctica, India, Australia, and in smaller Gondwanan crustal fragments now distributed in Asia and the Arabian Peninsula provide information on the extent of glaciation over the southern supercontinent (Fig. 1; Laskar and Mitra, 1976; Collinson et al., 1994; López Gamundí, 1997; Visser, 1997; Garzanti and Sciunnach, 1997; Wopfner and Casshyap, 1997; Isbell et al., 2003a, 2003b,

2008a, 2008c; Fielding et al., 2008a; Henry et al., 2008a; Martin et al., 2008; among others). It is currently thought that the LPIA commenced over Gondwana in present-day South America in the Late Devonian (Caputo et al., 2008; Glacial I of Isbell et al., 2003b; Fig. 1), and glaciation over western South America was at its maximum during the Namurian-Westphalian (Late Mississippian to Early Pennsylvanian; López Gamundí, 1997; Glacial II of Isbell et al., 2003b; Fig. 1). In the latest Carboniferous to Early Permian, the LPIA reached its acme as ice centers occurred across eastern South America, South Africa, Antarctica, Australia, India, southern Asia, and the Arabian Peninsula (Caputo and Crowell, 1985; Garzanti and Sciunnach, 1997; Wopfner and Casshyap, 1997; Glacial III of Isbell et al., 2003b, 2008a; Fielding et al., 2008a; Martin et al., 2008; Fig. 1). The shift in glaciation from western Gondwana to central and eastern Gondwana is related to the migration of Gondwana across the South Pole (Fig. 1; Caputo and Crowell, 1985; Powell and Li, 1994; Crowell, 1999; Li and Powell, 2001; Fielding et al., 2008b; Lawver et al., 2008). The main phase of the LPIA ended in Australia during the Sakmarian (Early Permian), when Earth transitioned into a greenhouse state; yet localized alpine glaciers continued in eastern Australia through the end of the Capitanian (Late Permian; Fielding et al., 2008a, 2008b).

### **Causes of Gondwana Glaciation**

The interplay of shifting lithospheric plates (Caputo and Crowell, 1985; Smith and Read, 2000; Saltzman, 2003) and atmospheric partial pressure of CO<sub>2</sub> ( $p\text{CO}_2$ ) fluctuations (Montañez et al., 2007) influenced the waxing and waning of LPIA glaciation. The shift in glaciation from northwestern South America to across the Gondwanan mainland to Australia has long been associated with continental drift across

the South Pole (Du Toit, 1921; Wegener, 1929; Crowell and Frakes, 1975; Crowell, 1978), and the collapse of the ice age was strongly influenced by the northward migration and clockwise rotation of the supercontinent (Caputo and Crowell, 1985). Another major tectonic event in the late Paleozoic, the docking of Euramerica with Gondwana to form Pangea in the Late Mississippian, may have also strongly influenced glaciation. Closing the oceanic gateway between Euramerica and Gondwana may have increased precipitation in the southern hemisphere, fostering growth of ice sheets (Fig. 2; Smith and Read, 2000; Saltzman, 2003). Divergent  $\delta^{13}\text{C}$  isotope signatures in the Panthalassan and Tethyan Oceans (Saltzman, 2003) support this hypothesis.

Close correlation of  $p\text{CO}_2$  levels with certain Permian glacial/interglacial intervals demonstrated by Montañez et al. (2007) indicate that greenhouse gases were also a major driver of climate in the late Paleozoic. Montañez et al. (2007) used  $p\text{CO}_2$  measurements from soil minerals and marine invertebrate shells to show that  $p\text{CO}_2$  levels were low, typically  $< 500$  parts per million by volume (ppmv), during glacial intervals in the Asselian and Artinskian (P1 and P2 glacial intervals of Fielding et al., 2008a; Fig. 3). In contrast, during non-glacial intervals in the Gzhelian, the Sakmarian, and the late Artinskian,  $p\text{CO}_2$  levels increased, to as high as 5000 ppmv in the Artinskian. In addition, the global  $\delta^{13}\text{C}$  and  $\delta^{18}\text{O}$  curves also correlate moderately well with glacial/interglacial fluctuations during the LPIA, shifting positively during periods of glaciation (Frank et al., 2008). Therefore events affecting the carbon cycle, such as organic carbon burial in peat forming forests and heavy siliciclastic erosion, are hypothesized to also influence glaciation (Berner, 2004).

A final major control on glaciation during the LPIA was the presence of elevated paleotopography produced by tectonic uplift. Powell and Veevers (1987) and Eyles (1993) identify compressive tectonics along the Panthalassan margin of Gondwana (Fig. 1), beginning with the collision of the Chilenia terrane against western South America in the Late Tournasian-Early Viséan, as an instigating condition for the LPIA. Further, Powell and Veevers (1987) call attention to the latitudinal position of South America and Australia when glaciation began in those areas. In South America, glaciation occurred in Peru, Bolivia, and Brazil in the latest Devonian to Viséan (Glacial I of Isbell et al., 2003b; Fig. 4), and in Australia, glaciation began in the Namurian (Glacial II of Isbell et al., 2003b; C1 and C2 of Fielding et al., 2008a; Fig. 4). During the onset of glaciation, both of these sites were located at mid-latitudes ( $30^{\circ}$  -  $60^{\circ}$ ), not high latitudes, and glaciation went on to spread across each respective crustal block. Therefore, rather than polar latitude, onset of glaciation appears to coincide with orogenesis: in South America, convergence and accretion along the Panthalassan margin, and in Australia, uplift along the Tasman Fold Belt (Powell and Veevers 1987). This availability of topographic surfaces above the equilibrium line altitude (ELA) in South America and Australia allowed glaciers to nucleate and grow (cf. Isbell et al., 2010). The ELA is the altitude/boundary on a glacier that separates areas of annual net ablation below from annual net accumulation above. Because the ELA rises and falls with climatic fluctuations and tectonic events, paleotopography and the ELA should be considered controlling factors on glacier distribution throughout the many phases of the LPIA.

## **The Dissertation Work**

The primary focus of this project is on glaciation during the early stages of the LPIA in western Argentina and the main phase of the LPIA in Tasmania, Australia (Glacial II and III of Isbell et al., 2003b, respectively). Both western Argentina and Tasmania contain excellent exposures of Late Carboniferous to Permian glacigenic rocks and are ripe for detailed sedimentologic studies, as the present body of work on the two areas is mostly limited to stratigraphic summaries (e.g., Clarke, 1989; López Gamundí, 1997; Azcuy et al., 1999; Limarino et al., 2006; Rogala et al., 2007). The advent of geomorphology and sedimentology studies of modern glacimarine environments (e.g., Dowdeswell et al., 1994; Powell et al., 1996; Anderson, 1999; Cowan et al., 1999) has provided a vast new source of information, making it possible for scientists to gain a more accurate and detailed characterization of ancient glacigenic strata. Study of the sedimentology of the glacigenic formations of western Argentina and Tasmania will provide information on the size, timing, and thermal regime of glaciers during the early stages and the acme of glaciation over Gondwana.

An ultimate question concerning the initiation, fluctuations, and end of the LPIA is: What caused the climate to change? Isbell et al. (2008b) suggested that the causes for LPIA deglaciation may have been the same as the drivers that resulted in the Late Permian extinctions, because both events are linked to increased  $p\text{CO}_2$  (Fig. 3), and fluctuations in  $p\text{CO}_2$  have long been linked to corresponding temperature changes. The link between increasing  $p\text{CO}_2$  and elevated temperatures is especially significant to modern society, as  $p\text{CO}_2$  has increased by one-third since the industrial revolution, to 380 ppmv, and may reach 2000 ppmv when fossil fuel resources are expended (Kump, 2002). Thus, the secondary focus of this project is to examine sources of  $\text{CO}_2$  (such as

volcanism) during the late Paleozoic in order to examine the drivers of the climatic fluctuations during the LPIA and the Middle and Late Permian extinctions. From the Late Carboniferous to the Triassic, volcanism occurred along the convergent Panthalassan margin of Gondwana, and may be a previously unrecognized contributor to the end of the LPIA and the end-Guadalupian and end-Permian extinctions. This portion of the dissertation will use a literature review to test the hypothesis that the large volume of volcanism along the Panthalassan margin released a substantial amount of CO<sub>2</sub> into the atmosphere that contributed to late Paleozoic environmental and ecological disturbances.

Therefore, this project aims to answer specific questions about climate fluctuations during the late Paleozoic: 1) How can the sedimentology and sequence stratigraphy of glacially influenced strata in western Argentina inform our understanding of the early stages of the LPIA? 2) What information does the sedimentology of Tasmanian glacial deposits provide on glacial dynamics and size during the peak of Gondwanan glaciation? 3) Is the collapse of the LPIA related to later environmental changes in the Permian, such as the end-Guadalupian and end-Permian mass extinctions? This project examines the initiation, peak, and collapse of the LPIA using sedimentology field methods, laboratory work, and literature review in order to provide new data and produce and test informed hypotheses on climate change throughout the LPIA. Below are the objectives for the work produced in this dissertation.

### **Dissertation Objectives**

1. In order to characterize glaciation over western Gondwana during the beginning of the ice age, I studied the glacial sedimentology and sequence stratigraphy of Serpukhovian – Bashkirian glacially influenced strata in west-central Argentina.

The Serpukhovian – Bashkirian glacial interval is the last time western Argentina was glaciated during the LPIA, and a sedimentologic and stratigraphic study establishes a record of depositional processes, paleoredox conditions, and glacial advance/retreat cycles. The Agua de Jagüel and El Imperial Formations are the focus of this portion of the study, and the nearby Hoyada Verde and Tramojo Formations are also included in the analysis of regional glacial conditions.

2. I also performed a detailed sedimentology analysis of the latest Carboniferous – Early Permian (Gzhelian - Sakmarian?) Wynyard Formation in Tasmania, Australia in order to characterize glaciation in the region during the main phase of the LPIA. In addition, Tasmanian glacial and post-glacial stratigraphy is compared to that in neighboring basins in Gondwana. Glacigenic strata in the Wynyard Formation of Tasmania are a thick, poorly-documented succession that are palaeogeographically important to the LPIA, because they provide a link to help correlate better studied glacigenic successions in Antarctica and Australia. Synthesizing the stratigraphic records of these three areas will better identify and constrain the effects that the LPIA had on Earth's physical systems, and will better enable climate models to deduce the major drivers of ice growth and deglaciation during the LPIA.
3. Finally, I examined the role of CO<sub>2</sub> as a driver of climate change during the LPIA and the Middle and Late Permian, exploring volcanism along the Panthalassan margin as a source of CO<sub>2</sub> and thus a contributing driver of climate change during the late Paleozoic. Shifting CO<sub>2</sub> levels have been linked to the initiation, fluctuations, and break-up of LPIA glaciers (Montañez et al., 2007), and increased



CO<sub>2</sub> from volcanism is considered the ultimate cause of the Middle and Late Permian extinctions (end-Guadalupian and end-Changhsingian; Fig. 3; Zhou et al., 2002; Payne and Kump, 2007). In this portion of the dissertation, I investigated emissions from volcanic provinces along the Panthalassan margin of Gondwana from the literature as driving both of these major Paleozoic events.

### **Significance of Research**

The work presented in this dissertation is valuable to multiple audiences. This project provides detailed information on glacial to post-glacial transitions during the LPIA in understudied areas in Argentina and Australia. The present body of work on LPIA sedimentary rocks in the western basins of Argentina is made up primarily of reviews of stratigraphy, with less than ten detailed sedimentology publications. The deficiency of glacial sedimentology studies of Tasmania is even greater, as there is no detailed published work on the Wynyard Formation. Therefore, this research provides valuable information to scientists working in western Argentina and Tasmania and on the LPIA. But most importantly, this project caters to a wider audience because it investigates ancient climate change by determining the size, thermal regime, and timing of glaciers during the commencement and main phase of the LPIA, and explores Panthalassan margin volcanism as a driver of both LPIA deglaciation and Permian extinctions. Investigating the LPIA deglaciation and CO<sub>2</sub> as a driver of climate change will inform society why climate change occurs and how global warming is manifested in Earth systems.

This project also implements new methods in sedimentology research: micromorphology and x-ray analytical techniques. Presently, micromorphology studies

on glacial deposits are rare but are gaining popularity as a method of understanding depositional dynamics (cf. Menzies, 2000; van der Meer et al., 2003). Similarly, mineralogical (as determined by XRD) and elemental (as determined by XRF) studies are underutilized in LPIA studies, despite the information these methods can provide on depositional settings (cf., Scheffler et al., 2003, 2006). Therefore, use of these methods introduces new perspectives on LPIA research.

### **Dissertation Structure**

This dissertation consists of five manuscripts written to be published in scientific journals, followed by a final ‘concept’ chapter that explores the idea of the elevation of paleotopography as a control on glaciation. The formatting style of the journal *Palaeogeography, Palaeoclimatology, Palaeoecology* has been adopted for this dissertation, because the manuscripts of Chapter 3 (Agua de Jagüel Formation) and Chapter 5 (Wynyrd Formation) have been published in this journal.

#### *Chapter 2*

Chapter 2 is titled “Carboniferous glacial deposits of the Protoprecordillera of west-central Argentina” and describes the Namurian glacial and post-glacial record of the basins surrounding the Protoprecordillera in west central Argentina. Based on the sedimentary record in seven different formations in the Calingasta-Uspallata, Río Blanco, and Paganzo Basins, it is hypothesized that the region was glaciated by alpine glaciers located in the Protoprecordillera, and that the melting of these glaciers in the Bashkirian did not affect eustatic fluctuations, because the glaciers were too small to instigate a change in global sea-level. This paper was published in 2008 in a Geological Society of

America special publication titled “Resolving the Late Paleozoic Ice Age in Time and Space,” edited by Christopher Fielding, Tracy Frank, and John Isbell.

### *Chapter 3*

Chapter 3 is titled “Mid-Carboniferous deglaciation of the Protoprecordillera, Argentina, recorded in the Agua de Jagüel paleovalley.” In this paper, the sedimentology and stratigraphy of the Agua de Jagüel Formation of west central Argentina is described and interpreted, and includes a geochemical and mineralogical study of mudrocks in the formation conducted using x-ray diffraction and x-ray fluorescence. Using these methods, the depositional environment is reconstructed and a glacial sequence stratigraphy model is developed for west central Argentina. This manuscript was published in 2010 in a *Palaeogeography, Palaeoclimatology, Palaeoecology* special volume titled “Environmental processes and biotic responses at high latitudes: a study of Late Palaeozoic sequences, biotas and palaeoenvironmental changes in Gondwana and northern Eurasia,” edited by Guang Shi and Bruce Waterhouse. Preliminary data for this project were reported in a national Geological Society of America poster, “Deglaciation in a Pennsylvanian paleovalley of western Argentina: the Agua de Jagüel Formation” (Henry et al., 2008b) and in a paper providing an overview of the glacial record of west central Argentina, “Carboniferous glacial deposits of the Protoprecordillera of west central Argentina” (Henry et al., 2008a).

### *Chapter 4*

Chapter 4 is titled “The late Paleozoic El Imperial Formation, western Argentina: Glacial to post-glacial transition and stratigraphic correlations with arc-related basins in southwestern Gondwana.” This paper describes the sedimentology of the El Imperial

Formation and correlates the stratigraphy of the San Rafael Basin in western Argentina with the Protoprecordilleran basins to the north and the Tepuel Basin to the south. This paper is in press in *Gondwana Research*.

### *Chapter 5*

Chapter 5 is titled “Proglacial deposition and deformation in the Wynyard Formation, Tasmania: a process analysis.” This paper analyzes the sedimentology of the Wynyard Formation in detail, and the micromorphology of Wynyard diamictites is also described. The Tasmanian glacial and post-glacial stratigraphy is then compared to the glacial and post-glacial successions of southern Africa, Antarctica, and eastern Australia. Preliminary results were presented at a regional Geological Society of America talk, “Early Permian glacial advance-retreat cycles recorded in the Wynyard Formation of Tasmania, Australia” (Henry et al., 2009a). This paper was published in *Palaeogeography, Palaeoclimatology, Palaeoecology* in 2012.

### *Chapter 6*

Chapter 6 is titled “Panthalassan margin volcanism: a driver of deglaciation and extinction in the late Paleozoic?” This paper describes the role of  $p\text{CO}_2$  in environmental events during the late Paleozoic and explores volcanism along the Panthalassan margin of Gondwana as a contributor of  $\text{CO}_2$  during these events. The volcanic rocks of the Choiyoi Group of Argentina compose the largest known volcanic province generated along the Panthalassan margin during the late Paleozoic – early Mesozoic (cf. López Gamundí et al., 1994), and  $\text{CO}_2$  output is estimated for these rocks. The ideas of this paper were presented in the talk “Potential environmental consequences of Panthalassan

margin volcanism in the late Paleozoic” (Henry et al., 2009b) at the national Geological Society of America conference.

### *Chapter 7*

Chapter 7 is the concluding chapter that also explores paleotopography as a control on glaciation during the LPIA. This chapter explores potential explanations for the initiation and collapse of glaciation over western Argentina during Glacial II (mid-Carboniferous) and over Tasmania during Glacial III (Early Permian; Fig. 4) are explored. The work presented in this chapter contributed to the paper “Evaluations of glacial paradoxes during the late Paleozoic Ice Age using the concept of the equilibrium line altitude (ELA) as a control on glaciation” by Isbell et al. (2012) published in *Gondwana Research*.

## Figures

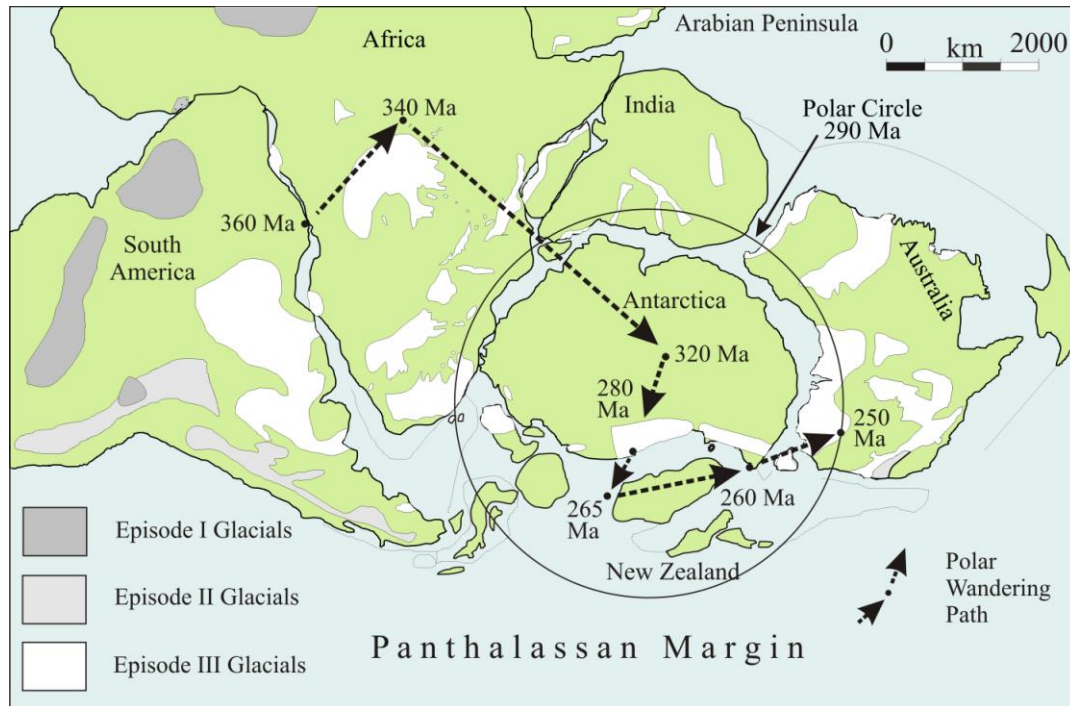
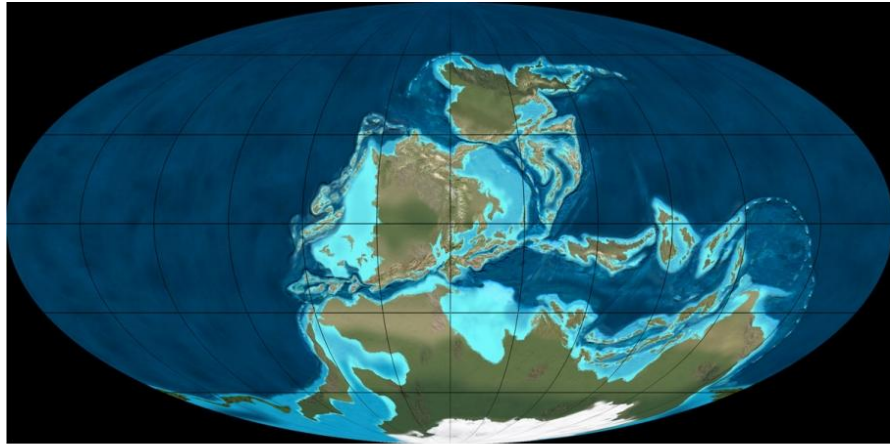
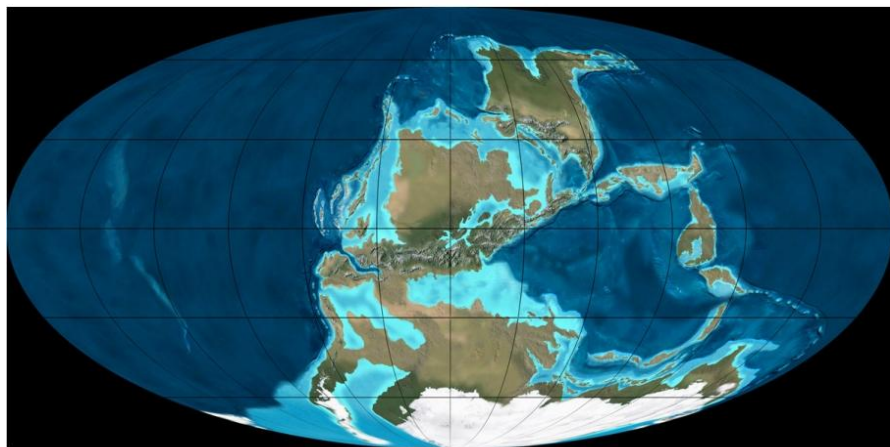


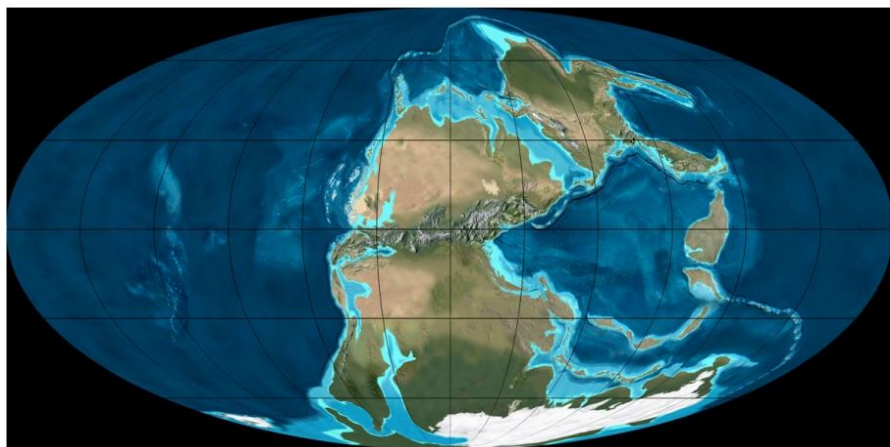
Figure 1. Gondwanan basins containing glacial deposits of the LPIA. Estimates by Powell and Li (1994) and Lawver et al. (2008) of the path of polar wander throughout the Carboniferous and Permian are illustrated. Yellow dots in the Lawver et al. (2008) polar wander path represent 10 million year time intervals. Modified from Isbell et al. (2003b).



Mississippian - 340 Ma



Pennsylvanian - 300 Ma



Early Permian - 280 Ma

Figure 2. Paleogeographic reconstructions of Gondwana throughout the late Paleozoic from Blakey (2008). The series of illustrations shows the docking of Laurussia with Gondwana to form Pangea in the Early Permian.

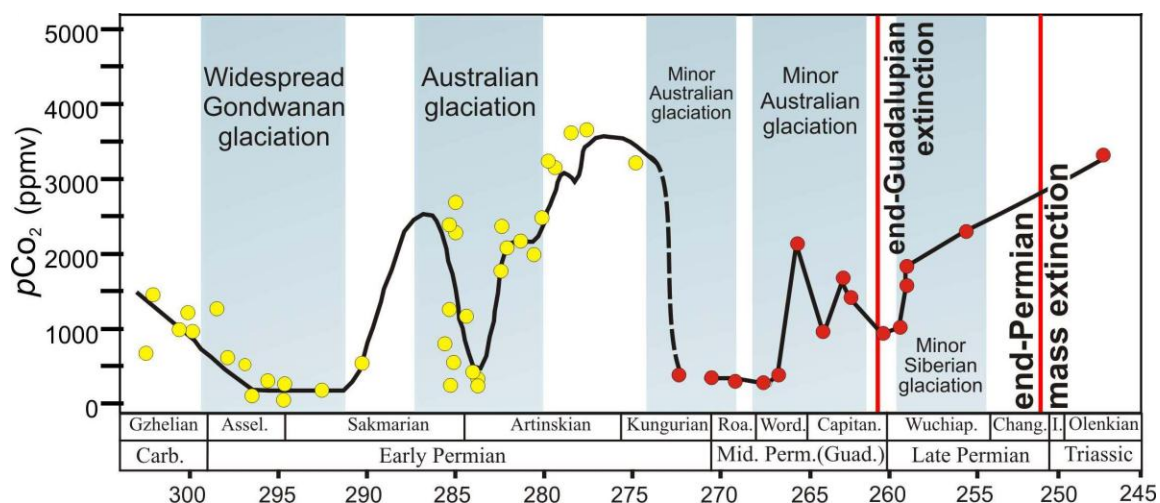


Figure 3.  $\text{CO}_2$  fluctuations correlate with glacial and non-glacial intervals in the Permian. Yellow dots are from Montañez et al. (2007), red dots represent data compiled by Royer (2006), and the dashed line links the two data sets.



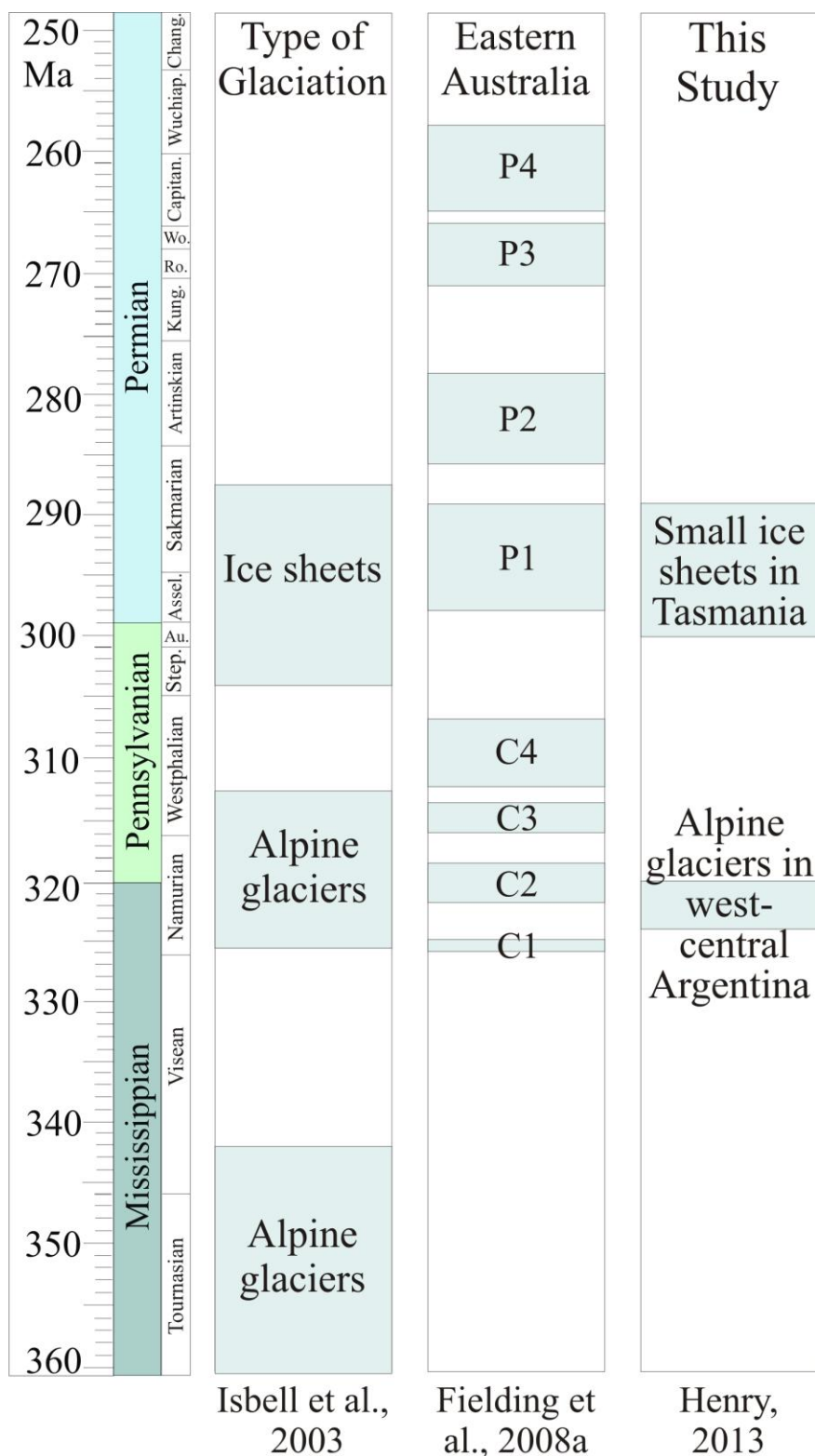


Figure 4. Glaciation during the LPIA occurred as alternating glacial and non-glacial intervals beginning in the Late Devonian, reaching its peak during the late Pennsylvanian – Early Permian, and ending in the Capitanian (middle Permian).

## References

- Anderson, J.B., 1999. Antarctic marine geology. Cambridge University Press, Cambridge, United Kingdom, 289 p.
- Azcuy, C.L., Carrizo, H.A., Caminos, R., 1999. Carbonífero y Pérmico de las Sierras Pampeanas, Famatina, Precordillera, Cordillera Frontal y Bloque de San Rafael. Instituto de Geología y Recursos Minerales Geología Argentina 29, 261–318.
- Berner, R.A., 2004. The Phanerozoic carbon cycle: Oxford, Oxford University Press, 150 p.
- Blakey, R.C., 2008. Gondwana paleogeography from assembly to breakup – A 500 m.y. odyssey. In: Fielding, C.R., Frank, T.D., Isbell, J.L. (Eds.), Resolving the late Paleozoic ice age in time and space. Geological Society of America Special Paper 441, 1–28.
- Caputo, M.V., Crowell, J.C., 1985. Migration of glacial centers across Gondwana during Paleozoic Era. Geological Society of America Bulletin 96, 1020–1036.
- Caputo, M.V., Gonçalves de Melo, J.H., Streel, M., Isbell, J.L., 2008. Late Devonian and Early Carboniferous glacial records of South America. In: Fielding, C.R., Frank, T.D., Isbell, J.L. (Eds.), Resolving the late Paleozoic ice age in time and space. Geological Society of America Special Paper 441, 161–173.
- Chumakov, N.M., 1994. Evidence of Late Permian glaciation in the Kolyma River Basin: a repercussion of the Gondwanan glaciations in Northeast Asia? Stratigraphy and Geological Correlation 2, 130–150.
- Clarke, M.J., 1989. Lower Permian Supergroup. In: Burrett, C.F. and Martin, E.L., eds., Geology and Mineral Resources of Tasmania, Geological Society of Australia Special Publication 15, 295–309.
- Collinson, J.W., Isbell, J.L., Elliot, D.H., Miller, M.F., Miller, J.M., 1994. Permian-Triassic Transantarctic basin. In: Veevers, J., Powell, C. (Eds.), Permian-Triassic Pangea Basins and foldbelts along the Panthalassan margin of Gondwanaland. Geological Society of America Memoir 184, 173–222.
- Cowan, E.A., Seramur, K.C., Cai, J., Powell, R.D., 1999. Cyclic sedimentation produced by fluctuations in meltwater discharge, tides and marine productivity in an Alaskan fjord. Sedimentology 46, 1109–1126.
- Crowell, J.C., 1978. Gondwanan glaciation, cyclothems, continental positioning, and climate change. American Journal of Science 278, 1345–1372.
- Crowell, J.C., 1999. Pre-Mesozoic ice ages; their bearing on understanding the climate

- system. Geological Society of America Memoir 192, 106.
- Crowell, J.C., Frakes, L.A., 1975. The late Paleozoic glaciation. In: Cresswell, M.M., Vela, P. (Eds.), *Gondwana Five*: Rotterdam, A.A. Balkema Publishers, 105–110.
- Crowley, T.J., Baum, S.K., 1991. Estimating Carboniferous sea-level fluctuations from Gondwana ice extent. *Geology* 19, 975–977.
- DeConto, R.M., Pollard, D., 2003. A coupled climate-ice sheet modeling approach to the Early Cenozoic history of the Antarctic ice sheet. *Palaeogeography, Palaeoclimatology, Palaeoecology* 198, 39–52.
- Denton, G.H., Armstrong, R.L., Stuiver, M., 1971. The late Cenozoic glacial history of Antarctica. In: Turekian, K.K., (Ed.), *The late Cenozoic glacial ages*. New Haven, Connecticut, Yale University Press, 267–306.
- Dickins, J.M., 1996. Problems of a late Palaeozoic glaciation in Australia and subsequent climate in the Permian. *Palaeogeography, Palaeoclimatology, Palaeoecology* 125, 185–197.
- Dickins, J.M., 1997. Some problems of the Permian (Asselian) glaciation and the subsequent climate in the Permian. In: Martini, I.P., (Ed.), *Late glacial and postglacial environmental changes: Quaternary, Carboniferous-Permian, and Proterozoic*. Oxford, U.K., Oxford University Press, p. 243–245.
- DiMichele, W.A., Pfefferkorn, H.W., Gastaldo, R.A., 2001. Response of Late Carboniferous and Early Permian plant communities to climate change. *Annual Review of Earth and Planetary Sciences* 29, 461–487.
- Dowdeswell, J.A., Whittington, R.J., Marienfeld, P., 1994. The origin of massive diamicton facies by iceberg rafting and scouring, Scoresby Sund, East Greenland. *Sedimentology* 41, 21–35.
- DuToit, A.L., 1921. The Carboniferous glaciation of South Africa. *Geological Society of South Africa Transactions* 24, 188–277.
- Eyles, N., 1993. Earth's glacial record and its tectonic setting. *Earth-Science Reviews* 35, 1–248.
- Fielding, C.R., Frank, T.D., Birgenheier, L.P., Rygel, M.C., Jones, A.T., Roberts, J., 2008a. Stratigraphic imprint of the Late Paleozoic Ice Age in eastern Australia: a record of alternating glacial and nonglacial climate regime. *Journal of the Geological Society, London* 165, 129–140.
- Fielding, C.R., Frank, T.D., Isbell, J.L., 2008b. The late Paleozoic ice age—A review of current understanding and synthesis of global climate patterns. In: Fielding, C.R.,

- Frank, T.D., Isbell, J.L. (Eds.), Resolving the Late Paleozoic Ice Age in Time and Space. Geological Society of America Special Paper 441, 343–354.
- Frakes, L.A., 1979, *Climates throughout geologic time*. Elsevier, Amsterdam, 310 p.
- Frakes, L.A., Matthews, J.L., Neder, I.R., Crowell, J.C., 1966. Movement directions in late Paleozoic glacial rocks of the Horlick and Pensacola mountains, Antarctica. *Science* 153, 746–748.
- Frakes, L.A., Crowell, J.C., 1969. Late Paleozoic glaciation: I, South America. *Geological Society of America Bulletin* 80, 1007–1042.
- Frank, T.D., Birgenheier, L.P., Montañez, I.P., Fielding, C.R., Rygel, M.C., 2008. Late Paleozoic climate dynamics revealed by comparison of ice-proximal stratigraphic and ice-distal isotopic records. In: Fielding, C.R., Frank, T.D., Isbell, J.L. (Eds.), *Resolving the Late Paleozoic Ice Age in Time and Space*: Geological Society of America Special Paper 441, 331–342.
- Garzanti, E., Sciunnach D., 1997. Early Carboniferous onset of Gondwanian glaciation and Neo-tethyan rifting in South Tibet. *Earth and Planetary Science Letters* 148, 359–365.
- Gastaldo, R.A., DiMichele, W.A., Pfefferkorn, H.W., 1996. Out of the icehouse into the greenhouse: a late Paleozoic analogue for modern global vegetational change. *GSA Today* 10, 1–7.
- Gulbranson, E.L., Montañez, I.P., Schmitz, M.D., Limarino, C.O., Isbell, J.L., Marensi, S.A., Crowley, J.L., 2010. High-precision U-Pb calibration of Carboniferous glacial deposits, Río Blanco and Paganzo basins, Northwest Argentina. *Geological Society of America Bulletin* 122, 1480–1498.
- Hansen, T.A., 1978. Larval dispersal and species longevity in lower Tertiary gastropods: *Science* 199, 885–887.
- Heckel, P.H., 1977. Origin of phosphatic black shale facies in Pennsylvanian cyclothems of mid-continent North America. *American Association of Petroleum Geologists Bulletin* 61, 1045–1068.
- Heckel, P.H., 1990. Evidence for global (glacial-eustatic) control over upper Carboniferous (Pennsylvanian) cyclothems in midcontinent North America. In: Hardman, R.F.P., Brooks, J. (Eds.), *Tectonic events responsible for Britain's oil and gas reserves*. Geological Society Special Publication 55, 35–47.
- Henry, L.C., Isbell, J.L., Limarino, C.O., 2008a. Carboniferous glacial deposits of the Protoprecordillera of west central Argentina. In: Fielding, C.R., Frank, T.D., and Isbell, J.L. (Eds.), *Resolving the Late Paleozoic Ice Age in Time and Space*:

Geological Society of America Special Paper 441, 131–142.

- Henry, L.C., Isbell, J.L., Limarino, C.O., McHenry, L.M., Fraiser, M.F., 2008b. Deglaciation in a Pennsylvanian paleovalley of western Argentina: the Agua de Jagüel Formation. *GSA Abstracts with Programs* 40.
- Henry, L.C., Isbell, J.L., Fielding, C.R., Frank, T.D., Fraiser, M.L., 2009a. Early Permian glacial advance-retreat cycles recorded in the Wynyard Formation of Tasmania, Australia. *GSA Abstracts with Programs* 41, 72.
- Henry, L.C., Limarino, C.O., Fraiser, M.L., Isbell, J.L., 2009b. Potential environmental consequences of Panthalassan margin volcanism in the late Paleozoic. *GSA Abstracts with Programs* 41, 360.
- Henry, L.C., Isbell, J.L., Limarino, C.O., in press. The late Paleozoic El Imperial Formation, western Argentina: glacial to post-glacial transition and stratigraphic correlations with arc-related basins in southwestern Gondwana. *Gondwana Research*, <http://dx.doi.org/10.1016/j.gr.2012.08.023>.
- Horton, D.E., Poulsen, C.J., 2009. Paradox of late Paleozoic glacioeustasy. *Geology* 37, 715–718.
- Isbell, J.L., Lenaker, P.A., Askin, R.A., Miller, M.F., Babcock, L.E., 2003a. Reevaluation of the timing and extent of late Paleozoic glaciation in Gondwana: Role of the Transantarctic Mountains. *Geology* 31, 977–980.
- Isbell, J.L., Miller, M.F., Wolfe, K.L., Lenaker, P.A., 2003b. Timing of late Paleozoic glaciation in Gondwana: was glaciation responsible for the development of northern hemisphere cyclothems? In: Chan, M.A., Archer, A.W. (Eds.), *Extreme depositional environments: mega end members in geologic time*. Geological Society of America Special Paper 370, 5–24.
- Isbell, J.L., Cole, C.I., Catuneanu, O., 2008a. Carboniferous-Permian glaciation in the main Karoo Basin, South Africa : Stratigraphy, depositional controls, and glacial dynamics. In: Fielding, C.R., Frank, T.D., Isbell, J.L. (Eds.), *Resolving the Late Paleozoic Ice Age in Time and Space*: Geological Society of America Special Paper 441, 71–82.
- Isbell, J.L., Fraiser, M.L., Henry, L.C., 2008b. Examining the complexity of environmental change during the late Paleozoic and early Mesozoic. *Palaios* 23, 267–269.
- Isbell, J.L., Koch, Z.J., Szablewski, G.M., Lenaker, P.A., 2008c. Permian glacial deposits in the Transantarctic Mountains, Antarctica. In: Fielding, C.R., Frank, T.D., Isbell, J.L. (Eds.), *Resolving the Late Paleozoic Ice Age in Time and Space*. Geological Society of America Special Paper 441, 59–70.

- Isbell, J.L., Henry, L.C., Limarino, C.O., Koch, Z.J., Fraiser, M.L., Dineen, A.A., 2010. The relationship between equilibrium line altitude and latitude as a control on Gondwana glaciation during the late Paleozoic ice age. *International Sedimentological Congress Abstracts with Programs* 18.
- Isbell, J.L., Henry, L.C., Gulbranson, E.L., Limarino, C.O., Fraiser, M.L., Koch, Z.J., Ciccioli, P.L., Dineen, A.A., 2012. Evaluations of glacial paradoxes during the late Paleozoic Ice Age using the concept of the equilibrium line altitude (ELA) as a control on glaciation. *Gondwana Research* 22, 1–19.
- Jablonski, D., 1986. Larval ecology and macroevolution in marine invertebrates. *Bulletin of Marine Science* 39, 565–587.
- Kump, L.R., 2002. Reducing uncertainty about carbon dioxide as a climate driver. *Nature*, v. 419, 188.
- Laskar, B., Mitra, N.D., 1976. Paleoclimatic vicissitudes in India during Lower Gondwana sedimentation. *Geophytology* 6, 162–169.
- Lawver, L.A., Dalziel, I.W.D., Norton, I.O., Gahagan, L.M., 2008. The Plates 2007 Atlas of Plate Reconstructions (750 Ma to Present Day), Plates Progress Report No. 305-0307, University of Texas Technical Report No. 195, 160 pp.
- Li, Z.X., Powell, C.M., 2001. An outline of the palaeogeographic evolution of the Australasian region since the beginning of the Neoproterozoic. *Earth-Science Reviews* 53, 237–277.
- Limarino, C., Tripaldi, A., Marensi, S., Fauqué, L., 2006. Tectonic, sea-level, and climatic controls on Late Paleozoic sedimentation in the western basins of Argentina. *Journal of South American Earth Sciences* 33, 305–226.
- López Gamundí, O. R., 1997. Glacial-postglacial transition in the late Paleozoic basins of Southern South America. In: Martini, I. P. (Ed.), *Late glacial and postglacial environmental changes: Quaternary, Carboniferous-Permian, and Proterozoic*: Oxford, U.K., Oxford University Press, 147–168.
- López Gamundí, O.R., Espejo, I.S., Conaghan, P.J., Powell, C.M., Veevers, J.J., 1994, *Southern South America: Geological Society of America Memoir* 184, 281–329.
- Martin, J.R., Redfern, J., Aitken, J.F., 2008. A regional overview of the late Paleozoic glaciation in Oman. In: Fielding, C.R., Frank, T.D., Isbell, J.L. (Eds.), *Resolving the Late Paleozoic Ice Age in Time and Space*. Geological Society of America Special Publication, 175–186.
- Menzies, J., 2000. Microstructures in diamictites of the lower Gowganda Formation (Huronian), near Elliot Lake, Ontario: evidence for deforming-bed conditions at

- the grounding line? *Journal of Sedimentary Research* 70, 210–216.
- Montañez, I.P., Tabor, N.J., Niemeier, D., DiMichele, W.A., Frank, T.D., Fielding, C.R., Isbell, J.L., Birgenheier, L.P., Rygel, M.C., 2007. CO<sub>2</sub>-forced climate and vegetative instability during late Paleozoic deglaciation. *Science* 315, 87–91.
- Paterson, W.S.B., 1972. Laurentide ice sheets: Estimated volumes during late Wisconsin. *Reviews of Geophysics and Space Physics* 10, 885–917.
- Payne, J.L., Kump, L.R., 2007. Evidence for recurrent Early Triassic massive volcanism from quantitative interpretation of carbon isotope fluctuations: Earth and Planetary Science Letters 256, 264–277.
- Powell, C.M., Veevers, J.J., 1987. Namurian uplift in Australia and South America triggered the main Gondwanan glaciation. *Nature* 326, 177–179.
- Powell, C. M., Li, Z.X., 1994. Reconstruction of the Panthalassan margin of Gondwanaland. In: Veevers, J., Powell, C. (Eds.), *Permian-Triassic Transantarctic basin, Permian-Triassic Pangea Basins and foldbelts along the Panthalassan margin of Gondwanaland*. *Geologic Society of America Memoir* 184, 5–9.
- Powell, M.G., 2005. Climatic basis for sluggish macroevolution during the late Paleozoic ice age. *Geology* 33, 381–384.
- Powell, R.D., Dawber, M., McInnes, J.N., Pyne, A.R., 1996. Observations of the grounding line area at a floating glacier terminus. *Annals of Glaciology* 22, 217–223.
- Raymond, A., Kelley, P.H., Lutken, C.B., 1989. Polar glaciers and life at the equator: the history of Dinantian and Namurian (Carboniferous) climate. *Geology* 17, 408–411.
- Rogala, B., James, N.P., Reid, C.M., 2007. Deposition of Polar carbonates during interglacial highstands on an Early Permian shelf, Tasmania. *Journal of Sedimentary Research* 77, 587–606.
- Ross, C.A., Ross, J.R.P., 1987. Late Paleozoic sea levels and depositional sequences. In: Ross, C.A., Haman, D. (Eds.), *Timing and Depositional History of Eustatic Sequences: Constraints on Seismic Stratigraphy*. *Cushman Foundation for Foraminiferal Research, Special Publication* 24, 137–149.
- Ross, J.R.P., 1981. Biogeography of Carboniferous ectoproct Bryozoa. *Paleontology* 24, 313–341.
- Royer, D., 2006. CO<sub>2</sub>-forced climate thresholds during the Phanerozoic. *Geochimica et Cosmochimica* 70, 5665–5675.

- Rygel, M.C., Fielding, C.R., Frank, T.D., Birgenheier, L.P., 2008. The magnitude of late Paleozoic glacioeustatic fluctuations: a synthesis. *Journal of Sedimentary Research* 78, 500–511.
- Saltzman, M.R., 2003. Late Paleozoic ice age: Oceanic gateway or  $p\text{CO}_2$ ? *Geology* 31, 151–154.
- Scheffler, K., Hoernes, S., Schwark, L., 2003. Global changes during Carboniferous – Permian glaciation of Gondwana: linking of polar and equatorial climate evolution by geochemical proxies. *Geology* 31, 605–608.
- Scheffler, K., Buehmann, D., Schwark, L., 2006. Analysis of late Palaeozoic glacial to postglacial sedimentary successions in South Africa by geochemical proxies – Response to climate evolution and sedimentary environment. *Palaeogeography, Palaeoclimatology, Palaeoecology* 240, 184–203.
- Scotese, C.R., 1999. The PALEOMAP Project: paleogeographic atlas and plate tectonics Software, Department of Geology, University of Texas, TX.
- Smith, L.B., Jr., Read, J.F., 2000. Rapid onset of late Paleozoic glaciation on Gondwana: Evidence from Upper Mississippian strata of the Midcontinent, United States. *Geology* 28, 279–282.
- Soreghan, G.S., Giles, K.A., 1999. Amplitudes of late Pennsylvanian glacioeustasy. *Geology* 27, 255–258.
- Stanley, S.M., Powell, M.G., 2003. Depressed rates of origination and extinction during the late Paleozoic ice age: A new state for the global marine ecosystem. *Geology* 31, 877–880.
- van der Meer, J. J. M., Menzies, J., Rose, J. 2003. Subglacial till: the deforming glacier bed. *Quaternary Science Reviews*, 22, 1659–1685.
- Veevers, J.J., Powell, M., 1987. Late Paleozoic glacial episodes in Gondwanaland reflected in transgressive-regressive depositional sequences in Euramerica. *Geological Society of America Bulletin* 98, 475–487.
- Visser, J.N.J., 1997. Deglaciation sequences in the Permo-Carboniferous Karoo and Kalahari basins of southern Africa: a tool in the analysis of cyclic glaciomarine basin fills. *Sedimentology* 44, 507–521.
- Wanless, H.R., Shepard, F.P., 1936. Sea level and climatic changes related to late Paleozoic cycles. *Geological Society of America Bulletin* 47, 1177–1206.
- Wegener, A., 1929. The origin of continents and oceans (English translation by John



Biram of Die Entstehung der Kontiente und Ozeane, 4<sup>th</sup> ed.); New York, Dover Publications, Inc., 1966, 246 p.

Wopfner, H., Casshyap, S.M., 1997. Transition from freezing to subtropical climates in the Permo-Carboniferous of Afro-Arabia and India. In: Martini, I.P. (Ed.), Late glacial and postglacial environmental changes: Quaternary, Carboniferous-Permian, and Proterozoic. Oxford, U.K., Oxford University Press, 192–212.

Zhou, M., Malpas, J., Song, X.-Y., Robinson, P.T., Min, S., Kennedy, A.K., Leshner, C.M., Keays, R.R., 2002. A temporal link between the Emeishan large igneous province (SW China) and the end-Guadalupian mass extinction. *Earth and Planetary Science Letters* 196, 113–122.

## Chapter 2: Carboniferous glacial deposits of the Protoprecordillera of west-central Argentina

Lindsey C. Henry<sup>\*a</sup>, John L. Isbell<sup>a</sup>, Carlos O. Limarino<sup>b, c</sup>

<sup>a</sup>Department of Geosciences, University of Wisconsin–Milwaukee, Milwaukee, Wisconsin 53201, USA

<sup>b</sup>Consejo Nacional de Investigaciones Científicas y Técnicas (CONICET), Departamento de Ciencias Geológicas

<sup>c</sup>Universidad de Buenos Aires, Pabellón 2, Ciudad Universitaria C1428EHA, Buenos Aires, Argentina

### Abstract

Glacial strata associated with the Protoprecordillera were deposited in the Calingasta-Uspallata and Río Blanco back-arc basins and the Paganzo foreland basin in west-central Argentina during the early Pennsylvanian (upper Namurian; Bashkirian). These basins were formed due to tectonic loading and later postcollisional extension in a convergent-margin setting along the western margin of Gondwana during the Chañic and Río Blanco tectonic events. Uplift of the Protoprecordillera fold-and-thrust belt during the latest Viséan–earliest Namurian (Serpukhovian) resulted in the development of a widespread unconformity that formed the pre-glacial basin floors. During the Namurian, alpine glaciers carved deep valleys into the upland, and ice drained radially away from the Protoprecordillera. Valley glaciers or an ice cap also occupied basement uplifts in the Sierras Pampeanas to the east. Ice was grounded below sea level in the Calingasta-Uspallata and Río Blanco Basins, where thick glacial successions were deposited. In the Paganzo Basin, a thin glacial succession was deposited in both terrestrial and glacial settings. Throughout the Protoprecordilleran region, deposition is interpreted to have occurred (1) subglacially, (2) in moraine banks, (3) as a result of settling from

---

\* Corresponding author.

Email addresses: [christi9@uwm.edu](mailto:christi9@uwm.edu) (L.C. Henry), [jisbell@uwm.edu](mailto:jisbell@uwm.edu) (J.L. Isbell), [oscarlimarino@ciudad.com.ar](mailto:oscarlimarino@ciudad.com.ar) (C.O. Limarino)

suspension out of meltwater plumes, (4) as rain-out from melting icebergs, and/or (5) from mass movement and sediment gravity flows. An abrupt upward transition from diamictites to marl-bearing, dropstone-free mudrocks marks glacial retreat and establishment of sediment-starved marine conditions. Above this, coarsening-upward successions and truncation surfaces signal either postglacial deltaic progradation during a forced regression or fluvial incision associated with a base-level fall. Although much is known about these strata, many questions remain, including the age of the deposits, environments of deposition, and the mechanisms responsible for the observed stratigraphic architecture.

Keywords: Protoprecordillera, late Paleozoic ice age (LPIA), Argentina, Namurian.

## **1. Introduction**

Lowermost Pennsylvanian (upper Namurian; Bashkirian) strata exposed in the Precordillera of west-central Argentina were deposited along the convergent margin of Gondwana in valleys cut into a fold-and-thrust belt, the Protoprecordillera, and in adjacent basins (Calingasta-Uspallata, Río Blanco, and Paganzo Basins; Figs. 5, 6, and 7; cf. Azcuy et al., 1999; Limarino and Spalletti, 2006; Limarino et al., 2006). These strata represent an important record of sedimentation because they were deposited during the initial stages (Bashkirian) of the main phase of the late Paleozoic ice age (LPIA) (Limarino et al., 2006). Important summaries of the rocks in this region may be found in reports by Salfity and Gorustovich (1983), Archangelsky et al. (1987), López-Gamundí (1987, 1997), López-Gamundí et al. (1994), Limarino et al. (1993, 2002, 2005, 2006), and Azcuy et al. (1999). Many of these studies represent regional-scale investigations without much attention given to glacial sedimentology. Only recently have investigators

begun to look at the glacial deposits in greater detail (e.g., González, 1981; López-Gamundí, 1987; Limarino and Gutiérrez, 1990; Marensi et al., 2005; Kneller et al., 2004; Dykstra et al., 2006).

This paper summarizes previous research on LPIA deposits in the Protoprecordillera and preliminary investigations conducted by the authors in the area. The paper also identifies and discusses a number of questions concerning the deposits that need further investigation, including:

- What was the age of the glaciation (initial advance and final retreat)?
- What was the nature of the preglacial and postglacial transitions?
- Under what environmental conditions were the strata deposited?
- Were the strata deposited from an ice sheet, ice cap, or from valley glaciers draining the Protoprecordillera and adjacent areas?
- What mechanisms drove deposition of the strata and the resulting stratigraphy?

## **2. Geologic Setting**

Namurian strata of the LPIA reported in this paper are exposed in and adjacent to an actively deforming Cenozoic fold-and-thrust belt, the Precordillera, which is superimposed on a late Paleozoic fold-and-thrust belt, the Protoprecordillera (Fig. 5A). According to the tectonic model described by Limarino et al. (2006), the Protoprecordillera formed during the Middle Devonian to earliest Mississippian Chañic orogeny and evolved from an obducted accretionary prism (eastward subduction) into a collisional fold-and-thrust belt (both eastward- and westward directed thrusting) during the accretion of the Chilenia terrane to the western margin of Gondwana (Fig. 6; Ramos et al., 1984, 1986; López-Gamundí et al., 1994; Limarino et al., 2006). In this model, the

Calingasta-Uspallata, Río Blanco, and Paganzo Basins were formed as foreland basins. By the Pennsylvanian, subduction had shifted westward, and postcollisional extension (Río Blanco tectonic phase) allowed these basins to widen in a back-arc setting (Limarino et al., 2006). Initial sedimentation in the Río Blanco and Calingasta-Uspallata Basins produced intercalated continental and marine sandstones, mud rocks, diamictite, and conglomerate (De Rosa, 1983; Limarino and Spalletti, 2006). At the top of this succession, Fauqué and Limarino (1990) and Limarino et al. (1993) interpreted rare local accumulations of dropstone-bearing mud rocks, mud rocks containing diamictite lenses, and thin diamictite that contained striated and faceted clasts as glacially influenced ice-rafted, iceberg-dump, and sediment gravity flow deposits. These strata contain palynomorphs of probable Visean age (Limarino et al., 2006). Visean glacial strata are highly deformed and have not been extensively studied. Uplift of the Protoprecordillera and synorogenic sedimentation in the Río Blanco and Calingasta-Uspallata Basins culminated with intense folding and faulting during the late Mississippian (latest Visean–earliest Namurian) Río Blanco tectonic event (López-Gamundí et al., 1994; Limarino et al., 2006). This event is marked by a regional unconformity, which along the margins of the Río Blanco and Calingasta-Uspallata Basins separates more deformed Visean and older strata below from less deformed Namurian and younger strata above.

During the Pennsylvanian, the Protoprecordilleran highland separated the mainly continental Paganzo Basin from open marine conditions in the Río Blanco and Calingasta-Uspallata Basins (Fig. 5A; Limarino et al., 2006). The latter two basins were located between the fold-and-thrust belt and a volcanic arc located to the west in present-day Chile (Azcuay et al., 1999; Limarino and Spalletti, 2006). Namurian sedimentation

occurred in paleovalleys cut into the Protoprecordillera and on an irregular erosion surface in the adjacent basins (López-Gamundí et al., 1994; Kneller et al., 2004; Limarino et al., 2006). The eastern part of the Paganzo Basin was broken by uplifts of cratonic Pampean basement rocks, which included Precambrian metamorphic and lower Paleozoic granitic rocks (López-Gamundí et al., 1994).

Namurian sedimentation associated with the Protoprecordillera was glacigenic in nature and occurred within paleovalleys in the fold-and-thrust belt (e.g., Agua de Jagüel Formation, Jejenes Formation; López-Gamundí et al., 1994; Kneller et al. 2004; Limarino et al., 2006), on the adjacent Río Blanco and Calingasta-Uspallata marine basin floors (Figs. 5A and 7; e.g., Hoyada Verde Formation), and in the western portion of the Paganzo Basin (Guandacol Formation). Throughout western Argentina, glacigenic rocks are overlain by marine mudrocks deposited during a Namurian postglacial transgression (Limarino et al., 2002). These strata are in turn overlain by either regressive sandstone and mudrocks deposited in shoreface environments (Paganzo Basin), or they are erosionally truncated by fluvial deposits (Calingasta-Uspallata and Río Blanco Basins).

### **3. Age**

The age of the uppermost Mississippian and lowermost Pennsylvanian glacigenic succession in west-central Argentina is constrained by fossils and lithostratigraphy. The Río Blanco unconformity at the base of the succession truncates strata with probable Viséan palynomorphs, and, based on regional correlations in Argentina, it is estimated to be no younger than earliest Namurian (Serpukhovian; Limarino and Gutiérrez, 1990). At Hoyada Verde in the Calingasta-Uspallata Basin, post glacial mudrocks contain brachiopods, bivalves, crinoids, and bryozoans. These fossils are assigned to the

Namurian to early Westphalian (Serpukhovian to Bashkirian; *Levipustula* zone; Amos and Roller, 1965; Cisterna, 1999). Therefore, glacial strata deposited west of the Protoprecordillera are considered to be late Namurian (Bashkirian; Fig. 7). In the Huaco area of the Paganzo Basin, basal strata of the Guandacol Formation rest on the Río Blanco unconformity. These strata contain palynomorphs assigned to the *Raistrickia densa*–*Convolutispora muriornata* assemblage biozone (DM, subzone A). Césari and Gutiérrez (2000) correlated this zone with late Namurian (Bashkirian) strata elsewhere in Gondwana. The occurrence of plant fossils belonging to the *Nothorhacopteris*–*Botrychiopsis*–*Ginkgophyllum* (NBG zone) indicates a Namurian–Westphalian age for the postglacial mudrocks (Gutiérrez et al., 1995). Based on fossils in the Río Blanco and Paganzo Basins, it is reasonable to assign a late Namurian (Bashkirian) age to the glaciation and a latest Namurian (late Bashkirian) to early Westphalian age (early Moscovian) to the ensuing postglacial transgression (Fig. 7; Limarino et al., 2002, 2006). However, biostratigraphic constraints have only been established at a few sites, and a precise correlation with international time scales that are based on invertebrate fossils remains problematic (Césari and Gutiérrez, 2000).

#### **4. Glacigenic deposits of the Protoprecordillera**

This paper focuses on Namurian glacigenic strata deposited within paleovalleys cut into the Protoprecordillera, and strata that were deposited in the nearby Paganzo, Río Blanco, and Calingasta-Uspallata Basins. Figures 5A and 7 show the names, locations, and ages of glacigenic deposits described in this report.

##### **4.1. Paleovalleys**

A number of paleovalleys containing Namurian deposits are exposed in the Precordillera and adjacent areas (Kneller et al., 2004; Limarino et al., 2005; Dykstra et al., 2006). These valleys, which contain deposits of glacial and postglacial diamictite, conglomerate, sandstone, and mudrock, were tens to hundreds of meters deep and as much as several kilometers wide. The paleovalleys are oriented perpendicular to oblique to the trend of the Protoprecordillera. However, some small paleovalleys within the range are oriented subparallel to the trend of the ancient fold-and-thrust belt. Three of the largest paleovalleys are exposed at Agua de Jagüel, Quebrada de las Lajas, and Quebrada Grande (Fig. 5A). These valleys and their deposits are described next.

#### **4.1.1. Agua de Jagüel**

Strata of the Agua de Jagüel Formation, located 17 km NNE of Uspallata in the Calingasta-Uspallata Basin, were deposited in a large paleovalley located along the southwestern margin of the Protoprecordillera (Figs. 5A and 5B). These strata, which are steeply dipping due to Cenozoic tectonism, overlie an angular unconformity cut into highly folded and faulted Mississippian and older siliciclastic rocks deformed during the Chañic and Río Blanco orogenies (Fig. 8).

At least three unconformity-bounded depositional sequences occur within strata of the Agua de Jagüel Formation (Fig. 8). These sequences consist of a thick, lower glacial sequence overlain by two sequences containing fluvial and shallow marine deposits. The lower two sequences occur in an area where the base of the formation is mainly covered by Quaternary and recent bajada deposits. However, in the northern portion of their outcrop, these sequences lap onto sedimentary basement rocks (Fig. 8). The third sequence rests on a relatively low-relief (tens of meters) erosion surface that



either truncates deposits of sequence two or cuts sedimentary basement rocks deformed during the Río Blanco tectonic movement. We estimate that the paleovalley containing the lower two depositional sequences was at least 700 m deep, and at least 5 km wide.

This estimate is based on the following observations:

- onlap of sequences I and II and part of III onto basement rocks (Fig. 8),
- the thickness of sequences I and II (Figs. 5B and 8),
- the width of the outcrop belt where sequences I and II occur (Fig. 8), and
- the low-relief character of the truncation surface separating sequence III from sequence II and from sedimentary basement rocks where sequences I and II are not present, which suggests that sequences I and II were never deposited in the northern portion of the outcrop belt (Fig. 8).

Glacigenic deposits occur within sequence I in the Agua de Jagüel Formation and are displayed in the stratigraphic column in Figure 5B. These strata consist of massive and stratified diamictite, massive conglomerate, massive and graded sandstone, crossbedded sandstone, dropstone-bearing mudrock (dropstones are faceted and striated), and mudrock containing thin marl beds. Throughout the glacigenic sequence, centimeter- to meter-scale deformational structures, including slumps, slides, folds, loading, and dewatering structures are common. However, slumps, slides, and folds are especially abundant within diamictite facies in the lower portion of the formation. A transition from glacigenic to postglacial deposits occurs above the last dropstone interval (Fig. 5B). Above this surface, mudrocks predominate and pass upward into a dropstone-free coarsening-upward succession. An incision surface separates strata in sequence I from fluvial and shallow-marine deposits in sequence II.

We interpret the clast-poor and clast-rich diamictites as having been deposited in ice-proximal settings, by rain-out from meltwater plumes, iceberg rafting, and sediment gravity flows (slides, slumps, and debris flows). Interbedded sandstones are interpreted as turbidity current deposits, which may have been triggered by larger-scale sediment gravity flows and mass movement. The combination of these deposits suggests that initial deposition may have been along a morainal bank, in front of a tidewater glacier that occupied the paleovalley or fjord. Mudrocks were deposited by clay and silt settling from suspension following retreat of the glacier up the fjord. However, the occurrences of dropstone intervals indicate that either a calving ice front was still in contact with marine waters or the glacial ice had readvanced into the paleovalley, and icebergs were rafting debris down the fjord. The coarsening-upward mudrock to crossbedded sandstone succession near the top of sequence I suggests either that a shoreface prograded down the fjord, or that marine currents (e.g., longshore currents) built a bar (e.g., spit) across the mouth of the fjord. A flooding surface overlain by dropstone-bearing mudrocks suggests the occurrence of icebergs in the area until late in the deposition of sequence I. The transition to dropstone-free mudrocks is indicative of the retreat of the ice margin from the area. Truncation surfaces capping each depositional sequence within the Agua de Jagüel Formation suggest fluctuations in relative base level.

Paleocurrent orientations taken from sole marks (groove, bounce, and flute marks and striations) and the orientation of conglomerate and sandstone channel bodies indicate flow down the paleovalley toward the SW, away from the Protoprecordillera.

Mudrocks in sequences II and III of the Agua de Jagüel Formation contain brachiopods, gastropods, bivalves, cephalopods, and corals (cf. Taboada, 1985). Based on

the presence of the brachiopod *Cancrinella*, Amos and Rolleri (1965) and Taboada (1985) identified these strata as Upper Carboniferous (Pennsylvanian) to Lower Permian. Because diamictites occur at the base of the Agua de Jagüel Formation in sequence I, they are considered to be the same age as the diamictites in the Hoyada Verde Formation described later in this paper (López-Gamundí, 1987).

#### **4.1.2. Quebrada de las Lajas and Quebrada Grande**

Paleovalley complexes at Quebrada de las Lajas and Quebrada Grande are exposed in the Sierra Chica del Zonda near the city of San Juan and have been described by Bercowski (1983), Kneller et al. (2004), Limarino et al. (2005), and Dykstra et al. (2006). Glacigenic deposits are contained within strata defined as the Jejenes Formation of the Paganzo Basin (Figs. 5A, 5C, and 7).

The paleovalley at Quebrada de las Lajas is cut into limestones of the Ordovician San Juan Formation. The valley is ~5 km long, up to 1000 m deep, and varies in width from 200 to 1000 m; the original valley walls slope at up to 50°–70° (Dykstra et al., 2006). The valley is oriented SW-NE and widens toward the NE. Paleocurrent orientations indicate that flow was NE down the axis of the paleovalley (Fig. 5A). The glacigenic and postglacial portion of the valley fill is ~300 m thick and consists of a complicated succession of conglomerate, sandstone, and siltstone facies (Fig. 5C). Dykstra et al. (2006) interpreted the basal conglomerate, sandstone, and siltstone as having been deposited in ice-contact deltas and deep-water lacustrine settings with deposition from iceberg rafting. Deformation within the conglomerates may have been the result of glacitectonic activity. Breccias along the sides of the paleovalley represent talus and scree deposits. These strata also include an abundance of large-scale

deformation (tens of meters thick and hundreds of meters long) in the form of slump and slide blocks. Upward, within the paleovalley fill, up to 135 m of laminated mudstone with rare sandstone and conglomerate sheets indicate marine inundation of the valley. These strata grade upward into a sandstone succession, as much as 90 m thick, deposited from turbidity flows. These strata are overlain by a coarsening-upward succession of sandstone and conglomerate interpreted as a prograding coarse-grained delta.

A larger paleovalley is exposed 17 km to the SSE at Quebrada Grande (Fig. 5A; Kneller et al., 2004). This paleovalley was cut into limestone of the San Juan Formation and deformed siliciclastic turbidites of the Ordovician-Silurian Rinconada Formation. The paleovalley has a N-S orientation, but toward the south, it changes to a NW-SE trend. Valley width is <1 km in the north but widens to ~2 km in the SE. A large tributary valley, ~0.5 km wide, enters the main valley from the west. Smaller tributary valleys enter from the northeast. Within the main paleovalley, relief on the basal unconformity is >900 m, and the glacial and postglacial deposits constitute ~500 m of the valley fill.

Massive diamictite and crudely stratified diamictite up to 13 m thick occur at the base of the fill in depressions cut in the valley floor (Kneller et al., 2004). Clasts in the diamictites consist of local Lower Paleozoic sedimentary clasts and clasts composed of crystalline basement rocks, which may have been derived from known basement outcrops 10 km to the SE or in the Sierras Pampeanas, 30 km to the east. Kneller et al. (2004) interpreted these strata as lodgment tills and resedimented debrites. Overlying sandstones with 10-m-thick, NNW-dipping clinoforms suggest marine inundation followed by rapid progradation of Gilbert type deltas and associated delta-plain braided streams. Upward, an ~150-m-thick dropstone-bearing, mudstone succession with thin sandstones and

conglomeratic beds occurs. These strata were probably deposited from glacial meltwater plumes, iceberg rafting, and turbidity currents. The succession is capped by over 300 m of sandstone deposited by underflows (hyperpycnal flows) and other mass movement and sediment gravity flow deposits.

Kneller et al. (2004) reported that ice flow in the valley was toward the NW, with the valley swinging toward the north, which is supported by the directions of the prograding Gilbert-type deltas and the clasts derived from crystalline basement rocks. Kneller et al. (2004) and Dykstra et al. (2006) interpreted both paleofjord fills as the record of a deglaciation event resulting in a relative sea-level rise and later relative sea-level fall, which they concluded was the result of glacial rebound. Both paleovalley fills are remarkably thick. In order to explain such great thicknesses, the authors suggested that initial accommodation was created by overdeepening of the valley due to glacial erosion.

#### **4.2. Calingasta-Uspallata Basin—Hoyada Verde**

Strata of the Hoyada Verde Formation were deposited in the Calingasta-Uspallata Basin and are now exposed in an anticline in the Sierra de Barreal, located 2.5 km east of the town of Barreal (Figs. 5A, 5D, and 7). This unit forms the core of the anticline and consists of 175 m of glacigenic deposits and 85 m of postglacial mudrocks. The base of the formation is not exposed at this locality, and a fluvial incision surface at the base of the overlying Tres Saltos Formation truncates strata in the Hoyada Verde Formation to a depth of over 200 m (Buatois and Limarino, 2003).

Strata in the Hoyada Verde Formation are divided into four lithofacies (López-Gamundí, 1987):

- (1) massive sandy diamictites with and without a striated boulder pavement,
- (2) stratified muddy diamictites,
- (3) pebbly mudrocks with dropstones, and
- (4) laminated fossiliferous mudstones and fine sandstones.

Strata in the Hoyada Verde Formation are perhaps the most-studied glacial glacial strata in western Argentina (Frakes and Crowell, 1969; González, 1981; López-Gamundí, 1987, 1997; Azcuy et al., 1999). Nevertheless, interpretations of depositional environments remain ambiguous. The occurrence of stratified diamictites, dropstone-bearing mud rocks, and invertebrate fossils indicates the importance of subaqueous marine deposition. However, the occurrence of a striated boulder pavement provides evidence for ice contact or grounded ice advance, at least locally, within the area (López-Gamundí, 1987). González (1981) interpreted all diamictites in the Hoyada Verde Formation as sub-glacial in origin. López-Gamundí (1987, 1989) and López-Gamundí and Martínez (2000), however, suggested that massive diamictites were deposited by subglacial processes, while stratified diamictites represent deposition from sediment gravity flows and iceberg rafting. In our study, some massive diamictites display gradational contacts with underlying dropstone-bearing mudrocks, suggesting that these diamictites resulted from either high rates of iceberg rain-out or settling from suspension from meltwater plumes coupled with iceberg rain-out. The change from stratified diamictite to mudrocks containing *Levipustula*-zone fossils indicates a change from ice-proximal to open-marine conditions. This change may represent glacial retreat from the area, and/or a relative rise in sea level (González, 1981; López-Gamundí, 1989). Sandstone and conglomerate in the overlying Tres Saltos Formation have been

interpreted as braided-stream–incised valley fills, which cut deeply into the underlying Hoyada Verde Formation during a relative fall in sea level (Buatois and Limarino, 2003).

Paleocurrent orientations taken from the striated boulder pavement (clast *a*-axes and striations) in the Hoyada Verde Formation indicate that ice flowed toward the SSW (González, 1981; López-Gamundí and Martínez, 2000). These directions are parallel to orientations taken from cross-laminations contained within the fine-grained postglacial sandstones near the top of the formation (López-Gamundí and Martínez, 2000).

#### **4.3. Paganzo Basin—Huaco Area**

Glacigenic strata exposed on the northeastern side of the Precordillera along Los Pozuelos Creek, Loma de Los Piojos, and in the Agua Hedionda anticline (López-Gamundí et al., 1992; López-Gamundí and Martínez, 2000; Limarino et al., 2002, 2005; Pazos, 2002; Marensi et al., 2005) occur at the base of the Guandacol Formation (Fig. 7). These strata were deposited in the western portion of the Paganzo Basin along the eastern flank of the Protoprecordillera (Figs. 5A and 5E).

In this area, glacigenic strata rest on striated pavements cut into either Ordovician Limestone (San Juan Formation) or Ordovician siliciclastic rocks (Los Azules Formation). The pavements contain striations, nailhead striations, and streamline erosional features that resemble roches moutonnées. A striated pebble pavement also occurs within diamictite at Los Pozuelos Creek. The orientation of these structures indicates that ice flowed toward the NW (López-Gamundí and Martínez, 2000; Marensi et al., 2005).

#### **4.4. Los Pozuelos Creek**

At Los Pozuelos Creek, a complex succession of diamictites, rhythmites, and mud rocks overlies a sloping striated basement surface cut into limestones of the San Juan Formation (Marensi et al., 2005). Diamictite units consist of decimeter- to meter-thick lens-shaped bodies of coarse-grained matrix-supported massive and stratified diamictite. Clasts are locally derived and are almost exclusively (90%) limestone. Some of the diamictites display clast support, normal grading, inverse grading, and/or deformational structures including internal shear planes. Erosional surfaces and/or boulder pavements separate the diamictites into four, meter-thick packages that together form a diamictite complex. Laterally, individual packages grade into stratified clinoform facies, which consist of dropstone-bearing couplets of thinly bedded diamictite and parallel-laminated mudstone. Upward within the complex, the packages display a back-stepping or retro-gradational architecture where the uppermost package onlaps onto the sloping basement surface. The diamictite complex is overlain by meter-thick stratified facies that consist of dropstone-bearing couplets of thinly bedded diamictite and parallel-laminated mudstone. Clasts within the stratified facies consist of both locally derived limestone clasts and exotic granite and metamorphic clasts derived from the Sierras Pampeanas, located 50 km to the east. In turn, the stratified facies are overlain by a meter-thick succession of mudstone containing thin marl beds and rare fine-grained sandstones.

Marensi et al. (2005) interpreted the diamictites as subglacial (matrix-supported massive and sheared diamictites), subaqueous rain-out (stratified diamictites), and noncohesive sediment gravity flow deposits (graded and clast-supported diamictites) that formed as part of a retrogradational morainal bank. Such banks form along fluctuating grounding lines of retreating temperate to subpolar tidewater glaciers (Cai et al., 1997;



Powell and Alley, 1997). Stratified lithofacies at Los Pozuelos Creek resulted from resedimentation by subaqueous cohesive sediment gravity flows derived from the morainal bank, debris flows following retreat of the glacier out of the area, rain-out of debris from icebergs, and settling of fines from suspension. Overlying mudstone and marl have been interpreted to be the result of settling of fines from suspension and carbonate deposition due to periods of sediment starvation in open-marine conditions during the post glacial transgression following retreat of the ice front (cf. Limarino et al., 2002; Marensi et al., 2005). The glacial successions at Los Pozuelos Creek are overlain by thick sandstones interpreted as deltaic deposits of a prograding, postglacial, highstand systems tract (Limarino et al., 2002).

#### **4.5. Agua Hedionda Anticline**

A 50-m-thick glacial successions exposed along the Río Huaco and in the Agua Hedionda anticline overlies irregular topography cut into limestone of the San Juan Formation (Fig. 5E; López-Gamundí and Martínez, 2000; Pazos, 2002; Limarino et al., 2005). In places, the contact is a polished striated surface. Although the striated surface at the base of the section was clearly the result of subglacial erosion, the origin of the overlying massive diamictites is ambiguous. López-Gamundí and Martínez (2000) and Pazos (2002) interpreted the lower portion of the successions as lodgment tills. However, Limarino et al. (2002) pointed out that these deposits could also have been deposited as sediment gravity flows or by ice rafting/iceberg dump in a proximal glaciomarine setting. Stratified diamictites with dropstones were likely deposited by debris flows, while mud rocks represent settling from suspension. Clasts within both stratified diamictite and mud rock facies represent debris released from icebergs (Limarino et al., 2002, 2005).

Overlying black shales suggest deposition during the postglacial transgression, while the overlying coarsening-upward succession suggests deposition from prograding deltas (Limarino et al., 2002, 2005; Pazos, 2002).

## **5. Ice-flow directions and ice-spreading centers**

Ice-dispersal patterns in western Argentina are identified from the orientation of glacial valleys, striations on bedrock surfaces and boulder pavements, cross-lamination and sole marks from associated sandstone beds, orientation of channel bodies, clast compositions, and from cross-stratification within postglacial sandstones (López-Gamundí et al., 1994; Kneller et al., 2004; Dykstra et al., 2006; Marensi et al., 2005). Paleocurrent orientations within glacial and postglacial deposits suggest a complex radial drainage pattern away from the Protoprecordillera and flow away from the area of the Quaternary Pie de Palo and Famatina uplift of the Sierras Pampeanas located to the east (Fig. 5A). Clasts within diamictites and dropstone-bearing mud rocks in the Calingasta-Uspallata Basin consist primarily of sandstone derived from Middle to Lower Paleozoic strata now exposed along the western side of the Precordillera (López-Gamundí and Martínez, 2000). However, rare granite, volcanic, metamorphic and limestone clasts also occur as dropstones near the top of the glacial succession at Agua de Jagüel, suggesting that these exotic clasts were rafted in by far-traveled icebergs. Along the eastern margin of the Precordillera, conglomerates in the Quebrada de las Lajas paleovalley contain limestone, chert, volcanic, and metasedimentary clasts. The limestone and chert were derived from local limestones of the San Juan Formation exposed in the valley walls. Although volcanic and metamorphic clasts are not currently exposed in the adjacent Precordillera, the NW paleoflow directions in the paleovalley suggest a provenance in the

Protoprecordillera (Dykstra et al., 2006). Elsewhere along the eastern margin, limestone, sandstone, granite, gneiss, and metamorphic clasts also occur (López-Gamundí and Martínez, 2000; Kneller et al., 2004; Marensi et al., 2005; Dykstra et al., 2006).

Paleoflow directions suggest that the granite, gneiss, and other metamorphic clasts were derived from the east, where they are currently exposed in the major part of the Sierras Pampeanas, including the Pie de Palo uplift (cf. López-Gamundí and Martínez, 2000; Marensi et al., 2005; Kneller et al., 2004). Scarce Mississippian age granitic rocks occur in the northern portion of the Precordillera (Limarino et al., 2006), but flow directions from around the Huaco area indicate ice flow from the SE.

During the late Namurian, facies and paleo-ice-flow patterns suggest that at least two ice centers occurred in the Precordilleran region of west-central Argentina (Figs. 5A and 6). The Protoprecordillera was likely the location of alpine glaciation, as suggested by the abundance of paleovalleys, or paleofjords (López-Gamundí et al., 1992; López-Gamundí, 1997; López-Gamundí and Breitzkreuz, 1997). Flow directions suggest that another ice center was located to the east on the Pie de Palo Arch (cf. López-Gamundí and Martínez, 2000; Kneller et al., 2004; Marensi et al., 2005). It is unknown whether ice in this area was contained within valley glaciers or in an ice cap ( $<50,000 \text{ km}^2$ ). Sparse data indicating flow off the Famatina System suggest that an ice center may have also occurred to the north (Fig. 5A). López-Gamundí and Breitzkreuz (1997) suggested that only small glacial centers were scattered around southern South America at this time. These centers were likely located on uplifts and arches that broke this portion of Gondwana into a series of cratonic, retroarc, and arc-related basins (Fig. 6; cf. Limarino and Spalletti, 2006). While it has been suggested that an ice sheet was present in the

Paraná Basin based on striated pavements and a lack of paleorelief (Rocha-Campos et al., 2000), other workers maintain that there is little evidence that any large ice sheet occurred in Gondwana at that time (López-Gamundí, 1997; Isbell et al., 2003).

## **6. Postglacial transgression**

The transition from glacial to postglacial deposits occurs over a short stratigraphic interval in west-central Argentina (Fig. 9). The transition is recorded by a progressive vertical change from diamictites to dropstone-bearing mudrocks or rhythmites and then into marl-bearing mud rocks without dropstones. The change occurs locally over a few decimeters (e.g., Los Pozuelos Creek), or over several tens of meters (e.g., Agua de Jagüel; López-Gamundí and Martínez, 2000; Marensi et al., 2005).

In the Calingasta-Uspallata and Río Blanco Basins, the change from glacial to postglacial conditions occurs over a stratigraphic interval of up to a few tens of meters. Here, postglacial mudrocks up to 100 m thick occur. These mudrocks contain thin marl beds near their base, followed by a coarsening-upward succession of interstratified fine-grained sandstones and mud rocks (e.g., Hoyada Verde). A fluvial erosion surface with up to 200 m of relief truncates the glacial and postglacial succession in these basins (Limarino et al., 2002).

In the Paganzo Basin, the glacial to postglacial transition occurs over a few decimeters to a few meters. Along the western margin of the basin, the postglacial mudrocks are only a few meters thick. These strata consist of massive and stratified black mudrocks containing thin marl beds. The mudrocks coarsen upward and are overlain by a thick (tens of meters) succession of thick-bedded (decimeter to meter) sandstone beds

interpreted as prograding deltas deposited during a forced regression (cf. Limarino et al., 2002; Pazos, 2002; Dykstra et al., 2006).

## **7. Sequence stratigraphy**

The glacial and postglacial successions in western Argentina (Fig. 9) are attributed to a combination of forcing mechanisms, including glacial advance-retreat cycles, glacio-eustasy, and glacio-isostasy. In sequence stratigraphic terms, Pazos (2002) ascribed the basal unconformity to the onset of glaciation and to a concomitant glacio-eustatic fall in sea level. In his scenario, he assigned the glacial deposits to the early portion of a transgressive system tract. Although this might be true for the Paganzo Basin, López-Gamundí and Martínez (2000) noted that glacial pavements within the Hoyada Verde Formation suggest that multiple glacial advances and retreats occurred in the Calingasta-Uspallata Basin, and that glaciers were likely grounded well below sea level to the west of the Protoprecordillera. The change from diamictites to dropstone-bearing mudrocks signals retreat of the ice front during deglaciation and likely reflects an early stage of transgression (transgressive systems tract; Limarino et al., 2002). Many authors have interpreted the change from dropstone-bearing mudrocks to dropstone-free mudrocks as the result of rapid marine flooding during the late stage of transgression (e.g., López-Gamundí, 1997; Limarino et al., 2002; Pazos, 2002; Kneller et al., 2004; Dykstra et al., 2006; Marensi et al., 2005). Therefore, they consider marl deposition synonymous with sediment starvation (condensed zone) during maximum marine inundation (Fig. 9). Finally, deltaic progradation is interpreted to have occurred during a highstand systems tract, and deltaic progradation and fluvial incision are interpreted to have occurred during a forced regression during glacial rebound (Fig. 9; falling-stage

systems tract; Limarino et al., 2002; Pazos, 2002; Kneller et al., 2004; Dykstra et al., 2006).

The sequence stratigraphic model for western Argentina during the Namurian glacial cycle assumes that the glacial successions were closely linked to continental-scale glaciation, and that the drivers of glacial sequence stratigraphy were similar to drivers of stratigraphic sequences on low-latitude continental shelves. Powell and Cooper (2002) cautioned against linking apparent changes in water depth in glacial marine successions to eustasy or, in many cases, even to relative sea-level changes. As an example, fining- and/or coarsening-upward stratal successions on low-latitude shelves are typically linked to changes in relative sea level. However, in a glacial marine setting, facies changes and changes in grain size can be due to either changes in water depth or changes in proximity to an ice front without a change in water depth. It is important to point out that the waxing and waning of alpine glaciers and/or ice caps associated with the Protoprecordillera would have had little effect on world sea level. Therefore, a wide range of factors (i.e., eustasy; tectonics; glacial style; and local, regional, and global climate change) needs to be considered when interpreting controls on accommodation and sedimentation across glaciated basin margins (cf. Powell, 1984; Boulton, 1990; Powell and Cooper, 2002).

Although the currently accepted stratigraphic model for the Protoprecordillera provides a reasonable interpretation of the Pennsylvanian geology in western Argentina, there are several inconsistencies between model predictions and the observed record. The model is valid for continental glaciation where glacial advance and retreat cycles drive or are synchronous with eustatic changes. However, the Protoprecordillera and the adjacent

Pie de Palo Arch were likely the site of either alpine glaciers or small ice caps. Mass balance fluctuations of a single ice cap ( $<50,000 \text{ km}^2$ ) would have produced eustatic change of no more than 0.62 m (Isbell et al., 2003). Additional ice caps to the east would also have had negligible impact on world sea level. Therefore, an ice sheet of immense size located elsewhere in Gondwana waxing and waning in concert with ice in west-central Argentina is required to make such a scenario work.

The magnitude of subsidence and uplift due to glacial loading and unloading is dependent on ice volume. Ice sheets ( $>50,000 \text{ km}^2$ ) produce the greatest lithospheric response where flexural subsidence is greatest beneath the center of the ice sheet and decreasing subsidence outward. Likewise, the greatest amount of postglacial rebound occurs beneath the ice sheet and decreases to zero some distance beyond the former ice margins. Smaller ice volumes produce smaller flexural response, and ice caps and alpine glaciers produce minor amounts of subsidence and/or uplift (cf. Benn and Evans, 1998). Glacio-isostasy may have played a role in the creation and destruction of accommodation space in the basins surrounding the Protoprecordillera, as suggested by the occurrence of a postglacial forced regression in the Paganzo Basin and the development of a fluvial incision surface in the Calingasta-Uspallata and Río Blanco Basins. However, observations suggest that loss of accommodation space was greatest to the west ( $\sim 200 \text{ m}$  of fluvial incision). This scenario is untenable because it requires a large ice sheet, and it also suggests that the center of the ice sheet would have been located over the Calingasta-Uspallata Basin rather than to the east. Available evidence indicates that glacio-isostasy associated with alpine glaciers in the Protoprecordillera could not have produced the observed incision. The importance of ice in the western Sierras Pampeanas is presently

poorly constrained. Future study in that region may help to resolve issues concerning glacio-isostasy in this part of Gondwana.

The role that tectonism may have played during and following the Namurian glaciation in western Argentina is unknown. Because all of the basins were actively subsiding during this interval, it is reasonable to assume that tectonic forcing exerted an influence on the stratigraphy. Further studies in western Argentina, including subsidence analysis, are required to resolve the roles that tectonic, glacial, eustatic, and climatic drivers played in contributing to the stratigraphy in this region.

## **8. Conclusions**

Glacigenic strata in the Protoprecordillera were deposited in a glacialmarine environment during the late Namurian within sedimentary basins (Fig. 6). However, glacial terrestrial conditions may have occurred in the Paganzo Basin during early stages of glacigenic deposition. The glaciation was characterized by alpine glaciation and the possible occurrence of an ice cap ( $<50,000 \text{ km}^2$ ) to the east in the area of the Pie de Palo Arch (Fig. 9). Current data do not support the occurrence of an ice sheet ( $>50,000 \text{ km}^2$ ) in this part of Gondwana during the early Pennsylvanian. Strata characterized by massive and stratified diamictites, dropstone-bearing mudrocks, and strata containing slump and slide blocks indicate that deposition occurred in ice-proximal to ice-distal settings, from settling from suspension out of melt water plumes, rain-out from icebergs, sediment gravity flows (debris and turbidity flows), and mass wasting. Sheared diamictite and striated surfaces suggest that subglacial deposition also occurred. A transition from glacial deposits to mudrocks indicates glacial retreat and development of sediment-starved marine conditions (Fig. 9). This change may have been due to marine inundation,



deepening of marine waters, or simply due to retreat of ice fronts out of the various basins. Base-level fall within all three basins is signaled by rapid delta progradation (during forced regression) or by fluvial incision (Fig. 9). However, the causes for this base-level fall are unknown.

Although strata in the Precordilleran area of Argentina are of great interest in understanding the LPIA, because they mark the initial stage of the main phase of Gondwana glaciation, and because of their location along the western margin of the supercontinent, a number of important questions need further investigation. These include: (1) What is the age of the probable Visean glacial strata, and under what conditions were they deposited? (2) Did glacial conditions persist from the Visean into the Namurian? (3) When did glaciation begin and end during the Namurian glacial stage? (4) Under what environmental conditions were the Namurian strata deposited? (5) Did glacial loading and unloading play a critical role in the development of the glacial and postglacial stratigraphy? (6) What were the thermal conditions and size of the depositing glaciers? (7) Was an ice sheet present anywhere in South America during this time interval? (8) What role did glacio-eustasy, glacio-isostasy, and/or tectonism play during deposition of these strata? Answers to these and other questions are critical in understanding the history of Gondwana glaciation and the influence that the LPIA had on Earth's physical, chemical, and biological systems.

### **Acknowledgments**

We thank Patricia Ciccioli and Ana Tedesco for assistance and discussions in the field. Discussions with Luis Buatois, Zelenda Koch, John Menzies, and Ellen Cowan are also appreciated. The authors are grateful to Luis Buatois, Edison Jose Milani, and Chris

Fielding for their comments on an earlier version of the manuscript. Lindsey Henry and John Isbell acknowledge support from the Center of Latin American and Caribbean Studies, the graduate school (Research Grant Initiative), the Department of Geosciences at the University of Wisconsin–Milwaukee, and from the National Science Foundation (grant ANT-0440919). Carlos O. Limarino acknowledges funding from the Agencia Nacional de Promoción Científica y Tecnológica of Argentina (PICT 04821) and from the Departamento de Ciencias Geológicas at the Universidad de Buenos Aires. We also thank the Departamento de Ciencias Geológicas for logistic support. This paper is a contribution to International Geoscience Programme Project 471.

# Figures

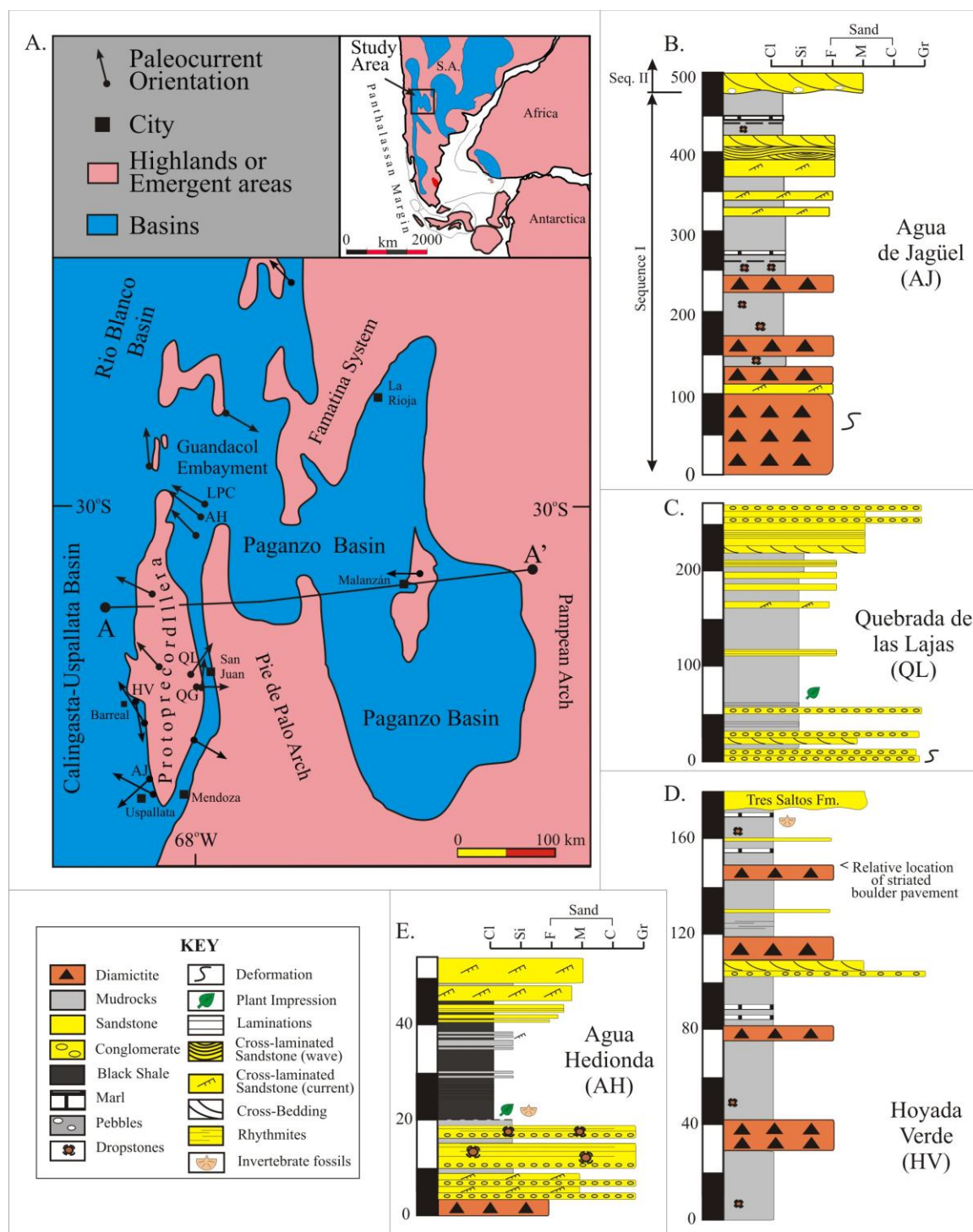


Figure 5. (A) Map showing the location of key stratigraphic sections in the Calingasta-Uspallata, Río Blanco, and Paganzo Basins (modified from Limarino et al., 2006).

Sections mentioned in the text are Agua de Jagüel (AJ), Quebrada Grande (QG), Quebrada de las Lajas (QL), Hoyada Verde (HV), Los Pozuelos Creek (LPC), and the

Agua Hedionda Anticline (AH). Arrows show paleo-ice-flow directions. Paleocurrent data are from Scalabrini Ortiz (1972), Andreis et al. (1975), López-Gamundí and Amos (1985), Buatois and Mángano (1994), López-Gamundí and Martínez (2000), Kneller et al. (2004), Marensi et al. (2005), Dykstra et al. (2006), and this paper. Line A–A' is the line of cross section shown in Figure 2. Inset map shows the location of the study area and the location of other basins that contain Lower Pennsylvanian glacigenic strata (modified from Isbell et al., 2003; Limarino and Spalletti, 2006). (B) The glacigenic succession in sequence 1 of the Agua de Jagüel Formation; (C) Quebrada de las Lajas, Jejenes Formation, redrafted from Dykstra et al. (2006); (D) Hoyada Verde Formation; (E) Agua Hedionda Anticline, Guandacol Formation, redrafted from Pazos (2002). All section thicknesses are in meters.

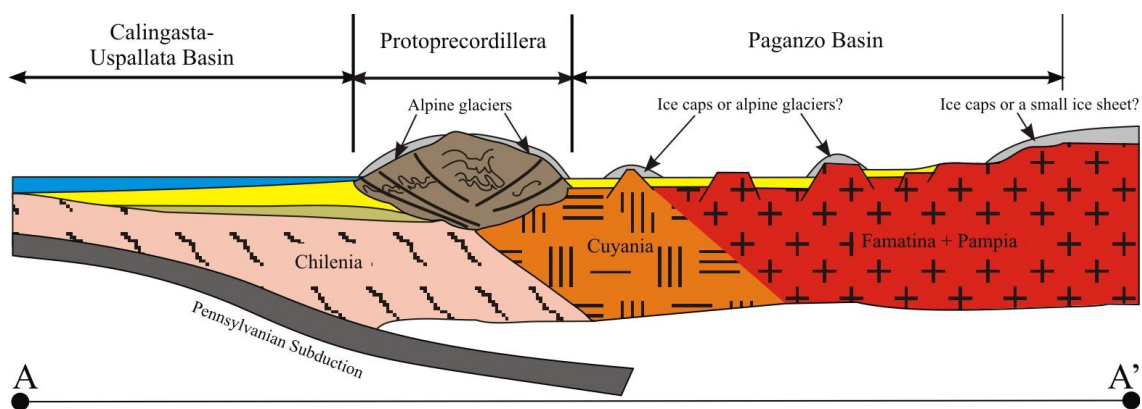


Figure 6. Cross section along transect A–A' (Fig. 1A) showing the tectonic configuration of the Calingasta-Uspallata Basin, the Protoprecordillera, and the Paganzo Basin, and the location and type of glaciers present (modified from Limarino et al., 2006).

Age (Ma)	System	Stage		Location and lithostratigraphy			
				Agua de Jagüel	Hoyada Verde	Quebrada de las Lajas	Huaco and Los Pozuelos Creek
300	Permian	Asselian		Agua de Jagüel	Esquina Gris		Patquía
	Pennsylvanian	Steph.	Gzhelian		El Retamo		Tupe
			Kasimovian		Tres Saltos		
		West.	Muscovian		Hoyada Verde	Jejenes	Guandacol
			Bashkirian				
325	Mississippian	Namurian	Serpukhovian				

Figure 7. Correlation chart for uppermost Mississippian, Pennsylvanian, and Lower Permian strata for sites in the Calingasta-Uspallata, Río Blanco, and Paganzo Basins

mentioned in the text (units and ages are based on Taboada, 1985; López-Gamundí et al., 1994; Azcuy et al., 1999; López-Gamundí and Martínez, 2003; Limarino et al., 2005).

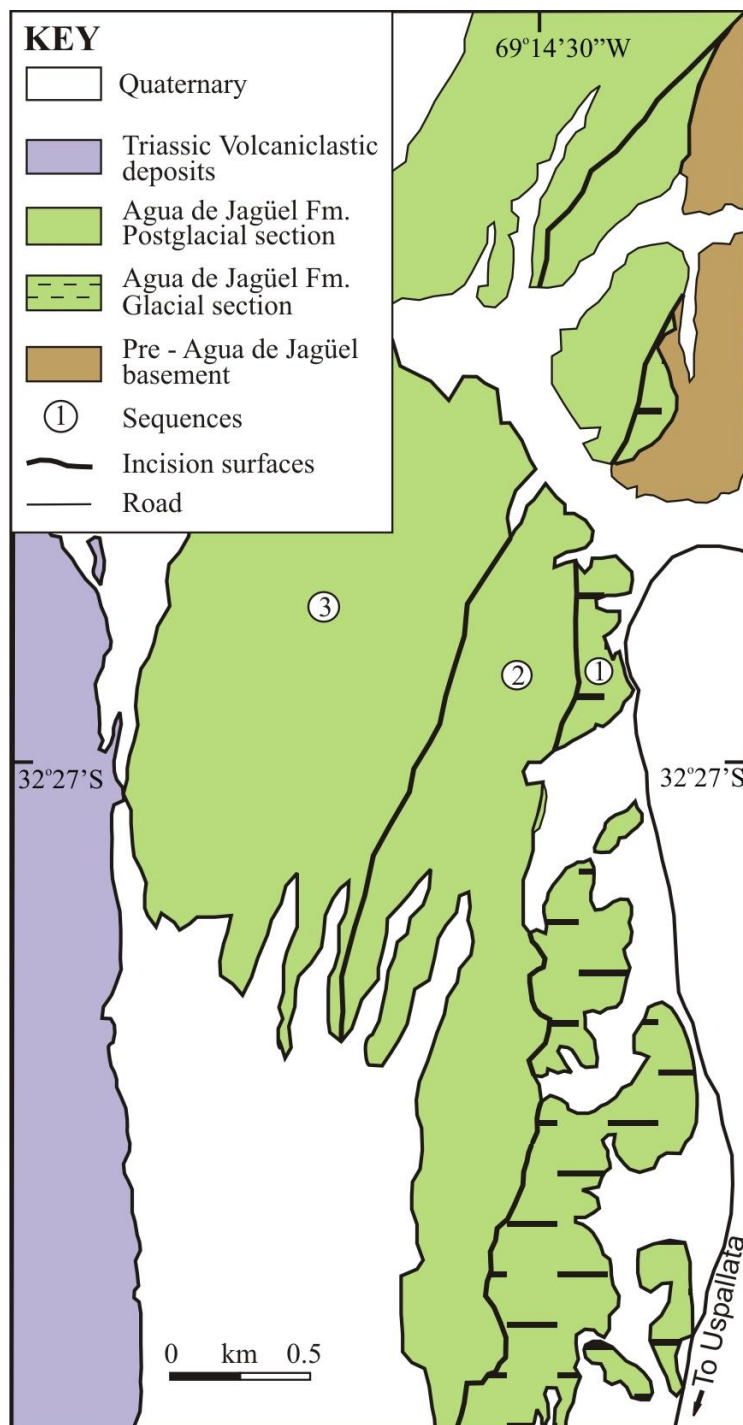


Figure 8. Geologic map of the Agua de Jagüel area showing depositional sequences in the Pennsylvanian to Permian Agua de Jagüel Formation. Strata in the Agua de Jagüel Formation dip at up to 90°.

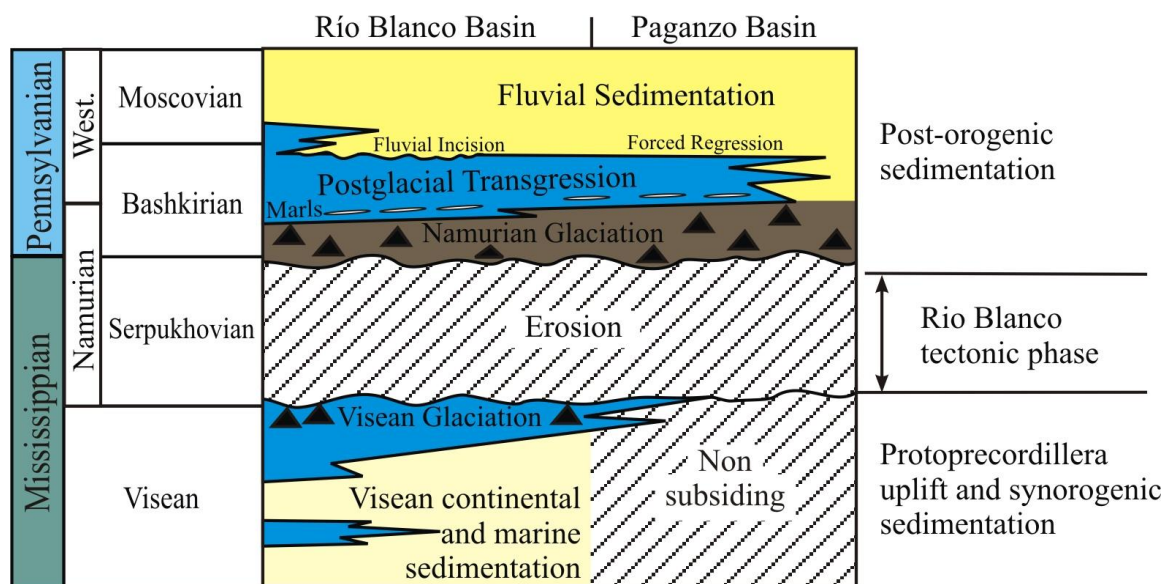


Figure 9. Time-space diagram summarizing the Carboniferous depositional history of the Protoprecordillera. The line of section traverses the Río Blanco Basin, Guandacol Embayment, and the Paganzo Basin (see Fig. 1A) (modified from Limarino et al., 2006).

## References

- Amos, A.J., Rolleri, E., 1965. El Carbónico marino en el valle Calingasta-Uspallata, San Juan-Mendoza. Boletín de Informaciones Petroleras 368, 50–71.
- Andreis, R.R., Spalletti, L.A., Mazzoni, M.M., 1975. Estudio geológico del Subgrupo Sierra de Maz, provincia de La Rioja, República Argentina. Revista de la Asociación Geología Argentina 30, 247–273.
- Archangelsky, S., Azcuy, C.L., Gonzalez, C.R., Sabattini, N., Acenolaza, F.G., 1987. Paleontología, bioestratigrafía y paleoecología de las cuencas Paganzo, Calingasta-Uspallata y Río Blanco (Paleontology, biostratigraphy and paleoecology of the Paganzo, Calingasta-Uspallata and Río Blanco Basins). In: Archangelsky, S. (Ed.), El Sistema Carbonífero en la República Argentina. Córdoba, Academia Nacional De Ciencias, p. 133–151.
- Azcuy, C.L., Carrizo, H.A., Caminos, R., 1999. Carbonífero y Pérmico de las Sierras Pampeanas, Famatina, Precordillera, Cordillera Frontal y Bloque de San Rafael. Instituto de Geología y Recursos Minerales Geología Argentina 29, 261–318.
- Benn, D.I., Evans, D.J.A., 1998. Glaciers and Glaciation. London, Arnold, 734 p.
- Bercowski, F., 1983. Estudio Sedimentológico y Paleoambiental del Carbonífero de la Quebrada de Las Lajas, Sierra Chica de Zonda, Provincia de San Juan [Ph.D. thesis]. Buenos Aires, Universidad de Buenos Aires, 157 p.

- Boulton, G.S., 1990. Sedimentary and sea level changes during glacial cycles and their control on glacial marine facies architecture. In: Dowdeswell, J.A., Scourse, J.D. (Eds.), *Glacial Marine Environments: Processes and Sediment*. Geological Society of London Special Publication 53, 15–52.
- Buatois, L.A., Limarino, C.O., 2003. El contacto entre las Formaciones Hoyada Verde y Tres Saltos, Carbonífero de la cuenca Calingasta-Uspallata: Su reinterpretación como una superficie de incisión fluvial. In: III Simposio Argentino del Paleozoico Superior y II Reunión del Proyecto International Geoscience Programme 471. La Plata, Argentina, Resúmenes, 5.
- Buatois, L.A., Mángano, M.G., 1994. Lithofacies and depositional processes from a Carboniferous lake of Gondwana, Sierra de Narváez, northwest Argentina. *Sedimentary Geology* 93, 25–49.
- Cai, J., Powell, R.D., Cowan, E.A., Carlson, P.R., 1997. Lithofacies and seismic-reflection interpretation of temperate glacial marine sedimentation in Tarr Inlet, Glacier Bay, Alaska. *Marine Geology* 143, 5–37.
- Césari, S.N., Gutiérrez, P.R., 2000. Palynostratigraphy of Upper Paleozoic sequences in central-western Argentina. *Palynology* 24, 113–146.
- Cisterna, G.A., 1999. Paleoeología de niveles políticos de la sección superior de la Formación Hoyada Verde, Carbonífero Superior, Precordillera de San Juan, Argentina. *Ameghiniana* 36, 259–267.
- De Rosa, L., 1983. Sedimentitas continentales del Carbónico inferior en el flanco occidental de la Precordillera, departamento Calingasta, provincial de San Juan. *Revista de la Asociación Argentina de Mineralogía, Petrografía y Sedimentología* 14, 51–69.
- Dykstra, M., Kneller, B., Milana, J.P., 2006. Deglacial and postglacial sedimentary architecture in a deeply incised paleovalley-paleofjord: The Pennsylvanian (Late Carboniferous) Jejenes Formation, San Juan, Argentina. *Geological Society of America Bulletin* 118, 913–937.
- Fauqué, L.E., Limarino, C.O., 1990. El Carbonífero de Agua de Carlos (Precordillera de La Rioja), su importancia tectónica y paleoambiental: The Carboniferous of the Agua de Carlos region (La Riojan Pre cordillera); its tectonic and paleoenvironmental importance. *Revista de la Asociación Geológica Argentina* 46, 103–114.
- Frakes, L.A., Crowell, J.C., 1969. Late Paleozoic glaciation: I. South America. *Geological Society of America Bulletin* 80, 1007–1042.
- González, C.R., 1981. Pavimento glaciario en el Carbónico de la Precordillera (Glacial



- pavement in the Carboniferous of the Precordillera). *Revista de la Asociación Geológica Argentina* 36, 262–266.
- Gutiérrez, P.R., Césari, S.N., Martínez, M., 1995. Presencia de *Nothorhacopteris Argentina* (Geinitz) Archangelsky en la Formación Guandacol (Carbonífero), Argentina. *Ameghiniana* 32, 169–172.
- Isbell, J.L., Miller, M.F., Wolfe, K.L., Lenaker, P.A., 2003. Timing of late Paleozoic glaciation in Gondwana: Was glaciation responsible for the development of Northern Hemisphere cyclothems? In: Chan, M.A., Archer, A.W. (Eds.), *Extreme Depositional Environments: Mega End Members in Geologic Time*. Geological Society of America Special Paper 370, 5–24.
- Kneller, B., Milana, J.P., Buckee, C., Al Ja'aidi, O.S., 2004. A depositional record of deglaciation in a paleofjord (Late Carboniferous [Pennsylvanian] of San Juan Province, Argentina): The role of catastrophic sedimentation. *Geological Society of America Bulletin* 116, 348–367.
- Limarino, C.O., Gutiérrez, P., 1990. Diamictites in the Agua Colorada Formation (northwestern Argentina); new evidence of Carboniferous glaciation in South America. *Journal of South American Earth Sciences* 3, 9–20.
- Limarino, C.O., Spalletti, L.A., 2006. Paleogeography of the Upper Paleozoic basins of southern South America: An overview. *Journal of South American Earth Sciences* 22, 134–155.
- Limarino, C.O., Page, R., Caselli, A., 1993. Origen y significado estratigráfico de las diamictitas del Miembro Superior de la Formación Cortaderas, Precordillera de San Juan. XII Congreso Geológico Argentino Actas I, 157–164.
- Limarino, C.O., Césari, S.N., Net, L.I., Marensi, S.A., Gutiérrez, P.R., Tripaldi, A., 2002. The Upper Carboniferous postglacial transgression in the Paganzo and Río Blanco Basins (northwestern Argentina): Facies and stratigraphic significance. *Journal of South American Earth Sciences* 15, 445–460.
- Limarino, C.O., Buatois, L.A., Gutiérrez, P.R., 2005. Upper Paleozoic basins and fossil record, northwest Argentina. In: *Gondwana 12: Geological and Biological Heritage of Gondwana*. Mendoza, Argentina, Academia Nacional De Ciencias, Field Trip Guidebook A4, 59 p.
- Limarino, C., Tripaldi, A., Marensi, S., Fauqué, L., 2006. Tectonic, sea level, and climatic controls on late Paleozoic sedimentation in the western basins of Argentina. *Journal of South American Earth Sciences* 33, 205–226.
- López-Gamundí, O.R., 1987. Depositional models for the glaciomarine sequences of Andean late Paleozoic basins of Argentina. *Sedimentary Geology* 52, 109–



126.

- López-Gamundí, O.R., 1989. Postglacial transgressions in late Paleozoic basins of western Argentina; a record of glacioeustatic sea level rise. *Palaeogeography, Palaeoclimatology, Palaeoecology* 71, p. 257–270.
- López-Gamundí, O.R., 1997. Glacial-postglacial transition in the late Paleozoic basins of southern South America. In: Martini, I.P. (Ed.), *Late Glacial and Postglacial Environmental Changes: Quaternary, Carboniferous-Permian, and Proterozoic*. Oxford, UK, Oxford University Press, 147–168.
- López-Gamundí, O.R., Amos, A.J., 1985. Consideraciones paleoambientales de las secuencias carbónicas del sector Precordillerano de la cuenca Calingasta-Uspallata, San Juan y Mendoza. *Primeras Jornadas sobre Geología de la Precordillera, Serie “A” Monografías y Reuniones, Asociación Geológica Argentina, Actas*, 289–294.
- López-Gamundí, O.R., Breitzkreuz, C., 1997. Carboniferous to Triassic evolution of the Panthalassan margin in southern South America. In: Dickins, J.M. (Ed.), *Late Palaeozoic and Early Mesozoic Circum-Pacific Events and Their Global Correlation*. Cambridge, Cambridge University Press, 8–19.
- López-Gamundí, O.R., Martínez, M., 2000. Evidence of glacial abrasion in the Calingasta-Uspallata and western Paganzo Basins, mid-Carboniferous of western Argentina. *Palaeogeography, Palaeoclimatology, Palaeoecology* 159, 145–165.
- López-Gamundí, O.R., Martínez, M., 2003. Esquema estratigráfico cosecuencial para las unidades Neopaleozoicas de la cuenca Calingasta-Uspallata en el flanco occidental de la Precordillera (Sequence stratigraphy of Upper Paleozoic units in the Calingasta-Uspallata Basin, western flank of Precordillera). *Revista de la Asociación Geológica Argentina* 58, 367–382.
- López-Gamundí, O.R., Limarino, C.O., Césari, S.N., 1992. Late Paleozoic palaeoclimatology of central west Argentina. *Palaeogeography, Palaeoclimatology, Palaeoecology* 91, 305–329.
- López-Gamundí, O.R., Espejo, I.S., Conaghan, P.J., Powell, C.M., Veevers, J.J., 1994, Southern South America. In: Veevers, J., Powell, C. (Eds.), *Permian-Triassic Pangea Basins and Foldbelts along the Panthalassan Margin of Gondwanaland*. Geological Society of America Memoir 184, 281–329.
- Marenssi, S.A., Tripaldi, A., Limarino, C.O., Caselli, A.T., 2005. Facies and architecture of a Carboniferous grounding-line system from the Guadacol Formation, Paganzo Basin, northwestern Argentina. *Gondwana Research* 8, 187–202.
- Pazos, P.J., 2002. The Late Carboniferous glacial to postglacial transition: Facies and

- sequence stratigraphy, western Paganzo Basin, Argentina. *Gondwana Research* 5, 467–487.
- Powell, R.D., 1984. Glacimarine processes and inductive lithofacies modeling of ice shelf and tidewater glacier sediments based on Quaternary examples. *Marine Geology* 57, 1–52.
- Powell, R.D., Alley, R.B., 1997. Grounding-line systems: Processes, glaciological inferences and the stratigraphic record. In: Barker, P.F., Cooper, A.C. (Eds.), *Geology and Seismic Stratigraphy of the Antarctic Margin 2*. Washington, D.C., Antarctic Research Series, American Geophysical Union 71, 169–187.
- Powell, R.D., Cooper, J.M., 2002. A glacial sequence stratigraphic model for temperate, glaciated continental shelves. In: Dowdeswell, J.A., Cofaigh, C.Ó. (Eds.), *Glacier-Influenced Sedimentation on High-Latitude Continental Margins*. Geological Society of London Special Publication 203, 215–244.
- Ramos, V.A., Jordan, T.E., Allmendinger, R.W., Kay, S.M., Cortes, J.M., Palma, M.A., 1984. Chilenia; un terreno alóctono en la evolución Paleozoica de los Andes centrales (Chilenia; an allochthonous terrane in the Paleozoic evolution of the Central Andes). *Actas del Congreso Geológico Argentino* 2, 84–106.
- Ramos, V.A., Jordan, T.E., Allmendinger, R.W., Mpodozis, M.C., Kay, S.M., Cortes, J.M., Palma, M., 1986. Paleozoic terranes of the central Argentine–Chilean Andes. *Tectonics* 5, 855–880.
- Rocha-Campos, A.C., dos Santos, P.R., Canuto, J.R., 2000. Late Paleozoic glacial history of the Rio Grande do Sul Arch, southern Brazil. *Geological Society of America Abstracts with Programs* 32, 57.
- Salfity, J.A., Gorustovich, S.A., 1983. Paleogeografía de la cuenca del Grupo Paganzo (Paleozoico Superior). *Revista de la Asociación Geológica Argentina* 38, 437–453.
- Scalabrini Ortiz, J., 1972. El Carbónico en el sector septentrional de la Precordillera Sanjuanina. *Revista Asociación Geológica Argentina* 27, 351–377.
- Taboada, A.C., 1985. Estratigrafía y contenido paleontológico de la Formación Agua del Jagüel, Pérmico Inferior de la Precordillera Mendocina. *Primeras Jornadas Sobre Geología de Precordillera, San Juan Acta I*, 181–186.

## Chapter 3: Mid-Carboniferous deglaciation of the Protoprecordillera, Argentina recorded in the Agua de Jagüel paleovalley

Lindsey C. Henry<sup>\*a</sup>, John L. Isbell<sup>a</sup>, Carlos O. Limarino<sup>b</sup>, Lindsay J. McHenry<sup>a</sup>, Margaret

L. Fraiser<sup>a</sup>

<sup>a</sup>Department of Geosciences, University of Wisconsin-Milwaukee, 3209 N. Maryland Avenue, Milwaukee, WI 53211-0413, USA

<sup>b</sup>Departamento de Ciencias Geológicas, Universidad de Buenos Aires, Pabellón 2, Ciudad Universitaria C1428EHA, Buenos Aires, Argentina

### Abstract

The Agua de Jagüel Formation near Uspallata, Mendoza Province, Argentina, was deposited within a paleovalley along the southeastern margin of the Calingasta-Uspallata Basin adjacent to the Protoprecordillera. The basal glacial sequence of the formation was deposited in the Serpukhovian – Early Bashkirian, near the beginning of the late Paleozoic ice age. The sequence is composed of diamictite, conglomerate, sandstone, and mudrock and records four depositional stages within a paleofjord: 1. morainal bank deposition by a wet-based tidewater glacier, 2. glacial retreat succession where ice retreated up the fjord out of the immediate area, allowing iceberg deposition of dropstones and dump deposits, 3. continued glacial retreat with ice receding onto land, allowing a shoreface to develop within the paleovalley, and 4. transgression across the shoreface and resumption of iceberg deposition. The thickness and facies of this succession are similar to deposits within modern Alaskan fjords housing temperate tidewater glaciers. Comparison of the Agua de Jagüel Formation with Alaskan fjords

---

<sup>\*</sup> Corresponding author.

Email addresses: [christi9@uwm.edu](mailto:christi9@uwm.edu) (L.C. Henry), [jisbell@uwm.edu](mailto:jisbell@uwm.edu) (J.L. Isbell), [oscarlimarino@ciudad.com.ar](mailto:oscarlimarino@ciudad.com.ar) (C.O. Limarino), [lmchenry@uwm.edu](mailto:lmchenry@uwm.edu) (L.J. McHenry), [mfraiser@uwm.edu](mailto:mfraiser@uwm.edu) (M.L. Fraiser).

indicates that sequence stratigraphy used for low latitude deposits must be applied with caution, as glacimarine ice retreat within a fjord produces strata surfaces that are easily misidentified as flooding surfaces resulting from changes in water depth. Likewise, the transgression during stage 4 is significant as it indicates a rise in sea level that occurred during glaciation of the Protoprecordillera, thus suggesting that the transgression between stage 3 and 4 was not driven by input of glacial meltwater. Additionally, the sediment geochemistry indicates that the bottom waters of the paleovalley were anoxic, which may help explain the absence of bioturbation in the sequence as well as in other ancient glacimarine paleovalleys. The deglaciation succession and transgression are also recorded in the nearby Hoyada Verde and Tramojo Formations, so it is proposed that all three formations record one glacial event in the Protoprecordillera. Overlying fluvial and shallow marine strata in the Agua de Jagüel, Hoyada Verde, and Tramojo Formations show no indication of continued glaciation in the Protoprecordillera following stage 4 and equivalent strata. The deglaciation succession of the Agua de Jagüel Formation affirms the emerging concept that the late Paleozoic ice age was characterized by alpine glaciers, ice caps, and small ice sheets that were not massive enough to have driven eustatic fluctuations of 100 m+ as previously understood, and that ice never covered westernmost Gondwana during later LPIA events.

Keywords: Agua de Jagüel Formation, Protoprecordillera, late Paleozoic ice age, Argentina

## **1. Introduction**

The late Palaeozoic ice age (LPIA) is one of the most significant icehouse intervals in Earth's history because the ice age, which lasted for 73 million years, exerted

significant effects on Earth's physical and biological systems during the mid-Carboniferous to mid-Permian. These effects include: 1) cyclic eustatic change that formed the palaeoequatorial Euramerican cyclothems, 2) a second-order mass extinction, 3) retarded rates of origination and extinction, and 4) dominance of terrestrial plants adapted to subhumid to everwet conditions (Frakes et al., 1992; Gastaldo et al., 1996; Stanley and Powell, 2003; Montañez and Soreghan, 2006; Montañez et al., 2007; Isbell et al., 2008b). Further, the LPIA provides the last complete record of the transition from icehouse to greenhouse conditions on a vegetated Earth (Gastaldo et al., 1996), and therefore serves as a proxy for Earth's inevitable transition out of its present glaciated state.

During the LPIA, glaciation occurred in both the southern hemisphere over Gondwana and in the northern hemisphere on the Siberian crustal block (Frakes and Crowell, 1969; Chumakov, 1994). The LPIA commenced over Gondwana in present-day western Argentina in the Visean (middle Mississippian), with its maximum extent in this region occurring during the Namurian (Serpukhovian to early Bashkirian: Late Mississippian to Early Pennsylvanian; Limarino et al., 2006; Henry et al., 2008; Gulbranson et al., 2010). In the latest Carboniferous through Early Permian, glaciation shifted southeastward and reached its acme as individual ice centers occurred across eastern South America, South Africa, Antarctica, Australia, India, southern Asia, and the Arabian Peninsula as Gondwana migrated across the South Pole (Laskar and Mitra, 1976; Caputo and Crowell, 1985; Garzanti and Sciunnach, 1997; López Gamundí, 1997; Visser, 1997; Wopfner and Casshyap, 1997; Collinson et al., 1994; Isbell et al., 2003a; Fielding et al., 2008; Martin et al., 2008). The main phase of the LPIA ended near the Sakmarian-

Artinskian boundary (Early Permian), when Earth began transitioning into a greenhouse state; however, small ice sheets, ice caps, and localized alpine glaciers continued in eastern Australia until the Capitanian (Bembrick, 1983; Bamberry et al., 1995; Fielding et al., 2008).

The traditional understanding of the LPIA is that a single, supercontinent-sized ice sheet covered Gondwana for over 90 Ma (Ziegler et al., 1997; Hyde et al., 1999). Many reconstructions display ice extending over much of Gondwana throughout the LPIA, and even recent models show that ice covered western Argentina throughout the Carboniferous and Permian (e.g., Scotese, 1997; Scotese et al., 1999; Horton and Poulsen, 2009). Climatic fluctuations affecting the mass balance of the ice sheet were considered to have resulted in Milankovitch-scale eustatic changes of as much as 100-120 m and contributed to the development of Pennsylvanian coal-bearing cyclothems in the present northern hemisphere (Wanless and Shepard, 1936; Heckel, 1994; Rygel et al., 2008). However, recent modeling by Horton and Poulsen (2009) questions whether large ice sheets would have been capable of producing such changes in sea level due to Milankovitch forcing. Expanded fieldwork on Gondwanan glacigenic deposits has recently led to the interpretation of multiple, smaller glaciers during the LPIA, with small ice sheets, ice caps, and alpine glaciers waxing and waning across Gondwana (Dickins, 1997; López Gamundí, 1997; Isbell et al., 2003a; Fielding et al., 2008; Henry et al., 2008). Improved chronostratigraphic control of LPIA glacigenic deposits is revealing that the LPIA consisted of numerous shorter glacial intervals of 1-8 My duration separated by non-glacial conditions of equal duration (Fielding et al., 2008; Stollhofen et al., 2008; Gulbranson et al., 2010).

The Agua de Jagüel Formation was deposited during the LPIA in present-day west-central Argentina (Fig. 10), which was located on the southwestern margin of Gondwana, at an estimated palaeolatitude of 40° - 50° S (Scotese and Barrett, 1990; Torsvik and Cocks, 2004; Blakey, 2008). However, reconstructions by Lawver et al. (2007) place the basin between 50 to 60° S palaeolatitude during the Namurian (Serpukovian to Early Bashkirian). The glacial sequence of the formation described in this paper was deposited in the Namurian, when glaciation was at its maximum over western Argentina but had not yet expanded across central and western Gondwana (Glacial II of Isbell et al., 2003b). The goals of this paper are to characterize the lithofacies of the glacial sequence in the Agua de Jagüel Formation, interpret the depositional setting based on sedimentary features, mineralogy (x-ray diffraction), and bulk geochemistry (x-ray fluorescence analysis), and thereby elucidate glacial dynamics and climate changes during this time. A detailed sedimentologic analysis of the glacial retreat succession of the Agua de Jagüel Formation enables the development of glacial sequence stratigraphy of the region and a better understanding of how glacial facies signal glacial dynamics in ancient environments. This will allow for refinement of high latitude proxy records for glacial advance/retreat cycles and glacioeustatics during the late Palaeozoic. Furthermore, sedimentologic and stratigraphic analysis of this formation will test the emerging concept that Gondwana was glaciated by small ice sheets, ice caps, and alpine glaciers that waxed and waned over 1–8 My timeframes, and that this area was not glaciated during the Late Pennsylvanian and Early Permian, thus refining the history of the LPIA in this region of Gondwana.

## **2. Geologic Setting and Stratigraphy**

The Agua de Jagüel Formation was deposited along the present eastern margin of the Calingasta-Uspallata Basin, adjacent to a late Palaeozoic mountain range, the Protoprecordillera (Fig. 11). The Protoprecordillera was a fold-thrust belt that is now overprinted by the Precordillera, an active Cenozoic fold-thrust belt located just east of the Andes. The Protoprecordillera formed as the Chilenia terrain accreted to the western margin of Gondwana from the Middle Devonian to Early Mississippian (Fig. 11). As a result, the Calingasta-Uspallata Basin developed as a peripheral foreland basin on the western side of the Protoprecordillera (Ramos et al., 1984, 1986; Limarino et al., 2006). During the Mississippian, the Calingasta-Uspallata Basin transitioned into a back-arc basin as subduction shifted westward, encasing the basin between a volcanic arc on the west and the Protoprecordillera fold-thrust belt on the east (Azcuy et al., 1999; Limarino and Spalletti, 2006; Limarino et al., 2006). Termination of Protoprecordillera uplift was marked by Río Blanco tectonism that resulted in an unconformity that cuts across older strata in the Calingasta-Uspallata and neighboring Paganzo and Río Blanco Basins (Fig. 10, Limarino et al., 2006). Along the eastern margin of the Calingasta-Uspallata Basin, the Río Blanco unconformity separates highly deformed Upper Devonian and Mississippian strata below from latest Mississippian and younger strata above.

The Protoprecordillera formed a topographic high from which alpine glaciers nucleated during the Namurian (Limarino et al., 2006; Henry et al., 2008). Glacigenic strata were deposited in both palaeovalley and open marine settings and are identified in the three basins that surround the Protoprecordillera: the Calingasta-Uspallata, Río Blanco, and the Paganzo Basins (Fig. 10; López Gamundí, 1997; Henry et al., 2008). These basins record glacigenic sedimentation followed by mudrock deposition that



formed during a post-glacial transgression at the end of the Namurian (Limarino et al., 2002), although data from the Agua de Jagüel Formation (discussed below) indicates that glaciers were still present at the beginning of the transgression. The transgressive deposits are incised by a regional unconformity that extends throughout the three basins. Above the unconformity, regressive sandstones and mudstones were deposited in the Paganzo Basin, and incised valleys filled with fluvial and shallow marine shelfal deposits occur in the Calingasta-Uspallata and Río Blanco Basins.

Three depositional sequences have been identified in the Agua de Jagüel Formation: a lower sequence containing glacigenic deposits and two overlying sequences containing fluvial and shallow marine deposits (Ciccioli et al., 2008; Henry et al., 2008). The lower sequence is greater than 530 m thick, contains diamictite, conglomerate, sandstone, and mudrock (Henry et al., 2008), and is analyzed in detail herein. Namurian spores have been identified from the lower glacigenic sequence (Césari, personal communication). In the two overlying fluvial and shallow marine sequences, brachiopods (*Costatumulus amosi*), gastropods, bivalves, cephalopods, and corals have been identified in mudrock, constraining these strata as Pennsylvanian to Lower Permian (Amos and Roller, 1965; Taboada, 1985, 2006). However, a dacitic lava at the base of sequence 3 returned a date of  $307.2 \pm 5.2$  Ma (Lech, 2002; Koukharsky et al., 2009) indicating a Middle Pennsylvanian (Moscowian) age for the middle portion of the formation.

The lower two sequences of the Agua de Jagüel Formation were deposited in a palaeovalley/palaeofjord cut into Mississippian and older siliciclastic bedrock of the Protoprecordillera (Henry et al., 2008). An angular unconformity separates the basement

rocks, which are highly deformed due to Río Blanco tectonism, from overlying Agua de Jagüel strata. Although the base of the formation is not exposed, the older, deformed basement rocks form the walls of the palaeovalley. Based on the geometry of the Agua de Jagüel outcrop, the palaeovalley is estimated to be greater than 700 m deep and up to 5 km wide (Fig. 12).

### **3. Study Area and Methodology**

The Agua de Jagüel Formation is located 17 km northeast of the town of Uspallata, Mendoza, at S 32° 27', W 69° 14' (Figs. 10, 12). Stratigraphic sections of the formation were logged through three different exposures in the formation (Figs. 12, 13). Palaeoflow measurements were collected using a Brunton compass and were corrected for structural dip. Pebble counts noting lithology, rounding, and sphericity were recorded from pebbles  $\geq 4$  mm in diameter, and apparent dip angle perpendicular to bedding planes was measured for pebbles  $\geq 2$  cm in diameter. Strata of the Agua de Jagüel Formation have been lightly metamorphosed as a result of Cenozoic deformation and therefore are pervasively cleaved and dip at  $\sim 90^\circ$  with a north-south strike. The outcrop belt is essentially oriented perpendicular to depositional strike.

Mineralogical and geochemical analyses of mudrock and marl from the glaciogenic sequence of the Agua de Jagüel Formation were conducted using x-ray diffraction (XRD) and x-ray fluorescence (XRF). Seven samples of mudrock and marl were analyzed by XRD and XRF, and samples were numbered based on the logged section and elevation in the section. For example, sample 1-258 was from Log 1, at 258 m in the logged section (Fig. 13). Samples were first powdered in a tungsten carbide shatterbox. XRD analyses of random powder mounts were obtained using a Bruker D8 Focus XRD (Cu Ka

radiation, 0.8 s per 0.02° 2 $\theta$ , 2°–50° range, Sol-X energy dispersive detector). Initial mineral identification was done by comparison to the International Centre for Diffraction Data PDF database, and relative abundances were determined by quantitative Rietveld analysis using Bruker's TOPAS software. For XRF analysis, samples were dried for 8 hours at 105 ° C, and then 1.000 g of sample was mixed with 1 g ammonium nitrate (oxidizer) and 10.000 g LiT:LiM flux with an integrated LiBr non-wetting agent. From the mixture, a glass bead was made using a 21 minute routine on a Claisse M4 fluxer (maximum temperature ~1050 ° C). The XRF measurements were made using a Bruker S4 Pioneer WD-XRF spectrometer, and results were computed using a calibration curve based on 11 USGS rock standards. More detailed methods, including error determination, are presented in McHenry (2009).

#### **4. Facies Analysis**

Sequence 1 of the Agua de Jagüel Formation can be divided into four groups of facies: diamictite (massive, weakly stratified, and bedded diamictite), conglomerate and sandstone, pebbly mudrock, and mudrock and sandstone. Lithological classifications for poorly sorted sediment were made according to Moncrieff's (1989) system based on sediment sorting. Descriptions and interpretations of the four facies are organized in Table 1.

##### **4.1. Diamictite Facies**

The diamictite facies forms a thick interval at the base of the section (Fig. 13).

##### **4.1.1. Diamictite Facies Description**

Diamictites occur as massive to weakly stratified to bedded (cm to m scale). The diamictites range from clast-poor (<5% clasts) to clast-rich (>5% clasts, cf. Moncrieff,

1989), and clast richness fluctuates horizontally (m scale) and changes vertically both abruptly and gradationally (cm to m scale). The diamictites are matrix-supported, with a matrix composed of mud and fine sand (Fig. 14). Basal contacts are sharp to gradational with adjacent units. Clasts within diamictite are most commonly sandstone and quartz, but shale and granite clasts rarely occur (< 1% of clasts in the sequence). Approximately 20% of clasts are striated. In clast counts (n=100), 64% of clasts are quartz, 36% of clasts are sandstone, average diameter is 1.8 cm (ranging from 4 mm to 8 cm), average sphericity is 0.75, and average roundness is 0.69 using visual estimates based on Wadell's (1932) scale. Additionally, thin beds of massive and horizontally laminated sandstones with sole-marked bases are interbedded within the diamictite facies (Fig. 14E).

Massive diamictites, 1 – 6 m thick, exhibit no stratification or bedding. However, occasional dewatering structures (dish and pipe structures) are present and were observable due to an increase in sorting within the structures. These units occur as clast-rich (Fig. 14A) and clast-poor diamictites. They are in sharp to gradational contact with adjacent units of weakly stratified diamictite, bedded diamictite, sandstone, and conglomerate. Typically these strata are deformed.

Weakly stratified diamictites contain cm-scale wisps of sand, faint laminations, and/or cm- to m-scale bedding (Fig. 14B). The diamictites may be 0.5 to several meters thick and may consist of clast-poor to clast-rich diamictite. These units often grade both vertically and laterally into clast-poor to clast-rich massive diamictite, which together may contain intercalations of structureless pebbly sandstone and lonestone-bearing laminated mudrock. Clasts in both the weakly stratified diamictite and mudrock units are

preferentially oriented with long axes at high angles to bedding, and some clasts penetrate laminations.

Bedded diamictite consists of distinct beds of thinly (3-10 cm thick) to thickly (10-cm – 1m thick) bedded, clast-poor and clast-rich diamictite (Fig. 14C, D). Basal and upper contacts are sharp with underlying and overlying units, and the long axes of clasts show no preferential orientation. These diamictites are interstratified with massive and weakly stratified diamictite, sandstone, and conglomerate. Individual beds can be traced for several tens of meters.

The diamictite interval is profusely deformed, with cm- to m-scale slumps (Fig. 14F), slides, and folds. Some slumps are stacked, suggesting that they slid on top of each other. Many slumps end in fold noses, and it is common for a 1 – 25 cm thick bed of fine to coarse-grained sand to encase the fold. In Log 1, analysis of the folds reveals that the slumps appear to have slid to the north or northeast. Load structures, such as undulating basal contacts, are also common within sandstones contained in the facies. Finally, dewatering structures, such as pipes and dish structures, also occur in sandy portions of diamictite.

#### **4.1.2. Diamictite Facies Interpretation**

Diamictites were deposited in ice proximal settings by a combination of the following processes: melt-out from the glacier front, rain-out from meltwater plumes, iceberg rafting, and sediment gravity flows (slides, slumps and debris flows). Massive diamictites can be deposited by several methods (including a combination of the following): 1) rain-out of clay- to boulder-sized sediment from icebergs, 2) rain-out of clay, silt, and sand from meltwater plumes emanating from the glacier terminus with

clasts introduced by ice rafting, 3) subaqueous debris flows, 4) melt-out of material from the base of the glacier near the grounding line, and 5) iceberg turbation (Anderson et al., 1983, 1991; Eyles et al., 1985; Moncrieff and Hambrey, 1990; Hambrey et al., 1991; Dowdeswell et. al, 1994; Visser, 1994; Woodworth-Lynas and Dowdeswell, 1994; Smith and Andrews, 2000; Evans and Pudsey, 2002). Weakly stratified diamictites are likely produced by a combination of settling from meltwater plumes with clasts introduced as iceberg rafted debris (Visser, 1994). Bedded diamictites are deposited by cohesive debris flows (López Gamundí, 1991). Debris flows commonly emanate from the grounding line, an unstable environment where activity such as calving, pushing, and squeezing takes place in front of the glacier (Powell and Domack, 2002). However, activity such as waves from storms, release of biogenic gas, shock due to calving icebergs striking the substrate, and movement from earthquakes can also instigate debris flows in a glacialmarine environment. Deformation such as slumping and folding occurred in the diamictites as material slid downslope, and folding occurred due to frictional differences along the basal surface of the bed as it moved across the substrate (López Gamundí, 1991). Deformation caused by slumping such as folding and buckling often resembles tectonic deformation when the original sedimentary features are often preserved (Woodcock, 1976).

Due to the thickness (Figs. 13, 14D), interfingering with multiple facies and subfacies of diamictite, and deformation (Fig. 14F) in the diamictite interval, it is interpreted that initial deposition was probably along a morainal bank at the terminus of a wet-based tidewater glacier that occupied the palaeovalley. A morainal bank is an elongate mound of diamictite, conglomerate, sandstone, and mud that forms from rapid

sedimentation in front of a grounded tidewater glacier (Powell, 1981; 1983; Powell and Molnia, 1989; Powell, 1990; bank-core subenvironment of Cai et al., 1997). Many different depositional processes work together to form a morainal bank, such as melt-out from the glacier, rain-out from ice bergs, meltwater stream deposition, and pushing and squeezing from glacial advance. Subsequent resedimentation as gravity flows occurred due to the slope of a morainal bank and as the glacier front advanced and retreated, creating instability of bank deposits (cf. Powell and Domack, 2002). Many of these processes are evident in the lower diamictite interval in the Agua de Jagüel Formation. In studies of modern glacimarine settings, morainal banks have been recorded as thick as 175 m (Cai et al., 1997). Because the basal diamictite unit is up to 150 m thick and contains only rare amounts of mudrock, deposition solely from rain-out is unlikely.

The high roundness and sphericity average values indicate that clasts have endured extensive weathering, which is common in glacial environments and likely are the result of multiple cycles of transport within glacial and glacially influenced systems. Sandstone clasts were eroded from the Lower Palaeozoic sedimentary rocks that formed the Protoprecordillera and quartz and granite clasts were derived from mid- to Late Carboniferous granitic intrusions in the Protoprecordillera (Azcuy et al., 1999).

Slumped diamictite formed from remobilized cohesive debris flow deposits, and orientations of some of the slumps may have resulted from the geometry of the palaeovalley. Debris flows are common around morainal banks, which are unstable environments due to the high sedimentation rate and glacial activity such as calving of icebergs and pushing and squeezing by the glacier front (Powell and Domack, 2002). The rim of sand blanketing the slumps may have been deposited by turbidity currents or

hyperconcentrated flows that resulted from mixing of the top of the debris flow with the surrounding fluid (cf. Mulder and Alexander, 2001; Winsemann et al., 2007). The north/northeast flow direction of the debris flows from the southern side of the formation may have been caused by the southwest palaeovalley wall (Fig. 12). As material was shed off the morainal bank at the southern end of the palaeovalley, sediments flowed away from the wall and down the axis of the palaeovalley.

## **4.2. Conglomerate and Sandstone Facies**

The conglomerate and sandstone facies is interbedded with the diamictite facies and thus occurs throughout the lower portion of the sequence.

### **4.2.1. Conglomerate and Sandstone Facies Description**

The conglomerate and sandstone facies consists of sandy conglomerate and fine- to coarse-grained sandstone (Fig. 15). Conglomerates are clast-supported with a sandy matrix (Fig. 15A). Clast sizes range from 4 mm to 29 cm in diameter. Clast counts reveal that the average clast size is 2.4 cm in diameter ( $n = 50$ ). Conglomerate bedding ranges from massive (rare), to 10 cm thick beds (Fig. 15B), to up to 50 cm thick beds. Basal contacts are sharp or erosive. Upper contacts of conglomerate are typically sharp but occasionally gradational when conglomerate passes up into diamictite. Conglomerates form sheets that are laterally extensive but, when traced several tens to hundreds of meters laterally, eventually pinch out into the surrounding diamictite. Internally, conglomerates are massive, normally graded, or inversely graded. Thinner beds (~10 cm thick) are typically normally graded, whereas some thick beds (~50 cm) are inversely graded. Occasionally, conglomerates are trough cross-bedded.



Sandstone is fine- to coarse-grained, and bed thickness ranges from 5 cm to 50 cm. Current structures usually are not visible within sandstones (structureless), however, faint to well developed laminations often appear (Fig. 15C), and cross-laminations also rarely appear (Fig. 15D). Laminated sandstones contain some clasts that penetrate laminations. Dewatering structures (flame structures, dish structures, pipes) were also identified. Sandstone bed contacts are sharp except where conglomerate grades into sandstone, and where thin sandstone layers occur as discontinuous “blobs” loaded into underlying diamictite.

A 48 m-wide, 15 m-thick channel composed of alternating conglomerate and sandstone beds occurs in the southern side of the outcrop belt for the Agua de Jagüel Formation (Log 1, Fig. 13). The channel has erosional basal and lateral contacts with surrounding clast-poor diamictite. Conglomerate in the channel exhibits trough cross beds, and the sandstone has sharp basal contacts with underlying conglomerate and contains primary current lineations. The channel is normally graded along its edges, but conglomerates appear massive in the center of the channel.

#### **4.2.2. Conglomerate and Sandstone Facies Interpretation**

The conglomerate and sandstone facies was deposited by a combination of processes occurring in a grounding line fan: 1) effluent flow emanating from the base of the glacier, 2) settling from suspension where subglacial jets began to float, 3) hyperconcentrated density flows, and 4) possibly from density driven underflows. Grounding-line fans are composed of outwash sediments ranging from clay- to gravel-size, and fans build up by input from outwash and sediment gravity flows (Powell, 1990). Outwash enters the sea as effluent jets exit the glacier from either an englacial or

subglacial position. These jets of water flow through ‘pipes’, or melted pathways, in the glacier. Sediment buildup or freezing water can block the pipe, and therefore flow is often episodic. Furthermore, glacial discharge can fluctuate according to seasonal temperature patterns and even fluctuate according to the lunar tidal cycle (e.g., Cowan and Powell, 1990; Cowan et al., 1999). Deposits resulting from episodic flow will therefore have a range of grain sizes, which records fluctuations in discharge during deposition. After water exits the glacier, flow is turbulent, driven by momentum flux. The jet will flow along the substrate for up to  $13.4D$ , where  $D$  is the diameter of the subglacial pipe from which the jet exited (Powell, 1990). Additionally, the higher the jet discharge, the longer the jet will stay in contact with the substrate. Farther away from the discharge point, sand and gravel deposits take the form of sheets and/or cut-and-fill geometries, the latter forming if the point of efflux migrates laterally. As velocity in the unconfined jet diminishes, the jet will detach from the substrate and transition into a buoyant plume when buoyancy flux becomes dominant over momentum flux. Once the jet has transformed into a plume in the zone of detachment, fine sand, silt, and clay rain down from the plume. In Alaska, growth rates for grounding line fans associated with temperate tidewater glaciers are estimated up to  $10^6 \text{ m}^3/\text{yr}$  (Powell and Molnia, 1989).

Where basal contacts of conglomerate and sandstone beds are erosive, deposition occurred due to sedimentation from an effluent jet. Sandstones that have sharp basal contacts and are normally graded were deposited by unconfined flow just upstream from the detachment point, or by rain-out from a meltwater plume just downstream of where the plume becomes buoyant. However, massive sandstone with sharp basal contacts was likely deposited by hyperconcentrated density flows (cf. Mulder and Alexander, 2001).

Inversely graded conglomerates were deposited by grain flows, because finer grains are sieved to the bottom and back of a grain flow as it travels over the substrate (Middleton, 1970; Parsons et al., 2001).

### **4.3. Pebbly Mudrock Facies**

The pebbly mudrock facies occurs between diamictite intervals in Log 2, above the diamictite interval and passing up into mudrock and sandstone in Log 1 and 2, and above an interval of mudrock and sandstone in Log 3 at the top of the glacial sequence in the Agua de Jagüel Formation (Fig. 13).

#### **4.3.1. Pebbly Mudrock Facies Description**

The pebbly mudrock facies consists of claystone and siltstone containing outsized clasts, rare fine- and medium-grained sandstone, and rare marl (Fig. 16). Siltstone and claystone are dark grey to olive in color, and bedding ranges from massive to 5 mm thick beds. In places, siltstone and claystone are rhythmically bedded (Fig. 16A). Occasionally, siltstone and claystone exhibit slumps, slides, and fold structures. Clasts are 4 mm to 30 cm in diameter, but most commonly in the pebble range (4 to 64 mm). Clast frequency varies, but pebble content is always less than 3% of rock volume. Clast lithologies are predominantly sandstone and quartz, but limestone and granite clasts occur rarely. From clast counts in pebbly mudrock, clasts are 82% sandstone, 18% quartz, and have an average diameter of 6.9 cm (n=50). Approximately 25% of clasts are striated (i.e., Fig. 16B), and are rarely (less than 1%) faceted and polished. Overall, clasts do not exhibit a preferred orientation, but many clasts have long axes that are oriented at high angles to bedding and downwarp or penetrate stratification. Wisps or clumps of fine and medium-grained sand, less than 10 cm across, occur rarely. In Log 1, marl occurs within

an interval of mudrock with occasional pebbles. The marl is composed of micritic limestone without observable fossils. Body fossils and bioturbation were not observed in this facies.

Fourteen pods composed of diamictite, conglomerate, and sandstone occur within the thick mudrock interval overlying the basal diamictite unit (Fig. 16C). The pods are lens-shaped and range from 50 cm to 2 m in diameter. The pods occur throughout 15 m of section, and several pods are stacked en echelon against each other. Between these stacked pods is mudrock containing outsized clasts. The pods are typically normally graded, ranging from conglomerate at the base to fine sandstone at the top; however, most beds are moderately normally graded diamictites, and some pods are simply composed of massive sandstone. No current structures were observed in the pods. The pods do not have erosional basal contacts, yet the surrounding mudrock bedding appears deformed by the base and sides of the pods. From clast counts in the pods, the average dip angle is  $40^\circ$  ( $n = 25$ ,  $\sigma = 25^\circ$ ), and 72% of counted clasts have long-axis dip angle greater than  $20^\circ$  (angles are rotated back to horizontal to account for  $90^\circ$  dip of the succession). A clast fabric analysis ( $n=25$ ) was done for clasts on the top of a bed, where the azimuth of the a-axes of clasts were measured (cf. Visser, 1994). Upon rotating the measurements, the average dip angle was  $\sim 45^\circ$ . The stratigraphic interval containing the coarse-grained pods grades laterally, over a distance of 400 m to the north, into an interval of clast-rich finely stratified to massive diamictite intercalated with structureless pebbly sandstone and laminated mudrock containing lonestones.

#### **4.3.2. Pebbly Mudrock Facies Interpretation**

The pebbly mudrock facies was deposited by a combination of suspension settling and rain-out from floating ice. Siltstone and claystone were deposited from suspension settling of fine particles, and rhythmic bedding of clay and siltstone suggests either turbidity current or tidal action. A single siltstone/claystone couplet may represent distal deposition from underflow currents or tidally-influenced settling from suspension out of meltwater plumes (Cowan et al., 1999). Slumps, slides, and folds formed from soft sediment deformation as mud with high water content resulting from high sedimentation rates moved downslope (Boulton, 1990). The combination of mudrock and pebbles formed from multiple glacial-marine processes, e.g., “two component mixing” (Powell and Domack, 2002), because in addition to clay- and silt-sized particles settling from suspension, clasts were deposited from rain-out from floating ice, likely icebergs that calved from a tidewater glacial terminus. Similarly, wisps and clumps of sand were deposited from melt-out from floating ice and represent sediment that underwent sorting due to differences in settling velocities through the water column. Clasts that bend and penetrate stratification are classified as dropstones (cf. Thomas and Connell, 1985). Clast lithologies of sandstone, quartz, and granite indicate provenance from the Protoprecordillera (Azcuy et al., 1999). Rare limestone clasts may have originated from the Ordovician San Juan Formation located to the east and north of this portion of the Protoprecordillera and could have been transported into the mouth of the palaeovalley from icebergs that originated from that region of the Protoprecordillera. The striations and polished and faceted surfaces of the larger clasts indicate a glacial influence (Gilbert, 1990). The presence of marl stratigraphically adjacent to outsized clasts is counterintuitive, as the presence of marls has been interpreted as indicators of sediment

starved conditions within these successions (e.g., López Gamundí, 1997; Pazos, 2002). However, it is quite feasible that marl marks an interval of ice rain-out quiescence when carbonate deposition occurred through pelagic material settling through the water column before dropstone deposition resumed (see discussion below).

The pods were deposited by rain-out from ice, because normal grading, absence of current structures, and high clast dip angles suggest deposition through the water column (cf. Domack and Lawson, 1985). The presence of outsized clasts in the mudrock between pods also indicates that rain-out was occurring at the time of pod deposition. The deformed contacts between the pods and surrounding mudrock suggest that the muddy substrate failed under the weight of the pod sediments. Furthermore, pods resemble iceberg dump structures (e.g., Thomas and Connell, 1985) because of their elongated geometries and coarse texture in contrast to the surrounding mudrock. Dump structures form from icebergs that become unstable as they melt and thus roll over in the water column, dropping loose sediment from their upper surface down onto the substrate (Ovenshine, 1970; Anderson et al., 1980). Following deposition as dumps, the pods likely experienced slight resedimentation as they slid, slumped or floundered into the soft substrate. The relatively flat upper surfaces of the pods in contrast to a conical mound shape (*sensu* Thomas and Connell 1985) signals some sort of resedimentation. The resedimentation was likely syndepositional with iceberg dumping; as the sediment reached the sea floor, it likely slid or slumped down the palaeoslope and sunk into the soft substrate. Lateral to the pods, clast-rich, weakly stratified and massive diamictite with clasts penetrating stratification represent deposition by iceberg rafting and settling

from suspension. The lateral facies changes along the outcrop indicate how localized different depositional processes may have been within the fjord.

#### **4.4. Mudrock and Sandstone Facies**

The mudrock and sandstone facies occurs above the thick diamictite interval in Logs 1 and 2 and composes the majority of Log 3 (Fig. 13).

##### **4.4.1. Mudrock and Sandstone Facies Description**

The mudrock and sandstone facies consists of claystone and siltstone, with occasional occurrences of marl and interbedded very fine- to medium-grained sandstone (Fig. 17). Claystone and siltstone are dark gray to olive in color, and bedding ranges from massive to 5 mm thick beds. Rare slumping is observable in the siltstone. Marl occurs as both beds and oblate concretions, composed of micritic limestone without observable fossils (Fig. 17A). Bioturbation is absent from the facies.

Sand is fine- to medium-grained and occurs in both lens and sheet geometries. At the base of the section, beds of fine sandstone progressively extend farther south (Fig. 17B). Sandstone beds are frequently deformed, often slumped, folded, loaded, or boudinaged (Fig. 17C, D, E). Boudinaged structures typically occur at the base of sandstone bodies. Some sandstone bodies at the base of the coarsening upward succession pinch out abruptly (Fig. 17B) or occur as isolated blocks within mudstone. Cross laminations, cross bedding, plane bedding and hummocky cross beds occur frequently, although some beds are massive. Hummocky cross-stratification occurs in very fine sandstone near the base of the thick coarsening upward sandstone unit at ~425 m, Log 3. Upwards, trough cross bedding becomes dominant. Additionally, very fine

sand often appears to be rhythmically bedded with siltstone. Rip-up clasts of mudrock were observed in one bed of fine sandstone.

#### **4.4.2. Mudrock and Sandstone Facies Interpretation**

The mudrock and sandstone facies exhibits no glacial indicators, which suggests that the facies was deposited in the absence of glaciers and icebergs in the palaeovalley, or were isolated from the direct influence of glaciers or floating ice. The presence of marl has been used previously to suggest clastic starved conditions (López Gamundí, 1997; Pazos, 2002), and mineralogical and bulk geochemical analysis (below) suggests that terrestrial sedimentation was still occurring, but at reduced levels, when marl was deposited. Where mudrock is dominant, fine sand beds signal underflow deposition, perhaps from meltwater emanating from the base of a terrestrial glacier or from streams entering from the sidewalls of the palaeovalley. Fold structures in the very fine sand were generated by failure of the substrate and sliding of the body down the palaeoslope. Sand boudins formed at the base of sandstone bodies due to the ductility contrast between the sand and surrounding mud as the material was stretched and sheared along glide and slide planes (Woodcock, 1976). Abrupt lateral termination of sand bodies and sand bodies encased anomalously in mudstone also suggest instability of the substrate and downslope sliding and floundering of deposits within the fjord.

In contrast, where sandstone forms thick units and exhibits hummocky and trough cross stratification (Log 3), sandstone was deposited above storm wave base to normal wave base. Boulton (1990) reports that storm waves in protected fjords rarely occur more than 20 m below sea-level, so it can be assumed that the sandstone was probably deposited (initially) in water depths of  $\leq 20$  m. Deformed, massive sandstone was



resedimented by hyperconcentrated density flows. The coarsening-upward shale to sandstone succession and the upward change from hummocky cross stratification to trough cross bedding near the top of the sequence suggests that a shoreface prograded down or across the fjord. Additionally, the geometry created by fine sandstone beds progressively extending further south at the base of the succession indicates progradation of these deposits (Fig. 17B).

## 5. X-ray Diffraction and Fluorescence Analysis

A mineralogical and geochemical study of mudrocks and marls of the Agua de Jagüel Formation was conducted using x-ray analysis to help constrain sediment sources and oxygenation of the water column in the palaeovalley. Marl is commonly used as a signal for clastic sediment starvation in these deposits (i.e., López Gamundí, 1997; Pazos, 2002), and x-ray diffraction (XRD) analysis can test this assumption by indicating if the minerals present are of likely terrestrial or marine origin. If only minerals that can form in marine environments are present (e.g., smectite), then it can be inferred that the mudrocks formed in situ as a result of truly ‘sediment-starved’ conditions (cf. Griffin et al., 1968; Hathaway, 1979). However, if minerals of likely terrestrial origin are present (e.g., albite), then sediment was likely supplied by streams, possibly meltwater emanating from the base of a glacier or from streams entering the fjord from the valley walls.

An XRF study of mudrocks and marls can enable characterization of the redox conditions of the water column by using ratios of elements such as V/Cr. Determining the oxygenation of the bottom waters of the Agua de Jagüel palaeovalley may explain why bioturbation is absent in the glacial sequence of the formation. However, *Bergaueria* and *Conostichus* are identified in the upper sequence (Lech and Buatois,

1990), so the palaeovalley must have become more hospitable to benthic organisms following deposition of the lower glacial sequence. Similarly, bioturbation is conspicuously absent in the glacial portions of the nearby and coeval Hoyada Verde and Tramojo Formations (cf. López Gamundí and Martínez, 2000; Henry, 2007), but resume in overlying strata (Lech and Buatois, 1990).

Geochemical studies of glacial and post-glacial sediments can provide a fresh approach to work on the LPIA, as very few mineralogical and bulk geochemical analyses of sedimentary rocks associated with the LPIA have been published to date (e.g., Scheffler et al., 2003, 2006), despite the information such work could yield on sedimentation trends, palaeoredox conditions, and ultimately palaeoclimate. Samples were selected from 1) mudrock interbedded with diamictite, conglomerate, and sandstone at the base of the formation (1-20a, 1-20b), 2) pebbly mudrock between the basal diamictite interval and the diamictite pods (1-224), 3) marl above the diamictite pods (1-251, 1-258), 4) the base of the uppermost pebbly mudrock interval (3-471), and 5) marl at the top of the uppermost pebbly mudrock interval (3-511, see Figure 13 and Tables 2 and 3).

### **5.1. XRD results**

Albite, muscovite, calcite, and quartz were present in the samples, and relative concentrations of the minerals are listed in Table 2. It is suspected that the muscovite readings represent illite instead, as the two minerals have very similar structures and are thus difficult to differentiate using their XRD patterns. The four marl samples all contained calcite, with relative concentrations ranging from 18.3% – 45.9%. Additionally, minor chlorite was qualitatively identified in the XRD patterns of 1-258, 1-

224, 3-511, and 1-251-07 but was not discernable by Rietveld analysis using the chlorite structure available in Bruker's TOPAS structure database. In summary, quartz and calcite (when present) are the dominant minerals in the mudrocks, but there are also significant amounts of albite and illite in the mudrock and marl, and chlorite is also present in four of the samples in unknown (but minor) amounts.

## **5.2 XRF results**

XRF data are presented in Table 3, including loss on ignition (LOI) values. LOI values are elevated (21-24.5%) for samples with high CaO values (25.5-30.7%), indicating increased CO<sub>2</sub> loss for samples containing carbonate. V/Cr ratios are used to determine anoxia in the presence of H<sub>2</sub>S (Ernst, 1970; Jones and Manning, 1994; Tenesch et al., 2007). V concentrations for five of the seven samples analyzed are at least twice the lower limit of detection for this element, as are Cr concentrations from samples 1-258 and 3-511. The V and Cr values of the other samples reported are lower than twice the lower limit of detection and thus not reported, though the statistical error for each is under 10%. V/Cr ratios range for available samples are both above 2 (Table 3).

## **5.3 Discussion of x-ray results**

The XRD and XRF results indicate how marl and mudrock formed in the Agua de Jagüel palaeovalley and provide information about the oxygenation of the bottom waters of the palaeovalley. The presence of albite and the high concentrations of Al<sub>2</sub>O<sub>3</sub> and TiO<sub>2</sub> suggest that marl and mudrock formed in the presence of terrestrial sediment influx (Griffin et al., 1968; Hathaway, 1979; Rais et al., 2008). Albite, a plagioclase feldspar, is derived from continental crust, and Al and Ti are insoluble in seawater and thus must have been transported in particulates into the water column. The presence of terrestrial

sediment in every mudrock and marl sample signals that none of the rocks formed purely ‘in situ’ from marine clay or organisms. Therefore, marl cannot be construed as representing pure clastic sediment starvation in the water column. The samples were taken from or adjacent to intervals with glacial indicators, such as dropstones or diamictite. The source of the terrestrial sediment is likely rain-out from icebergs or meltwater emanating from the base of the glacier. Calcium carbonate was likely sourced from pelagic material settling from suspension. While marl does indicate reduced clastic input so that calcium carbonate can precipitate, the assumption of ‘sediment starvation’ in the presence of marl should not exclude minor fine-grained terrestrial sediment influx.

The XRF results are consistent with an interpretation of anoxia in the Agua de Jagüel palaeovalley. V/Cr ratios above 2 indicate that mudrock deposition occurred in water that is anoxic, because  $\text{H}_2\text{S}$  was present in the water column (Ernst, 1970; Jones and Manning, 1994; Tenesch et al., 2007). Therefore, anoxia is indicated throughout the sequence. Anoxia likely resulted from isolation of the palaeovalley from Panthalassan waters at the mouth of the fjord, especially if the palaeovalley was silled or separated into subbasins due to multiple morainal banks (cf. Willems et al., 2009). A cap of glacial meltwater on top of the water column may have further stratified the water column in the palaeovalley.

The interpretation of anoxia can be further strengthened by future work using other redox-sensitive elements such as zinc, nickel, and cobalt (cf. Powell, 2009). However, the concentrations of these elements are too low in the Agua de Jagüel mudrocks for XRF analysis using the current calibration. ICP-MS analysis is recommended for future work to determine the relative abundances of these elements.

Evidence for anoxia provides one explanation for the absence of bioturbation and body fossils in this fjordal setting. Another factor that would make the Agua de Jagüel palaeovalley an inhospitable environment to benthos is the high sedimentation rate of a proglacial environment. Rapid sedimentation may explain the absence of bioturbation in the lower diamictite and pebbly mudrock portion of the sequence, but bioturbation is absent from the entire sequence, even where glacial indicators are absent. Thus, anoxia was likely a major factor in preventing bioturbation in the glacial sequence of the Agua de Jagüel Formation. Morainal banks could have acted as “sills” that separated the fjord into separate sub-basins, which would likely have limited circulation and promoted anoxic bottom waters within the fjord.

This research presents a line of reasoning for the absence of bioturbation in proglacial environments in palaeovalley settings. It is likely that the unbioturbated glacial portions of the Tramojo and Hoyada Verde Formations (cf. López Gamundí and Martínez, 2000; Henry, 2007) were also deposited under anoxic conditions. Thus, where bioturbation is absent from proglacial environments, anoxia should be explored as the cause, especially in restricted environments such as fjords. For example, the Guandacol Formation in the Paganzo Basin (Fig. 10B, Huaco locality) contains unbioturbated postglacial black shale overlain by bioturbated sandstones and siltstones reported to contain both freshwater trace fossils and marine acritarchs (Buatois and Mángano, 2003; Buatois et al., 2006). The presence of freshwater trace fossils in a frequently marine basin has been interpreted as resulting from the large release of meltwater from glaciers that pushed the salinity barrier seaward, allowing freshwater biota to migrate into the environment (Buatois et al., 2006). In light of the anoxia data

from the Agua de Jagüel Formation, future geochemical studies on the Guandacol Formation may indicate anoxia during deposition of black shales and may provide more information on this little-studied depositional system.

## **6. Filling the Palaeovalley**

A facies analysis of the glacial sequence of the Agua de Jagüel Formation and a geochemical analysis of mudrock and marl in the sequence enables the interpretation of four stages of depositional regimes that occurred in the palaeovalley (Fig. 13). Stage 1 is characterized by deposits of a morainal bank: the thick interval of diamictite, conglomerate, and sandstone in Logs 1 and 2. In stage 2, diamictite passes up into pebbly mudrock as rain-out of sediments from icebergs becomes the dominant depositional process. Next, stage 3 is marked by glacial retreat out of the fjord and progradation of the shoreface, evidenced by an absence of glacial indicators and a thickening and coarsening-upward succession of fine-grained, cross-stratified sandstones. Finally, stage 4 is characterized by mudrock with dropstones that signal a transgression and the return of iceberg rafting. At its top, stage 4 is incised by the sandstones of sequence 2.

### **6.1 Stage 1: Morainal Bank Deposition**

The thick diamictite interval with interbedded conglomerate, sandstone, and mudrock in Logs 1 and 2 (Fig. 13) contains several indicators that suggest it was deposited as a morainal bank. The overall thickness of diamictite and the profuse folds and slumps suggest a morainal bank in the proximal proglacial environment where rapid sedimentation and deformation due to glacial shoving and mass movement (i.e., slumping, sliding) occur. The conglomerate and sandstone channel within the diamictite

interval (Fig. 13) was likely deposited by meltwater discharge flowing as an effluent jet from the base of the glacier (e.g., Powell, 1990) and formed channel and grounding line fan facies that made up part of the morainal bank. After depositing the bedload of gravel- to fine sand-sized sediment, the jet then transformed into a buoyant plume. The buoyant plume floated to the top of the water column due to the density difference between the freshwater effluent and the saline water in the palaeovalley and spread down the fjord, raining out clay, silt, and very fine to fine sand with sediment fining in a proximal to distal direction. Because of the evidence for deposition by meltwater in stage 1, and the abundant evidence for the occurrence of debris-laden icebergs throughout much of the succession, which are characteristic of temperate glaciers, deposition by wet-based, temperate glaciers is interpreted for the Agua de Jagüel Formation. The depositional environment for stage 1 is illustrated in Figure 18.

There is a temptation to interpret thick diamictite successions deposited in the ancient record, like that of stage 1 in Agua de Jagüel Formation, to represent composite glaciations spanning millions of years. There is also a tendency to interpret individual diamictite intervals within a succession, such as those between 100 and 130 m in log 2, as separate glacial events, or as advance and retreat cycles. These tendencies may be inspired by focusing on the thin diamictite deposits produced by terrestrial glaciers instead of taking into account the rapid sedimentation rates and lateral variability of processes and environments in glacimarine settings. For example, glaciations that deposited up to 20 m of diamictite in the marine setting produced only 1-2 m of till on land (cf. De Geer, 1910; Lamplugh, 1911; Boulton, 1990). Studies from modern glaciers have recorded high rates of sedimentation that decrease logarithmically with distance

from the glacier front (Powell and Cowan, 1986; Boulton, 1990). Sedimentation rates can exceed 1000 mm/yr in the immediate proglacial area, and taper off to 1-10 mm/yr in the outer proximal zone ~10 km from the glacial front (Powell and Cowan, 1986; Boulton, 1990). Morainal banks up to 175 m thick have been reported from modern glacimarine settings in Alaska (Cai et al., 1997), therefore the thick diamictite interval within the glaciogenic sequence at the base of the Agua de Jagüel Formation, which is here interpreted as a morainal bank associated with a temperate tidewater glacial system, is consistent with deposition during a single glaciation. If this interpretation is correct, then other glacimarine deposits in the rock record containing multiple diamictites and interpreted as the deposits of multiple glacial events may need to be reinvestigated to test whether they may have been deposited during a single glacial event like that of the Agua de Jagüel Formation.

## **6.2 Stage 2: Iceberg Rain-Out**

Stage 2 represents glacial retreat, as the glacier terminus pulled farther up into the palaeovalley and was no longer resting against the morainal bank. The transition from diamictite to mudrock is not necessarily evidence of a transgression but is more likely a facies transition caused by glacial retreat within deep water (Boulton, 1990; Powell and Cooper, 2002). During stage 2, icebergs calved from the glacier front and shed dropstones as they floated down the fjord. Several episodes of iceberg dumping occurred in this stage, depositing dump structures consisting of diamictite and normally graded conglomerate and sandstone pods (Fig. 16C). The mud that dominates stage 2 would have provided a soupy substrate, and the iceberg dumps and dropstones sunk down into the underlying mud when they impacted the bottom. Additionally, meltwater plumes



rising away from the glacier base deposited mud and sand. Anoxic conditions are known to have occurred following the iceberg dumps, although it is possible that the palaeovalley was perpetually anoxic. The anoxic bottom waters and soupy substrate prevented colonization by benthic organisms and may have been the result of restricted circulation within subbasins within the fjord separated by morainal bank “sills” (cf. Cai et al., 1997; Willems et al., 2009).

### **6.3 Stage 3: Glacial Retreat, Shoreface Progradation**

In stage 3, sandstone beds in mudrock thicken upwards, and structures in sandstone indicate a shallowing-upward trend, as hummocky cross-bedding passes up into trough cross-bedding (Fig. 13). The thickening and coarsening-upwards beds and shallowing-upward indicators suggest progradation of a shoreface in or across the palaeovalley. Water depth is estimated at 20 m or less during this stage (cf. Boulton, 1990). The sandstone beds in stage 3 are pervasively deformed, which we interpret to be a result of slumping due to the uneven substrate of the palaeovalley and/or high sedimentation rates. The absence of glacial indicators in stage 3 suggests that icebergs were not present in the palaeovalley, therefore the glacier front had retreated out of the sea and onto land. Alternately, the shallow crests of morainal banks farther up the fjord may have trapped icebergs in a more proximal setting.

### **6.4 Stage 4: Transgression, Iceberg Rain-Out**

A shift back to mudrock with dropstones and marl characterizes stage 4. Dropstones indicate the return of icebergs to the palaeovalley, thus glacial advance down the fjord likely occurred. The top of the shoreface deposits in underlying stage 3 is deformed, which may be the result of grounding of iceberg keels. However, it is possible

that this renewed iceberg deposition may have been from icebergs that calved from glaciers outside the Agua de Jagüel palaeovalley and were transported into the mouth of the palaeovalley by ocean currents. Additionally, the shift from cross-bedded sandstone to mudrock is interpreted as a flooding surface. This flooding surface correlates with the Namurian – early Westphalian transgression described in Limarino et al. (2002). Another scenario that explains this stage is that shallow morainal banks up the palaeovalley may have trapped icebergs in the proximal portion of the fjord during deposition of stage 3, and following the Namurian – early Westphalian transgression, deeper waters allowed icebergs to again transit into more distal portions of the fjord.

## **7. Discussion**

The Protoprecordillera was glaciated by temperate alpine glaciers that flowed radially off the Protoprecordillera into the surrounding Río Blanco, Calingasta-Uspallata, and Paganzo Basins (López Gamundí, 1997; Henry et al., 2008), and the Agua de Jagüel Formation records this Namurian glacial event. Similar stratigraphic records of glacial retreat occur in two other nearby formations in the Calingasta-Uspallata Basin: the Hoyada Verde and Tramojo Formations (Fig. 10). Both formations occur adjacent to the Protoprecordillera and contain thick glacial diamictites overlain by mudrock with dropstones that pass up into pebble-free mudrock. In the Hoyada Verde Formation, several layers of glacial diamictite, one containing a striated boulder pavement, pass up into pebbly mudrock and mudrock with marl (López Gamundí and Martínez, 2000; Henry et al., 2008; Fig. 19). In the lower member of the Tramojo Formation, the deglaciation is recorded in a syncline, with the two limbs of the syncline representing different environments. The northwest limb contains diamictite passing up into mudrock

containing marl, and the southeast limb contains diamictite and mudrock that are overlain by conglomerate and sandstone sheets (Fig. 19). The two successions of the Tramojo Formation, which were likely deposited within a few hundred meters of each other, record glacial retreat into a terrestrial environment. A thick coarsening-upward proglacial alluvial or fan delta system developed in the proximal environment (southeast limb), whereas the distal setting shows an abrupt change from diamictite to shale (northwest limb), which is typically identified as a flooding surface. Therefore, the Tramojo Formation records an apparent proximal to distal out of phase regression/transgression succession that is not easily explained by a eustatic rise. As with the Agua de Jagüel Formation, the transitions from diamictite to mudrock in both the Hoyada Verde and Tramojo Formations may not represent a transgression associated with a eustatic rise, but instead may record abrupt facies transitions associated with glacial retreat in areas of the fjord distal to the ice front. Although this abrupt change is often described as a transgression or flooding surface, the diamictite to mudrock transition can occur without a change in water depth (cf. Boulton, 1990).

Temperate glacial environments can be characterized by a sequence stratigraphy interpretation that is independent of eustasy, because glacial advance and retreat cycles are often more important controls on glacial sedimentation and systems tracts than eustatic changes (Powell and Cooper, 2002). Under Powell and Cooper's (2002) glacial sequence stratigraphy model, the base of the glacier is a major control on base level in addition to sea level, because a marine glacier is able to create erosional surfaces below sea level and deposit accumulations of sediment that rise above sea level. Examining the Agua de Jagüel Formation in this paradigm, stage 1 is a glacial maximum systems tract,

stage 2 is a glacial retreat systems tract, stage 3 is a glacial minimum systems tract, and stage 4 may be a glacial advance systems tract, especially if the dropstones from that stage were deposited from icebergs that calved off a glacier in the Agua de Jagüel palaeovalley. Stage 4 is unique in that the transition into shale is a fining upwards succession, but the return of dropstones in stage 4 indicates glaciation. Although stage four represents a transgression, it was not caused by input of glacial meltwater from glaciers in the Protoprecordillera, as there is evidence of synchronous glaciation, and because the waxing and waning of alpine glaciers have little influence on eustasy. This rise in relative sea-level may have lifted icebergs that were grounded on morainal banks in the Agua de Jagüel and other fjords, allowing them to travel more freely and rain out debris onto the substrate. Stage 4 corresponds with the Namurian-Westphalian post-glacial transgression documented for the basins surrounding the Protoprecordillera (Limarino et al., 2002), and the identification that glaciation occurred at the same time as the beginning of this transgression supports the hypothesis that the transgression was not caused by input of glacial meltwater.

The Agua de Jagüel, Hoyada Verde, and Tramojo Formations of the Calingasta-Uspallata Basin record the same Namurian glacial event, instead of multiple glaciations as proposed by Taboada (2006) and Pazos (2007). The Hoyada Verde Formation is dated as Namurian to early Westphalian (Serpukhovian to Bashkirian) by brachiopods, bivalves, crinoids, and bryozoans of the *Levipustula* zone found in mudrocks that overlie diamictite (Amos and Rolleri, 1965; Cisterna, 1999). In the Tramojo Formation, the post-glacial mudrock contains Serpukhovian-Bashkirian spores (Césari, personal communication). Thus, based on their proximity to each other and coeval timing, it can

be concluded that the Hoyada Verde, Tramojo, and Agua de Jagüel Formations record the same deglaciation succession of the Protoprecordillera. In the adjacent Río Blanco Basin, post-glacial strata from a similar glacial retreat succession from the Río del Peñon Formation have been dated as  $319.57 \pm 0.09$  (Bashkirian; Gulbranson et al., 2010). In the Paganzo Basin, the Guandacol Formation contains a glacial succession, and post-glacial strata from the Huaco section was dated as  $318.79 \pm 0.10$  (Bashkirian). These dates are likely transferrable to the formations of the Calingasta-Uspallata Basin, constraining the end of the glaciation of the Protoprecordillera to the Early Bashkirian (Fig. 20).

The deglaciation of the Protoprecordillera marks the end of glaciers in western Argentina during the LPIA. After the glaciation of the Protoprecordillera, ice centers shift to the Paraná Basin of Brazil and the Kalahari and Karoo Basins in South Africa later in the Pennsylvanian (Schneider et al., 1974; França and Potter, 1988; Visser, 1997; Holz et al., 2008; Isbell et al., 2008a; Rocha Campos et al., 2008; Stollhofen et al., 2008). However, palaeogeographic models often represent western Argentina as glaciated throughout the entire LPIA (i.e., Scotese, 1997). Thus, this and other work on near-field Gondwanan glacial deposits show inconsistencies from the geologic record with palaeoclimate models for the LPIA. Continued near-field research is necessary for ‘groundtruthing’ these models. Finally, this research on the Protoprecordillera highlights that glaciation during the LPIA occurred as smaller glaciers that waxed and waned over different time intervals instead of occurring as a supercontinental-sized glacier that endured from the Late Carboniferous – Early Permian. Following the deposition of the lower portion of the Agua de Jagüel formation, fluvial and shallow marine sedimentation dominated western Argentina with a progressive shift toward arid climates from the

Pennsylvanian into the Permian (Limarino et al., 2002; 2006; Henry et al., 2008; Gulbranson et al., 2010).

## **8. Conclusions**

The lower sequence of the Agua de Jagüel Formation records the deglaciation of the Protoprecordillera of western Argentina in the Namurian (Serpukhovian to Early Bashkirian). The depositional sequence is characterized by a thick (150 m) interval of diamictite near the base of the formation, which passes up into pebbly mudrock. Above these facies is a thickening-upward succession of cross-stratified sandstones, which are then overlain by another interval of pebbly mudrock. XRD analysis of mudrock and marl in the succession indicate that terrestrial sedimentation was still occurring during marl formation based on the presence of albite, which informs the present understanding of marl deposition under ‘sediment starvation.’ Additionally, XRF data suggest that anoxia occurred in the palaeovalley, which explains the absence of bioturbation in the strata. Overall, this succession represents a deglaciation in a restricted palaeovalley. Initially, a temperate, wet-based valley glacier deposited a morainal bank, and then the glacier retreated and deposition shifted to iceberg rafting. Next, the glacier completely retreated from the sea, and shoreface progradation occurred. Finally, a transgression occurred, ushering in another interval of iceberg rafting that may have also been caused by glacial readvance. This sequence represents one glacial event in the Protoprecordillera and indicates that glacial retreat in this area occurred before and therefore independently of the regional Namurian-Westphalian transgression.

## **Acknowledgments**

We thank Luis Spalletti and an anonymous reviewer for constructive feedback that helped improve this paper. Financial support was provided by the Center of Latin American and Caribbean Studies, the Graduate School (Research Growth Initiative), and the Department of Geosciences at UWM; the National Science Foundation (ANT-0440919; ANT-0635537; OISE-0825617); the Wisconsin Geological Society; the Geological Society of America (GSA); GSA Coal Division; and Universidad de Buenos Aires. Patricia Ciccioli and Ana Tedesco provided support in the field.

## Tables

Table 1. Facies descriptions of the lower glacial sequence of the Agua de Jagüel Formation

<b>Facies</b>	<b>Lithology</b>	<b>Sedimentary Structures</b>	<b>Interpretation</b>	<b>Depositional Environment</b>
Massive Diamictite	Massive diamictite, massive sandstone	Slumps, folds, load structures, dewatering structures	Deposition by rain-out from icebergs and meltwater plumes, debris flows	Morainial bank
Weakly Stratified Diamictite	Weakly stratified diamictite, fine sandstone	Faint laminations, faint bedding, high-angle clasts, sole marks	Rain-out from icebergs and meltwater plumes	Morainial bank
Bedded Diamictite	Thinly to thickly bedded diamictite	Sharp lower and upper contacts, slumps, folds	Cohesive debris flows	Morainial bank
Conglomerate and Sandstone	Clast-supported sandy conglomerate, fine- to coarse-grained sandstone	Massive bedding, normal and inverse grading, trough cross beds, primary current lineations, dewatering structures	Sheets deposited by an effluent jet emanating from the base of the glacier. Pods were deposited as iceberg dumps.	Sheets: Grounding line fan Pods: bank-front environment
Pebbly Mudrock	Claystone and siltstone with outsized clasts, diamictite pods, marl, wisps and clumps of fine sand	Slumps, slides, folds	Mud is deposited by suspension settling; icebergs rain out clasts, sand, and mud; diamictite pods form from iceberg dumping; marl forms from setting pelagic under clastic sediment starved conditions.	Bank-front environment



Mudrock and Sandstone	Claystone, siltstone, very fine-to-medium-grained sandstone, marl	Slumping, folding boudins, cross-laminations, trough cross-bedding, hummocky cross-bedding, massive bedding, rip-up clasts	Sandstone is deposited due to shoreface progradation in the absence of glaciers; debris flows resediment sand; mud is deposited by suspension settling.	Shoreface prograding down the fjord
-----------------------	---	--	---	-------------------------------------

Table 2. X-ray Diffraction Data

Sample	Albite (%)	Calcite (%)	Quartz (%)	Muscovite (%)
1-20a	19.3	0	80.7	0
1-224	21.69	0	61.35	17.0
1-251	19.1	43.4	26.0	11.5
1-251-07	17.2	45.9	22.5	14.4
1-258	18.9	42.9	25.6	12.6
3-471	29.74	0	64.3	5.9
3-511	15.1	38.1	24.7	22.1

Table 3. X-ray Fluorescence Data

Sample	Na <sub>2</sub> O (%)	MgO (%)	Al <sub>2</sub> O <sub>3</sub> (%)	SiO <sub>2</sub> (%)	P <sub>2</sub> O <sub>5</sub> (%)	K <sub>2</sub> O (%)	CaO (%)	TiO <sub>2</sub> (%)	Fe <sub>2</sub> O <sub>3</sub> (%)	Zr (ppm)
1-20a	1.98	0.57	7.62	82.73	0.20	0.89	0.32	0.85	3.09	338
1-20b	1.96	0.51	7.68	82.74	0.20	0.88	0.7	0.83	3.34	325
1-224	1.97	1.65	12.4	71.55	0.18	2.13	1.08	0.83	5.14	316
1-251	1.36	1.28	7.26	31.44	0.44	1.23	30.78	0.42	2.66	82
1-258	1.31	1.25	7.79	31.66	0.24	1.37	29.7	0.50	3.17	95
3-471	2.97	0.53	10	76.46	0.28	1.02	2.13	0.94	2.98	614
3-511	0.86	1.85	10.17	33.24	0.26	2.3	25.58	0.51	4.50	93

Sample	V (ppm)	Zn (ppm)	Cr (ppm)	Ce (ppm)	Sr (ppm)	Ba (ppm)	Mn (%)	LOI (%)	Sum (%)
1-20a	64	<LLOD	<LLOD	<LLOD	48	159	0.02	1.53	99.91
1-20b	<LLOD	72	<LLOD	<LLOD	44	156	0.04	1.91	100.89
1-224	99	76	<LLOD	<LLOD	74	421	0.04	3.05	100.15
1-251	54	<LLOD	<LLOD	<LLOD	238	197	0.56	24.51	102.02
1-258	78	<LLOD	27	<LLOD	297	227	0.50	24.07	101.65
3-471	<LLOD	<LLOD	<LLOD	216	116	177	0.04	2.86	100.36
3-511	90	66	36	<LLOD	223	305	0.24	21.77	101.37

## Figures

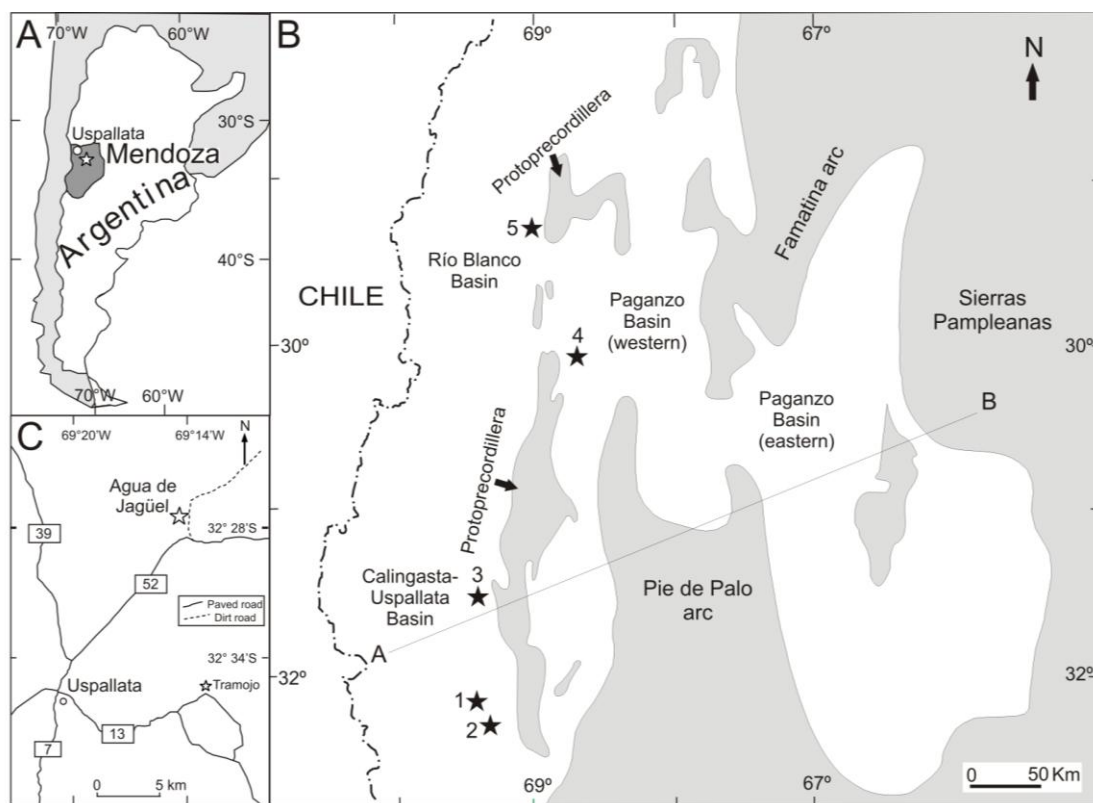


Figure 10. Location map of the Agua de Jagüel Formation and other formations described in the text. A. The Agua de Jagüel Formation is located 17 km northeast of the town of Uspallata, northern Mendoza, Argentina. B. Palaeogeography of the Carboniferous basins of western Argentina: the Calingasta-Uspallata, Río Blanco, and Paganzo Basins. Numbers indicate the localities mentioned in the text, 1. Agua de Jagüel Formation, 2. Tramojo Formation, 3. Hoyada Verde, 4. Huaco, and 5. Río del Peñón. A-B indicates the orientation of the cross section in Figure 2. C. Location of the Agua de Jagüel and Tramojo Formations outside the town of Uspallata.

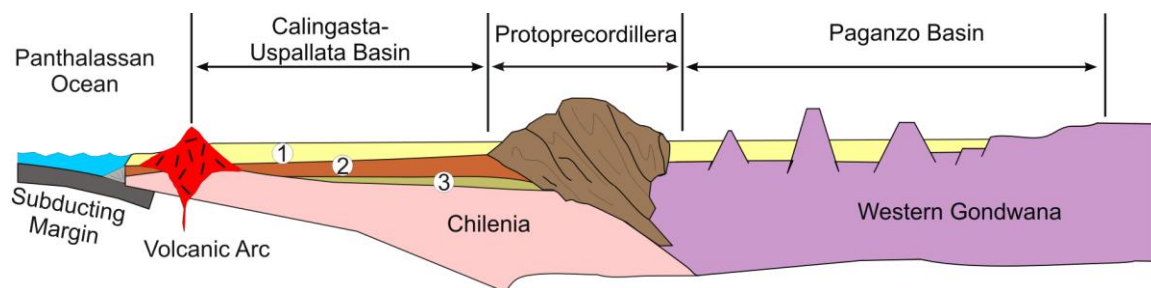


Figure 11. Cross-section of Early Permian geology through the Calingasta-Uspallata Basin, Protoprecordillera, and Paganzo Basin in western Argentina. 1. Middle Carboniferous - Permian sedimentary rocks, including the Agua de Jagüel Formation, 2. Lower Carboniferous sedimentary rocks (below the Río Blanco unconformity), 3. Pre-

Carboniferous basement sedimentary rocks. After Azcuy et al. (1999) and Limarino et al. (2006).

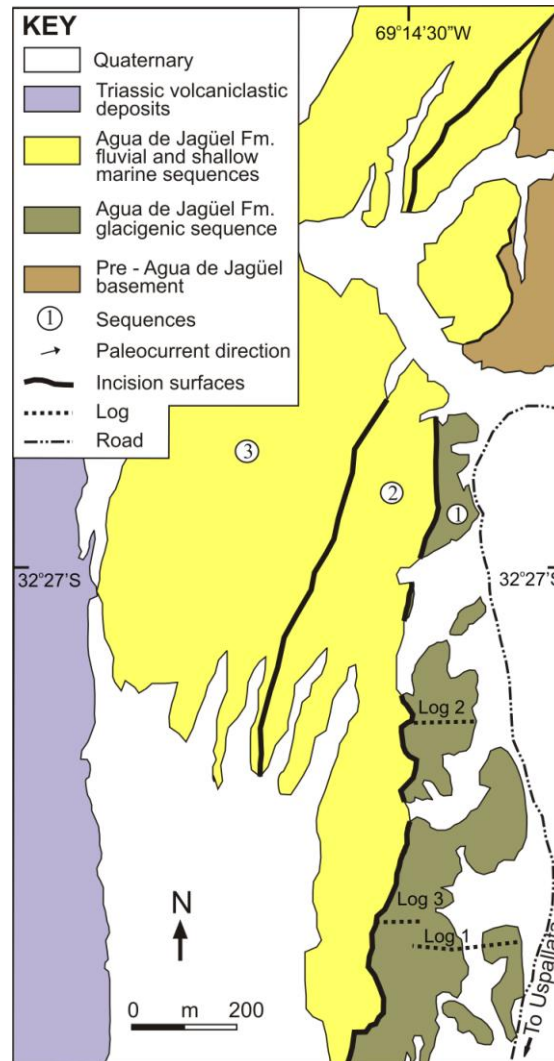


Figure 12. Geologic map of the three sequences of the Agua de Jagüel Formation. Strata of the Agua de Jagüel Formation dip at  $90^\circ$ . Based on the geometry of the formation and contacts with basement rocks, the Agua de Jagüel Formation was deposited in a palaeovalley at least 700 m deep and at least 5 km wide. Modified from Henry et al. (2008).

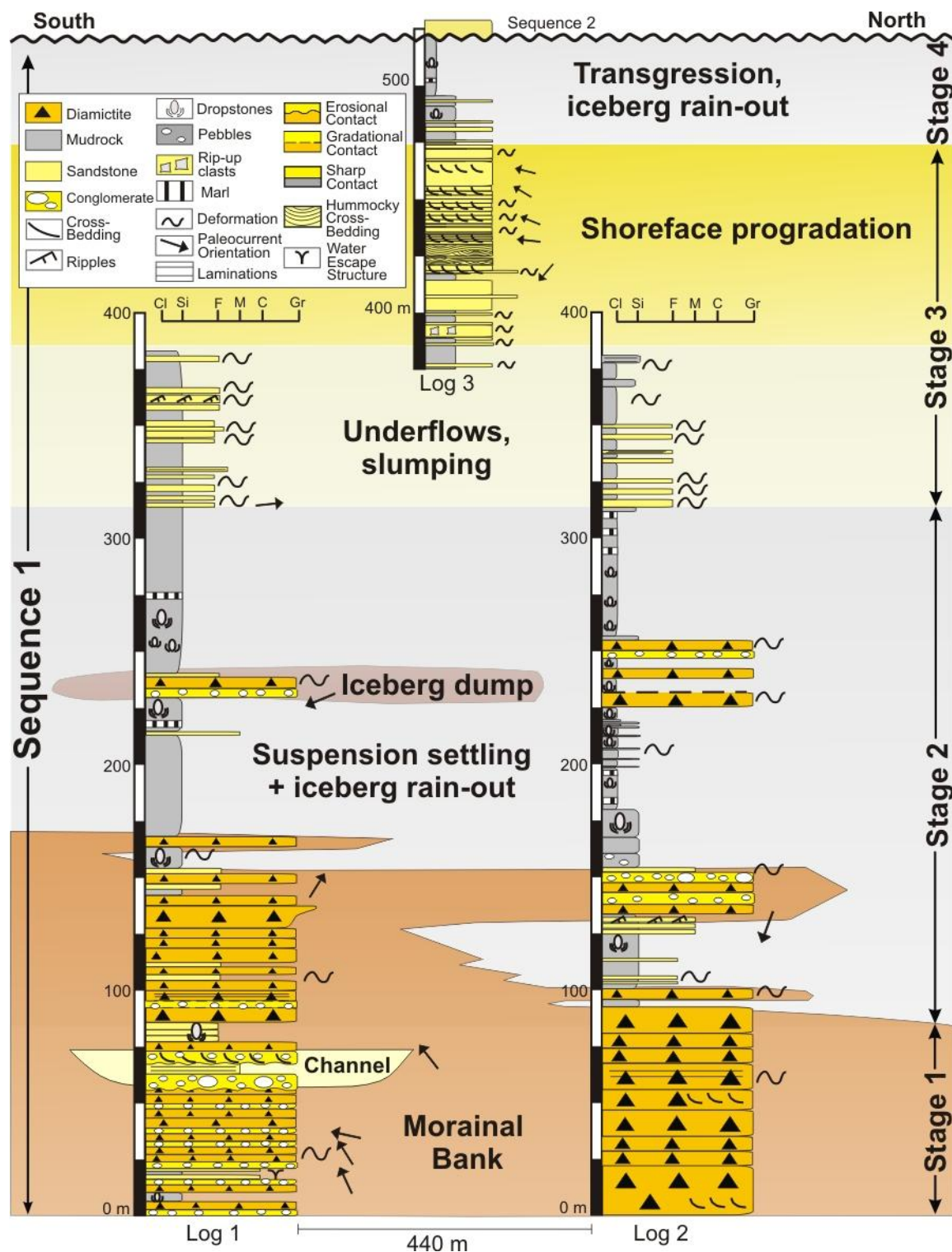


Figure 13. Logs and interpreted depositional processes for sequence 1 of the Agua de Jagüel Formation.



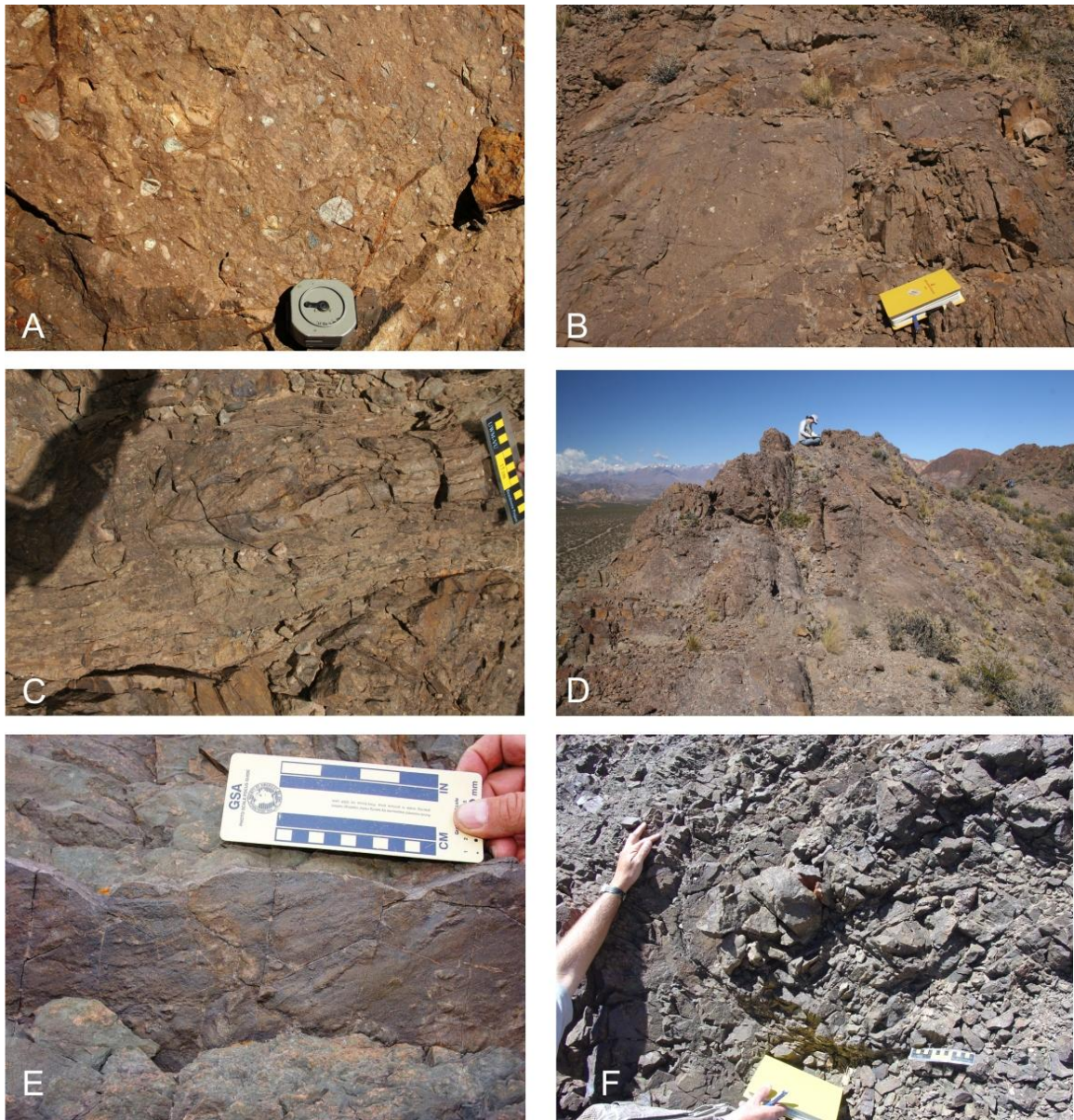


Figure 14. The diamictite facies association. A. Clast-rich massive diamictite B. Weakly stratified diamictite C. Thinly bedded diamictite D. Diamictite from the thick lower diamictite interval of the Agua de Jagüel Formation. Bedded Diamictite occurs just behind the person. E. Sandstone bed with sole marks, interbedded with diamictite in Log 1 F. Slumped diamictite rimmed by fine sand.



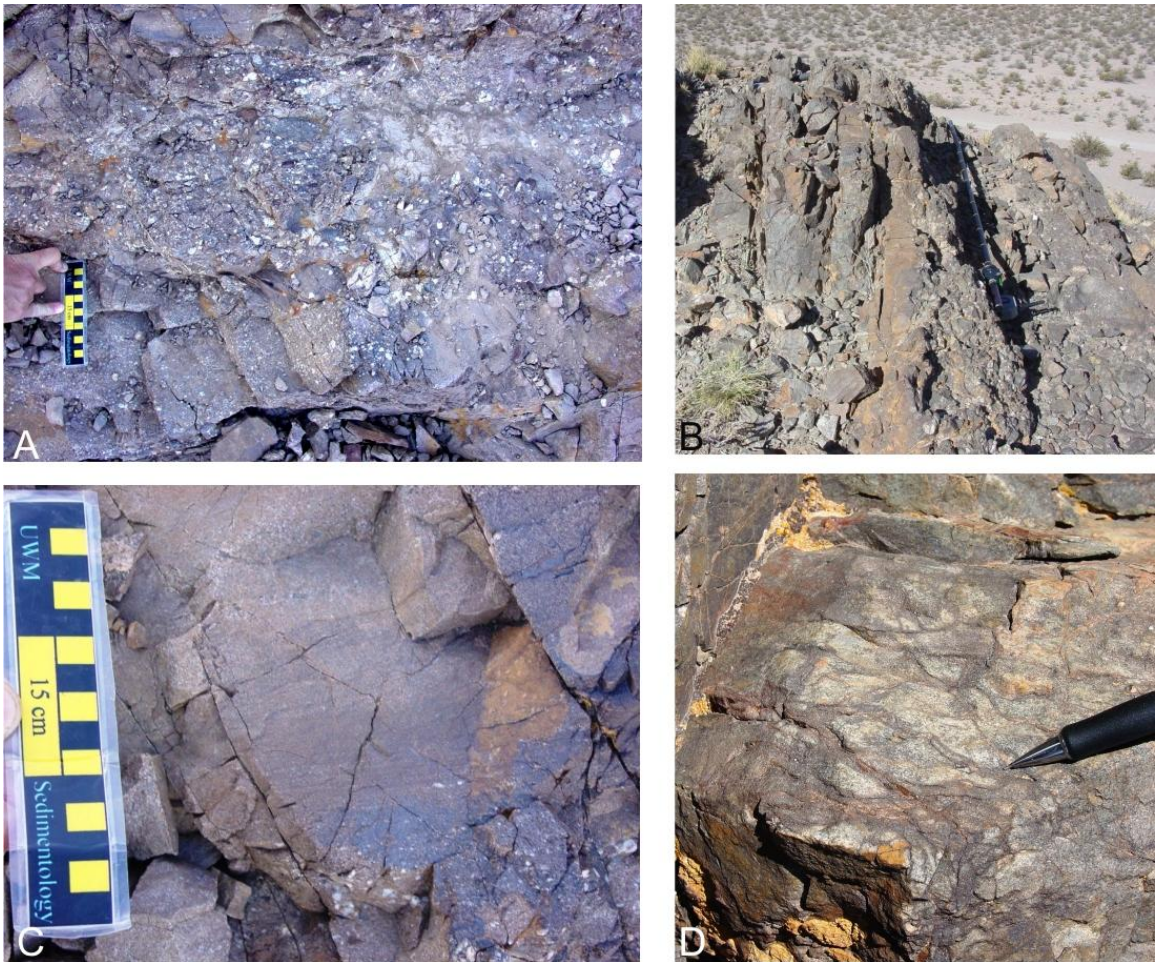


Figure 15. The conglomerate and sandstone facies association. A. Bedded conglomerate with a sandy matrix B. Interbedded conglomerate and sandstone. Jacob's staff for scale. C. Laminated sandstone D. Cross-laminated fine-grained sandstone.





Figure 16. The pebbly mudrock facies association. A. Rhythmically bedded siltstone and claystone that has been deformed and folded B. Striated sandstone clast in mudrock C. Lens-shaped pods of diamictite, conglomerate, and sandstone occur within a thick pebbly mudrock interval.





Figure 17. The mudrock and sandstone facies association. A. Marl (orange rock fragments) in mudrock B. Deformed beds of fine sandstone interbedded with mudrock, overlying a thick mudrock with marl interval. Sand beds progressively extend further south (towards the camera), indicating progradation. C. Very fine sandstone folded around siltstone. Yellow lines on Jacob's staff occur every 10 cm. D. Bulbous load structures on base of sandstone bed in mudrock E. Boudinaged sandstone in mudrock.



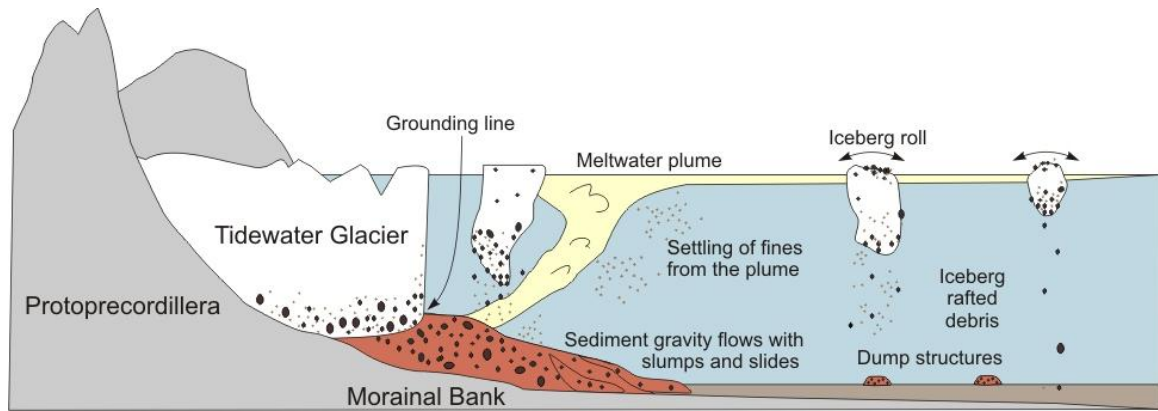


Figure 18. Depositional environment of the Agua de Jagüel Formation.

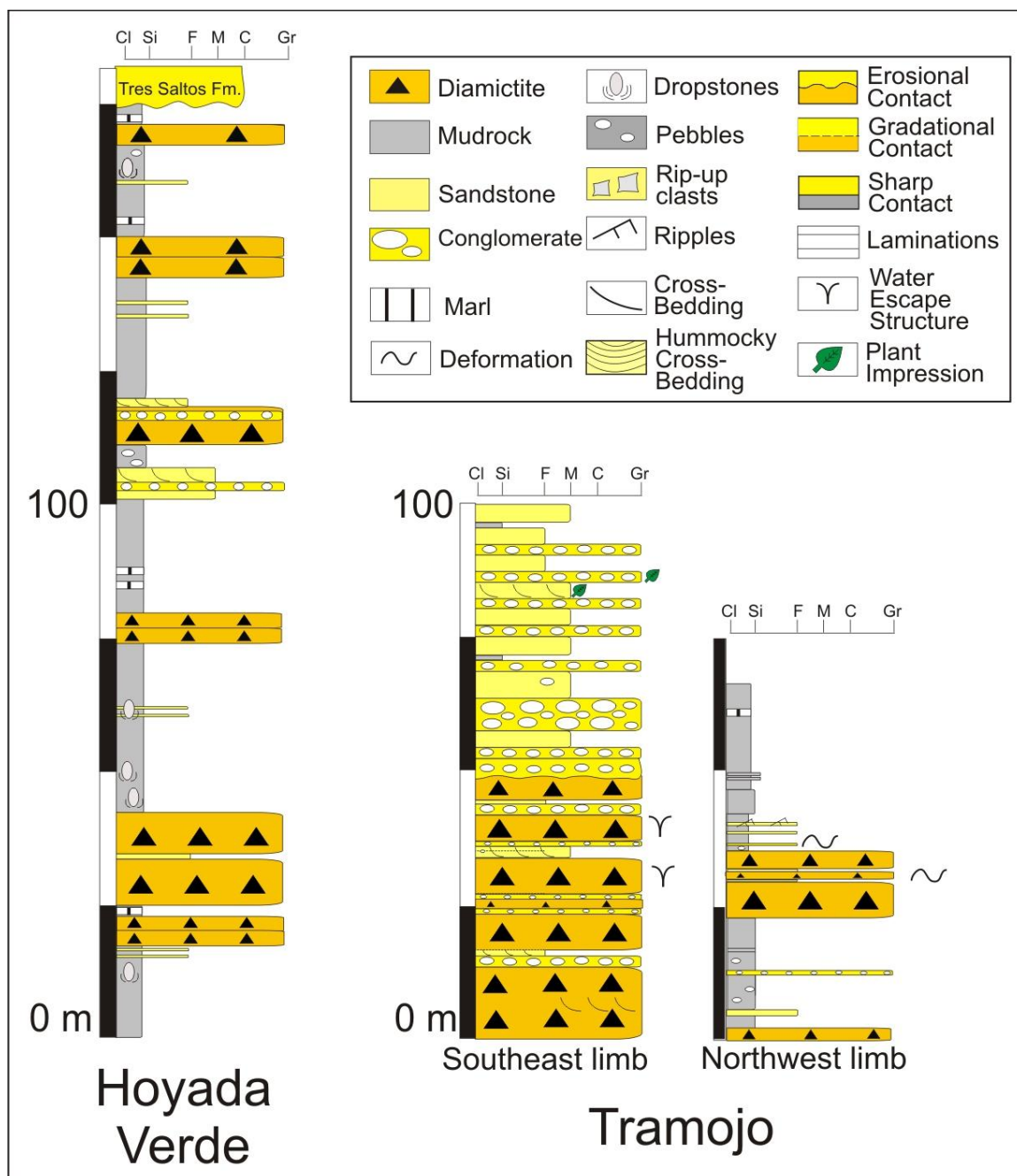


Figure 19. Graphic logs of the Hoyada Verde Formation and the Namurian lower member of the Tramojo Formation. The Tramojo Formation occurs as an anticline, and the two limbs of the anticline record different deglaciation successions. The Hoyada Verde and Tramojo Formations are located in the Calingasta-Uspallata Basin and occur adjacent to the Protoprecordillera (Fig. 1B).

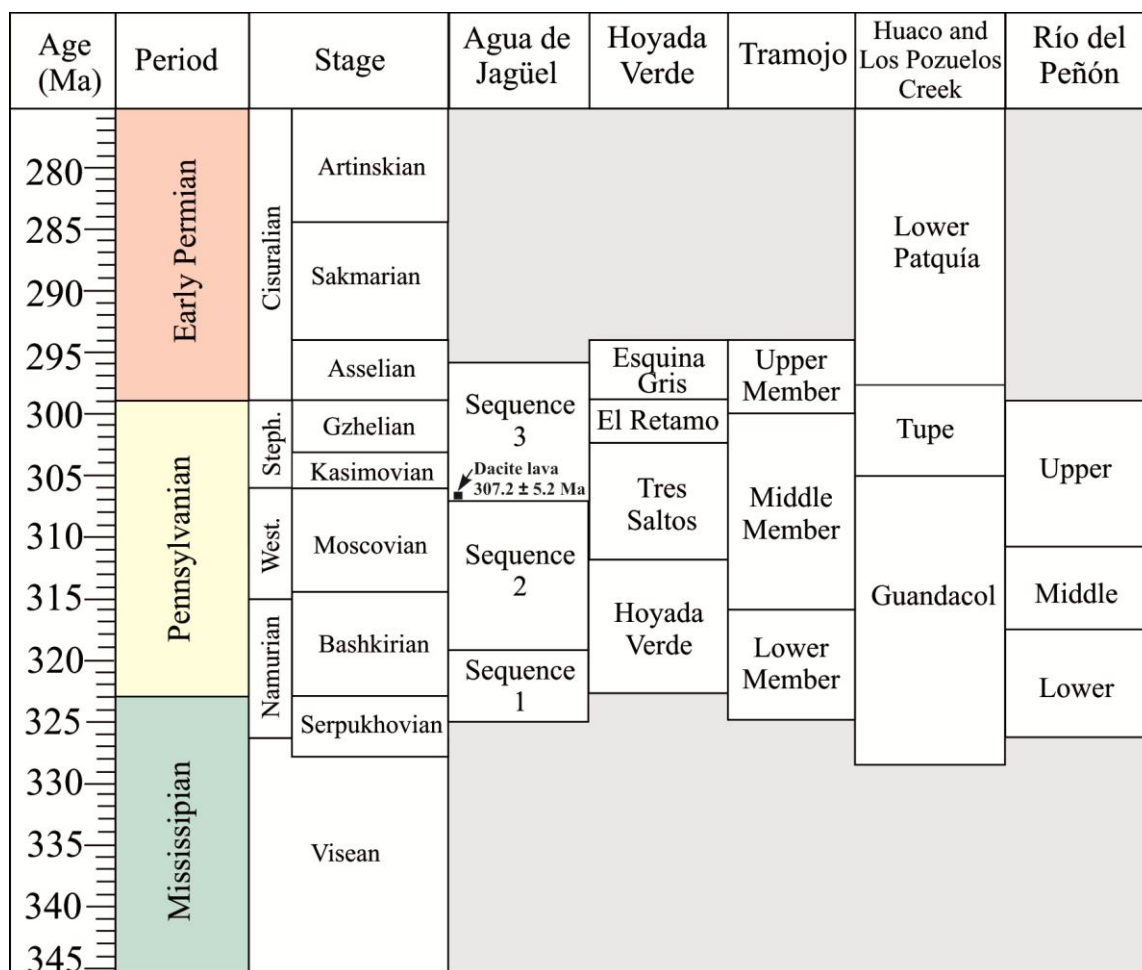


Figure 20. Correlation diagram for uppermost Mississippian, Pennsylvanian, and Lower Permian strata for sites in the Calingasta-Uspallata, Río Blanco, and Paganzo Basins mentioned in the text (units and ages are based on Taboada, 1985; Archangelsky and Lech, 1985; Archangelsky and Archangelsky, 1987; Fernandez-Seveso and Tankard, 1995; Azcuy et al., 1999, López-Gamundí and Martínez, 2000; Gulbranson et al., 2010; Césari, personal communication).

## References

- Amos, A.J., Rolleri, E., 1965. El Carbónico marino en el valle Calingasta-Uspallata, San Juan-Mendoza. Boletín de Informaciones Petroleras, 368, 50–71.
- Anderson, J.B., Domack, E.W., Kurtz, D.D., 1980. Observations of sediment-laden icebergs in Antarctic waters: implications to glacial erosion and transport. Journal of Glaciology 25, 387–396.
- Anderson, J. B., Brake, C., Domack, E., Myers, N., Wright, R., 1983. Development of a polar glacial-marine sedimentation model from Antarctic quaternary deposits and

- glaciological information. In: Molina, B.F. (Ed.) *Glacial Marine Sedimentation*. New York, Plenum Press, p. 233–264.
- Anderson, J. B., Kennedy, D.S., Smith, M.J., Domack, E.W., 1991. Sedimentary facies associated with Antarctica's floating ice masses. In: Anderson, J.B., Ashley, G.M. (Eds.), *Glacial marine sedimentation; paleoclimatic significance*. Geological Society of America Special Publication 261, 1–25.
- Archangelsky, A., Lech, R.R., 1985. Presencia de *Cancrinella* aff. *Farleyensis* (Eth. & Dun) en las capas plegadas de la “Serie Tramojo,” Pérmico inferior de la Precordillera de Mendoza. *Internacional Jornal de Geologia Precordillera*, San Juan, p.13.
- Archangelsky, A., Archangelsky, S., 1987. Tafoflora de la formacion Tramojo, Paleozoico tardio, en la region de Uspallata, provincial de Mendoza, republica Argentina. *Ameghiniana* 24, 251–256.
- Azcuy, C.L., Carrizo, H.A., Caminos, R., 1999. Carbonífero y Pérmico de las Sierras Pampeanas, Famatina, Precordillera, Cordillera Frontal y Bloque de San Rafael. *Instituto de Geología y Recursos Minerales, Geología Argentina* 29, 261–318.
- Bambery, W.J., Hutton, A.J., Jones, B.G., 1995. The Permian Illawarra Coal Measures, southern Sydney Basin, Australia: a case study of deltaic sedimentation. In: Postma, G., Oti, M.N. (Eds.), *Geology of Deltas*. Balkema, Rotterdam, 153–166.
- Bembrick, C.S., 1983. Stratigraphy and sedimentation of the Late Permian Illawarra Coal Measures in the Western Coalfield, Sydney Basin, New South Wales. *Journal and Proceedings of the Royal Society of New South Wales* 116, 105–117.
- Blakey, R.C., 2008. Gondwana paleogeography from assembly to breakup- a 500 m.y. odyssey In: Fielding, C.R., Frank, T.D., Isbell, J.L., (Eds.), *Resolving the Late Paleozoic Ice Age in Time and Space: Geological Society of America Special Paper* 441, 1–28.
- Boulton, G.S., 1990. Sedimentary and sea level changes during glacial cycles and their control on glacimarine architecture. In: Dowdeswell, J.A., Scourse, J.D. (Eds.), *Glacimarine Environments: Processes and Sediments*. Geological Society Special Publication 53, 15–52.
- Buatois, L.A., Mángano, M.G., 2003. Caracterización icnológica y paleoambiental de la localidad tipo de *Orchosteropus atavus*, Huerta de Huachi, provincial de San Juan, Argentina. *Ameghiniana* 40, 53–70.
- Buatois, L.A., Netto, R.G., Mángano, M.G., Balistieri, P.R.M.N., 2006. Extreme freshwater release during the late Paleozoic Gondwana deglaciation and its impact on coastal ecosystems. *Geology* 34, 1021–1024.

- Cai, J., Powell, R.D., Cowan, E.A., Carlson, P.R., 1997. Lithofacies and seismic-reflection interpretation of temperate glacial-marine sedimentation in Tarr Inlet, Glacier Bay, Alaska. *Marine Geology* 143, 5–37.
- Caputo, M.V., Crowell, J.C., 1985. Migration of glacial centers across Gondwana during Paleozoic Era. *Geological Society of America Bulletin* 96, 1020–1036.
- Chumakov, N.M. 1994. Evidence of Late Permian glaciation in the Kolyma River Basin: a repercussion of the Gondwanan glaciations in Northeast Asia? *Stratigraphy and Geological Correlation*, 2, 130–150.
- Ciccioli P.L., Limarino, C.O., Tedesco, A.M., Henry, L.C., Isbell, J.L., 2008. Paleoenvironmental evolution of the Agua de Jagüel Formation (Late Carboniferous – Early Permian): an example of glacial-postglacial transition in open marine basins. V Simposio Argentino del Paleozoico Superior.
- Cisterna, G.A., 1999. Paleoecología de niveles politicos de la sección superior de la Formación Hoyada Verde, Carbonífero Superior, Precordillera de San Juan, Argentina. *Ameghiniana* 36, 259–267.
- Collinson, J.W., Isbell, J.L., Elliot, D.H., Miller, M.F., Miller, J.M., 1994. Permian-Triassic Transantarctic basin. In: Veevers, J., Powell, C., (Eds.), *Permian-Triassic Pangea Basins and foldbelts along the Panthalassan margin of Gondwanaland*. Geological Society of America Memoir 184, 173–222.
- Cowan, E.A., Powell, R.D., 1990. Suspended sediment transport and deposition of cyclically interlaminated sediment in a temperate glacial fjord, Alaska, U.S.A. In: Dowdeswell, J.A., Scourse, J.D. (Eds.), *Glacial-marine Environments: Processes and Sediments*. Geological Society Special Publication 53, 75–89.
- Cowan, E.A., Seramur, K.C., Cai, J., Powell, R.D., 1999. Cyclic sedimentation produced by fluctuations in meltwater discharge, tides and marine productivity in an Alaskan fjord. *Sedimentology* 46, 1109–1126.
- De Geer, G., 1910. Guide de l'excursion au Spitzberg. Excursion A1. XI<sup>3</sup> Congrès Geologique Internationale, Stockholm.
- Dickins, J.M., 1997. Some problems of the Permian (Asselian) glaciation and the subsequent climate in the Permian. In: Martini, I.P. (Ed.), *Late glacial and postglacial environmental changes: Quaternary, Carboniferous-Permian, and Proterozoic*. Oxford, U.K., Oxford University Press, 243–245.
- Domack, E.W., Lawson, D.E., 1985. Pebble fabric in an ice-rafted diamicton. *Journal of Geology* 93, 577–591.

- Dowdeswell, J. A., Whittington, R.J., Marienfeld, P., 1994. The origin of massive diamicton facies by iceberg rafting and scouring, Scoresby Sound, East Greenland. *Sedimentology* 41, 21–35.
- Ernst, T.W., 1970. *Geochemical Facies Analysis*. Elsevier, Amsterdam, 152 p.
- Evans, J., Pudsey, C.J., 2002. Sedimentation associated with Antarctic Peninsula ice shelves; implications for palaeoenvironmental reconstructions of glacial marine sediments. *Journal of the Geological Society of London* 159, 233–237.
- Eyles, C. H., Eyles, N., Miall, A.D., 1985. Models of glacial marine sedimentation and their application to the interpretation of ancient glacial sequences. *Palaeogeography, Palaeoclimatology, Palaeoecology* 57, 15–84.
- Fernandez-Seveso, F., Tankard, A.J., 1995. Tectonics and stratigraphy of the late Paleozoic Paganzo Basin of western Argentina and its regional implications. In: Tankard, A.J., Soruco, R.S., Welsink, H.J. (Eds.), *Petroleum Basins of South America*. AAPG Memoir 62, 285–301.
- Fielding, C.R., Frank, T.D., Birgenheier, L.P., Rygel, M.C., Jones, A.T., Roberts, J., 2008. Stratigraphic imprint of the Late Paleozoic Ice Age in eastern Australia: a record of alternating glacial and nonglacial climate regime. *Journal of the Geological Society, London* 165, 129–140.
- Frakes, L.A., Crowell, J.C., 1969. Late Paleozoic glaciation: I, South America. *Geological Society of America Bulletin* 80, 1007–1042.
- Frakes, L.A., Francis, J.E., Syktus, J.I., 1992. *Climate modes of the Phanerozoic*. Cambridge, Cambridge University Press, 274 p.
- França, A.B., Potter, P.E., 1988. Estratigrafia, ambiente deposicional e análise de reservatório do Grupo Itararé (Permo-Carbonífero), Bacia do Paraná (parte 1): *Boletim de Geociências da Petrobrás* 2, 147–191.
- Garzanti, E., Sciunnach D., 1997. Early Carboniferous onset of Gondwanian glaciation and Neo-tethyan rifting in South Tibet. *Earth and Planetary Science Letters* 148, 359–365.
- Gastaldo, R.A., DiMichele, W.A., Pfefferkorn, H.W., 1996. Out of the icehouse into the greenhouse: a late Paleozoic analogue for modern global vegetational change. *GSA Today* 10, 1–7.
- Gilbert, R., 1990. Rafting in glacial marine environments. In: *Glacial marine environments: Processes and Sediments*, Dowdeswell, J.A., Scourse, J.D. (Eds.), Geological Society Special Publication 53, 105–120.

- Griffin, J.J., Windom, H., Goldberg, E.D., 1968. The distribution of clay minerals in the world ocean. *Deep Sea Research* 15, 433–459.
- Gulbranson, E.L., Montañez, I.P., Schmitz, M.D., Limarino, C.O., Isbell, J.L., Marensi, S.A., Crowley, J.L., 2010. High-precision U-Pb calibration of Carboniferous glacigenic deposits, Río Blanco and Paganzo basins, Northwest Argentina. *Geological Society of America Bulletin* 122, 1480–1498.
- Hambrey, M.J., Ehrmann, W.U., Larsen, B., 1991. Cenozoic glacial record of the Prydz Bay continental shelf, East Antarctica. In: Barron, J., Larsen, B. (Eds.), *Proc. Ocean Drilling Program, Scientific Results* 119, 77–131.
- Hathaway, J.C., 1979. Clay Minerals In: Burns, R.G., ed., *Marine Minerals. Reviews in Mineralogy* 6, 123–150.
- Heckel, P.H., 1994. Evaluation of evidence for glacio-eustatic control over marine Pennsylvanian cyclothems in North America and consideration of possible tectonic effects. In: Dennison, J.M., and Ettensohn, F.R. (Eds.), *Tectonic and eustatic controls on sedimentary cycles. Tulsa, Oklahoma, SEPM (Society for Sedimentary Geology) Concepts in Sedimentology and Paleontology* 4, 65–87.
- Henry, L.C., 2007. Carboniferous glacigenic deposits of the Hoyada Verde and Tramojo Formations of the Calingasta-Uspallata Basin, west central Argentina. M.S. Thesis, University of Wisconsin-Milwaukee, 151 p.
- Henry, L.C., Isbell, J.L., Limarino, C.O., 2008. Carboniferous glacigenic deposits of the Protoprecordillera of west central Argentina. In: Fielding, C.R., Frank, T.D., Isbell, J.L., (Eds.), *Resolving the Late Paleozoic Ice Age in Time and Space. Geological Society of America Special Paper* 441, 131–142.
- Holz, M., Souza, P.A., Iannuzzi, R., 2008. Sequence stratigraphy and biostratigraphy of the Late Carboniferous to Early Permian glacial succession (Itararé subgroup) at the eastern-southeastern margin of the Paraná Basin, Brazil. In: Fielding, C.R., Frank, T.D., and Isbell, J.L., (Eds.), *Resolving the Late Paleozoic Ice Age in Time and Space: Geological Society of America Special Paper* 441, 115–129.
- Horton, D.E., Poulsen, C.J., 2009. Paradox of late Paleozoic glacioeustasy. *Geology* 37, 715–718.
- Hyde, W.T., Crowley, T.J., Tarasov, L., Paltier, W.R., 1999. The Pangean ice age: studies with a coupled climate-ice sheet model. *Climate Dynamics* 15, 619–629.
- Isbell, J.L., Lenaker, P.A., Askin, R.A., Miller, M.F., Babcock, L.E., 2003a. Reevaluation of the timing and extent of late Paleozoic glaciation in Gondwana: Role of the Transantarctic Mountains. *Geology* 31, 977–980.

- Isbell, J.L., Miller, M.F., Wolfe, K.L., Lenaker, P.A., 2003b, Timing of late Paleozoic glaciation in Gondwana: was glaciation responsible for the development of northern hemisphere cyclothems? In: Chan, M.A., Archer, A.W., (Eds.), *Extreme depositional environments: mega end members in geologic time*. Geological Society of America Special Paper 370, 5–24.
- Isbell, J.L., Cole, D.I., Catuneanu, O., 2008a. Carboniferous-Permian glaciation in the main Karoo Basin, South Africa; stratigraphy, depositional controls, and glacial dynamics. In: Fielding, C.R., Frank, T.D., Isbell, J.L., (Eds.), *Resolving the Late Paleozoic Ice Age in Time and Space*. Geological Society of America Special Paper 441, 71–82.
- Isbell, J.L., Fraiser, M.L., Henry, L.C., 2008b. Examining the complexity of environmental change during the late Paleozoic and early Mesozoic. *Palaios* 23, 267–269.
- Jones, B., Manning, D.A.C., 1994. Comparison of geochemical indices used for the interpretation of palaeoredox conditions in ancient mudstones. *Chemical Geology* 111, 111–129.
- Koukharsky, M., Kleiman, L., Etcheverría, M., Quenardelle, S., Bercowski, F., 2009. Upper Carboniferous retroarc volcanism with submarine and subaerial facies at the western Gondwana margin of Argentina. *Journal of South American Earth Sciences* 27, 299–308.
- Lamplugh, G.W., 1911. On the shelly moraine of the Sefström glacier and other Spitsbergen phenomena illustrative of British glacial conditions. *Proceedings of the Yorkshire Geological Society* 17, 216–241.
- Laskar, B., Mitra, N.D., 1976. Paleoclimatic vicissitudes in India during Lower Gondwana sedimentation. *Geophytology* 6, 162–169.
- Lawver, L.A., Dalziel, I.W.D., Norton, I.O., Gahagan, L.M., 2008. The Plates 2007 Atlas of Plate Reconstructions (750 Ma to Present Day), Plates Progress Report No. 305-0307, University of Texas Technical Report No. 195, 160 pp.
- Lech, R.R., Buatois, L.A., 1990. Trazas fósiles del Pérmico Marino de la Precordillera Mendocina, República Argentina. V Congreso Argentino de Paleontología y bioestratigrafía, Actas I, 97–102.
- Lech, R.R., 2002. Consideraciones sobre la edad de la Formación Agua de Jagüel (Carbonífero superior-Pérmico inferior de Mendoza, Argentina. *Ameghiniana* 23, 57–60.
- Limarino, C.O., Césari, S.N., Net, L.I., Marensi, S.A., Gutiérrez, P.R., Tripaldi, A., 2002. The Upper Carboniferous postglacial transgression in the Paganzo and Río



- Blanco Basins (northwestern Argentina): Facies and stratigraphic significance. *Journal of South American Earth Sciences* 15, 445–460.
- Limarino, C.O., Spalletti, L.A., 2006. Paleogeography of the Upper Paleozoic basins of southern South America: An overview. *Journal of South American Earth Sciences* 22, 134–155.
- Limarino, C., Tripaldi, A., Marensi, S., Fauqué, L., 2006. Tectonic, sea level, and climatic controls on late Paleozoic sedimentation in the western basins of Argentina. *Journal of South American Earth Sciences* 33, 205–226.
- López Gamundí, O. R., 1991. Thin-bedded diamictites in the glacial-marine Hoyada Verde Formation (Carboniferous), Calingasta-Uspallata Basin, western Argentina; a discussion on the emplacement conditions of subaqueous cohesive debris flows: *Sedimentary Geology*, v. 73, p. 247–255.
- López Gamundí, O.R., 1997. Glacial-postglacial transition in the late Paleozoic basins of southern South America. In: Martini, I.P., (Ed.), *Late Glacial and Postglacial Environmental Changes: Quaternary, Carboniferous-Permian, and Proterozoic*. Oxford, UK, Oxford University Press, 147–168.
- López Gamundí, O.R., Martínez, M., 2000. Evidence of glacial abrasion in the Calingasta-Uspallata and western Paganzo Basins, mid-Carboniferous of western Argentina. *Palaeogeography, Palaeoclimatology, Palaeoecology* 159, 145–165.
- Martin, J.R., Redfern, J., Aitken, J.F., 2008. A regional overview of the late Paleozoic glaciation in Oman. In: Fielding, C.R., Frank, T.D., and Isbell, J.L., (Eds.), *Resolving the Late Paleozoic Ice Age in Time and Space*. Geological Society of America Special Publication., 175–186.
- McHenry, L.J., 2009. Element mobility during zeolitic and argillic alteration of volcanic ash in a closed-basin lacustrine environment: Case study Olduvai Gorge, Tanzania. *Chemical Geology* 265, 540–552.
- Middleton, G.V., 1970. Experimental studies related to problems of flysch sedimentation. In: Lajoie, J. (Ed.), *Flysch Sedimentology in North America*. Geological Association of Canada Special Paper 7, 253–272.
- Moncrieff, A.C.M., 1989. Classification of poorly-sorted sedimentary rocks. *Sedimentary Geology* 65, 191–194.
- Moncrieff, A.C.M., Hambrey, M.J., 1990. Marginal-marine glacial sedimentation in the late Precambrian succession of East Greenland. In: Dowdeswell, J.A., Scourse, J.D. (Eds.), *Glacial-marine Environments: Processes and Sediments*. Special Publication of the Geological Society 53, 387–410.

- Montañez, I., Soreghan, G.S., 2006. Earth's fickle climate. *Geotimes* 51, 24–27.
- Montañez, I.P., Tabor, N.J., Niemeier, D., DiMichele, W.A., Frank, T.D., Fielding, C.R., Isbell, J.L., Birgenheir, L.P., and Rygel, M.C., 2007. CO<sub>2</sub>-forced climate and vegetative instability during late Paleozoic deglaciation. *Science* 315, 87–91.
- Mulder, T., Alexander, J., 2001. The physical character of subaqueous sedimentary density flows and their deposits. *Sedimentology* 48, 269–299.
- Ovenshine, T.A., 1970. Observations of iceberg rafting in Glacier Bay, Alaska, and the identification of ancient ice-rafted deposits. *Geological Society of America Bulletin* 81, 891–894.
- Parsons, J.D., Whipple, K.X., Simoni, A., 2001. Experimental study of the grain-flow, fluid-mud transition in debris flows. *Journal of Geology* 109, 427–447.
- Pazos, P.J., 2002. The Late Carboniferous glacial to postglacial transition: facies and sequence stratigraphy, western Paganzo Basin, Argentina. *Gondwana Research* 5, 467–487.
- Pazos, P.J., 2007. Cyclostratigraphy during the Carboniferous glaciations in central western Argentina: glacial ageism and tectonic framework. In: Iannuzzi, R., Boardman, D.R. (Eds.), *Problems in Western Gondwana Geology I*. Gramado, Brasil, pp. 108–114.
- Powell, R.D., 1981. A model for sedimentation by tidewater glaciers. *Annals of Glaciology* 2, 129–134.
- Powell, R.D., 1983. Glacial-marine sedimentation processes and lithofacies of temperate tidewater glaciers, Glacier Bay, Alaska. In: Molnia, B.F. (Ed.), *Glacial-Marine Sedimentation*. Plenum Press, New York, 185–232.
- Powell, R.D., 1990. Glacimarine processes at grounding-line fans and their growth to ice-contact deltas. In: Dowdeswell, J.A., Scourse, J.D. (Eds.), *Glacimarine Environments: processes and sediments*. Geological Society Special Publication 53, 53–73.
- Powell, R.D., Cowan, E.A., 1986. Depositional processes at McBride Inlet and Riggs glacier. In: Anderson, P.G., Goldthwait, R.P., McKenzie, G.D. (Eds.), *Observed processes of glacial deposition in Glacier Bay, Alaska*. Ohio State University, Institute of Polar Studies, Miscellaneous Publications 256, 140–156.
- Powell, R.D., Molnia, B.F., 1989. Glacimarine sedimentary processes, facies, and morphology of south-southeast Alaska shelf and fjords. *Marine Geology* 85, 359–390.

- Powell, R.D., Cooper, J.M., 2002. A glacial sequence stratigraphic model for temperate, glaciated continental shelves. In: Dowdeswell, J.A., Ó Cofaigh, C. (Eds.), *Glacier-influenced sedimentation on high-latitude continental margins*. Geological Society, London, Special Publications 203, 215–244.
- Powell, R.D., Domack, E., 2002. Modern glacimarine environments. In: Menzies, J. (Ed.) *Modern and past glacial environments*. Oxford, Butterworth-Heinemann Ltd., 361–389.
- Powell, W., 2009. Comparison of geochemical and distinctive mineralogical features associated with the Kinzers and Burgess Shale formations and their associated units. *Palaeogeography, Palaeoclimatology, Palaeoecology* 277, 127–140.
- Rais, P., Louis-Schmid, B., Bernasconi, S.M., Reusser, E., Weissert, H., 2008. Distribution of authigenic albites in a limestone succession of the Helvetic Domain, eastern Switzerland. *Swiss Journal of Geosciences* 101, 99–106.
- Ramos, V.A., Jordan, T.E., Allmendinger, R.W., Kay, S.M., Cortes, J.M., Palma, M.A., 1984. Chilenia; un terreno alóctono en la evolución Paleozoica de los Andes centrales. *Actas del Congreso Geológico Argentino* 2, 84–106.
- Ramos, V.A., Jordan, T.E., Allmendinger, R.W., Mpodozis, M.C., Kay, S.M., Cortes, J.M., Palma, M., 1986. Paleozoic terranes of the central Argentine–Chilean Andes. *Tectonics* 5, 855–880.
- Rocha Campos, A.C., dos Santos, P.R., Canuto, J.R., 2008. Late Paleozoic glacial deposits of Brazil; Parana Basin. In: Fielding, C.R., Frank, T.D., Isbell, J.L., (Eds.), *Resolving the Late Paleozoic Ice Age in Time and Space*. Geological Society of America Special Paper 441, 97–114.
- Rygel, M.C., Fielding, C.R., Frank, T.D., Birgenheier, L.P., 2008. The magnitude of late Paleozoic glacioeustatic fluctuations: a synthesis. *Journal of Sedimentary Research* 78, 500–511.
- Scheffler, K., Hoernes, S., Schwark, L., 2003. Global changes during Carboniferous–Permian glaciation of Gondwana: Linking polar and equatorial climate evolution by geochemical proxies. *Geology* 31, 605–608.
- Scheffler, K., Buehmann, D., Schwark, L., 2006. Analysis of late Palaeozoic glacial to postglacial sedimentary successions in South Africa by geochemical proxies – Response to climate evolution and sedimentary environment. *Palaeogeography, Palaeoclimatology, Palaeoecology* 240, 184–203.
- Schneider, R.L., Mühlmann, H., Tommasi, E., Medeiros, R.A., Daemon, R.F., Nogueira, A.A., 1974. Revisão estratigráfica da Bacia do Paraná: Porto Alegre, XXVIII Congresso Brasileiro de Geologia, Anais 1, 41–65.

- Scotese, C.R., 1997. The PALEOMAP Project: paleogeographic atlas and plate tectonic software, Department of Geology, University of Texas, TX.
- Scotese, C.R. Barrett, S.F., 1990. Gondwana's movement over the South Pole during the Palaeozoic: evidence from lithological indicators of climate. In: McKerrow, W.S., Scotese, C.R. (Eds.), *Palaeozoic Palaeogeography and Biogeography*, Geological Society, London, Memoirs 12, 75–85.
- Scotese, C.R., Boucot, A.J., McKerrow, W.S., 1999. Gondwanan palaeogeography and palaeoclimatology. *Journal of African Earth Sciences*, 28: 99–114.
- Smith, L.M., Andrews, J.T., 2000. Sediment characteristics in iceberg dominated fjords, Kangerlussuaq region, East Greenland. *Sedimentary Geology* 130, 11–25.
- Stanley, S.M., Powell, M.G., 2003. Depressed rates of origination and extinction during the late Paleozoic ice age: A new state for the global marine ecosystem. *Geology* 31, 877–880.
- Stollhofen, H., Werner, M., Sanistreet, I.G., Armstrong, R.A., 2008. Single-zircon U-Pb dating of Carboniferous-Permian tuffs, Namibia, and the intercontinental deglaciation cycle framework. In: Fielding, C.R., Frank, T.D., Isbell, J.L., (Eds.), *Resolving the Late Paleozoic Ice Age in Time and Space*. Geological Society of America Special Paper 441, 83–96.
- Taboada, A.C., 1985. Estratigrafía Y contenido paleontológico de la Formación Agua del Jagüel, Pérmico Inferior de la Precordillera Mendocina. *Primeras Jornadas Sobre Geología de Precordillera*, San Juan Acta I, San Juan.
- Taboada, A.C., 2006. *Tivertonia* Archbold (Chonetidina, Brachiopoda) del Pérmico inferior de la subcuenca Calingasta-Uspallata, Precordillera argentina. *Ameghiniana* 43, 705–716.
- Tenesch, A., Hinman, N.W., Stanley, G., 2007. Geochemical and mineralogical insight into the environmental conditions for preservation of the Chengjiang biota. 12<sup>th</sup> International Conference on Water-Rock Interaction 12, 4 p.
- Thomas, G.S.P., Connell, R.J., 1985. Iceberg drop, dump, and grounding structures from Pleistocene glacio-lacustrine sediments, Scotland. *Journal of Sedimentary Petrology* 55, 243–249.
- Torsvik, T.H., Cocks, L.R.M., 2004. Earth geography from 400 to 250 Ma: a palaeomagnetic, faunal and facies review. *Journal of the Geological Society* 161, 555–572.
- Visser, J.N.J., 1994. The interpretation of massive rain-out and debris-flow diamictites

- from the glacial marine environment. In: Deynoux, M., Miller, J.M.G., Domack, E.W., Eyles, N., Fairchild, I.J., Young, G.M. (Eds.), *Earth's glacial record*. Cambridge University Press, Cambridge, p. 83–94.
- Visser, J.N.J., 1997. Deglaciation sequences in the Permo-Carboniferous Karoo and Kalahari basins of southern Africa: a tool in the analysis of cyclic glaciomarine basin fills. *Sedimentology* 44, 507–521.
- Wadell, H., 1932. Volume, shape and roundness of rock particles. *Journal of Geology* 40, 443–451.
- Wanless, H.R., Shepard, F.P., 1936. Sea level and climate changes related to late Paleozoic Cycles. *Geological Society of America Bulletin* 47, 1177–1206.
- Willems, B.A., Powell, R.D., Cowan, E.A., Jaeger, J., Trusel, L.D., 2009. A high-resolution record of advance/retreat phase glaciomarine sediments: implications in reconstructing glacial dynamics. *Geological Society of America Abstracts with Programs* 41, 71.
- Winsemann, J., Asprion, U., Meyer, T., Schramm, C., 2007. Facies characteristics of Middle Pleistocene (Saalian) ice-margin subaqueous fan and delta deposits, glacial Lake Leine, NW Germany. *Sedimentary Geology* 193, 105–129.
- Woodcock, N.H., 1976. Structural style in slump sheets: Ludlow Series, Powys, Wales. *Proceedings of the Geologists' Association* 87, 169–182.
- Woodworth-Lynas, C. M. T., Dowdeswell, J.A., 1994. Soft-sediment striated surfaces and massive diamicton facies produced by floating ice. In: *Earth's Glacial Record*. M. Deynoux, J. M. G. Miller, E. W. Domack, N. Eyles, I.J. Fairchild, G.M. Young (Eds.), Cambridge, U.K., Cambridge University Press, 241–259.
- Wopfner, H., Casshyap, S.M., 1997. Transition from freezing to subtropical climates in the Permo-Carboniferous of Afro-Arabia and India. In: Martini, I.P., (Ed.), *Late glacial and postglacial environmental changes: Quaternary, Carboniferous-Permian, and Proterozoic*. Oxford, U.K., Oxford University Press, 192–212.
- Ziegler, A.M., Hulver, M.L., Rowley, D.B., 1997. Permian World topography and climate. In: Martini, I.P., (Ed.), *Late glacial and postglacial environmental changes: Quaternary, Carboniferous-Permian, and Proterozoic*. Oxford, U.K., Oxford University Press, 111–146.

## **Chapter 4: The late Paleozoic El Imperial Formation, western Argentina: Glacial to post-glacial transition and stratigraphic correlations with arc-related basins in southwestern Gondwana**

Lindsey C. Henry<sup>\*a</sup>, John L. Isbell<sup>a</sup>, Carlos O. Limarino<sup>b</sup>

<sup>a</sup>Department of Geosciences, University of Wisconsin-Milwaukee, 3209 N. Maryland Avenue, Milwaukee, WI 53211-0413, USA

<sup>b</sup>Departamento de Ciencias Geológicas, Universidad de Buenos Aires, Pabellón 2, Ciudad Universitaria C1428EHA, Buenos Aires, Argentina

### **Abstract**

The El Imperial Formation of the San Rafael Basin records a succession of depositional environments during the latest Mississippian to earliest Permian that span before, during, and after the glaciation of west central Argentina. At the base of the formation, a restricted marine environment is recorded in mudstone containing marl and rippled and deformed sandstone beds. This unit, or sequence 1, is incised by a deltaic facies association composed of cross-bedded sandstone and conglomerate that form at least five stacked Gilbert deltas. The deltaic facies association grades upward into the glacially-influenced facies association, made up of stratified diamictite, mudstone with dropstones, and massive deformed sandstone, indicating deposition by wet-based tidewater glaciers that calved icebergs into the basin, with contributions from mass movement processes. The glacially-influenced facies association is overlain by mudstone and horizontally laminated and cross-bedded sandstone of the post-glacial open marine facies association, recording post-glacial transgression followed by relative sea level fall.

---

<sup>\*</sup> Corresponding author.

*Email addresses:* [christi9@uwm.edu](mailto:christi9@uwm.edu) (L.C. Henry), [jisbell@uwm.edu](mailto:jisbell@uwm.edu) (J.L. Isbell), [oscarlimarino@ciudad.com.ar](mailto:oscarlimarino@ciudad.com.ar) (C.O. Limarino), [lmchenry@uwm.edu](mailto:lmchenry@uwm.edu) (L.J. McHenry), [mfraiser@uwm.edu](mailto:mfraiser@uwm.edu) (M.L. Fraiser).

The deltaic, glacially-influenced, and post-glacial open marine facies associations comprise sequence 2. Sequence 2 is incised by conglomerate of the upper fluvial member, or sequence 3.

The strata of the El Imperial Formation are correlated to those of the other arc-related basins of western Argentina: Río Blanco, Calingasta–Uspallata, and Tepuel. A Bashkirian transgression and fluvial incision in the El Imperial Formation correlate with events in the Río Blanco and Calingasta–Uspallata Basins to the north, whereas glaciation continues to the south in the Tepuel Basin through the Early Permian. The deviating stratigraphic record of the Tepuel Basin may be the result of its higher latitudinal position during the Pennsylvanian–Early Permian and higher altitude due to either tectonic convergence of the Patagonian microplate or convergence along the Panthalassan margin of southwestern Gondwana.

## **1. Introduction**

The late Paleozoic ice age (LPIA) was a time of protracted icehouse conditions, during which alternating glacial and non-glacial intervals occurred in Gondwana (Isbell et al., 2003), lasting for 1-10 m.y. and separated by non-glacial intervals of similar duration (Fielding et al., 2008a,b; Gulbranson et al., 2010). The LPIA began in the Viséan, with glacial events identified in western Argentina, Brazil, and possibly South Africa (Caputo, 1985; Streel and Theron, 1999; Caputo et al., 2008; Isbell et al., 2008a; Rocha Campos et al., 2008; Gulbranson et al., 2010; Taboada, 2010). During the Serpukhovian–Bashkirian, glaciers expanded in western South America (López Gamundí, 1997) and first appeared in eastern Australia (Fielding et al., 2008a,b). In the Gzhelian to Sakmarian, widespread glaciation occurred across Gondwana in southern

Argentina, Brazil, Africa, India, and Australia (Laskar and Mitra, 1976; Collinson et al., 1994; López Gamundí, 1997; Visser, 1997; Fielding et al., 2008a,b; Isbell et al., 2008a,b; Mory et al., 2008; Rocha Campos et al., 2008; Taboada, 2010). Finally, from the late Sakmarian to the Capitanian, glacial centers were located only in Australia (cf. Fielding et al., 2008a,b; Mory et al., 2008).

The El Imperial Formation records glaciation over western Argentina in the San Rafael Basin (Fig. 21) during the Bashkirian and the subsequent transition to post-glacial conditions. Glaciation in western Argentina marked the beginning of the LPIA, but glaciation did not return to west central Argentina after the Bashkirian (López Gamundí, 1997; Limarino et al., 2006; Isbell et al., 2012). In contrast, glacial intervals continued to the south in the Tepuel Basin into the late Sakmarian-earliest Artinskian, coeval with the P2 glacial interval in eastern Australia (Fielding et al., 2008a; Taboada, 2010). Therefore, the El Imperial Formation provides an opportunity to compare the glacial records across western Argentina, because the San Rafael Basin lies between the Viséan and Serpukhovian to Bashkirian glacigenic formations in the Protoprecordilleran basins to the north and the Viséan to Artinskian glacial intervals recorded in the Tepuel Basin to the south (Fig. 21). A stratigraphic comparison of the basins of western Argentina allows for correlation of the glacial to post-glacial transition and other stratigraphic and tectonic events.

It is also worth noting that to the east in Brazil, glaciation continued later in the Pennsylvanian than it did in west central Argentina (Rocha Campos et al., 2008). The Itararé Group in the Paraná Basin may contain glacigenic deposits spanning the Late Mississippian to the latest Pennsylvanian (Rocha Campos et al., 2008), although recent



age dating of strata overlying glacial deposits in the Paraná Basin suggests that glaciation may have continued into the mid-Early Permian (cf. Mori et al., 2012). However, the focus of this paper is on the correlation of strata within “arc-related basins” of western Argentina (Limarino and Spalletti, 2006) because of their proximity and similar basinal settings.

The main goals of this paper are to 1) provide a sedimentologic analysis of the lower and middle units of the El Imperial Formation deposited before, during, and after the glacial maximum for the San Rafael Basin, 2) characterize the regional glacial depositional environments, and 3) compare and correlate depositional and tectonic events in the San Rafael Basin to the records from the Río Blanco and Calingasta–Uspallata Basins to the north and the Tepuel Basin to the south. Knitting the El Imperial Formation into the stratigraphic framework of western Argentina will improve our understanding of the environmental mechanisms occurring along western Gondwana during the LPIA and help to refine the understanding of glacial–non-glacial intervals of that region.

## **2. San Rafael Basin and neighboring western Gondwana basins**

The San Rafael Basin was located on the western margin of Gondwana at ~50° S paleolatitude during the Carboniferous–Early Permian (Torsvik and Cocks, 2004; Blakey, 2008). The basin is elongated in a NW–SE orientation, bounded by the Sierras Pampeanas/Pampean Arch/Chadileuvú Block to the east and south and a volcanic arc to the west (Fig. 21; López Gamundí et al., 1994; Andreis and Archangelsky, 1996). The basin occurs on the Cuyania terrane, which accreted to the Pampia terrane along the western margin of Gondwana in the Ordovician (Abre et al., 2011). The San Rafael and Las Matras blocks occur in the southern extension of the Cuyania terrane (Cingolani et

al., 2003; Sato et al., 2004). To the east, the Sierras Pampeanas/Pampean Arch–Chadileuvú Block–North Patagonian Massif complex was uplifted in the Ordovician during the Famatinian orogeny, and separates the San Rafael Basin from the craton proper (Caminos et al., 1988; López Gamundí et al., 1994; Azcuy et al., 1999). The western sector of the San Rafael Basin (studied in this paper) is a backarc basin adjacent to the magmatic arc that ran along west central Argentina in the late Paleozoic, and the eastern sector is a retroarc basin in a more stable tectonic setting (Limarino and Spalletti, 2006).

The basin is floored by Precambrian granites and contains deformed pre-Carboniferous sedimentary rocks, the top of which is the Devonian La Horqueta Formation, composed of lightly metamorphosed shale and sandstone (García, 1996; Azcuy et al., 1999). These strata were deformed and uplifted by the Chañic orogeny in the Late Devonian–earliest Carboniferous, which created the angular unconformity that separates the La Horqueta Formation from the overlying El Imperial Formation (López Gamundí et al., 1994).

Overlying the El Imperial Formation is the Cochicó Group, which consists of fluvial and eolian deposits that grade upwards into volcanic rocks and pyroclastic deposits (Stinco, 1986; López Gamundí et al., 1994). This volcanism was caused by a magmatic arc along western South America that is represented by strata known as the Choiyoi Group. Choiyoi volcanism occurred in two phases: first in the Early Permian as a large volcanic arc related to the subduction of the paleo-Pacific plate under the western margin of Gondwana, and then in the Late Permian to Early Triassic under an extensional tectonic regime (Nasi and Sepúlveda, 1986; López Gamundí et al., 1994). Above the

Cochicó Group are volcanic breccias of the Cerro Carrizalito Group that formed during the Late Permian–Early Triassic in the second phase of Choiyoi volcanism (Toubes and Spikermann, 1976; Linares et al., 1979).

To the north of the San Rafael Basin is the Protoprecordillera, a fold-thrust belt that also formed during the Chanic orogeny. The uplift of the Protoprecordillera and the tectonic extension that followed the Río Blanco tectonic event in the Late Mississippian (Viséan; Taboada, 2010) created three surrounding basins: the Río Blanco, Calingasta–Uspallata, and Paganzo Basins (Fig. 21; Limarino et al., 2006). The Protoprecordillera housed alpine glaciers in the Viséan, recorded by glacial diamictites of the Jagüel/Cortaderas Formation in the Río Blanco Basin (Perez Loinaze, 2008; Gulbranson et al., 2010; Taboada, 2010; Césari et al., 2011), and also in the Serpukhovian–Bashkirian, indicated by glacial deposits preserved in the Río Blanco, Calingasta–Uspallata, and Paganzo Basins (cf. López Gamundí et al., 1994; Limarino and Spalletti, 2006; Henry et al., 2008, 2010; Limarino et al., 2012). The Protoprecordillera collapsed in the early Pennsylvanian due to tectonic extension and a westward shift in the location of subduction along the Panthalassan margin (López Gamundí et al., 1994; Limarino et al., 2006; Isbell et al., 2012). This loss of altitude coincides with deglaciation in west central Argentina (Isbell et al., 2012).

The Tepuel Basin experienced a much different tectonic development than the San Rafael Basin and the Protoprecordilleran basins to the north. The Tepuel Basin formed on the Patagonian crustal block, which accreted first to the Antarctic Peninsula to the south in the mid- to Late Carboniferous, and then collided with Gondwana during the Early–Mid-Permian (Ramos, 2008). A competing hypothesis, that Patagonia originally

existed within Gondwana and did not accrete as an allochthonous terrane, has been proposed (e.g., Dalla Salda et al., 1990), however, recent geophysical, structural, and age dating studies support the accretion of Patagonia to Gondwana as an allochthonous terrane (Pankhurst et al., 2006; Ramos, 2008; Rapalini et al., 2010). The Tepuel Basin may have developed as a forearc basin adjacent to the western magmatic arc within Patagonia (Ramos, 2008). In the Tepuel Basin, at least six glacial intervals occurred from the Tournaisian to the Artinskian (Taboada, 2010; Isbell et al., 2011).

### 3. El Imperial Formation

The El Imperial Formation occurs in the western portion of the San Rafael Basin (Fig. 21), and the measured section is from the Atuel Canyon, as roadcuts along the Atuel River adjacent to Highway 173, 35 km southwest of the city of San Rafael, and as exposures in tributary canyons (Fig. 22). Palynology studies have dated the El Imperial Formation as latest Mississippian (Serpukhovian)–Early Permian (Asselian) based on the presence of flora of the *Raistrickia densa*–*Convolutispora muriornata* (DM) and *Fusacolopites fusus*–*Vittatina subsaccata* (FS) biozones (García, 1996; Césari and Gutiérrez, 2000; Césari et al., 2011). The El Imperial Formation is composed of three units: 1. mudstones and rippled and massive sandstones (Pazos et al., 2007), 2. deltaic sandstones, glaciogenic diamictites, and massive sandstones and mudstones (Arias and Azcuy, 1986; Espejo and López Gamundí, 1994; Pazos et al., 2007), and 3. fluvial sandstones and conglomerates (Arias and Azcuy, 1986; Espejo and López Gamundí, 1994). The lower two units were measured for this study.

Previously published stratigraphic sections of the El Imperial Formation vary widely from each other and the section provided herein (cf. Espejo and López Gamundí,

1994; López Gamundí et al., 1994; Loss, 2006; Pazos et al., 2007). These discrepancies are the result of the irregular floor of the paleovalley where the El Imperial Formation was deposited (Pazos et al., 2007), lateral facies variability inherent in glacimarine environments (Powell and Domack, 2002), and the broad distribution of the formation in the Atuel and Rio Diamante Canyons. In this study, diamictites were observed directly overlying the Devonian basement (Fig. 23) and also within a succession of sandstone and mudstone (167–177 m, Fig. 24) overlying stacked Gilbert deltas. The diamictite in Fig. 23 is probably stratigraphically equivalent to 155 to 180 m in the measured section in Fig. 24, where there are indicators of glacial affinity, such as dropstones, stratified diamictite, and thinly bedded fine-grained sandstones deposited by meltwater plumes. Above 180 m, there is an absence of glacial indicators, suggesting glacial retreat from the marine basin (Fig. 24).

#### **4. Sedimentology of the El Imperial Formation**

The lower two units of the El Imperial Formation occur in a paleovalley (Pazos et al., 2007) cut into the positive area that occurs to the north of the North Patagonian Massif (Fig. 21). The paleovalley is floored by steeply dipping metamorphosed green shale and thin sandstone beds of the La Horqueta Formation that exhibits an irregular, often angular surface, with relief of 75–100 m (Fig. 25). Strata of the El Imperial Formation onlap onto the paleovalley floor, forming an angular unconformity. Both units (sequences) directly overlie and onlap onto the La Horqueta bedrock at different locations within the paleovalley, the result of deposition within an irregularly-floored sub-basin. Additionally, irregularly shaped lenses of conglomerate 3–5 m long drape the eastern wall of the paleovalley and may have formed from scree lining the bedrock (Fig. 26). The

conglomerate is clast-supported, clasts are angular, and some clasts are composed of metamorphosed shale from the La Horqueta Formation.

The measured section for the El Imperial Formation was studied along Highway 173 at S 34° 58.31', W 68° 36.73' (Fig. 24), on both sides of the Atuel River, and an additional section of well exposed glacial-genic sediments (Fig. 23) was accessed along a northwest-flowing tributary to the Atuel River off of Highway 173 located at S 34° 58.40', W 68° 36.58'. Pazos et al. (2007) separated the lower glacial-deltaic member of the El Imperial Formation (cf. Espejo and López Gamundí, 1994) into a lower unit and a middle unit to reflect the divergent sedimentology of mudstones and fine sandstones at the base of the formation. We were able to access 108 m of this lower member (rather than 35 m as reported by Pazos et al., 2007) by working along a steep slope at S 34° 57.64', W 68° 36.82' on the west side of the Atuel River. In this analysis, the lower two units of the formation are divided into four facies associations: 1. restricted marine, 2. deltaic, 3. glacially-influenced, and 4. post-glacial open marine. The upper third unit is dominated by fluvial deposits of crossbedded medium- to coarse-grained sandstone (Espejo and López Gamundí, 1994) and rest on a regional truncation surface. Descriptions and interpretations of the four facies associations are presented below and in Table 1.

#### *4.1. Restricted marine facies association*

##### *4.1.1. Restricted marine facies association description*

The restricted marine facies association consists of claystone and siltstone, fine- to medium-grained sandstone, and paleosols. At the base of the formation, fine-grained massive sandstone containing rip-up clasts of metamorphosed shale lines the angular

unconformity with the La Horqueta Formation. Paleosols overlie this bed, occurring as 20–30 cm thick units with yellow and black horizons that contain root traces (Fig. 27A). However, faint bedding is present, and master horizons could not be distinguished, so the beds should be considered protosols (cf. Mack et al., 1993). Mudstone sharply overlies the paleosols, occurring as thinly bedded to massive, and many beds of clay coarsen up into silt or fine-grained sandstone. Some mudstone beds are deformed, showing load structures and disrupted or chaotic bedding, especially where squeezed between pods of sandstone (Fig. 27B). Within claystone are beds of marl 3–5 cm thick (Fig. 27C). Within the mudstone of this facies association, Pazos et al. (2007) identified *Diplichnites* and *Diplopodichnus* (arthropod locomotion traces) in siltstone, and *Archaeonassa* (possibly created by molluscs) in dark shale. Additionally, non-marine palynomorphs were identified.

Interbedded sandstone is fine-grained and occurs in beds 5–80 cm thick. Basal contacts of sandstone beds are sharp or erosional. Horizontal laminations and ripple cross-lamination also occur in sandstone. Ripples are asymmetrical, and climbing ripples also occur (Fig. 27D). Some beds show pipe, dish, and flame structures, diapirs, or deformed bedding. Some sandstone beds or pods (spheroids of sandstone surrounded by mudstone) are massive and internally deformed (Fig. 27E).

#### *4.1.2. Restricted marine facies association interpretation*

The fine-grained deposits and presence of limestone (marl) suggest that this facies association was deposited in a quiet marine setting, such as a restricted area of the paleovalley. At the base of the formation, rip-up clasts were derived from scree along the paleovalley wall. Above, the presence of two beds of paleosols indicates nonmarine

conditions that were later flooded. Overlying beds of deformed mudstone and sandstone beds and pods resulted from subaqueous deposition and slumping and sinking into water-saturated substrates with low cohesion (Allen, 1982; Shanmugam, 2006). Sandstone beds were deposited by density flows: massive beds suggest deposition by sandy debris flows, and beds with slight coarsening upward signatures, some containing ripple cross-stratification, suggest deposition by quasi-steady turbidity currents or reworking due to bottom currents (Mulder and Alexander, 2001; Shanmugam, 2006). Symmetrical ripples were observed in this unit by Pazos et al. (2007), restricting the water depth above storm wave base. No glacial indicators, such as dropstones or diamictite, were observed in this facies association, so glaciers may have been absent from the region, or at least absent from the paleovalley at that time.

The trace fossil assemblage supports a paleovalley or estuarine depositional environment with freshwater runoff adjacent to the sea (Pazos et al., 2007; Buatois et al., 2010). Additionally, *Diplopodichnus* was also observed in glacial marine strata by Schatz et al. (2011) in the Guandacol Formation in the Paganzo Basin. The presence of marl in the lower member is unequivocal in the steep slopes where we worked. Marl forms from sediment starvation and calcium carbonate deposition, and the presence of marl suggests a marine paleoenvironment (cf. Fernández Sevesso and Tankard, 1995).

## 4.2. Deltaic facies association

### 4.2.1. Deltaic facies association description

The deltaic facies association incises into the restricted marine succession and occurs from 108 to 155 m on the measured stratigraphic column (Fig. 24). A thin fluvial succession may sit on the incision surface, but steep slopes made these units inaccessible.



Horizontally laminated and cross-bedded medium-grained sandstone, conglomerate, and occasional interbedded siltstone compose the facies association. The sandstone predominantly occurs in foresets that are 1 cm–several m thick (Fig. 28A,B). Within the foresets, sandstone is medium-grained and displays horizontal lamination and some cross-stratification. At the base of the facies, the foresets interfinger with conglomerate, but otherwise sandstone beds have sharp basal contacts. Where beds are thicker (0.30–2 m thick), topsets and bottomsets are also apparent (Fig. 28B). Additionally, the average foreset dip is  $\sim 30^\circ$  in thicker beds. Paleocurrent analysis of foresets indicates variable dip directions, but most of the succession shows NNW paleoflow (Fig. 24). Interbedded with medium-grained sandstone is conglomerate with beds that range from 0.20 to 3 m in thickness, consisting of a matrix of fine to coarse sand and subrounded clasts up to 20 cm in diameter. Clast lithologies are mudstone, sandstone, and quartz. Basal contacts of conglomerate are erosive. Towards the top of the facies, sandstone foresets interbed with siltstone, until the foresets are replaced by massive, fine-grained sandstone, interbedded siltstone, and strata of the glacially-influenced facies association (Fig. 28C).

#### *4.2.2. Deltaic facies association interpretation*

The sandstone foresets represent prograding clinoforms forming stacked deltas; some deltas can be classified as Gilbert type deltas, but others do not have well-defined foresets and topsets, especially those that are interbedded with siltstone. At least five deltas can be distinguished (i.e., Fig. 28B) before interbedded siltstone appears in the section. The deltas most likely formed in a non-glacial environment, because 1) the angle of the foresets is higher than those in glacialmarine environments (cf. Postma, 1990; Benn, 1992), and 2) because there is no interbedded glacial diamictite or other glacial indicators

(i.e. dropstones, striations) interbedded with the deltaic facies. Steeply dipping foresets can be the result of friction-dominated processes at the river mouth where a river enters a shallow-water marine basin (Bhattacharya, 2006). Such deltas are also common as bay head deltas within areal restricted settings like flooded paleovalleys.

The erosive contact at the base of the deltaic facies association indicates a drop in base level and the start of a new depositional sequence (Fig. 28D; Loss, 2006). The presence of stacked deltas indicates that aggradation was occurring (cf. Posamentier and Allen, 1999; Coe, 2003; Catuneanu, 2006). The confined depositional environment of a paleovalley restricted the accommodation space, which fostered the ability of sediment supply to keep pace with relative sea level rise, allowing for the creation of multiple deltas.

At the top of the deltaic facies, the upwards transition to the glacially-influenced facies (Fig. 28C), characterized by a transition from thick packages of sand to interbedded siltstone and thin, fine-grained sandstone beds, most likely signals a rise in relative sea level. The relative sea level rise may have been caused by isostatic loading as the glacier encroached on the basin (cf. Boulton, 1990; Powell and Cooper, 2002), promoted by subsidence, and/or by a regional transgression. The Protoprecordilleran basins experienced transgression in the mid- to late Bashkirian, during the glacial interval in the El Imperial Formation, so the El Imperial Formation appears to record simultaneous glaciation and transgression during this relative sea-level rise (cf. Limarino et al., 2002; Henry et al., 2010).

### 4.3. *Glacially-influenced facies association*

#### 4.3.1. *Glacially-influenced facies association description*

The glacially-influenced facies association overlies La Horqueta bedrock (Fig. 23), and in the measured section, gradationally overlies the deltaic facies association (Figs. 24, 28C), occurring from 155 to ~180 m. The glacially-influenced facies association consists of stratified diamictite, sandstone, conglomerate, and siltstone. The stratified diamictite is weakly to well stratified (Fig. 29A, B), with beds ranging from 5 to 150 cm in thickness. Upper and lower contacts of beds are sharp. The stratified diamictite is matrix supported but clast rich, containing shale, sandstone, quartz, granite, and gneiss clasts in a matrix of muddy fine- to medium-grained sand. Clasts are subrounded on average, and clast fabric indicates aligned *a* axes (apparent, bed not disaggregated), and the dip of clasts is predominantly parallel to bedding. Fabric analysis on one bed indicated a preferred orientation (trend) of 290°–110° for the *a* axes (see rose diagram in Fig. 29C). Maximum clast size is 15 cm. In one area where stratified diamictite is in direct contact with the La Horqueta Formation, beds of stratified diamictite drape underlying bedrock and are stacked against each other like shingles (Fig. 29B, C). At this location, the top of the slate bedrock was a jagged surface draped by stratified diamictite, forming an angular unconformity. Stratified diamictite is interstratified with massive, deformed, fine-grained sandstone and conglomerate.

Sandstone occurs as laminated beds, as massive beds, and as deformed pods. Laminated sandstone is horizontally and cross-laminated, and climbing ripples also occur (Fig. 29D). Thin (5 mm–1 cm) beds of mudstone frequently occur in between beds of laminated sandstone. Massive sandstone is fine- to medium-grained, containing outsized

sandstone clasts up to 4 cm in diameter. Massive sandstone is interbedded with siltstone, either as pods floating in deformed siltstone (Fig. 29E), or as interbedded strata 20–30 cm thick. The sandstone pods are massive, composed of fine-grained sandstone, and 1–3 m in diameter with either a circular or teardrop shape. Interbedded massive sandstone and siltstone beds are deformed in one area into large fold noses, but internal structures are well preserved (Fig. 29F).

Conglomerate beds occur interbedded with diamictite and sandstone, and beds are 20–30 cm thick with erosive or sharp lower contacts. Conglomerate has a matrix of coarse sand and is clast supported, and clasts are subangular and predominantly shale, but quartz, sandstone, and granite are also present. Maximum clast size is 5 cm.

Conglomerate occurs as both massive and cross-bedded units.

Siltstone is interbedded with sandstone and diamictite and occurs as massive or very thinly bedded (1 cm thick beds). Some beds of massive siltstone are deformed. Within several beds of siltstone, lonestones 3–7 cm long bend and deform underlying bedding (Fig. 29G). Lonestones are highly weathered, and striations are not visible.

#### *4.3.2. Glacially-influenced facies association interpretation*

The glacially-influenced facies association was deposited by both a tidewater glacier that was calving icebergs into the water column and mass movement processes of slumps, slides, and debris flows. Calved icebergs shed clasts, sand, and mud onto the substrate, thereby depositing dropstones and stratified diamictite. Some beds of stratified diamictite also traveled downslope along the substrate in cohesive debris flows after iceberg deposition (cf. López Gamundí, 1991; Powell and Domack, 2002). Subsequent gravity flows of diamict formed the imbricate slices observed in Fig. 29B and C,

traveling as debris flows as far as frictional differences with the substrate permitted, then experiencing slumping, as indicated by variable dips of bedding surfaces (cf. López Gamundí, 1991; Shanmugam, 2006). Debris flows also oriented clast axes approximately parallel to bedding. The angular surface of the La Horqueta Formation indicates that it was not smoothed by overriding ice.

Clasts within diamictite indicate both local and extrabasinal provenance: intraformational pebbles of mud and sand may have been derived from the deltaic and restricted marine facies associations. Granite, gneiss, and quartz clasts were most likely derived from the North Patagonian Massif region and/or the Chadileuvú Block, which contains Paleozoic metamorphic rocks and granite intrusions (cf. Martínez Dopico et al., 2011). Detrital zircons in the El Imperial Formation dated as Cambrian (506 Ma and 528 Ma), during the Pampean orogeny (Rapela et al., 1998; Sims et al., 1998), suggest that the Sierras Pampeanas was also a sediment source (Rocha Campos et al., 2011). Additional possible sediment sources are plutonic and sedimentary rocks from the Las Matras and San Rafael Blocks (cf. Cingolani et al., 2003; Sato et al., 2004).

Rippled sandstone, interbedded mudstone, and horizontally laminated sandstone were deposited by subaqueous outwash from meltwater with fluctuating discharge rates (cf. Powell and Domack, 2002). Conglomerate also may have been deposited by a glaci-fluvial system, representing intervals of increased flow velocity, or by a subaqueous grain flow, as current structures are not present. Massive fine-grained sandstone beds and pods formed from sandy debris flows and slumps (cf. Mulder and Alexander, 2001; Shanmugam, 2006), although beds may also have been deposited by settling out of suspension from meltwater plumes (cf. Powell, 1990). Fold nose structures formed from

interbedded sandstone and siltstone sliding downslope and bending when frictional forces arrested the slide block (cf. Woodcock, 1976; López Gamundí, 1991; Shanmugam, 2006).

#### *4.4. Post-glacial open marine facies association*

##### *4.4.1. Post-glacial open marine facies association description*

The post-glacial open marine facies association gradationally overlies the glacially-influenced facies association, is composed of sandstone and mudstone, and features massive bedding, current structures, and soft-sediment deformation. Fine-grained sandstone beds are interbedded with claystone and siltstone and have predominantly massive bedding, although some beds exhibit deformed bedding, ripples, and horizontal lamination (Fig. 30A). Interbedded mudstone is massive or thinly bedded and often deformed into chaotic bedding (Fig. 30B). Beds of massive fine-grained sandstone become thinner upwards stratigraphically, from 60 cm thick beds on average to 20 cm thick beds which then pass upwards to predominantly deformed mudstone (180–210 m, Fig. 24).

Above this interval is a coarsening upwards succession of fine grained rippled or horizontally laminated sandstone beds that pass up into hummocky cross-bedded fine-grained sandstone (Fig. 30C) and trough cross-bedded medium-grained sandstone (228–297 m, Fig. 24). Siltstone beds 10–30 cm thick are interbedded. Fine-grained sandstone also contains climbing ripples and wavy bedding (Fig. 30D). The top of this facies association is eroded by conglomerate of the upper fluvial unit (Arias and Azcuy, 1986; Espejo, 1990).

#### *4.4.2. Post-glacial open marine facies association interpretation*

The post-glacial open marine facies association contains no apparent glacial indicators such as dropstones or diamictite and therefore signals the retreat of glaciers out of the water column, possibly from the region. The lower interval of fine-grained massive, horizontally laminated, and rippled sandstone and interbedded mudstone may have been deposited by sandy debris flows or traction currents from streams. Deformation in beds of sandstone and mudstone is the result of slumping and dewatering. The upwards thinning of beds suggests decreased input from streams or density flows, perhaps the result of increased relative sea level.

Above, the coarsening upwards succession indicates water depth from above storm wave base to normal wave base, potentially signaling a shallowing-upward cycle. This shallowing-upward cycle may represent part of a highstand systems tract or the distal record of a falling stage systems tract. Based on the presence of hummocky cross-bedding, water depth was probably  $\leq 20$  m within the paleovalley (cf. Boulton, 1990). Incision of the upper fluvial member of the El Imperial Formation indicates a drop in base level and the start of a new sedimentary sequence.

### **5. Discussion of depositional environments and sequence stratigraphy**

The El Imperial Formation records four distinct depositional environments within a paleovalley. During the first stage, the paleovalley was unglaciated, and low volumes of sediment entered the paleovalley, allowing marl to form within mudstone successions. The transition from paleosols with root traces to fine-grained sandstone and mudstone with marl suggests a rise in relative sea level, with a flooding surface located on top of the paleosols. The erosional contact between claystone at the top of the restricted marine

facies association and the conglomerate of the deltaic facies association represents a new depositional sequence (sequence 2, Fig. 28D; Loss, 2006), and this sequence persisted until the incision of the upper fluvial member. The conglomerate at the base of sequence 2 that incises the restricted marine facies association (Fig. 24) was likely deposited during a lowstand systems tract, and the overlying stacked deltas represent aggradation during relative sea level rise in the lowstand systems tract.

The transition to the glacially-influenced facies association indicates advancement of glaciers into the paleovalley and the glacial maximum of the region. It is possible that alpine glaciation occurred over the North Patagonian Massif and adjacent positive areas when other facies associations were being deposited, but the glacially influenced facies of the El Imperial Formation marks the growth of glaciers to sea level, shedding icebergs into the ocean that deposited dropstones and diamictite. This glacial maximum resulted from drivers such as the paleolatitude of the San Rafael Basin, low atmospheric  $p\text{CO}_2$  (cf. Montañez et al., 2007), and the altitude of the adjacent highlands that housed the glaciers, so that glaciers were able to nucleate above the equilibrium line altitude (cf. Isbell et al., 2012). To the north, the altitude of the Protoprecordillera allowed glaciers to nucleate and reach sea level in the Calingasta–Uspallata, Río Blanco, and Paganzo Basins in the late Serpukhovian–early Bashkirian (López Gamundí et al., 1994; Limarino et al., 2006; Isbell et al., 2012). In the Early Pennsylvanian, an extensional tectonic regime was established following the Chañic orogeny, which instigated the collapse of the Protoprecordillera (Limarino et al., 2006; Isbell et al., 2012). This loss of altitude was a major driver for the deglaciation of the Protoprecordillera (Isbell et al., 2012). A similar chain of events probably occurred in the upland areas adjacent to the El Imperial



Formation (the northwest region of the North Patagonian Massif), so that extensional tectonics in the Early Pennsylvanian resulted in a loss of altitude, corresponding with deglaciation. However, deglaciation in the two regions was somewhat diachronous. Deglaciation occurred in the Protoprecordilleran basins in the early to mid-Bashkirian (Limarino et al., 2002, 2006; Henry et al., 2008; Gulbranson et al., 2010). In the San Rafael Basin, deglaciation occurred in the late Bashkirian, based on the timing of the DM Subzone B identified in the middle unit of the El Imperial Formation (Pazos et al., 2007; Césari et al., 2011). Nevertheless, it is suggested here that the extensional tectonics in the Pennsylvanian that caused the collapse of the Protoprecordillera also caused relaxation of the highlands surrounding the San Rafael Basin in the late Bashkirian, contributing to deglaciation of the northwest highlands of the North Patagonian Massif.

The transition to the post-glacial open marine facies association indicates the retreat of glaciers out of the water column and possibly complete deglaciation of the highlands surrounding the San Rafael Basin, as glaciers never returned to the basin. Glaciation continued throughout the Pennsylvanian to the northeast in the Paraná Basin and to the south in the Tepuel Basin (Rocha Campos et al., 2008; Taboada, 2010), but the San Rafael Basin did not experience glaciation after the late Bashkirian.

Above the glacially-influenced facies association, a relative sea level rise continued, followed by a relative sea level fall, indicated by a coarsening upwards succession. This pattern of post-glacial transgressive deposits overlain by a coarsening upwards succession also occurs in the Protoprecordilleran basins, where glacial diamictites are overlain by Bashkirian–early Moscovian transgressive deposits, and in the western Paganzo Basin and surrounding area, transgressive mudstones are overlain by a

coarsening upwards succession (Limarino et al., 2002). For example, in the Calingasta–Uspallata Basin, the Hoyada Verde Formation contains late Serpukhovian–Bashkirian glacial diamictites that are overlain by transgressive mudstones containing *Levipustula* fauna. Transgressive deposits of marl-bearing mudstone overlying glacial deposits are also documented in the Agua de Jagüel and Tramojo Formations of the Calingasta–Uspallata Basin (Henry et al., 2010). Paleovalleys cut into the eastern side of the Protoprecordillera at Quebrada de las Lajas and Quebrada Grande (Fig. 21) contain glacial deposits that are overlain by mudstone, interpreted as relative sea-level rise, which are then overlain by sandstone (Quebrada Grande) or a coarsening upwards succession of sandstone and conglomerate (Quebrada de las Lajas), both interpreted as deposited during relative sea-level fall (Kneller et al., 2004; Dykstra et al., 2006). In the western Paganzo Basin, the Guandacol Formation contains post-glacial mudstones that grade upwards into thin, fine-grained sandstone interbedded with mudstone, which then grade upward into cross-bedded medium- to coarse-grained sandstone, interpreted as distal to proximal distributary mouth bars in front of a prograding delta (Limarino et al., 2002). That this succession is repeated in the El Imperial Formation suggests that the San Rafael Basin was experiencing similar depositional events controlled by similar tectonic activity as the Protoprecordilleran basins. Therefore, the late Bashkirian transgression may have occurred across west central Argentina, and not just in the Protoprecordillera region.

At the top of the post-glacial succession, a drop in base level occurs where the upper fluvial member of the El Imperial Formation incises the middle member, beginning sequence 3 in the formation (Espejo and López Gamundí, 1994; Loss, 2006). The coarsening upwards succession at the top of sequence 2 may indicate a highstand prior to

a relative sea level fall that resulted in the fluvial incision. The incision may also be synchronous to the fluvial incision at the base of the Pituil Formation (formerly known as the Tres Saltos Formation) that erodes into the Hoyada Verde Formation in the Calingasta–Uspallata Basin (Fig. 31), with both erosional surfaces representing a drop in relative sea level across west central Argentina.

## **6. Late Paleozoic stratigraphic framework of western Argentina**

Basins along the southwestern margin of Gondwana, in Chile, western Bolivia, Peru, and western Argentina, were clustered as “arc-related basins” by Limarino and Spalletti (2006), because they occur adjacent to the magmatic arc that formed along the active Panthalassan margin of southwestern Gondwana. Recent work on the Argentine basins (Río Blanco, Calingasta–Uspallata, El Imperial, Tepuel) has yielded new radiometric ages and biostratigraphic correlations (i.e., Gulbranson et al., 2010; Taboada, 2010; Césari et al., 2011; Rocha Campos et al., 2011), so herein the stratigraphy of the four arc-related basins of western Argentina is compared and correlated according to available data (Fig. 31).

### *6.1. Río Blanco Basin*

The Río Blanco Basin formed as a foreland basin adjacent to the Protoprecordillera during the Chanic orogeny and received marine and terrestrial sedimentation from the Early Carboniferous to the Permian (Scalabrini Ortiz, 1973). In the late Mississippian (middle Viséan?; Taboada, 2010), the Río Blanco tectonic event deformed older sediments and altered the basin into a backarc basin (Limarino et al., 2006). Following this event, sediments of the Paganzo Group were deposited in the Río Blanco Basin and in the Paganzo Basin to the east, composed of glacial, fluvio-

deltaic, and deep marine to shoreface successions (Limarino et al., 2006; Gulbranson et al., 2008, 2010).

The Río Blanco Basin provides a record of Viséan glaciation with diamictites in the Jagüel/Cortaderas Formation, dated by Gulbranson et al. (2010) as ~339–336 Ma by high-resolution U–Pb dating of zircons, and also with diamictites in the Malimán Formation (Limarino et al., 2006). These formations were deformed and eroded by the Río Blanco tectonic event. The overlying Paganzo Group outcrops in a number of locations (see Limarino et al., 2006), but the lower, middle, and upper members of the Río del Peñón Formation span deposition during the late Mississippian–Pennsylvanian (Gulbranson et al., 2010). The lower member contains deposits such as massive and stratified diamictite and pebbly mudstone (Gulbranson et al., 2008), and U–Pb dating has constrained these rocks as  $323\text{--}319.57 \pm 0.09$  Ma (late Serpukhovian–early Bashkirian; Gulbranson et al., 2010). Onset of the post-glacial transgression is dated as  $319.57 \pm 0.086$  Ma.

The middle unit of the Río del Peñón Formation unconformably overlies the lower unit and consists of fluvial sandstone overlain by fluvial/deltaic sandstone containing interbedded coal (Limarino et al., 2006; Gulbranson et al., 2010). The middle unit transitions to the upper unit within a transgressive facies that spans the mid-Bashkirian–early Moscovian (Limarino et al., 2002; Net and Limarino, 2006; Gulbranson et al., 2010). Above, the upper unit is composed of lower shoreface sandstones that grade into deltaic and terrestrial facies (Net and Limarino, 2006; Gulbranson et al., 2010). The middle and upper units of the Río del Peñón Formation contain the *Tivertonia*–*Streptorhynchus* fauna (Sabattini et al., 1990; Taboada, 2010), which is now considered

to be mid- to late Pennsylvanian in age (Césari et al., 2011). Choiyoi volcanism began in the Protoprecordilleran region in the Asselian, based on a rhyolite flow in the western Paganzo Basin dated as mid-Asselian ( $296.09 \pm 0.085$  Ma; Gulbranson et al., 2010).

## 6.2. Calingasta–Uspallata Basin

The Calingasta–Uspallata Basin experienced similar tectonic development to the Río Blanco Basin, as the two basins could be considered north and south sectors of the same elongated basin (cf. Azcuy et al., 1999). Glaciation began in the Calingasta–Uspallata Basin in the late Viséan, with glacial deposits including glacial diamictites and dropstone-bearing mudstones in the El Paso Formation that were associated with the *Rugosochonetes–Bulahdelia* brachiopod fauna that correlates to the late Viséan MQ palynozone (Perez Loinaze, 2007; Taboada, 2010; Césari et al., 2011). Glaciation also occurred in the late Serpukhovian–early Bashkirian in the El Paso, Hoyada Verde, Agua de Jagüel, and Tramojo Formations, featuring massive and stratified diamictite and mudstone with striated dropstones, dated with the NBG and *Levipustula* biozones (López Gamundí, 1991, 1997; Taboada, 1997, 2010; Limarino and Spalletti, 2006; Henry et al., 2008, 2010; Césari et al., 2011). A transgression began at the end of the glacial event, and marl-bearing mudstones up to 100 m thick were deposited in the Hoyada Verde, Agua de Jagüel, and Tramojo Formations (Limarino et al., 2002; Henry et al., 2008, 2010). The Hoyada Verde Formation is incised to a depth of 200+ m by the fluvial cross-bedded sandstones and conglomerates of the Pituil Formation, formerly known as the Tres Saltos Formation (Mésigos, 1953; Taboada, 1997, 2004; Buatois and Limarino, 2003). Above the fluvial incision, a short marine interval occurs in the Pituil Formation that contains

the *Marginovatia–Maemia* fauna of late Bashkirian–earliest Moscovian age (Taboada, 2010).

Arc magmatism began in the Calingasta–Uspallata Basin in the Pennsylvanian (Nasi and Sepúlveda, 1986; López Gamundí et al., 1994), with volcanism first occurring in the upper shallow marine sequence of the Agua de Jagüel Formation dated as  $307.2 \pm 5.2$  Ma (latest Moscovian; Lech, 2002; Koukharsky et al., 2009).

### 6.3. *San Rafael Basin*

The ages for some of the boundaries of the units of the El Imperial Formation are presently ambiguous. It is suggested here that the lower unit was deposited after the Río Blanco tectonic event in the Viséan that deformed Lower Carboniferous strata and created a regional unconformity (Limarino et al., 2006; Taboada, 2010), because the strata of the lower member are undeformed. The middle member of the El Imperial Formation is dated as mid- to late Bashkirian based on the presence of spores from the *R. densa–C. muriornata* (DM) Assemblage Biozone, Subzone B identified below the glacially-influenced facies association by Pazos et al. (2007). Therefore, the glacial interval in the El Imperial Formation occurred after the late Serpukhovian–early Bashkirian glacial interval in the Río Blanco and Calingasta–Uspallata Basins, but overlapped with the Bashkirian glacial interval in the Tepuel Basin (cf. Taboada, 2010). The glacial deposits in the El Imperial Formation (~25 m thick succession) are also thinner than the successions of glacial rocks 100–300 m thick in the Calingasta–Uspallata Basin (cf. Henry et al., 2010).

The upper member of the El Imperial Formation contains spores of the DM Subzone C, dated as mid- to late Pennsylvanian (Césari and Gutiérrez, 2000; Césari et al.,

2011). The top of the upper member of the El Imperial Formation is dated as  $297.2 \pm 5.3$  Ma (Asselian) with a U–Pb zircon age by Rocha Campos et al. (2011). Above the angular unconformity at the top of the upper member of the El Imperial Formation, volcanic rocks of the Cochicó Group are dated as Artinskian ( $281.4 \pm 2.5$  Ma). There is a pronounced delay in phase 1 Choiyoi volcanism in the San Rafael Basin compared to that in the Río Blanco Basin (Fig. 31), but this follows the pattern of volcanic arcs developing along the Panthalassan margin of Gondwana from west to east during the Early Permian to Triassic, the result of subduction and extension between the Panthalassa and Gondwana plates (Veevers et al., 1994; Henry et al., 2009).

#### *6.4. Tepuel Basin*

The Tepuel Basin provides a contrasting glacial history compared to the western Argentine basins to the north that experienced final deglaciation in the Bashkirian. Instead, the Valle Chico, Pampa de Tepuel, and Mojón de Hierro Formations record at least six glacial intervals ranging from 2 to 6 million years in duration that occurred from the Tournaisian to the Artinskian (Fig. 31; Taboada, 2010). The glacial intervals are indicated by massive and stratified diamictites and dropstones in mudstone, interpreted as deep water glacialmarine sedimentary environments, and dated using brachiopod fauna biozones (Taboada, 2010; Isbell et al., 2011). Presently, it appears that glaciation was diachronous among the Protoprecordilleran basins, the San Rafael, and the Tepuel Basin, with possible coeval glaciation during the Bashkirian in the Tepuel and San Rafael Basins. Choiyoi volcanism did not occur in the Tepuel region in the Permian (cf. Kay et al., 1989).

The multiple glacial intervals that extended from the Tournaisian to the Artinskian were likely the result of the paleolatitude and paleo-altitude of the Patagonian microplate. Patagonia was located near or within the south polar circle during much of the late Paleozoic (Blakey, 2008; Isbell et al., 2011; Taboada and Shi, 2011), and the position of South America within Gondwana rendered the Tepuel Basin closer to the South Pole than the San Rafael, Calingasta–Uspallata, or Río Blanco Basins in the Pennsylvanian–Permian (cf. Blakey, 2008). Additionally, the Patagonian microplate experienced convergence from both the Antarctic Peninsula in the south and Gondwana in the northeast (Ramos, 2008), which may have pushed the microplate into a higher altitude than that of the Río Blanco, Calingasta–Uspallata, and San Rafael Basins once Patagonia had accreted to Gondwana. This combination of factors, in addition to other drivers such as  $p\text{CO}_2$  and ocean circulation patterns (i.e., Jones et al., 2006; Montañez et al., 2007; Isbell et al., 2012), caused the divergent pattern of glacial intervals in the Tepuel Basin. Much remains to be investigated in the Tepuel Basin before its climactic and tectonic histories are well understood.

## **7. Conclusions**

The El Imperial Formation of the San Rafael Basin records a succession of depositional environments during the latest Mississippian to Early Permian that span before, during, and after the glaciation of west central Argentina. The El Imperial Formation is composed of a restricted marine facies association that is incised by a deltaic facies association that grades upward into the glacially-influenced facies association. The glacially-influenced facies association was deposited by tidewater glaciers emanating from highlands northwest of the North Patagonian Massif, in



conjunction with mass movement processes. The glacially-influenced facies association passes upward into the post-glacial open marine facies association that records a relative sea level rise overlain by a shallowing upward succession. These marine sediments are eroded by fluvial conglomerates.

The glacial event and subsequent deglaciation recorded in the San Rafael Basin was likely related to the late Serpukhovian–early Bashkirian glacial interval in the Protoprecordillera 300 km to the north. Deglaciation of the Protoprecordillera has been attributed, in part, to collapse of the Protoprecordillera due to regional tectonic extension resulting from the Río Blanco tectonic event (Limarino et al., 2006; Isbell et al., 2012), and thus it is proposed that deglaciation in the San Rafael Basin was the result of similar extensional tectonic forces causing loss of altitude in the highlands that supported glaciers.

To the south, the Tepuel Basin presents a contrasting record of glaciation, with at least six glacial intervals occurring from the Tournasian–Artinskian. The high paleolatitude of the Tepuel Basin and possibly higher altitude resulting from the convergence of the Patagonian crustal block with the Antarctic Peninsula and Gondwana are two drivers of protracted glaciation there.

Following deposition of post-glacial facies, Choiyoi volcanism began in the Río Blanco and Calingasta–Uspallata Basins in the Asselian (Gulbranson et al., 2010) and in the San Rafael Basin in the Artinskian (Rocha Campos et al., 2011) as the magmatic arc wrapped around southwestern Gondwana, but not erupting in Patagonia during the Permian (cf. Kay et al., 1989).

## **Acknowledgments**

Our sincere thanks go to Arturo Taboada and an anonymous reviewer for their helpful input on this manuscript. We thank Patricia Ciccioli and Ana Tedesco for help in the field and Erik Gulbranson for input on root trace interpretation. Financial support was provided by the Center of Latin American and Caribbean Studies, the Graduate School (Research Growth Initiative), the Advanced Opportunity Program, and the Department of Geosciences at UWM; the National Science Foundation (OISE-0825617, OPP-0943935, OPP-0944532); CONICET; the Wisconsin Geological Society; the Geological Society of America (GSA); GSA Coal Division; and the Universidad de Buenos Aires.

**Table**

Table 4. Facies descriptions and interpretations of the lower and middle units of the El Imperial Formation.

<b>Facies association</b>	<b>Unit</b>	<b>Lithologies</b>	<b>Sedimentary structures</b>	<b>Bed thickness</b>	<b>Interpreted mechanisms</b>	<b>Depositional environment</b>
Restricted marine	Lower	Claystone, siltstone, fine- and medium-grained sandstone, marl, paleosols	Load structures, disrupted/chaotic bedding, rip-up clasts, pipe, dish, and flame structures, massive bedding, asymmetrical ripples, climbing ripples, horizontal lamination, cross-bedding, root traces	Claystone: 1–5 cm Siltstone: 1–20 cm Sandstone: 5–80 cm Marl: 3–5 cm Paleosols: 20–30 cm	Sandy debris flows, turbidity currents, dewatering	Paleovalley, water depth above storm wave base
Deltaic	Middle	Medium-grained sandstone, conglomerate, siltstone	Horizontal laminations, cross-bedding, foresets, conglomerate pod	Sandstone: 1–50 cm Conglomerate: 20 cm – 2 m Siltstone: 2–5 cm	Prograding clinoforms forming stacked deltas, some Gilbert-type	Deltaic, non-glacial, probably bay head deltas
Glacially-influenced	Middle	Stratified diamictite, massive sandstone, laminated sandstone, conglomerate, siltstone	Diamictite imbricate slices, sandstone foresets, dropstones, sandstone pods, horizontal laminations, cross-bedding, deformed bedding	Stratified diamictite: 1–150 cm Massive sandstone: 20–30 cm Laminated sandstone: 0.20–1 m Conglomerate: 20–30 cm	Debris flows, iceberg rain-out, glacialfluvial outwash, slides, slumps	Proglacial, glacier(s) was tidewater and wet-based, shed icebergs into water column
Post-glacial	Middle	Massive sandstone,	Horizontal laminations,	Massive sandstone:	Sandy debris flows, traction	Non-glacial,

open marine		laminated sandstone, siltstone, claystone	cross-bedding, hummocky cross- stratification, asymmetrical ripples, deformed bedding, water escape structures	0.20–2 m Laminated sandstone: 0.50–2.5 m Siltstone: 1– 50 cm Claystone: 1–20 cm	currents, wave action, slumps	shoreface with water depth $\leq 20$ m
----------------	--	--	---	--	----------------------------------	---

## Figures

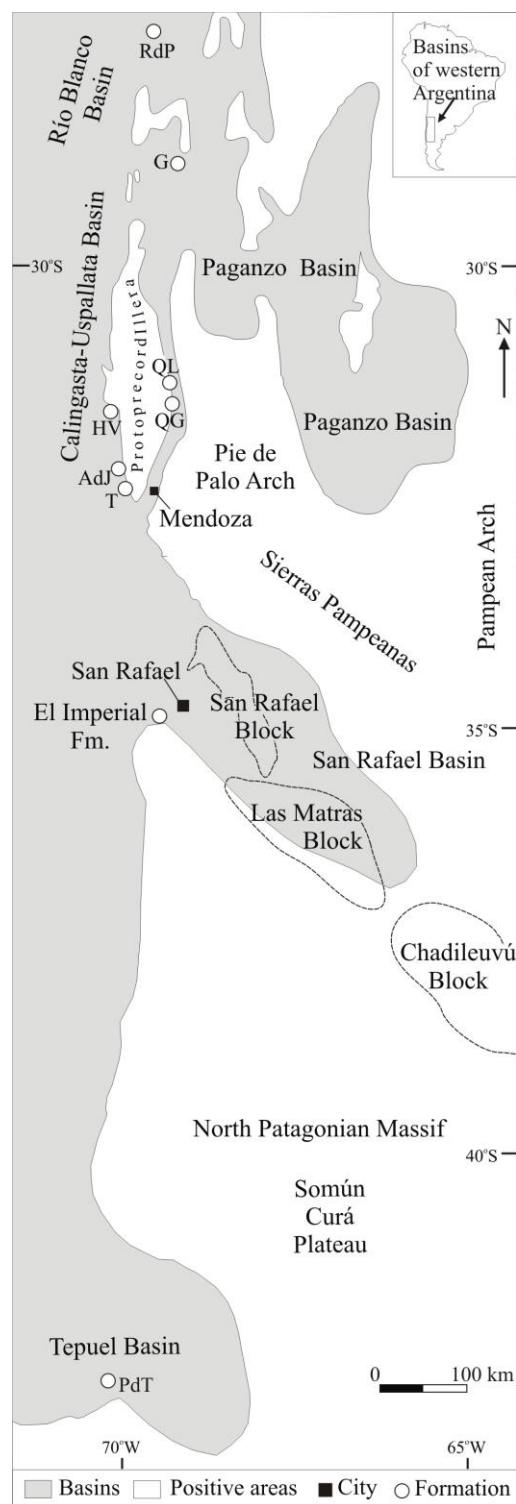


Figure 21. Map of the San Rafael Basin and other arc-related late Paleozoic basins in western Argentina (cf. López Gamundí et al., 1994; Sato et al., 2004; Limarino and Spalletti, 2006). Selected formations are denoted as RdP = Río del Peñón, G =

Guandacol, QL = Quebrada de las Lajas, QG = Quebrada Grande, HV = Hoyada Verde, AdJ = Agua del Jagüel, T = Tramojo, PdT = Pampa de Tepuel.

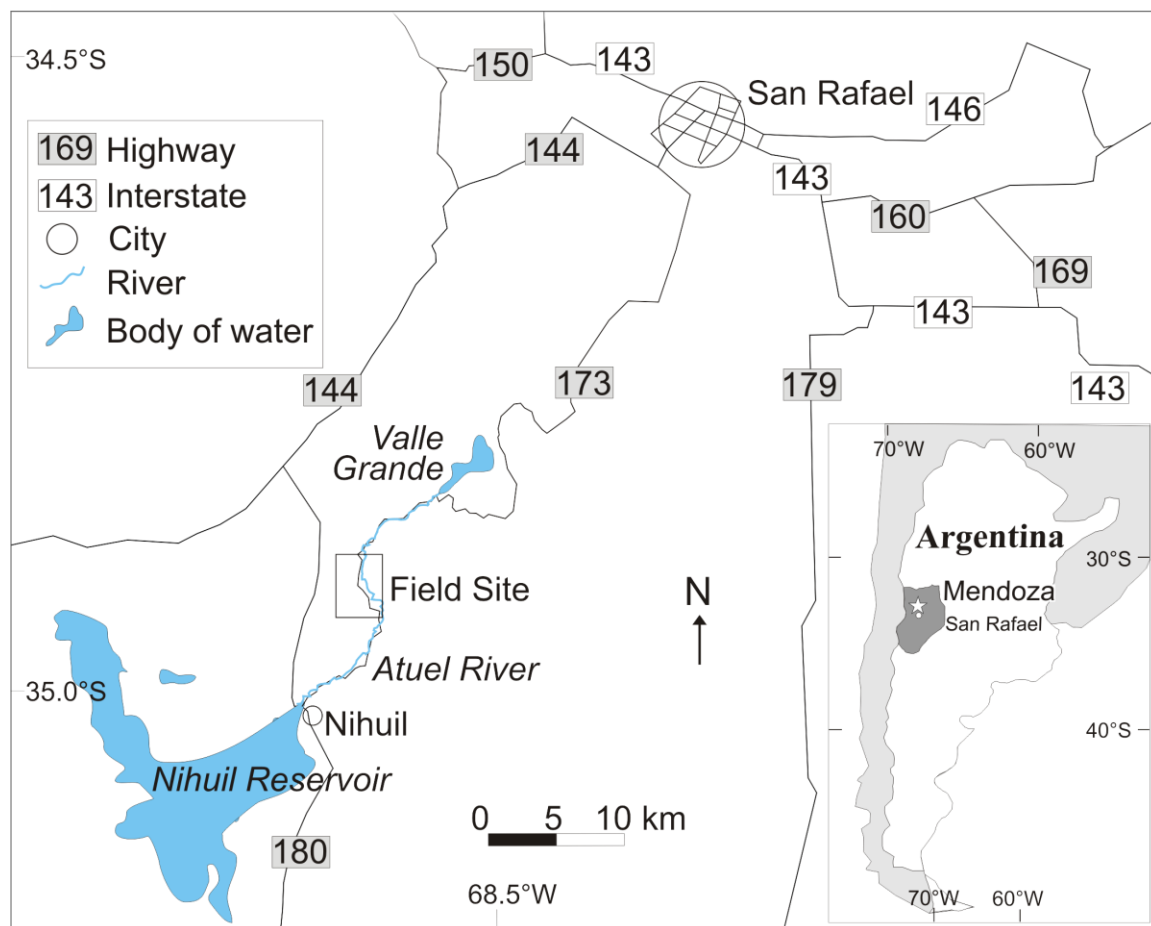


Figure 22 . Location map for the measured section of the El Imperial Formation southwest of San Rafael, Mendoza Province, Argentina.

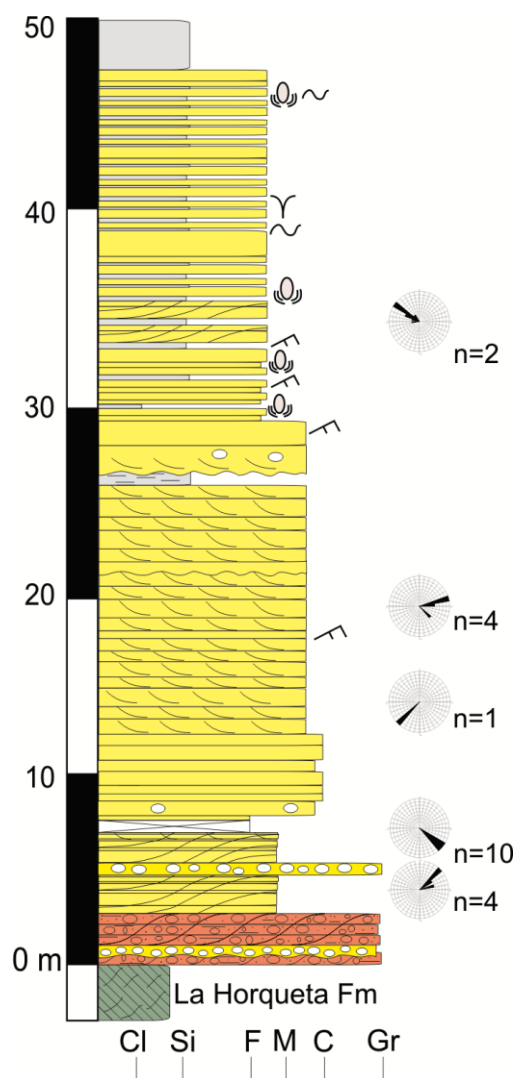


Figure 23. Contact of glacial deposits against Devonian bedrock from the middle unit of the El Imperial Formation. Section was measured on the west side of Highway 173, along a creek at S 34° 58.40', W 68° 36.58'. See Figure 24 for symbols key.

# El Imperial Formation: Lower and Middle Units

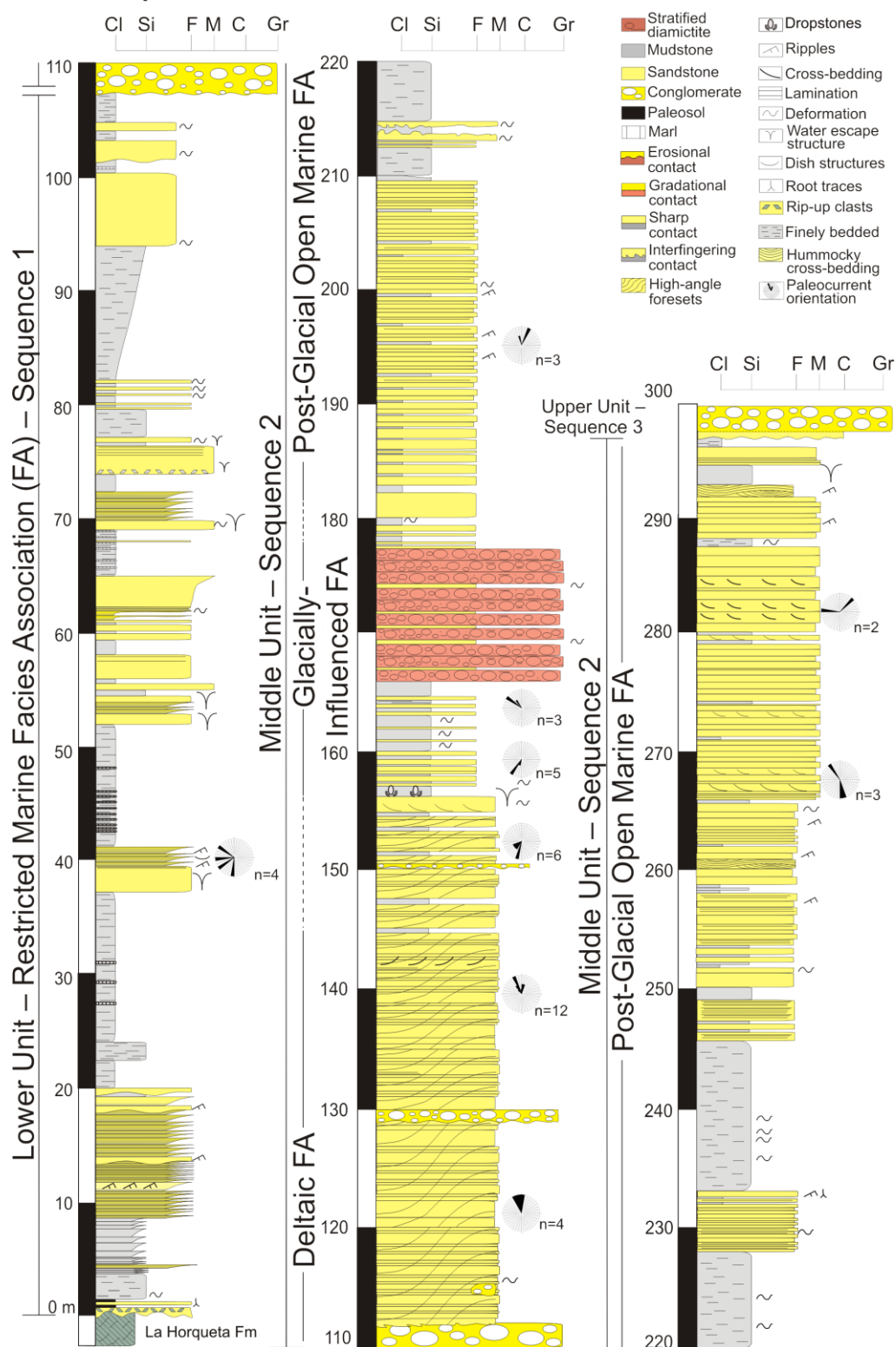


Figure 24. Measured section of the lower and middle units of the El Imperial Formation.





Figure 25. The lower two sequences of the El Imperial Formation occur in a paleovalley with 75–100 m relief that cuts into underlying Devonian bedrock (La Horqueta Formation). The present valley, incised by the Atuel River, is excavating the paleovalley. A close-up view of the paleo-scee is shown in Fig. 26.





Figure 26. Irregularly-shaped lenses of clast-supported conglomerate, with angular clasts derived from the underlying La Horqueta Formation, are interpreted as paleo-scree and line the walls of the paleovalley in places.

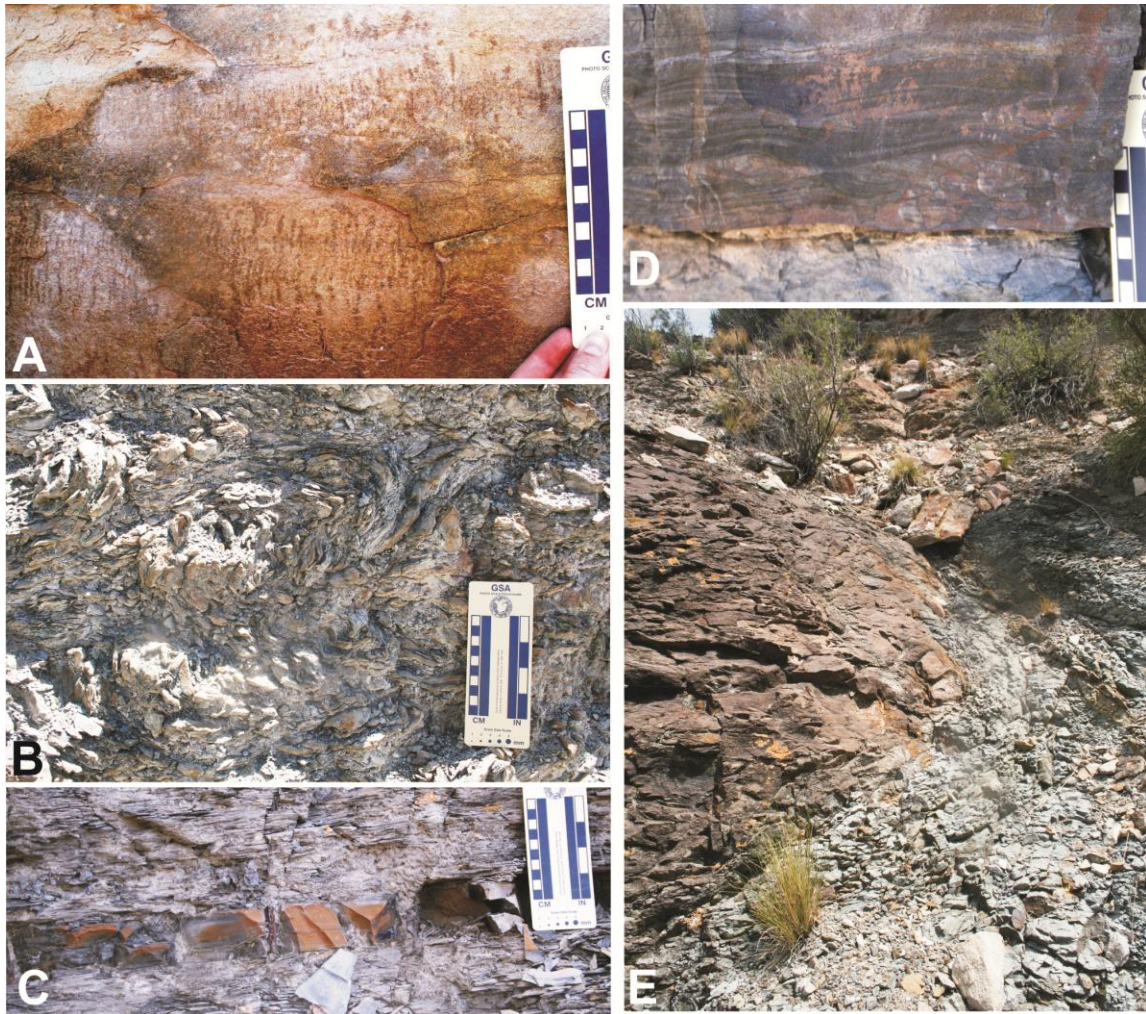


Figure 27. Restricted marine facies association. A. Root structures in paleosol. B. Deformed mudstone. C. Orange bed is marl within mudstone. D. Climbing ripples in fine-grained sandstone. E. Internally deformed sand pod on left surrounded by deformed mudstone. Shrub in foreground is 15 cm tall for scale.



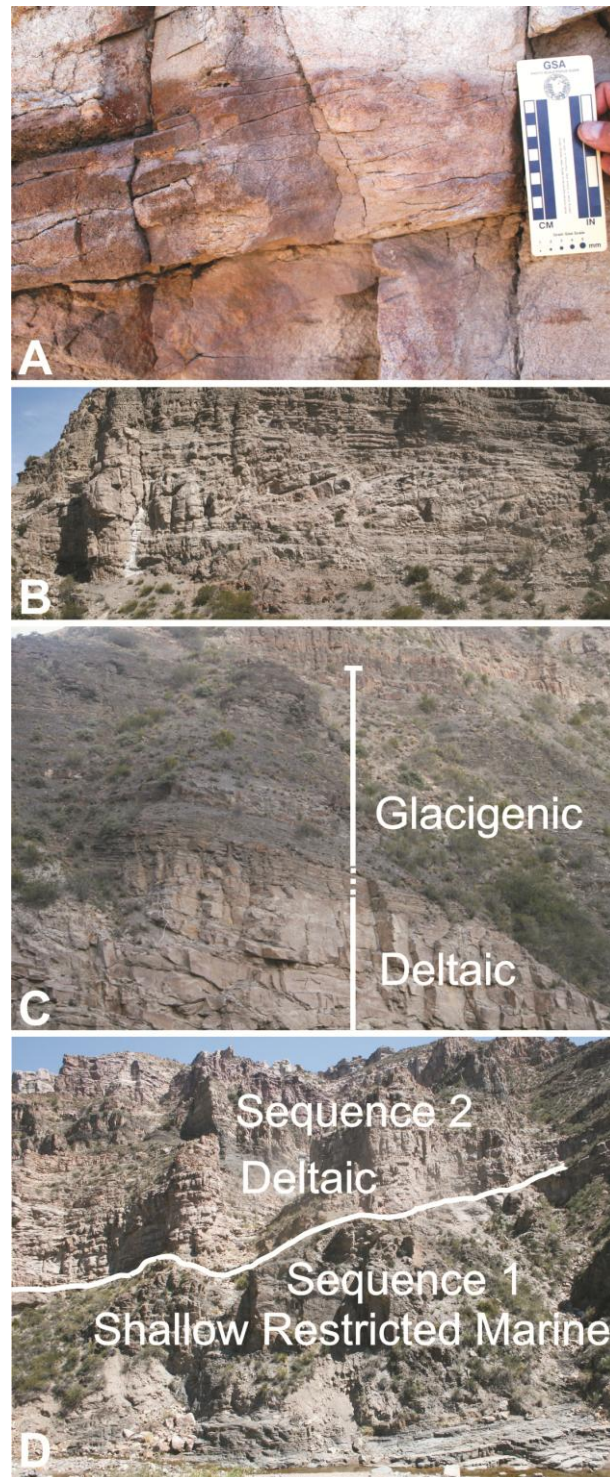


Figure 28. Deltaic facies association. A. Small-scale foresets in medium-grained sandstone. B. Gilbert delta. C. Deltaic facies association transitioning upwards into the glacigenic facies association (both in sequence 2). Sandstone is interbedded with siltstone in the transitional stage, a prodelta environment. D. Sequence 1, composed of the restricted marine facies association, incised by conglomerate at the base of sequence 2.



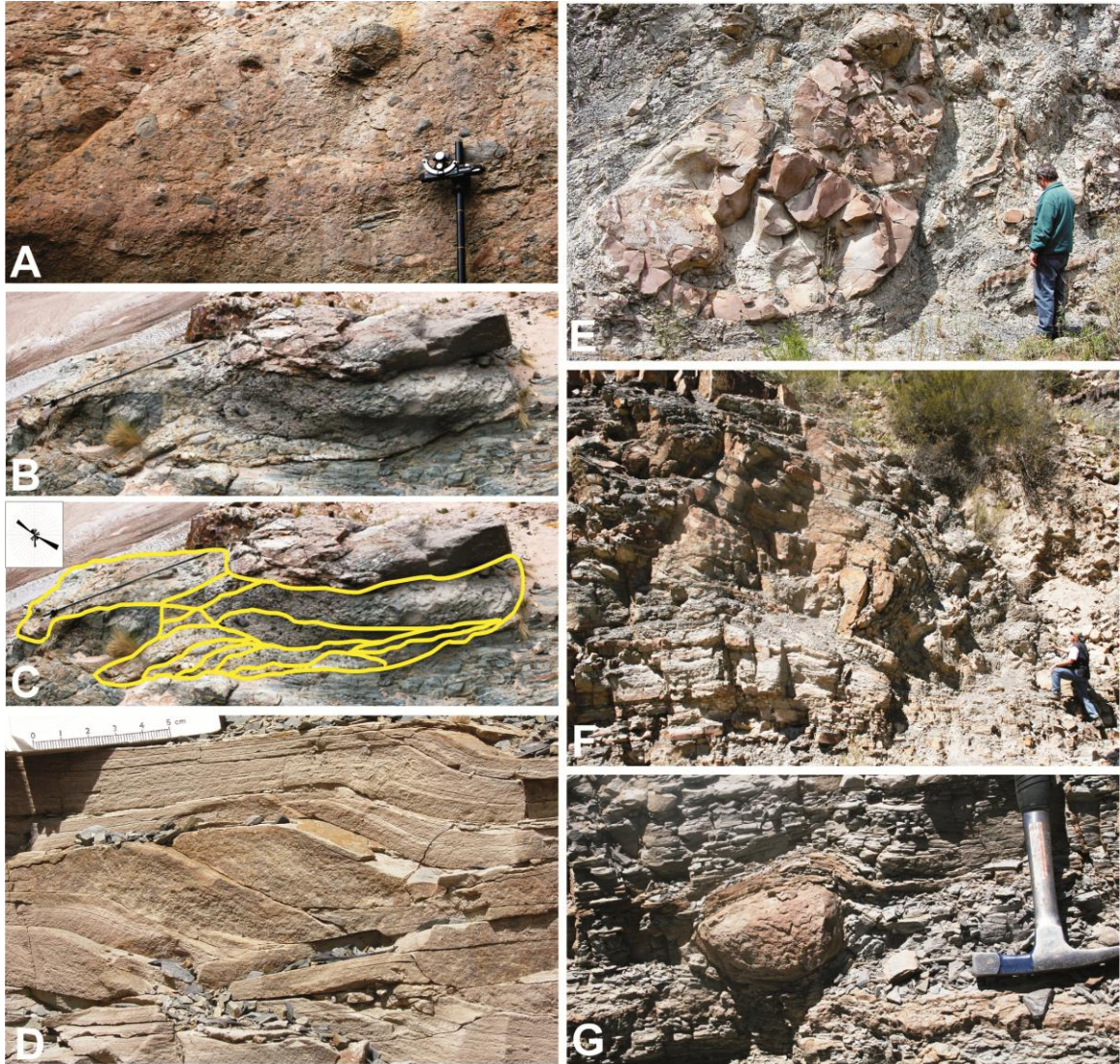


Figure 29. Glacially-influenced facies association. A. Clast rich, weakly stratified diamictite. B. Stratified diamictite stacked as imbricate slices draping underlying Devonian bedrock. Jacob staff for scale. C. Individual beds are outlined in yellow. Rose diagram shows preferred alignment of  $290^{\circ}$ – $110^{\circ}$  for clast a axes ( $n=25$ ) for bed surface where the Jacob staff lies. D. Climbing ripples in fine-grained sandstone. E. Internally deformed sand pod surrounded by deformed siltstone. F. Folded beds of sandstone and mudstone that slid along the substrate. G. Outsized clast in siltstone bends and deforms under- and overlying strata.



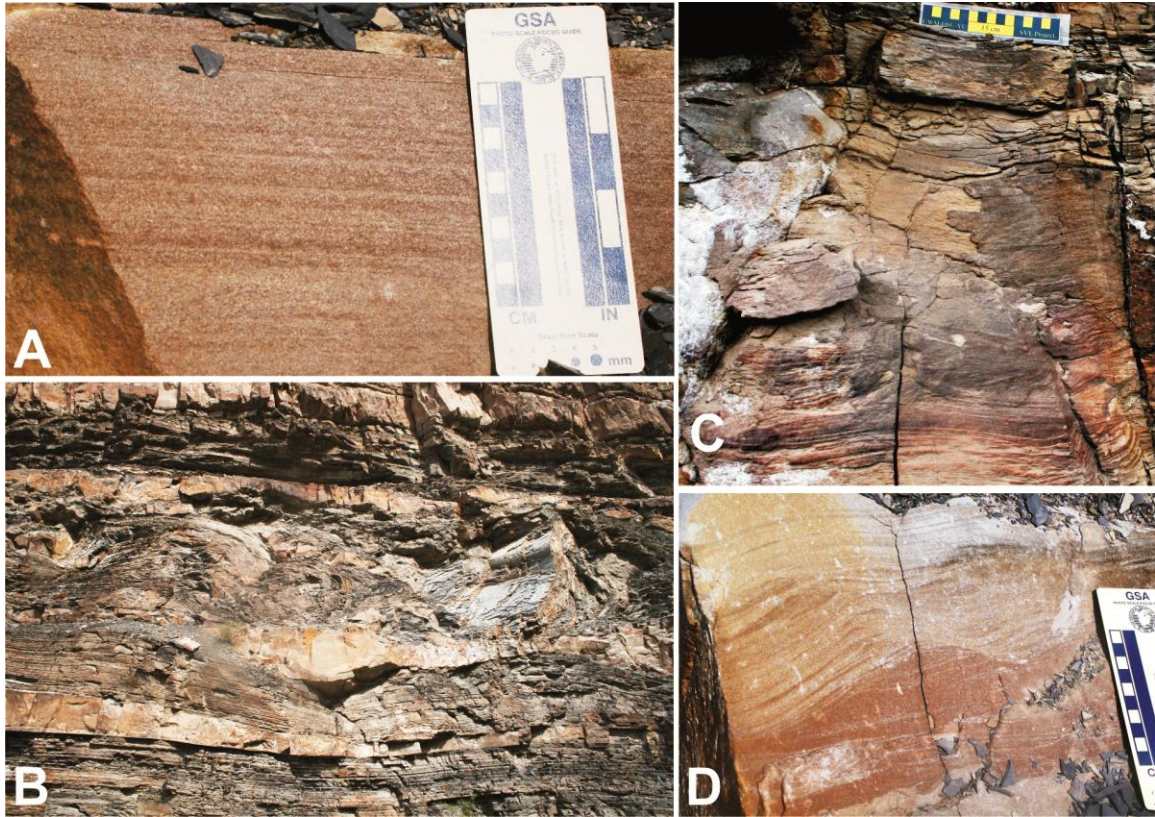


Figure 30. Post-glacial open marine facies association. A. Horizontally laminated fine-grained sandstone. B. Deformed siltstone interbedded with massive fine-grained sandstone. C. Hummocky cross-bedded fine-grained sandstone towards the top of the section. D. Wavy bedding of fine-grained sandstone and siltstone.

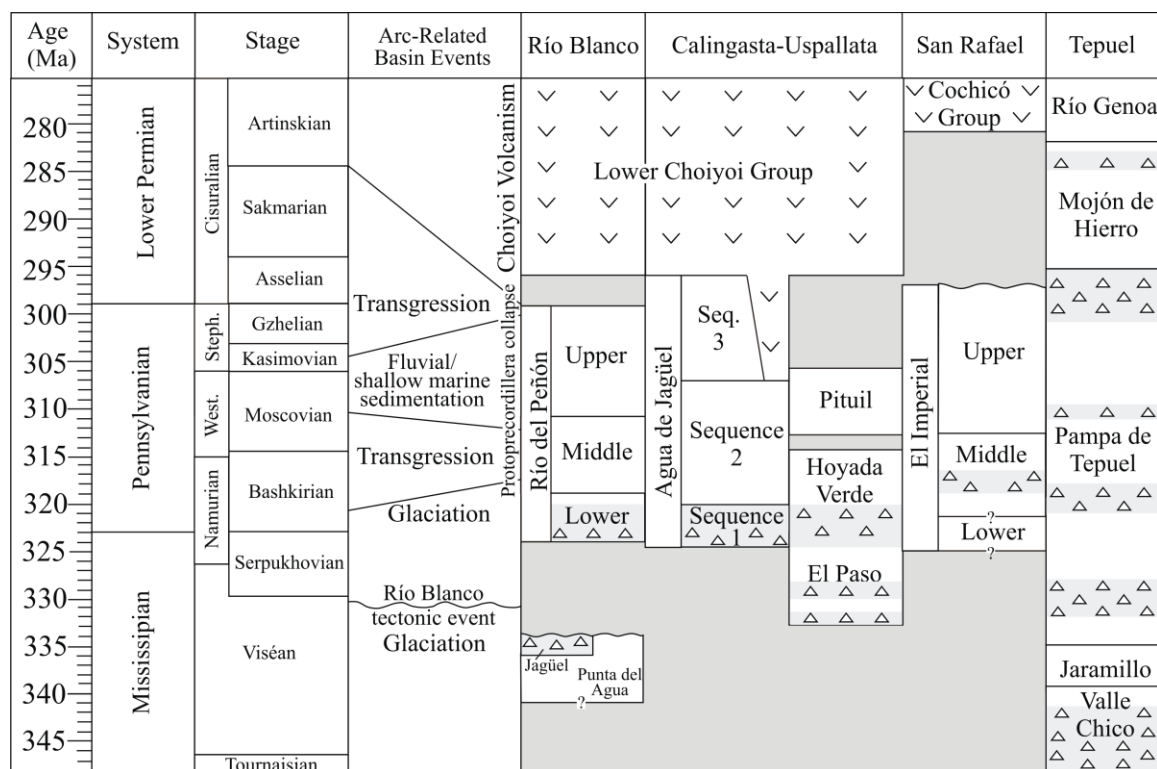


Figure 31. Stratigraphy and events in arc-related basins in western Argentina. Ages of events and formations are from Taboada (1985, 2010); Espejo (1993); García (1996); Azcuy et al. (1999); López Gamundí and Martínez (2000); Limarino and Spalletti (2006); Limarino et al. (2006); Strazzere et al. (2006); Gulbranson et al. (2010); Henry et al. (2010); Césari et al. (2011); and Rocha Campos et al. (2011). Carboniferous time scale is from Davydov et al. (2010); Permian time scale is from Gradstein et al. (2004).

## References

- Abre, P., Cingolani, C., Zimmermann, U., Cairncross, B., Chemale Jr., F., 2011. Provenance of Ordovician clastic sequences of the San Rafael block (central Argentina), with emphasis on the Ponón Trehué Formation. *Gondwana Research* 19, 275–290.
- Allen, J.R.L., 1982. *Sedimentary structures: their character and physical basis*. Developments in Sedimentology, 30. Elsevier, Amsterdam, p. 2 (663 pp.).
- Andreis, R.R., Archangelsky, S., 1996. The Neo-Paleozoic basins of southern South America. In: Moullade, M., Nairn, A.E. (Eds.), *The Phanerozoic Geology of the World, I, The Palaeozoic B*. Elsevier, Amsterdam, pp. 339–650.
- Arias, W.E., Azcuy, C.L., 1986. El Paleozoico superior del Cañón del Río Atuel, Provincia de Mendoza, Argentina. *Revista de la Asociación Geológica Argentina* 41, 262–269.

- Azcuy, C.L., Carrizo, H.A., Caminos, R., 1999. Carbonífero y Pérmico de las Sierras Pampeanas, Famatina, Precordillera, Cordillera Frontal y Bloque de San Rafael. *Geología Argentina*, 29. Instituto de Geología y Recursos Minerales, pp. 261–318.
- Benn, D.I., 1992. Scottish landform examples; 5, the Achnasheen terraces. *Scottish Geographical Magazine* 108, 128–131.
- Bhattacharya, J.P., 2006. Deltas. In: Posamentier, H.W., Walker, R.G. (Eds.), *Facies Models Revisited: SEPM (Society of Sedimentary Geology) Special Publication*, 84, pp. 237–292.
- Blakey, R.C., 2008. Gondwana paleogeography from assembly to breakup—a 500 m.y. odyssey. In: Fielding, C.R., Frank, T.D., Isbell, J.L. (Eds.), *Resolving the Late Paleozoic Ice Age in Time and Space: Geological Society of America Special Paper*, 441, pp. 1–28.
- Boulton, G.S., 1990. Sedimentary and sea level changes during glacial cycles and their control on glacimarine architecture. In: Dowdeswell, J.A., Scourse, J.D. (Eds.), *Glacimarine Environments: Processes and Sediments: Geological Society Special Publication*, London, 53, pp. 15–52.
- Buatois, L.A., Limarino, C.O., 2003. El contacto entre las Formaciones Hoyada Verde y Tres Saltos. Carbonífero de la cuenca Calingasta–Uspallata: Su reinterpretación como una superficie de incisión fluvial: III Simposio Argentino del Paleozoico Superior y II Reunión del Proyecto International Geoscience Programme, 471 (La Plata, Argentina, Resúmenes, 5).
- Buatois, L.A., Netto, R.G., Mángano, M.G., 2010. Ichnology of late Paleozoic postglacial transgressive deposits in Gondwana: reconstructing salinity conditions in coastal ecosystems affected by strong meltwater discharge. *Geological Society of America Special Paper* 468, 149–173.
- Caminos, R., Llambías, E., Rapela, C., Parica, C., 1988. Late Paleozoic–Early Triassic magmatic activity of Argentina and the significance of new Rb–Sr ages from northern Patagonia. *Journal of South American Earth Sciences* 1, 137–145.
- Caputo, M.V., 1985. Late Devonian glaciation in South America. *Palaeogeography, Palaeoclimatology, Palaeoecology* 51, 291–317.
- Caputo, M.V., de Melo, J.H.G., Streel, M., Isbell, J.L., 2008. Late Devonian and Early Carboniferous glacial records of South America. In: Fielding, C.R., Frank, T.D., Isbell, J.L. (Eds.), *Resolving the Late Paleozoic Ice Age in Time and Space: Geological Society of America Special Paper*, 441, pp. 161–173.
- Catuneanu, O., 2006. *Principles of Sequence Stratigraphy*. Elsevier, Amsterdam. (375



pp.).

- Césari, S.N., Gutiérrez, P.R., 2000. Palynostratigraphy of Upper Paleozoic sequences in Central–Western Argentina. *Palynology* 24, 113–146.
- Césari, S.N., Limarino, C.O., Gulbranson, E.L., 2011. An Upper Paleozoic Biochronostratigraphic scheme for the western margin of Gondwana. *Earth-Science Reviews* 106, 149–160.
- Cingolani, C.A., Manassero, M., Abre, P., 2003. Composition, provenance, and tectonic setting of Ordovician siliciclastic rocks in the San Rafael block: southern extension of the Precordillera crustal fragment, Argentina. *Journal of South American Earth Sciences* 16, 91–106.
- Coe, A.L. (Ed.), 2003. *The Sedimentary Record of Sea-level Change*. Cambridge University Press, Cambridge, U.K. (288 pp.).
- Collinson, J.W., Isbell, J.L., Elliot, D.H., Miller, M.F., Miller, J.M.G., 1994. Permian–Triassic Transantarctic basin. In: Veevers, J.J., Powell, C.M. (Eds.), *Permian–Triassic Pangean Basins and Fold Belts along the Panthalassan Margin of Gondwanaland: Geological Society of America Memoir*, 184, pp. 173–222.
- Dalla Salda, L., Cingolani, C., Varela, R., 1990. The origin of Patagonia. *Comunicaciones* 41, 55–61.
- Davydov, V.I., Crowley, J.L., Schmitz, M.D., Poletaev, V.I., 2010. High-precision U–Pb zircon age calibration of the global Carboniferous time scale and Milankovitch-band cyclicity in the Donets Basin, eastern Ukraine. *Geochemistry, Geophysics, Geosystems* (22 pp.).
- Dykstra, M., Kneller, B., Milana, J.P., 2006. Deglacial and postglacial sedimentary architecture in a deeply incised paleovalley-paleofjord: the Pennsylvanian (Late Carboniferous) Jejenes Formation, San Juan, Argentina. *Geological Society of America Bulletin* 118, 913–937.
- Espejo, I., 1990. Análisis estratigráfico, paleoambiental y de proveniencia de la Formación El Imperial, en los alrededores de los ríos Diamante y Atuel provincial de Mendoza). [Ph.D. Thesis]: Buenos Aires, Universidad de Buenos Aires, 338 p.
- Espejo, I.S., 1993. Reordenamiento de la estratigrafía neopaleozoica en el sector norte. XII Congreso de Geológico Argentino y II Congreso de Exploración de Hidrocarburos: Actas Tº II, pp. 57–62.
- Espejo, I.S., López Gamundí, O.R., 1994. Source versus depositional controls on sandstone composition in a foreland basin: the El Imperial Formation (mid

Carboniferous–Lower Permian), San Rafael Basin, western Argentina. *Journal of Sedimentary Research* 64, 8–16.

- Fernández Sevesso, F., Tankard, A.J., 1995. Tectonics and stratigraphy of the Late Paleozoic Paganzo Basin of western Argentina and its regional implications. In: Tankard, A.J., Suárez, R., Welsink, H.J. (Eds.), *Petroleum Basins of South America: American Association Petroleum Geologists, Memoir*, 62, pp. 285–301.
- Fielding, C.R., Frank, T.D., Birgenheier, L.P., Rygel, M.C., Jones, A.T., Roberts, J., 2008a. Stratigraphic imprint of the Late Paleozoic Ice Age in eastern Australia: a record of alternating glacial and nonglacial climate regime. *Journal of the Geological Society of London* 165, 129–140.
- Fielding, C.R., Frank, T.D., Isbell, J.L., 2008b. The late Paleozoic ice age — a review of current understanding and synthesis of global climate patterns. In: Fielding, C.R., Frank, T.D., Isbell, J.L. (Eds.), *Resolving the Late Paleozoic Ice Age in Time and Space: Geological Society of America Special Paper*, 441, pp. 343–354.
- García, G., 1996. Palinología de la Formación El Imperial, Paleozoico superior, Cuenca San Rafael, República Argentina; Parte II, Granos de polen, incertae sedis, acritarcas (Palynology of the El Imperial Formation, upper Paleozoic, San Rafael Basin, Argentina; part II, pollen grains, incertae sedis, acritarchs). *Ameghiniana* 33, 7–33.
- Gradstein, F.M., Ogg, J.G., Smith, A.G., 2004. *A Geologic Time Scale 2004*. Cambridge University Press, Cambridge, U.K.
- Gulbranson, E.L., Limarino, C.O., Marensi, S., Montañez, I.P., Tabor, N.J., Davydov, V.I., Colombi, C., 2008. Glacial deposits in the Río del Peñón Formation, late Carboniferous, Río Blanco Basin, northwestern Argentina. *Latin American Journal of Sedimentology and Basin Analysis* 15, 129–142.
- Gulbranson, E.L., Montañez, I.P., Schmitz, M.D., Limarino, C.O., Isbell, J.L., Marensi, S.A., Crowley, J.L., 2010. High-precision U–Pb calibration of Carboniferous glaciation and climate history, Paganzo Group, NW Argentina. *Geological Society of America Bulletin* 122, 1480–1498.
- Henry, L.C., Isbell, J.L., Limarino, C.O., 2008. Carboniferous glacial deposits of the Protoprecordillera of west central Argentina. In: Fielding, C.R., Frank, T.D., Isbell, J.L. (Eds.), *Resolving the Late Paleozoic Ice Age in Time and Space: Geological Society of America Special Paper*, 441, pp. 131–142.
- Henry, L.C., Limarino, C.O., Fraiser, M.L., Isbell, J.L., 2009. Potential environmental consequences of Panthalassan margin volcanism in the late Paleozoic. *Geological Society of America Abstracts with Programs* 41, 360.

- Henry, L.C., Isbell, J.L., Limarino, C.O., McHenry, L.J., Fraiser, M.L., 2010. Mid-Carboniferous deglaciation of the Protoprecordillera, Argentina, recorded in the Agua de Jagüel paleovalley. *Palaeogeography, Palaeoclimatology, Palaeoecology* 298, 112–129.
- Isbell, J.L., Miller, M.F., Wolfe, K.L., Lenaker, P.A., 2003. Timing of late Paleozoic glaciation in Gondwana: was glaciation responsible for the development of northern hemisphere cyclothems? In: Chan, M.A., Archer, A.W. (Eds.), *Extreme Depositional Environments: Mega End Members in Geologic Time*: Geological Society of America, Special Publication, 370, pp. 5–24.
- Isbell, J.L., Cole, D.I., Catuneanu, O., 2008a. Carboniferous–Permian glaciation in the main Karoo Basin, South Africa: stratigraphy, depositional controls, and glacial dynamics. In: Fielding, C.R., Frank, T.D., Isbell, J.L. (Eds.), *Resolving the Late Paleozoic Ice Age in Time and Space*: Geological Society of America Special Paper, 441, pp. 71–82.
- Isbell, J.L., Koch, Z.J., Szablewski, G.M., Lenaker, P.A., 2008b. Permian glacial deposits in the Transantarctic Mountains, Antarctica. In: Fielding, C.R., Frank, T.D., Isbell, J.L. (Eds.), *Resolving the Late Paleozoic Ice Age in Time and Space*: Geological Society of America Special Paper, 441, pp. 59–70.
- Isbell, J.L., Taboada, A.C., Koch, Z.J., Limarino, C.O., Fraiser, M.L., Pagani, M.A., Gulbranson, E.L., Ciccioli, P.L., Dineen, A.A., 2011. Emerging polar view of the late Paleozoic ice age as interpreted from deep-water, distal, glacial marine deposits in the Tepuel-Genoa Basin, Patagonia, Argentina. In: Hakansson, E., Trotter, J. (Eds.), *Programme & Abstracts, XVII International Congress on the Carboniferous and Permian Perth 3–8, July 2011*: Geological Survey of Western Australia 2011/20, 74.
- Isbell, J.L., Henry, L.C., Gulbranson, E.L., Limarino, C.O., Fraiser, M.L., Koch, Z.J., Ciccioli, P.L., Dineen, A.A., 2012. Evaluations of glacial paradoxes during the late Paleozoic Ice Age using the concept of the equilibrium line altitude (ELA) as a control on glaciation. *Gondwana Research* 22, 1–19.
- Jones, A.T., Frank, T.D., Fielding, C.R., 2006. Cold climate in eastern Australian mid to late Permian may reflect cold upwelling waters. *Palaeogeography, Palaeoclimatology, Palaeoecology* 237, 370–377.
- Kay, S., Ramos, V., Mpodozis, C., Sruoga, P., 1989. Late Paleozoic to Jurassic silicic magmatism at the Gondwanaland margin: analogy to the Middle Proterozoic in North America? *Geology* 17, 324–328.
- Kneller, B., Milana, J.P., Buckee, C., Al Ja'aidi, O.S., 2004. A depositional record of deglaciation in a paleofjord (Late Carboniferous [Pennsylvanian]) of San Juan

- Province, Argentina): the role of catastrophic sedimentation. *Geological Society of America Bulletin* 116, 348–367.
- Koukharsky, M., Kleiman, L., Etcheverría, M., Quenardelle, S., Bercowski, F., 2009. Upper Carboniferous retroarc volcanism with submarine and subaerial facies at the western Gondwana margin of Argentina. *Journal of South American Earth Sciences* 27, 299–308.
- Laskar, B., Mitra, N.D., 1976. Paleoclimatic vicissitudes in India during Lower Gondwana sedimentation. *Geophytology* 6, 162–169.
- Lech, R.R., 2002. Consideraciones sobre la edad de la Formación Agua de Jagüel (Carbonífero superior–Pérmico inferior) provincia de Mendoza, Argentina. *Ameghiniana* 23, 57–60.
- Limarino, C.O., Spalletti, L.A., 2006. Paleogeography of the upper Paleozoic basins of southern South America: an overview. *Journal of South American Earth Sciences* 22, 134–155.
- Limarino, C.O., Césari, S.N., Net, L.I., Marensi, S.A., Gutiérrez, P.R., Tripaldi, A., 2002. The Upper Carboniferous postglacial transgression in the Paganzo and Río Blanco Basins (northwestern Argentina): facies and stratigraphic significance. *Journal of South American Earth Sciences* 15, 445–460.
- Limarino, C.O., Tripaldi, A., Marensi, S., Fauqué, L., 2006. Tectonic, sea level, and climatic controls on late Paleozoic sedimentation in the western basins of Argentina. *Journal of South American Earth Sciences* 22, 205–226.
- Limarino, C.O., Césari, S.N., Spalletti, L.A., Taboada, A.C. Isbell, J.L., Geuna, S., Gulbranson, E.L., submitted for publication. Paleoclimatic evolution of southern South America during the late Paleozoic: a record from icehouse to extreme greenhouse conditions. *Gondwana Research*.
- Linares, E., Manavella, M.A., Piñeiro, A., 1979. Geocronología de las rocas efusivas de las zonas de los yacimientos “Dr. Baulés” y “Los Reyunos”, Sierra Pintada de San Rafael, Mendoza, República Argentina. 7th Congreso Geológico Argentino. *Actas* 2, 13–21.
- López Gamundí, O.R., 1991. Thin-bedded diamictites in the glacimarine Hoyada Verde Formation (Carboniferous), Calingasta–Uspallata Basin, western Argentina; a discussion on the emplacement conditions of subaqueous cohesive debris flows. *Sedimentary Geology* 73, 247–255.
- López Gamundí, O.R., 1997. Glacial–postglacial transition in the late Paleozoic basins of

- Southern South America. In: Martini, I.P. (Ed.), *Late Glacial and Postglacial Environmental Changes: Quaternary, Carboniferous–Permian, and Proterozoic*. Oxford University Press, Oxford, U.K., pp. 147–168.
- López Gamundí, O.R., Martínez, M., 2000. Evidence of glacial abrasion in the Calingasta–Uspallata and western Paganzo Basins, mid-Carboniferous of western Argentina. *Palaeogeography, Palaeoclimatology, Palaeoecology* 159, 145–165.
- López Gamundí, O.R., Espejo, I.S., Conaghan, P.J., Powell, C.M., Veevers, J.J., 1994. Southern South America. In: Veevers, J., Powell, C. (Eds.), *Permian–Triassic Pangea Basins and Fold Belts along the Panthalassan Margin of Gondwanaland: Geological Society of America Memoir*, 184, pp. 281–329.
- Loss, M.L., 2006. *Facies y estratigrafía secuencial en la Formación El Imperial, Cañón del Atuel, Cuenca de San Rafael [Thesis]*: Buenos Aires, Universidad de Buenos Aires, 194 p.
- Mack, G.H., James, W.C., Monger, H.C., 1993. Classification of paleosols. *Geological Society of America Bulletin* 105, 129–136.
- Martínez Dopico, C.I., López de Luchi, M.G., Rapalini, A.E., Kleinhanns, I.C., 2011. Crustal segments in the North Patagonian Massif, Patagonia: an integrated perspective based on Sm–Nd isotope systematic. *Journal of South American Earth Sciences* 31, 324–341.
- Mésigos, M., 1953. El Paleozoico superior de Barreal y su continuación austral. Sierra de Barreal. Provincia de San Juan. *Revista de la Asociación Geológica Argentina* 8, 65–109.
- Montañez, I.P., Tabor, N.J., Niemeier, D., DiMichele, W.A., Frank, T.D., Fielding, C.R., Isbell, J.L., Birgenheier, L.P., Rygel, M.C., 2007. CO<sub>2</sub>-forced climate and vegetative instability during late Paleozoic deglaciation. *Science* 315, 87–91.
- Mori, A.L.O., de Souza, P.A., Marques, J.C., Lopes, R.d.C., 2012. A new U–Pb zircon age dating and palynological data from a Lower Permian section of the southernmost Paraná Basin, Brazil: biochronostratigraphical and geochronological implications for Gondwanan correlations. *Gondwana Research* 21, 654–669.
- Mory, A.J., Redfern, J., Martin, J.R., 2008. A review of Permian–Carboniferous glacial deposits in western Australia. In: Fielding, C.R., Frank, T.D., Isbell, J.L. (Eds.), *Resolving the Late Paleozoic Ice Age in Time and Space: Geological Society of America Special Paper*, 441, pp. 29–40.
- Mulder, T., Alexander, J., 2001. The physical character of subaqueous sedimentary density flows and their deposits. *Sedimentology* 48, 269–299.

- Nasi, C., Sepúlveda, P., 1986. Avances en el conocimiento del Carbonífero en el norte de Chile. Late Paleozoic of South America, Abstracts: Annual Meeting of the Working Group, IUGS-IGCP Project, 211, pp. 27–43.
- Net, L.I., Limarino, C.O., 2006. Applying sandstone petrofacies to unravel the Upper Carboniferous evolution of the Paganzo Basin, northwest Argentina. *Journal of South American Earth Sciences* 22, 239–254.
- Pankhurst, R.J., Rapella, C.W., Fanning, C.M., Márquez, M., 2006. Gondwanide continental collision and the origin of Patagonia. *Earth-Science Reviews* 76, 235–257.
- Pazos, P.J., di Pasquo, M., Amenabar, C.R., 2007. Trace fossils of the glacial to postglacial transition in the El Imperial Formation (Upper Carboniferous), San Rafael Basin, Argentina. *SEPM Special Publication* 88, 137–147.
- Perez Loinaze, V.S., 2007. A Mississippian miospore biozone for Southern Gondwana. *Palynology* 31, 101–117.
- Perez Loinaze, V.S., 2008. Systematic palynological study of the Cortaderas Formation, (Mississippian) Río Blanco Basin, Argentina: part one. *Ameghiniana* 45, 33–57.
- Posamentier, H.W., Allen, G.P., 1999. Siliciclastic sequence stratigraphy — concepts and applications. *SEPM Concepts in Sedimentology and Paleontology*. (210 pp.).
- Postma, G., 1990. Depositional architecture and facies of river and fan deltas: a synthesis. In: Colella, A., Prior, D.B. (Eds.), *Coarse-grained Deltas*. International Association of Sedimentologists, Special Publication, 10. Blackwell, Oxford, pp. 13–27.
- Powell, R.D., 1990. Glacimarine processes at grounding-line fans and their growth to ice contact deltas. In: Dowdeswell, J.A., Scourse, J.D. (Eds.), *Glacimarine Environments: Processes and Sediments*. Geological Society Special Publication, 53, pp. 53–73.
- Powell, R.D., Cooper, J.M., 2002. A glacial sequence stratigraphic model for temperate, glaciated continental shelves. In: Dowdeswell, J.A., Ó Cofaigh, C. (Eds.), *Glacier Influenced Sedimentation on High-latitude Continental Margins*. Geological Society, London, Special Publications, 203, pp. 215–244.
- Powell, R.D., Domack, E., 2002. Modern glacimarine environments. In: Menzies, J. (Ed.), *Modern and Past Glacial Environments*. Butterworth-Heinemann Ltd., Oxford, pp. 361–389.
- Ramos, V.A., 2008. Patagonia: a Paleozoic continent adrift? *Journal of South American*

Earth Sciences 26, 235–251.

- Rapalini, A.E., López de Luchi, M., Martínez Dopico, C., Lince Klinger, F., Giménez, M., Martínez, P., 2010. Did Patagonia collide with Gondwana in the Late Paleozoic? Some insights from a multidisciplinary study of magmatic units of the North Patagonian Massif. *Geologica Acta* 8, 349–371.
- Rapela, C.W., Pankhurst, R.J., Casquet, C., Baldo, E., Saavedra, J., Galindo, C., Fanning, M., 1998. The Pampean orogeny of the southern proto-Andes: Cambrian continental collision in the Sierras de Córdoba. In: Pankhurst, R.J., Rapela, C.W. (Eds.), *The Proto Andean Margin of Gondwana*: Geological Society of London: Special Publication, 142, pp. 181–217.
- Rocha Campos, A.C., dos Santos, P.R., Canuto, J.R., 2008. Late Paleozoic glacial deposits of Brazil: Paraná Basin. In: Fielding, C.R., Frank, T.D., Isbell, J.L. (Eds.), *Resolving the Late Paleozoic Ice Age in Time and Space*: Geological Society of America Special Paper, 441, pp. 97–114.
- Rocha Campos, A.C., Basei, M.A., Nutman, A.P., Kleiman, L.E., Varela, R., Llambías, E., Canile, F.M., da Rosa, O., de, C.R., 2011. 30 million years of Permian volcanism recorded in the Choiyoi igneous province (W. Argentina) and their source for younger ash fall deposits in the Paraná Basin: SHRIMP U–Pb zircon geochronology evidence. *Gondwana Research* 19, 509–523.
- Sato, A.M., Tickyj, H., Llambías, E.J., Basei, M.A.S., González, P.D., 2004. *Gondwana Research* 7, 1077–1087.
- Scalabrini Ortiz, J., 1973. El Carbónico en el sector septentrional de la Precordillera sanjuanina. *Revista de la Asociación Geológica Argentina* 27, 351–377.
- Schatz, E.R., Mángano, M.G., Buatois, L.A., Limarino, C.O., 2011. Life in the late Paleozoic ice age: trace fossils from glacially influenced deposits in a late Carboniferous fjord of western Argentina. *Journal of Paleontology* 85, 502–518.
- Shanmugam, G., 2006. *Deep-water Processes and Facies Models: Implications for Sandstone Petroleum Reservoirs*. Elsevier, Amsterdam . (476 pp.).
- Sims, J.P., Ireland, T.R., Camacho, A., Lyons, P., Pieters, P.E., Skirrow, R.G., Stuart-Smith, P.G., 1998. U–Pb, Th–Pb and Ar–Ar geochronology from the southern Sierras Pampeanas, Argentina: implications for the Palaeozoic tectonic evolution of the western Gondwana margin. In: Pankhurst, R.J., Rapela, W.C. (Eds.), *The Proto-Andean Margin of Gondwana*: Geological Society of London Special Publication, 142, pp. 259–282.
- Stinco, L.P., 1986. *Análisis litoestratigráfico del Miembro inferior de la Formación Cochicó [Thesis]*: Buenos Aires, Universidad de Buenos Aires.

- Strazzere, L., Gregori, D.A., Dristas, J.A., 2006. Genetic evolution of Permo-Triassic volcanoclastic sequences at Uspallata, Mendoza Precordillera, Argentina. *Gondwana Research* 9, 485–499.
- Streel, M., Theron, J.N., 1999. The Devonian–Carboniferous boundary in South Africa and the age of the earliest episode of the Dwyka glaciation: new palynological result. *Episodes* 22, 41–44.
- Taboada, A.C., 1985. Estratigrafía y contenido paleontológico de la Formación Agua del Jagüel. Pérmico Inferior de la Precordillera Mendocina: Primeras Jornadas Sobre Geología de Precordillera. San Juan Acta I, San Juan.
- Taboada, A.C., 1997. Bioestratigrafía del Carbonífero marino del valle de Calingasta–Uspallata, provincias de San Juan y Mendoza. *Ameghiniana* 34, 215–246.
- Taboada, A.C., 2004. Braquiópodos y bioestratigrafía del Carbonífero del Cordón del Naranjo (subcuenca Calingasta–Uspallata), Argentina. *Ameghiniana* 41, 405–422.
- Taboada, A.C., 2010. Mississippian–Early Permian brachiopods from western Argentina: tools for middle- to high-latitude correlation, paleobiogeographic and paleoclimatic reconstruction. *Palaeogeography, Palaeoclimatology, Palaeoecology* 298, 152–173.
- Taboada, A.C., Shi, G.R., 2011. Taxonomic review and evolutionary trends of *Levipustulini* and *Absenticostini* (Brachiopoda) from Argentina; palaeobiogeographic and palaeoclimatic implications. *Memoirs of the Association of Australasian Palaeontologists* 41, 87–114.
- Torsvik, T.H., Cocks, L.R.M., 2004. Earth geography from 400 to 250 Ma: a palaeomagnetic, faunal and facies review. *Journal of the Geological Society* 161, 555–572.
- Toubes, R.O., Spikermann, J.P., 1976. Algunas edades K–Ar para la Sierra Pintada, provincial de Mendoza. *Revista de la Asociación Geológica Argentina* 31, 118–126.
- Veevers, J., Powell, C., Collinson, J., López Gamundí, O., 1994. Synthesis. In: Veevers, J., Powell, C. (Eds.), *Permian–Triassic Pangean Basins and Fold Belts along the Panthalassan Margin of Gondwanaland*. Boulder, Colorado: Geological Society of America Memoir, 184, pp. 331–353.
- Visser, J.N.J., 1997. A review of the Permo–Carboniferous glaciation in Africa. In: Martini, I.P. (Ed.), *Late Glacial and Postglacial Environmental Changes: Quaternary, Carboniferous–Permian, and Proterozoic*. Oxford University Press,



Oxford, U.K., pp. 169–191.

Woodcock, N.H., 1976. Structural style in slump sheets. Ludlow Series, Powys, Wales: Proceedings of the Geologists' Association, 87, pp. 169–182.

## **Chapter 5: Proglacial deposition and deformation in the Upper Carboniferous to Lower Permian Wynyard Formation, Tasmania: a process analysis**

Lindsey C. Henry<sup>\*a</sup>, John L. Isbell<sup>a</sup>, Christopher R. Fielding<sup>b</sup>, Eugene W. Domack<sup>c</sup>,  
Tracy D. Frank<sup>b</sup>, Margaret L. Fraiser<sup>a</sup>

<sup>a</sup>*Department of Geosciences, University of Wisconsin-Milwaukee, 3209 N. Maryland Avenue, Milwaukee, WI 53211-0413, USA*

<sup>b</sup>*Department of Earth and Atmospheric Sciences, University of Nebraska-Lincoln, 214 Bessey Hall, Lincoln, NE 68588-0340, USA*

<sup>c</sup>*Department of Geosciences, Hamilton College, 198 College Hill Road, Clinton, NY 13323, USA*

### **Abstract**

The Wynyard Formation of Tasmania, Australia, provides the last evidence of grounded ice during the Late Carboniferous – Early Permian in the Tasmania Basin of southeastern Gondwana during the late Paleozoic ice age. Within the Wynyard Formation, four facies associations are recognized: 1) massive diamictite, 2) stratified diamictite, 3) conglomerate and sandstone, and 4) deformed mudstone and fine sandstone. A detailed facies analysis was performed in order to interpret the depositional processes and environments. The massive diamictite facies association contains massive diamictite and massive sandstone and was deposited primarily by iceberg rain-out in a subaqueous morainal bank setting. The stratified diamictite facies association is composed of stratified diamictite, sandstone, and conglomerate, was deposited by debris flows and iceberg rain-out, and deformed by glacial pushing. The conglomerate and sandstone facies association is made up of cross-stratified, channelized conglomerate and

---

<sup>\*</sup> Corresponding author.

Email address: [christi9@uwm.edu](mailto:christi9@uwm.edu) (L.C. Henry).

pebbly sandstone that were deposited by glacial outwash on grounding-line fans. The deformed mudstone and fine sandstone facies association is composed of pervasively deformed pebbly mudstone and fine-grained sandstone that exhibit volcano, flame, and dyke structures. This facies association was deposited by a combination of suspension settling, iceberg rain-out, and soft sediment deformation, in a quiet distal proglacial setting. The facies analysis supports the interpretation that the Wynyard Formation was deposited by a wet-based, tidewater glacier or glaciers. The depositing glacier(s) occupied a ~40 km - wide trough in northwest Tasmania. Based on the distribution of the Wynyard Formation and the presence of glacial deposits in other eroded troughs in Tasmania, glaciation occurred in the region within broadly eroded valleys. The Wynyard Formation and overlying mudstone of the Inglis Formation provide a glacial-postglacial signature similar to those in South Africa, Antarctica, and eastern Australia during the latest Carboniferous – Early Permian, therefore the climate warmed in southern Gondwana following this glacial interval. Continued glaciation in eastern Australia was a result of regional topography and oceanographic processes.

*Keywords:* Wynyard Formation; late Paleozoic ice age; Tasmania; micromorphology

## **1. Introduction**

Glacigenic strata of the Wynyard Formation in Tasmania, Australia (Fig. 32), were deposited in southeastern Gondwana during the main phase (Gzhelian–Sakmarian; latest Carboniferous–Early Permian) of the late Paleozoic ice age (LPIA). During the LPIA, glaciation occurred over Gondwana in the southern hemisphere, and possibly in Siberia in the northern hemisphere (Du Toit, 1937; Crowell and Frakes, 1975; Frakes et al., 1992; Chumakov, 1994; López Gamundí, 1997; Biakov et al., 2010). In Gondwana,

the LPIA was characterized by multiple intervals of glaciation that lasted for 1–10 m.y., separated by non-glacial intervals of similar duration (Isbell et al., 2003b; Fielding et al., 2008a). Gondwana migrated across the South Pole during the late Paleozoic, and as a result, glaciation began in western Gondwana (present-day South America) in the Famennian (Late Devonian; Caputo et al., 2008) and ended in eastern Gondwana (eastern Australia) in the Capitanian (Middle Permian; Fielding et al., 2008b). The LPIA is one of the most significant climatic events in Earth's history, as glaciation resulted in dramatic changes in earth's physical and biological systems: eustatic fluctuations and consequential paleoequatorial Euro-American cyclothem deposition (Frakes et al., 1992), changes in tropical precipitation and vegetation (Poulsen et al., 2007; Peyser and Poulsen, 2008), a second-order extinction (Stanley and Powell, 2003), depressed evolution (Brezinski, 1999; Stanley and Powell, 2003), and population redistributions (Gastaldo et al., 1996; Raymond et al. 1989; Clapham and James, 2008; DiMichele et al., 2009). Further, the LPIA provides the last complete record of the transition from icehouse to greenhouse conditions on a biologically complex Earth (Gastaldo et al., 1996), a worthwhile record to study as Earth will inevitably transition back into greenhouse conditions in the future.

Glacigenic strata in the Wynyard Formation of Tasmania form a thick, poorly-documented succession that provides a correlative link between better-studied glacigenic successions in Antarctica and the mainland of Australia (cf. Isbell et al., 1997, 2003a; Fielding et al., 2001, 2008a). During the late Paleozoic, Tasmania connected eastern Australia with northern Victoria Land, Antarctica (Fig. 33). Synthesizing the stratigraphic records of these three areas will help to constrain the waxing and waning of

glacial intervals of the LPIA and will better enable climate models to deduce the major drivers of ice growth and deglaciation during the LPIA.

The South Pole was located in Antarctica during the Late Pennsylvanian and Early Permian (Fig. 33; Powell and Li, 1994; Li and Powell, 2001; Blakey, 2008; Lawver et al., 2008). Originally, Crowell and Frakes (1970, 1971) and Lindsay (1997) reported an ice center in northern Victoria Land that supplied ice northward into southeastern Australia. However, Isbell (2010) and Isbell et al. (2003a, 2008) reported that multiple small ice sheets occurred in Antarctica during this interval, and Fielding et al. (2008a, b) and Birgenheier et al. (2009) reported that ice sheets occurred in eastern Australia, known there as the P1 glacial interval. The glacial records of Antarctica and eastern Australia diverge in the Permian; glaciation in eastern Australia continued as the P2, P3, and P4 glacial intervals (Fielding et al., 2008a), but there is no record of glaciation in Antarctica after the Early Permian (Isbell et al., 2008), even though Antarctica occupied higher latitudes. Therefore, the stratigraphic record of Tasmania is a keystone for correlating the glacial records of Antarctica and eastern Australia.

The main purpose of this paper is to provide a detailed facies analysis and process interpretation of the Wynyard Formation based on facies data and micromorphology analysis of selected samples. Results are then compared to the Pennsylvanian – Lower Permian stratigraphic record of Antarctica and eastern Australia. The Wynyard Formation crops out as intertidal platforms, exposing extensive bedding planes. These exposures allow for three dimensional observations, which are rare in field-based sedimentologic studies of ancient glacial strata. Previous studies have interpreted the Wynyard Formation as a glacimarine environment (Banks and Clarke, 1987; Clarke,

1989; Powell, 1990; Hand, 1993), recording at least four major ice advances (Banks and Clarke, 1987). However, a detailed sedimentologic evaluation of all the facies associations of the Wynyard Formation has not been completed, as most studies involving the Wynyard Formation focus instead on the stratigraphy and basic paleontology of the Pennsylvanian – Permian strata of Tasmania (e.g., Clarke and Farmer, 1976; Banks and Clarke, 1987; Reid et al., in press). A process analysis of the Wynyard Formation clarifies the glacial history and dynamics of this region during the acme of the LPIA and provides insight into interregional correlation of the stratigraphic glacial to post-glacial transition between the Antarctic and Australian sectors of Gondwana.

## **2. Geologic setting and stratigraphy**

The Wynyard Formation and correlative glacigenic rocks form the lowermost part of the Parmeener Supergroup (Upper Carboniferous – Triassic) in the Tasmania Basin (Figs. 34, 35; Forsyth et al., 1974). The basin is an intracratonic basin that was located between Antarctica and Australia on the southeastern side of Gondwana, between ~75 – 80° S during the Pennsylvanian and Early Permian (Powell and Li, 1994; Li and Powell, 2001). This basin likely developed due to extensional block faulting during the late Paleozoic, with sub-basins within the Tasmanian Basin situated over 1000 m below adjacent highs (Clarke and Forsyth, 1989; Veevers et al., 1994; Reid et al., in press; Fielding et al., 2010). The Parmeener Supergroup unconformably overlies Precambrian and Paleozoic metamorphosed and folded igneous, metamorphic, and sedimentary rocks (McDougall and Leggo, 1965; Clarke and Farmer, 1976; Reid et al., in press). Striae and scour marks have been noted on basement surfaces below the basal glacigenic strata

(Clarke and Farmer, 1976). The glacial deposits occur in structural lows within the basin, which are interpreted to represent grabens or half-grabens that may have been further deepened by glacial erosion (Fig. 35, Fielding et al., 2010). For example, the Wynyard Formation occurs in a ~40 km wide trough in northwestern Tasmania (Fig. 32; Clarke and Forsyth, 1989).

The lower Parmeener Supergroup is composed predominantly of marine sediments with a minor freshwater interval (deltaic facies), ranging from Late Pennsylvanian to Middle Permian in age (Fig. 34), and the upper Parmeener Supergroup is composed primarily of Upper Permian and Triassic terrestrial rocks (Forsyth et al., 1974).

## **2.1. The lower Parmeener Supergroup**

The lower Parmeener Supergroup records glaciation, glacial retreat, and relative sea level fluctuations during the Late Pennsylvanian to Middle Permian (Reid et al., in press). The lithostratigraphic units of the lower Parmeener Supergroup have been assigned a variety of different names according to location. Figure 35 summarizes this stratigraphic nomenclature across Tasmania. An effort to streamline the nomenclature assigned to the lower Parmeener Supergroup was made by Reid et al. (in press) in their summary of the stratigraphy of the Parmeener Supergroup, and the adopted terminology and relative ages are presented in Figure 34.

The Wynyard Formation and correlative rocks consist of a 600+ m-thick succession of diamictites, conglomerates, sandstones, and lonestone-bearing mudstones, which records LPIA glaciation in Tasmania. Mudstones of the Inglis Formation, Woody Island Formation, and correlative rocks overlie the basal diamictites (Fig. 36).

## 2.2. Age

The lower Parmeener Supergroup is dated solely through biostratigraphy, as no radiometric ages are currently available. The Wynyard Formation and correlative diamictites are generally lacking in age-diagnostic fossils, although fossil palynomorphs, invertebrate body fossils, and plants have been identified (Truswell, 1978; Hand, 1993). Previously studied palynomorphs from the Wynyard Formation are from Australian palynostratigraphic zones (stages 1 and 2; Evans, 1969; Price et al., 1985), placing the diamictites in the uppermost Pennsylvanian to Lower Permian (Sakmarian?; Truswell, 1978; Veevers et al., 1994). The body fossils are *Trigonotreta*, *Deltopecten*, *Pyramus*, *Keenia*, *Eurydesma* and stenoporids, which are designated as Faunizone 1 of Clarke and Banks (1975), representing the latest Carboniferous to earliest Permian. The plant fossils are *Botrychiopsis plantiana* and *Aphlebia* sp., which also suggest a Late Carboniferous to earliest Permian age (Gould, 1975). Additionally, marine spinose acritarchs (*Veryhachium* and *Michrystidium*) were found in the Wynyard Formation and correlative Tasmanian diamictites (Downie and Sarjeant, 1964; Truswell, 1978).

## 3. Study area and methodology

Fieldwork on the Wynyard Formation occurred during the Austral winter of 2008 outside of the town of Wynyard.

### 3.1. Outcrop location

The outcrops at Wynyard are exposed in numerous intertidal platforms that occur immediately east of Doctors Rocks to immediately north-northwest of the mouth of the Inglis River (Fig. 37). Most outcrops along the shore are accessible only at low tide. Stratigraphic sections were logged at four different locations along the coast. The oldest



section occurs to the east (section A, Fig. 37) while progressively younger stratigraphic successions are exposed on intertidal platforms to the west. A continuous section is not exposed at any one locality because of tidal zones and breaks in exposure.

### **3.2. Sedimentology field methods**

Vertical sections were logged using standard methodologies. Paleoflow measurements and orientations of synsedimentary deformation structures were collected using a Brunton compass and corrected for structural dip and magnetic declination. Pebble counts noting lithology, rounding, sphericity, and apparent dip angles perpendicular to bedding planes were recorded from pebbles  $\geq 4$  mm in diameter. Samples for micromorphology analysis were taken from stratified diamictites in section A (Fig. 37). Thin sections were examined at 1 – 40 $\times$  magnification. Micromorphology terminology was developed from pedology, and descriptions herein are after the guidelines outlined by Menzies and van der Meer (2006).

## **4. Facies analysis**

Four facies associations are identified within the Wynyard Formation: 1. massive diamictite, 2. stratified diamictite, 3. conglomerate and sandstone, and 4. deformed mudstone and fine sandstone. Bioturbation is not observed in any of the facies associations. Descriptions and interpretations of the four facies associations are presented below and in Table 1.

### **4.1. Massive diamictite facies association**

The massive diamictite facies association occurs in sections A and D (Fig. 37).

#### **4.1.1. Massive diamictite facies association description**

The massive diamictite facies association consists of massive to weakly stratified diamictite and interbedded massive and normally graded sandstone (Table 1, Fig. 38). Basal and upper contacts of both diamictite and sandstone are typically sharp, although locally diamictite has gradational upper and lower contacts with massive sandstone. Massive diamictite beds have a matrix of gray sandy mudstone (Fig. 38A). The diamictite is clast-rich (cf. Moncrieff, 1989), maximum clast size is 20 cm, and clast lithologies (n=25) are on average 64% siltstone, 12% quartzite, 8% quartz, 8% red granite, 8% sandstone. The average diameter of clasts is 6.6 cm, and using visual estimates based on Wadell's (1932) scale, average sphericity is 0.6, and average roundness 0.5. Some clasts are striated, and bullet-shaped clasts are common. Long axis orientations of clasts appear to be random.

Sandstone is fine- to medium-grained and occurs as beds, lenses, and pods up to 4 m wide. Lenses of massive sandstone appear to fill depressions on surfaces of diamictite beds, and pods of massive and normally graded sandstone are loaded into underlying massive diamictite beds (Fig. 38B). Massive sandstone is soft-sediment-deformed. One massive pod exhibits small sand volcanoes (1 – 2 cm across). Multiple thin (5 mm – 1 cm thick) sandstone dykes of fine-grained sand cut through some massive medium-grained sandstone beds contained as interbeds within the diamictite (Fig. 38B).

#### **4.1.2. Massive diamictite facies association interpretation**

The massive and weakly stratified diamictites were deposited by a combination of rain-out of mud, sand, and clasts from floating icebergs; rain-out of clay, silt, and sand from meltwater plumes emanating from the base of a tidewater glacier; and subaqueous debris flows (cf. Eyles et al., 1985; Dowdeswell et al., 1994; Visser, 1994; Woodworth-

Lynas and Dowdeswell, 1994, Powell and Domack, 2002). A lack of internal structures in diamictite is common to deposits of rain-out and debris flows. The weak bedding of diamictites and sharp upper and lower contacts with other lithologies suggest deposition by rain-out with some resedimentation as debris flows. The presence of gradational contacts; an absence of shear structures, lineations, or grooves in the tops of beds; and an absence of an oriented low angle fabric for clasts discount a subglacial deposition interpretation (cf. Dreimanis, 1989; Boulton, 1990).

The moderately high roundness values of clasts suggest extensive transport of clasts prior to incorporation into ice. Based on clast provenance, Banks (1981) interpreted glacial movement into the Wynyard area from the southwest. Siltstone and sandstone clasts may have been derived from the Silurian to Lower Devonian Eldon Group south of Wynyard, quartzite from underlying Precambrian Burnie quartzite, and quartz and red granite from Devonian – Lower Carboniferous alkali-feldspar granite in the region of Mt. Meredith, Mt. Ramsay, and Mt. Hemmskirk, ~75 km south of Wynyard (cf. Banks, 1962; Spry, 1962).

Massive sandstone formed from hyperconcentrated density flows (cf. Mulder and Alexander, 2001). Normally graded pebbly sandstone was deposited by turbidity currents (cf. Lowe, 1982; Winsemann et al., 2007). Hyperconcentrated density flows and turbidity currents are common to the proximal proglacial environment, where unstable slopes associated with morainal banks can generate such flows (cf. Powell and Domack, 2002; Winsemann et al., 2007). Further, turbidity currents are often generated by debris flows through flow transformation as a result of dilution and stripping of surface materials from the original flow (cf. Winsemann et al., 2007).

Dewatering occurred in both diamictite and massive sandstone as a result of rapid deposition. The processes of settling from suspension out of buoyant melt-water plumes and rain-out of ice-rafted debris trap large volumes of water within diamict, and water is also trapped within sand in hyperconcentrated flows (cf. Mulder and Alexander, 2001; Powell and Domack, 2002). Sand volcanoes formed from dewatering, by water erupting out of sand along the sediment-water interface (cf. Burne, 1970). In massive sandstone, clastic dykes formed as water transported fine sand along conduits in medium-grained sand as water escaped upward (cf. Montenat et al., 2007).

The thick accumulation of massive and stratified diamictite in section A, 0 – 60 m (Fig. 37) likely represents a morainal bank, an elongate mound of diamict, gravel, sand, and mud that forms from rapid sedimentation in front of a grounded tidewater glacier (Powell, 1981; 1983; Powell and Molnia, 1989; Powell, 1990; bank-core subenvironment of Cai et al., 1997). Subsequent resedimentation as gravity flows are common due to the slope of the bank and from advance and retreat of the glacial front (cf. Powell and Domack, 2002). The first 60 m of section A fit the description of morainal bank deposits closely, with massive diamictite deposited primarily by rain-out; stratified diamictite deposited by debris flows; sandstone deposited by meltwater streams and hyperconcentrated flows; and conglomerate deposited as glacial outwash. The diamictite-rich portion of section A (0 – 60 m) grades up into a conglomerate-dominated succession (60 – 90 m) that likely represents a grounding-line fan, which is discussed further in the conglomerate and sandstone facies association section.

#### **4.2. Stratified diamictite facies association**

The stratified diamictite facies association occurs in sections A, B, C, and D (Fig. 37). Additional thin section micromorphology analysis was done on stratified diamictite from section A. Samples were taken from two 20 cm- and 30 cm-thick beds of stratified diamictite that showed macroscopic evidence of shearing.

#### **4.2.1. Stratified diamictite facies association description**

The stratified diamictite facies association consists of stacked thin beds of interstratified diamictite, fine- to medium-grained sandstone, and conglomerate (Fig. 39; Table 1). Stratified diamictite beds have sharp lower and upper contacts with sandstone, conglomerate, mudstone, and other beds of stratified diamictites (Fig. 39A). Stratified diamictite occurs as sheets, and massive fine-grained sandstone pods penetrate stratified diamictite beds as loads.

Stratified diamictite has a matrix of gray, sandy mud and is matrix-supported. Reverse grading occurs in some beds (Fig. 39B). In these inversely graded beds, basal layers exhibit faint lamination or fissility (cf. van der Meer, 1987). Wisps of fine sand, dewatering pipes, and vertically-oriented flame-like structures occur near the top of units, while arcuate-shaped compression ridges occur on the tops of beds. In some units, large clasts protrude from the tops of beds.

The stratified diamictite is clast-rich with a maximum clast size of 70 cm, and some clasts penetrate and deform bedding. A clast count from section D (n=25) indicates lithologies of 52% quartzite, 20% siltstone, 16% quartz, and 12% sandstone. Average diameter of clasts in the clast count is 3.9 cm, average sphericity is 0.6, and average roundness is 0.5 using visual estimates based on Wadell's (1932) scale. The average apparent dip angle of clast long axes is 31° (n=25). Striated clasts were observed in

stratified diamictite in all sections. In addition to clasts, clumps of small pebbles (maximum clast size 2 cm) and granules were observed on top of and within beds of stratified diamictite (Fig. 39C).

Many stratified diamictite beds are cut by brittle deformation structures. In several of these deformed intervals, stratified diamictites are interbedded with sandstones and occur as stacked deformed zones, both along bedding plane surfaces and up section. The deformed zones consist of a series of thrust faults that overlie decimeter-thick shear zones, which are identified by a fissile-like appearance and the presence of boudins within the zone (Fig. 39D). Additionally, upper and lower surfaces of sand beds contain crenulation folds. The shear zones separate the deformed zones from underlying undeformed massive and stratified diamictites. In sections A (20 m, see Fig. 37) and D (3 – 4 m), stratified diamictite beds bend upward so that they appear concave up in comparison to the normal dip of bedding (Fig. 39E, F). Despite this curvature, most beds are not internally deformed. Blocks of these upturned beds have trends of ESE – WNW, E – W, and NE – SW. Other beds of stratified diamictite are folded and overturned by soft-sediment deformation.

The fine- and medium-grained sandstone of the stratified diamictite facies association exhibits cross-lamination with occurrences of climbing ripples and low angle cross-bedding. The conglomerate is clast-supported with a matrix of muddy sand.

Micromorphologic analysis of diamictites from the Wynyard Formation reveals a high density of skeletal grains (grains larger than silt, cf. Menzies and van der Meer, 2006). The larger skeletal grains (0.2 – 1 mm) are subrounded, while smaller grains (0.05 – 0.2 mm) are subangular. Each grain is typically surrounded by plasmic fabric,

but where grain-on-grain contacts occur, there is no sign of grain crushing. Skeletal grains are primarily quartz and sandstone fragments, and no microfossils are observed. Rotational structures are profuse in thin section and are also visible to the naked eye on polished surfaces in hand samples. Rotational structures occur with and without core stones (Fig. 40). Pressure shadows rarely occur against grains. The plasmic fabric is well developed skelsepic fabric, where silt and finer grains are oriented parallel to grains.

#### **4.2.2. Stratified diamictite facies association interpretation**

The stratified diamictite facies association was deposited predominantly by debris flows, with contributions from rain-out from icebergs and deposition from hyperconcentrated flows. Stratified diamictite beds were deposited by cohesive debris flows; this interpretation is based on their bedding, stacking, sharp lower and upper contacts, sheet geometry, and reverse grading (cf. Middleton, 1970; López Gamundí, 1991; Parsons et al., 2001). Lamination and/or fissility at the base of stratified diamictite beds may be the result of shearing at the base of the original debris flow. Dewatering occurred after the flows came to rest. The interbedded sandstones may have been produced by flow transformation, when the tops of debris flows mixed with the water column, resulting in either hyperconcentrated flows or turbidity currents (cf. Mulder and Alexander, 2001; Winsemann et al., 2007). Clasts that pierce stratification were likely dropped in as iceberg rafted debris (Thomas and Connell, 1985). The clumps of small pebbles and granules in stratified diamictite were probably formed from frozen aggregates of coarse sediment that fell from icebergs to the sea floor, held together by interstitial ice (Gilbert, 1990). Conglomerate deposition likely occurred by cohesionless

debris flows/grain flows. The presence of mud in the conglomerate matrix precludes deposition by streams of glacial outwash.

Deformation in stratified diamictite is likely the result of glacial push and soft-sediment deformation. The deformed beds of stratified diamictite and sandstone bounded by shear zones (section A, 8 m; Fig. 38D) probably formed by intervals of glacial pushing. Similarly, the concave-up beds (section D, 1 – 4 m, Fig. 38E, F) formed from glacial readvance after stratified diamictite and interbedded sandstones were deposited (cf. Lønne, 2006). These units are similar to DeGeer moraines, which form in subaqueous settings from seasonal fluctuations in the position of the ice front (Hoppe, 1959). The upturned beds suggest development of numerous small-scale thrust blocks that mark the extent of ice push, yet formed under overall ice retreat conditions (cf. Boulton, 1986; Benn and Evans, 1998; Lønne, 2006). The trends of the structures indicate compression toward the ESE, E, and NE. Soft-sediment deformation in stratified diamictite such as slumping and folding occurred in the diamictites as material slid downslope, and folding occurred due to frictional differences along the basal surface of the bed as it moved across the substrate (cf. López Gamundí, 1991).

The microstructures in Wynyard diamictites indicate water-rich diamict that experienced abundant ductile deformation rather than subglacial shearing. The absence of tile structures and fissility suggests that deposition of diamictites could not have been purely subglacial, as ‘lodgment till’ (cf. van der Meer et al., 2003). Instead, the rotational structures and well-sorted domains align well with the above interpretations of deposition by iceberg rain-out and debris flow resedimentation in the proglacial environment of a wet-based tidewater glacier. The skelsepic plasmic fabric formed as a response to the



rotational structures, because clay and silt enveloped skeletal grains as they rotated, forming a fabric parallel to grain margins (Menzies and van der Meer, 2006).

### **4.3. Conglomerate and sandstone facies association**

The conglomerate and sandstone facies association occurs in sections A, B, C, and D (Fig. 37).

#### **4.3.1. Conglomerate and sandstone facies association description**

The conglomerate and sandstone facies association consists of sandy pebble conglomerate, cobble conglomerate, pebbly coarse-grained sandstone, and massive sandstone (Fig. 41, Table 1). Clast lithologies are quartzite, red granite, conglomerate, sandstone, and siltstone. Sandy pebble conglomerate is the dominant facies of the facies association and is clast-supported with a matrix of medium- to coarse-grained sand, and maximum clast size is 17 cm. Beds typically contain trough or planar cross-beds up to 80 cm thick (Fig. 41A). A few distinctive cross-beds have low angle, highly tangential foresets and display lunate geometries up to 15 m long in plan view from the toe of the cross-bed to the top of the bed. In these cross-beds, gravel foresets grade downward along the foreset and into bottomset beds consisting of medium-grained sand, forming a coarsening-upwards sequence up the foresets within individual cross-bed sets. Bottomset sandstone appears horizontally laminated to massive. Lower contacts within individual beds are either sharp, or appear to have destroyed sedimentary structures in the underlying beds and are therefore classified as erosional. Upper contacts are sharp.

Cobble conglomerate is normally graded, containing cobbles and pebbles with a maximum clast size of 20 cm and a matrix of medium to coarse sand (Fig. 41B). Lower contacts of beds are erosional, and upper contacts are sharp. Pebbly coarse-grained

sandstone is made up of coarse sandstone with granules and small pebbles. Maximum clast size is 2 cm. Pebbly coarse-grained sandstone exhibits trough cross-bedding, and granules and pebbles are aligned with cross-beds. Lower contacts are sharp, and upper contacts are sharp or eroded by sandy pebble conglomerate. Massive sandstone is composed of fine- and medium-grained sand with occasional pebbles. Maximum clast size is 3 cm. Lower contacts are sharp, and upper contacts are gradational with sandy pebble conglomerate. On the tops of massive sandstone beds are faint fissures (Fig. 41C). The fissures are connected to lenses of fine-grained sand that are visible from the side of the bed.

#### **4.3.2. Conglomerate and sandstone facies association interpretation**

The conglomerate and sandstone facies association was deposited by glacial outwash as parts of grounding-line fans (cf. Powell, 1990) and/or a glaciofluvial system. The stratigraphic proximity in section A of the conglomerate and sandstone facies to diamictite (Fig. 37), suggestive of a morainal bank, leads to the interpretation of a grounding-line fan depositional environment. Powell (1990) interpreted the area covered by section B as a grounding-line fan in which barchanoid bars formed from episodic turbulent jets that transformed into vertical turbulent jets. Alternately, the absence of mud in the conglomerate matrix and a lack of soft sediment deformation structures could also be explained as deposition in a braided outwash system. Additionally, it is possible that boundaries within the succession of the Wynyard Formation are disconformities, and unconformities are also possible between sections where outcrops are not exposed. Therefore, the conglomerate and sandstone facies, especially in section B, may have been

deposited in a different environment than the interpreted morainal bank in section A, such as glacialfluvial outwash.

Normally graded beds and rapid stratigraphic changes among conglomerate, sandstone, and diamictite occur as a result of fluctuating discharge common to glacialmarine effluent flow (cf. Powell, 1990; Hunter et al., 1996). Glacial outwash is discharged episodically and can fluctuate with seasonal temperatures (e.g., Cowan and Powell, 1990; Cowan et al., 1999). In the Wynyard Formation, the interbedding of cobble conglomerate, sandy pebble conglomerate, and pebbly coarse-grained sandstone may have resulted from cyclic changes in efflux (cf. Powell, 2003).

The sandy pebble conglomerate was deposited by high energy turbulent flows that formed 2-d and 3-d dunes (cf. Winsemann et al., 2007). The tangential, low-angle cross-beds that grade from gravel to medium sand down the foreset may have been deposited by turbulent flows that transformed into a plume, thus recording the ‘detachment zone’ (cf. Powell, 1990). The cobble conglomerate beds were deposited from hyperconcentrated density flows (cf. Lowe, 1982; Kneller, 1995; Mulder and Alexander, 2001; Winsemann et al., 2007). The pebbly coarse-grained sandstone was deposited by glacial outwash that formed 3-d dunes, based on the trough cross-bedding and sharp lower contacts with sandy pebble conglomerate. Fluctuations in grain-size in the pebbly coarse-grained sandstone suggest fluctuations in flow velocity. Massive sandstone was deposited by hyperconcentrated flows that dewatered following deposition, creating fissures (cf. Shanmugam, 1996; Marr et al., 2001).

#### **4.4. Deformed mudstone and fine sandstone facies association**

The deformed mudstone and fine sandstone facies association is characterized by conspicuous soft sediment deformation and occurs in section C (Fig. 37).

#### **4.4.1. Deformed mudstone and fine sandstone description**

The deformed mudstone and fine sandstone facies association consists of mudstone and very fine- to fine-grained sandstone (Fig. 42, Table 5). Most upper and lower contacts between units are sharp and often appear undulating. Where the mudstone transitions upward into conglomerate and sandstone in section C, the upper levels of mudstone bedding are partially destroyed and filled in by conglomerate, creating an erosional contact. Additionally, mudstone units locally exhibit convolute bedding and mix with underlying muddy stratified diamictite (Fig. 42A). Similarly, some mudstone beds exhibit cusp-shaped flame or diapir structures where overlain by medium-grained sandstone (Fig. 42B). Original laminations are not identifiable within the flames/diapirs, and bedding is chaotic. A clastic dyke over 90 cm long (in plan view) consisting of very fine-grained sandstone cuts obliquely through a mudstone bed (Fig. 42C). The dyke is pipe-shaped and internally deformed. Many mudstone beds contain outsized clasts ranging from 5 mm to 70 cm in diameter. Lithologies of outsized clasts are sandstone, siltstone, quartz, and red granite. Some clasts are striated. Larger clasts (> 20 cm diameter) show obvious breaking and penetrating of underlying strata and draping of overlying strata (Fig. 42D).

Sandstone occurs as both beds and pods with sharp upper and lower contacts. Where sandstone occurs as beds, current ripple cross-lamination is common (Fig. 42E). Rippled fine-grained sandstone beds have rib and furrow structures indicating an average paleoflow orientation of 149°. However, thin (1 – 5 cm) sandstone beds are typically

massive. Load structures of fine-grained sand also occur, which are internally deformed or massive (Fig. 42F).

Sedimentary volcano structures occur abundantly within this facies association, composed of siltstone to fine-grained sandstone. These dewatering structures consist of concentric rings of chaotic sediment that build upward with a shallow, small depression in the middle (Fig. 42G). The volcano structures range from 5 cm to 2 m in diameter and have a flat appearance, rising no more than 5 cm above the surrounding bed. At one locality, a sand volcano and a large (30 cm) dropstone were deposited adjacent to each other on the same mudstone bed, with the volcano lying conformably on top of the mudstone, and the dropstone penetrating into the mudstone (Fig. 42H).

#### **4.4.2. Deformed mudstone and fine sandstone interpretation**

The deformed mudstone and fine sandstone facies association displays profuse soft-sediment deformation and indications of ice rafted debris. Soft-sediment deformation typically occurs in subaqueous environments with interbedded mud and sand, where sediment is rapidly deposited and compaction is minimal (Lowe, 1975; Allen, 1982; Obermeier, 1996). The deformation structures indicate water escape (flames, clastic dyke, volcanoes) and sinking of denser material into underlying water-saturated units (loads).

Dewatering structures occur in interbedded mud and sand because the minimal porosity of mud pressurizes pore water in sand (Yassir, 1990). When pore water is overpressured, water moves upward and creates vertical shear stress on grains, dragging them upward (Allen, 1982; Owen, 1987; Oliveira et al., 2009).

Flame structures can form from liquefaction or fluidization, which both cause sediment to lose its strength and behave like a viscous fluid and to deform plastically (Lowe, 1975). The absence of original lamination from the dewatered beds in the flame structures indicates that fluidization was the deformational mechanism, as fluidization uplifts grains through turbulent flow and destroys original depositional structures (Lowe, 1975; Oliveira et al., 2009). Similarly, the convolute bedding between diamictite and overlying mudstone formed from hydroplastic deformation and failure of the two units following mud deposition on the water-rich diamict below (Lowe, 1975; Oliveira et al., 2009).

Clastic dykes form from injection from a source bed, as a slurry of sediment infiltrates a fissure in the host bed/beds in response to pressure from above (Obermeier et al., 1989). The deformation within the very fine-grained sandstone dyke suggests that the sediment was fluidized. Internal deformation in dykes indicates shearing of the material as it moved through the host.

Volcano structures can occur in deposits ranging from mud to medium-grained sand (Burne, 1970). The units containing the volcano structures were deposited by sandy to silty hyperconcentrated flows. After deposition, the sand/silt dewatered as it partially sunk down into underlying mud. The depositing current must have been brief, as the excellent preservation and circular shape of the volcano indicate quiet water. Subsequent deposition of mud also aided preservation.

Sand load structures indicate that after a sand bed was deposited, it ruptured and sank into underlying mud due to a gravitational inverse density gradient (Allen, 1982; Collinson and Thompson, 1982; Owen, 1987; Hindmarsh and Rijksijk, 2000). The sand

could not maintain cohesion as a single bed, and collapsed into a substrate that had low cohesion, minimal compaction, and high porosity.

The deformed mudstone and fine sandstone facies association was deposited in a distal, subaqueous proglacial setting with quiet water and ice-rafted debris. The presence of striated outsized clasts penetrating and deforming beds of mudstone and fine sandstone suggests dropstone deposition from icebergs (Thomas and Connell, 1985; Gilbert, 1990). The abundance of water-saturated sediments and the remobilization of sediment suggest rapid deposition, like that produced by meltwater plume deposition. Thus, fine sand and mud were likely deposited by meltwater plumes and waning turbidity currents, and ripple structures in sandstone formed by underflows. Rapid sedimentation rates are common to the glacial marine environment and would result in water-rich, unstable substrates (Powell and Cowan, 1986; Boulton, 1990; Powell and Domack, 2002). In addition, the force of large dropstones striking the substrate may have shocked underlying beds and instigated dewatering and the formation of clastic dykes and mud and sand volcanoes (i.e., Fig. 42H). The impact from the dropstones may have caused fluidization and/or liquefaction, the mechanisms necessary for dewatering to occur (Allen, 1982; Oliveira et al., 2009).

#### **4.5. Depositional environments of the Wynyard Formation**

The four facies associations of the Wynyard Formation were deposited in the proglacial environment of a wet-based tidewater glacier(s) that occupied a trough cut through northwestern Tasmania (Fig. 32). This facies analysis supports the glacial marine interpretation by Banks and Clarke (1987), Clarke (1989), Powell (1990), and Hand (1993). Evidence for a glacial marine environment includes marine acritarchs (Downie and Sarjeant, 1964; Truswell, 1978) and beds of fine sandstone and mudstone that were

deposited by meltwater plumes, which require a density contrast between inflowing waters and ambient waters in the depositional basin for their formation. The depositional setting may have been either fjordal, i.e., restricted within the trough cut through northwest Tasmania (Fig. 32), or open marine. Ice rain-out, gravity flows, glacial outwash, suspension settling, and dewatering were the primary depositional mechanisms for the formation and are illustrated in Figure 43. Microstructures indicate that deformation of diamictites at Wynyard was almost entirely ductile, due to the high water content in diamict as it was deposited. No evidence of subglacial shearing or scouring was identified in the Wynyard Formation in the studied sections. However, Banks (1981) described a striated surface east of Doctors Rocks where strata of the Wynyard Formation rest unconformably on Precambrian quartzite and schist. That site was not visited during this study.

Although the measured sections are not continuous, fluctuations of the depositional environment and glacial front can still be determined. Sections A and B record proximal proglacial deposition of a morainal bank that developed into a grounding-line fan. This transition may be the result of an increase in glacial outwash, possibly due to seasonal or climatic warming (cf. Powell, 1990), a decrease in iceberg calving, which can result from damming by sea ice (Powell and Domack, 2002), migration of the efflux point, or because the glacial front retreated out of the sea, onto land. The latter is unlikely, based on the deposits of section C. Section C records a more distal environment than A and B that received ice rafted debris, turbidity currents, and underflows. During the deposition of C, the glacier front retreated from the area but remained tidewater as indicated by the presence of dropstones and outsized clasts in



mudstone. If icebergs were still calving during deposition of C, when glacial retreat is obvious, they were probably also calving during deposition of B, when the glacier front was proximal. In addition, Powell (1990) identified large pebbles on the top of barchanoid bars in section B and interpreted them as ice rafted debris. In B, signatures of ice rafting were overwhelmed by glacial discharge.

In C, mudstone transitions upward into stratified diamictite, which may represent either 1) glacial readvance and the encroachment of debris flows emanating off the morainal bank, or 2) intensified iceberg rain-out and resedimentation of ice rafted debris along the substrate as debris flows. Lastly, section D records multiple glacial advances. First, the glacier front advanced (relative to the position in section C) and deposited diamictite and conglomerate. Next, the glacier front retreated and then readvanced to shove the interbedded diamictite and conglomerate, forming the concave-up beds in Figure 39D. Finally, the glacier deposited the conglomerate, sandstone, and diamictite in the upper 5 m of section D. Thus, the Wynyard Formation records a dynamic glacier front that produced a wide variety of proglacial deposits and structures.

The thick accumulation of glacialigenic strata in the Wynyard Formation is common to glacialmarine environments. In modern settings, individual morainal banks up to 175 m thick have been documented (Cai et al., 1997). Further, morainal banks can be stacked as a result of advance/retreat cycles (Willems et al., 2009). Therefore, the thickness of the Wynyard succession does not require that it was deposited by multiple glaciations. Instead, the Wynyard Formation could have been deposited in one glacial event by a dynamic glacial front that deposited large quantities of sediments (cf. Powell and Cowan, 1986; Boulton, 1990). However, because the sections are not complete, it is difficult to

ascertain whether these strata were deposited during a single glaciation or multiple glacial cycles during the Late Pennsylvanian to Early Permian glacial interval (cf. Truswell, 1978).

### **5. The Wynyard glacial record compared to nearby basins in Gondwana**

The last evidence of grounded ice in the Tasmania Basin is found in the Wynyard Formation and correlative diamictites, which is overlain by the Inglis Formation and correlative mudstones (Figs. 34, 35). The signature of thick Upper Pennsylvanian – Lower Permian glacial and glacial-marine deposits overlain by mudstone that is relatively dropstone-poor also occurs in Antarctica, South Africa, and eastern Australia (Fig. 44). The sharp contacts between glacial deposits and post-glacial mudstones in all the regions suggest abrupt environmental transitions as glaciers retreated from the depositional basins, resulting in an abrupt change in facies. Icebergs or sea ice deposited rare ice-rafted debris in the lower portions of the post-glacial facies, but the presence of grounded ice or ice-contact deposits are not recorded in post-Sakmarian strata of Tasmania, Antarctica, or South Africa following deposition of the Wynyard, Pagoda, Dwyka, or equivalent rocks (Fig. 44).

In contrast, ice sheets returned to eastern Australia in the late Sakmarian, classified as the P2 glaciation by Fielding et al. (2008a, b; Fig. 44). The glacial deposits of the P2 glaciation in eastern Australia are diamictites and outsized clasts deposited in glacial-marine environments in the Sydney, Gunnedah, and Bowen Basins (Fielding et al., 2008a). These glaciers must have had high mass balance budgets, which allowed the glaciers to reach sea level. During this interval, the South Pole was still in Antarctica (Fig. 33; Powell and Li, 1994; Li and Powell, 2001; Blakey, 2008; Lawver et

al., 2008). In Tasmania, the upper part of the Bundella Formation and the Liffey Group (Figs. 34, 35) have been correlated to P2 deposits in eastern Australia by Fielding et al. (2010) due, in part, to the presence of outsized clasts in these two formations. Although the presence of outsized clasts in these units indicates cold climatic conditions in the late Sakmarian, ice contact deposits have not been identified in Tasmania during P2. The absence of deposits from grounded ice elsewhere in Gondwana during P2 suggests that climatic conditions in Gondwana at this time were vastly different from those during the earlier Permian glaciation. Rather, Antarctica was characterized by fluvial deposits (Fairchild Formation) and coal-bearing fluvial deposits (Buckley Formation) during P2 (Figs. 33, 44; Collinson et al., 2006). In the Karoo Basin in South Africa, siltstone and mudstone of the Prince Albert Formation (Veevers et al., 1994; Faure and Cole, 1999; Herbert and Compton, 2007) was deposited during P2.

Because the Karoo, Transantarctic, and Tasmania basins all resided at sea level, the absence of glacial deposits suggests that the elevation of the snowline (or equilibrium line, the elevation that separates ice accumulation from areas of ablation) was elevated throughout the rest of the Permian within the South Polar Circle. During the P2, P3, and P4 glaciations, the elevation of the highlands in eastern Australia may have been favorable for ice to nucleate, forming ice sheets during P2 and ice caps and valley glaciers during P3 and P4 (Herbert, 1981; Eyles, 1993; Veevers, 2006; Fielding et al., 2008a) when  $p\text{CO}_2$  levels were higher than during P1 (Montañez et al., 2007). However, glaciers never flowed into the sea in basins farther to the south. Thus, a major control on glaciation in southern Gondwana by the late Sakmarian may have been elevation.

Another factor fostering glaciation in eastern Australia may have been cold upwelling waters along eastern Gondwana/eastern Australia (Jones et al., 2006). This hypothesis of upwelling of cold, nutrient rich, deep ocean water is supported by ikaite formation (Domack et al., 1993; Jones et al., 2006), high total organic carbon contents in offshore Permian strata in eastern Australia (Jones et al., 2006), and wind and ocean circulation reconstructions for the region (cf. Gibbs et al., 2002; Winguth et al., 2002).

Glaciation in Tasmania, Antarctica, South Africa, and eastern Australia occurs in an interval during the latest Carboniferous – Early Permian (early Sakmarian, Fig. 44). The end of this glacial interval has been correlated with a dramatic rise in atmospheric  $p\text{CO}_2$  in the mid- to late Sakmarian by Montañez et al. (2007). In the late Sakmarian, glaciation resumed in eastern Australia (P2; Fig. 44), and cold conditions may be inferred for Tasmania, based on the presence of dropstones and glendonites. Montañez et al. (2007) document a drop in  $p\text{CO}_2$  again in the late Sakmarian – early Artinskian, correlating with P2. The collapse of P2 glaciers in the early Artinskian corresponds to a rise in  $p\text{CO}_2$ , and then  $p\text{CO}_2$  declined ~25% by the time of P3. Present climate models for P3 do not support glaciers in Australia (Horton and Poulsen, 2009), but elevations for Australia are low in these simulations (< 500 m). Correction for elevation in eastern Australia may resolve inconsistencies between the climate models and the stratigraphic record, and attention to the role of elevation in other glacial intervals may inform other waxing and waning patterns during the LPIA.

## 6. Conclusions

The Wynyard Formation is composed of massive diamictite, stratified diamictite, conglomerate, sandstone, and deformed mudstone, and these deposits record ice rafting,

gravity flows, glacial outwash, and suspension settling and dewatering, respectively. Cycles of glacial advance and retreat are recorded by these strata, indicating a dynamic glacial front.

The Wynyard Formation and correlative diamictites in Tasmania are the last evidence of grounded ice in the Tasmania Basin and correlate with glacial facies of Antarctica, South Africa, and eastern Australia in the Late Carboniferous – Early Permian (early Sakmarian). This glaciation across southern Gondwana receded in the mid-Sakmarian, and post-glacial mudstone was deposited above glacial facies. However, glaciation resumed in eastern Australia in the late Sakmarian, even though eastern Australia was located at lower latitudes than non-glaciated areas of Gondwana farther south. Renewed glaciation in eastern Australia may have been enabled by elevated highlands in eastern Australia and ocean circulation patterns.

### **Acknowledgments**

We thank Steve Forsyth and Catherine Reid for their assistance with stratigraphy and field sites. Ross Powell also provided helpful input on exposures of the Wynyard Formation. Microscope equipment was provided by Dyanna Czeck and Lindsay McHenry at the University of Wisconsin-Milwaukee. We appreciate the helpful reviews by Finn Surlyk and two anonymous reviewers. Financial support was provided by the National Science Foundation – Office of Polar Programs/Earth Sciences grants 0635537, 0944532, and 0943935 to the University of Wisconsin-Milwaukee and 0635540 to the University of Nebraska- Lincoln, the American Association of Petroleum Geologists Student Grants-in-Aid, and the J. W. Johnson Family Chair in Environmental Studies at Hamilton College.

**Table**

Table 5. Facies descriptions and interpretations of the Wynyard Formation

<b>Facies association</b>	<b>Lithologies</b>	<b>Sedimentary structures</b>	<b>Bed thickness</b>	<b>Interpreted mechanisms</b>	<b>Depositional environment</b>
Massive diamictite	Massive to weakly stratified diamictite, massive sandstone, normally graded sandstone pods	Loads, flames, thin sandstone dykes	Massive diamictite: 50 cm – 1 m Weakly stratified diamictite: 20 cm – 1 m Massive sandstone: 15 – 80 cm	Rain-out from icebergs, debris flow resedimentation, dewatering	Morainial bank
Stratified diamictite	Stratified diamictite, fine- to medium-grained sandstone, conglomerate	Folded and slumped diamictite, sheared diamictite, concave-up beds of diamictite, cross-laminated and cross-bedded sandstone, climbing ripples, sand loads, dropstones, clumps of small pebbles and granules Micromorphology: skelsepic plasmic fabric, subrounded skeletal grains, rotational structures, pressure shadows, lineaments	Stratified diamictite: 5 – 50 cm Sandstone: 1 – 40 cm Conglomerate: 10 – 30 cm	Debris flows, iceberg rain-out, glacial shove, rapid suspension settling, underflows	Morainial bank
Conglomerate and sandstone	Sandy pebble conglomerate, cobble conglomerate, pebbly coarse-grained sandstone, and massive fine to medium sandstone	Planar and trough cross-bedding, massive bedding with dewatering structures, normal grading, channel incisions	Sandy pebble conglomerate: 20 cm – 1 m Cobble conglomerate: 50 cm – 1 m Pebbly coarse-grained sandstone: 10 – 40 cm Massive sandstone: 5 – 20 cm	Glacial outwash	Grounding-line fan, possibly ice-contact delta
Deformed mudstone and fine sandstone	Mudstone containing clay and silt, very fine- and fine-grained sandstone	Ripples, sand and mud volcanoes, flame structures, fine sandstone dykes, convoluted bedding, dropstones	Mudstone: 5 cm – 1 m Sandstone: 1 – 10 cm	Underflows, iceberg rain-out, dewatering due to liquefaction, fluidization,	Distal proglacial, quiet water

				and impact from dropstones hitting the substrate	
--	--	--	--	--	--

## Figures

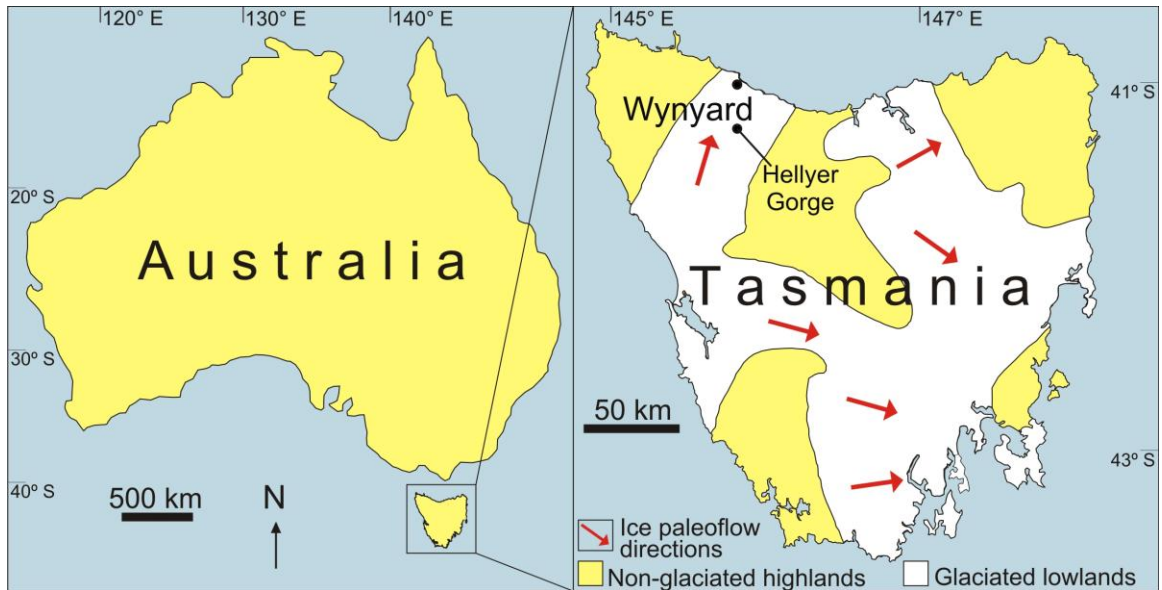


Figure 32. Location map of Wynyard, Tasmania, where the Wynyard Formation is located, and Hellyer Gorge, where equivalent diamictites occur. Glacial distributions after Rogala et al. (2007); ice flow directions after Hand (1993).



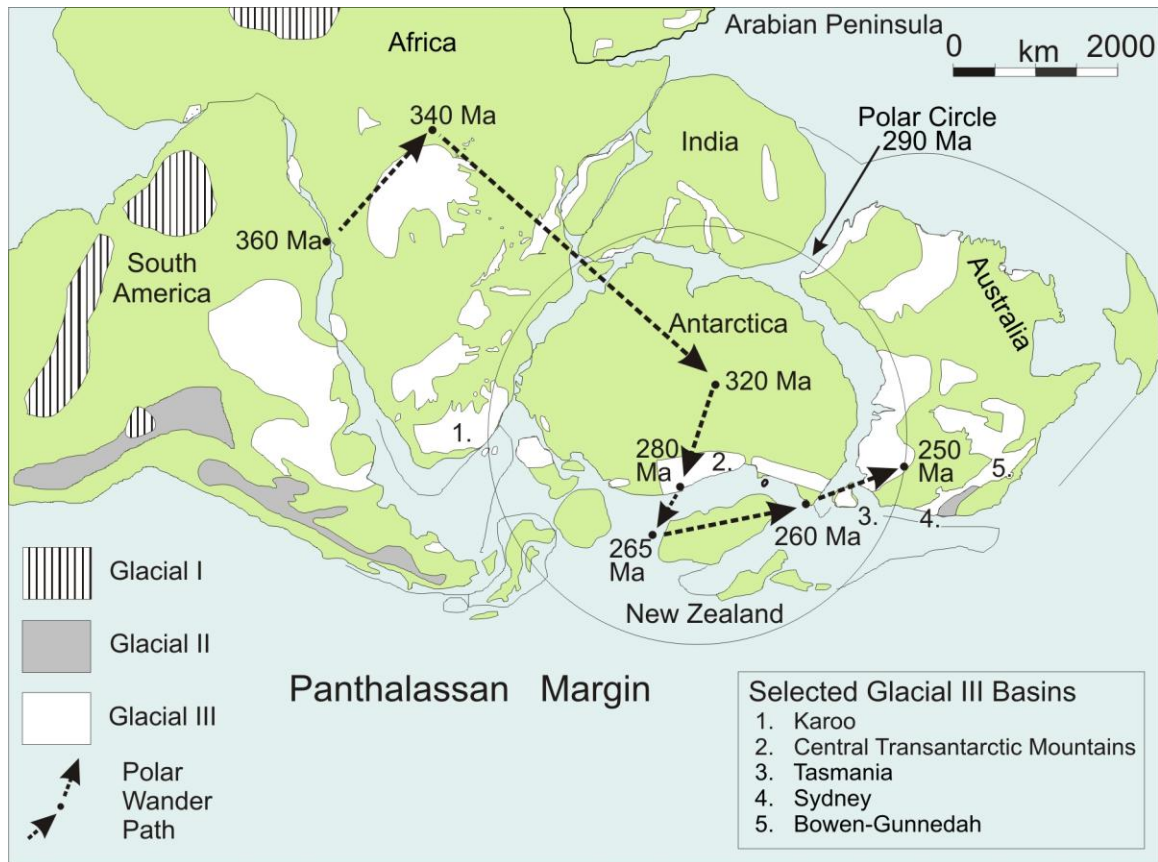


Figure 33. Paleozoic basins of Gondwana, after Isbell et al. (2003b). Arrows show the path of polar wander during the Carboniferous and Permian according to Powell and Li (1994).

Lower Parmeener Supergroup			
System		Stage	Formation
Permian	Middle	Capitanian	Abels Bay Formation
		— 266 —	
		Wordian	Malbina Formation
		— 268 —	
	Roadian		
	— 271 —		
	Kungurian	Deep Bay Fm.	
	— 274 —		
	Lower	Artinskian	Cascades Group
		— 285 —	Liffey Group
Sakmarian		Bundella Fm.	
		— 293 —	Woody Island Fm.
Asselian			Wynyard Formation
— 298 —			
Carb.	Upper	Gzhelian	

Figure 34. Major formations and corresponding ages estimated from biostratigraphy of the Lower Parmeener Supergroup of Tasmania, Australia. Modified from Reid et al. (in press).

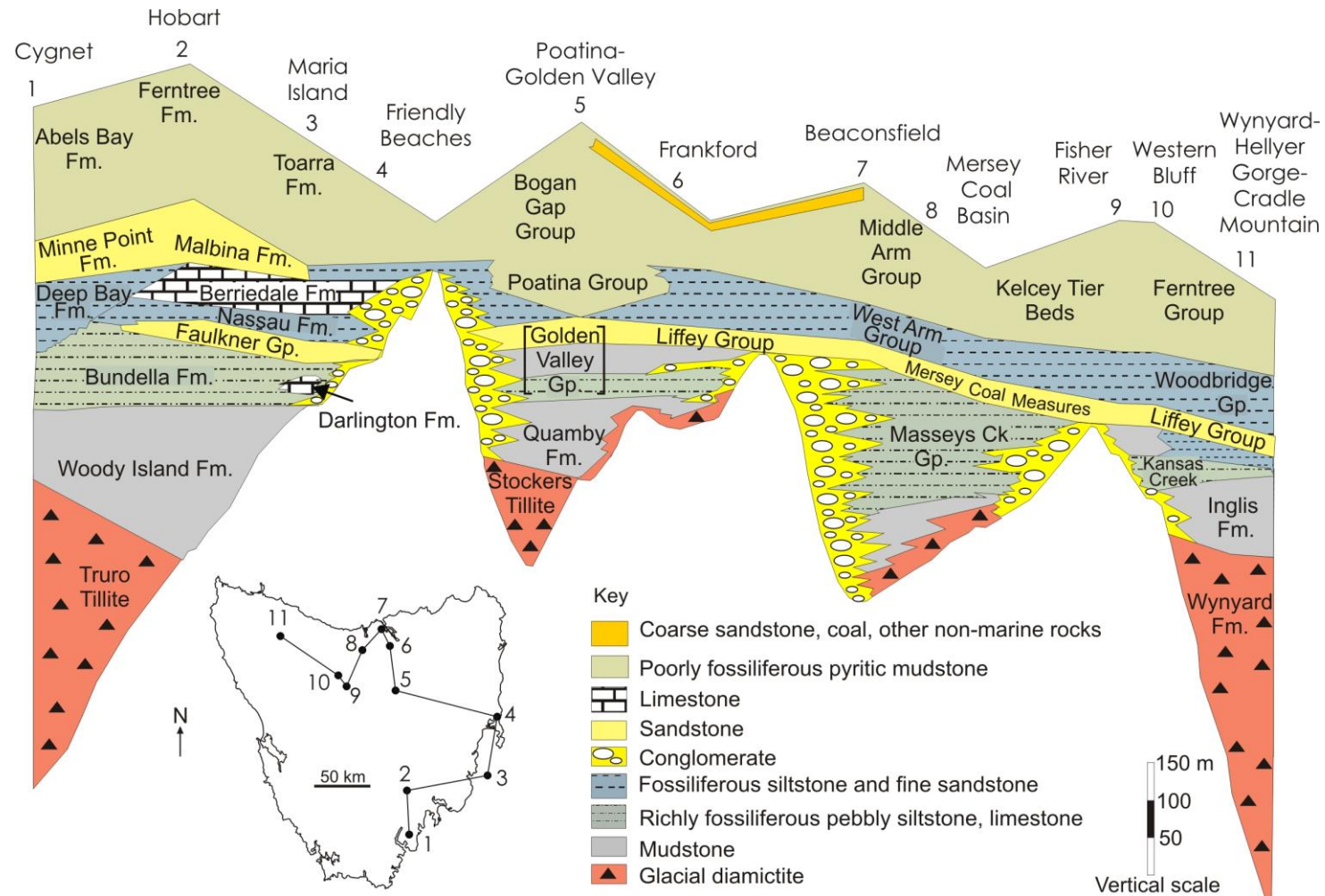


Figure 35. Cross section of the lower Parmeener Supergroup of Tasmania, Australia. Lithostratigraphic units are assigned multiple names depending on location within the Tasmania Basin. The distribution and varying thickness of the deposits illustrates the relief of the troughs that the glaciers occupied (see Fig. 32). Modified from Clarke and Forsyth (1989).

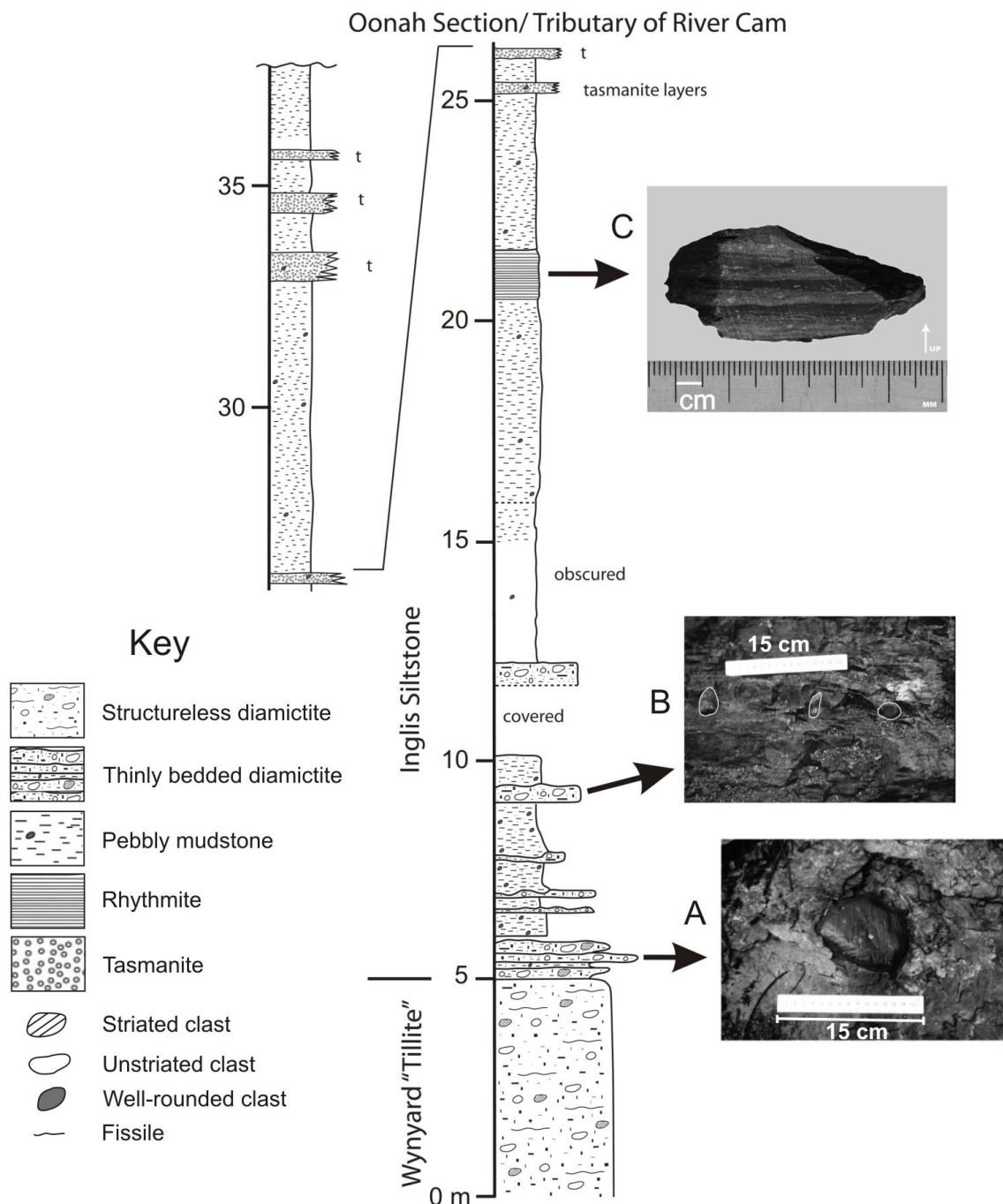


Figure 36. Measured section of the Wynyard Formation and Inglis Siltstone contact as exposed in a tributary of the River Cam, north of Hellyer Gorge and south of Wynard. Inset photographs illustrate from bottom to top: (A) striated dropstone in stratified diamictite, near contact with fissile, structureless diamictite, (B) vertical clasts in mudstone facies of Inglis Siltstone, and (C) rhythmic laminations of siltstone, very fine grained sandstone and mudstone. Also note layers of tasmanite oil shale (t).



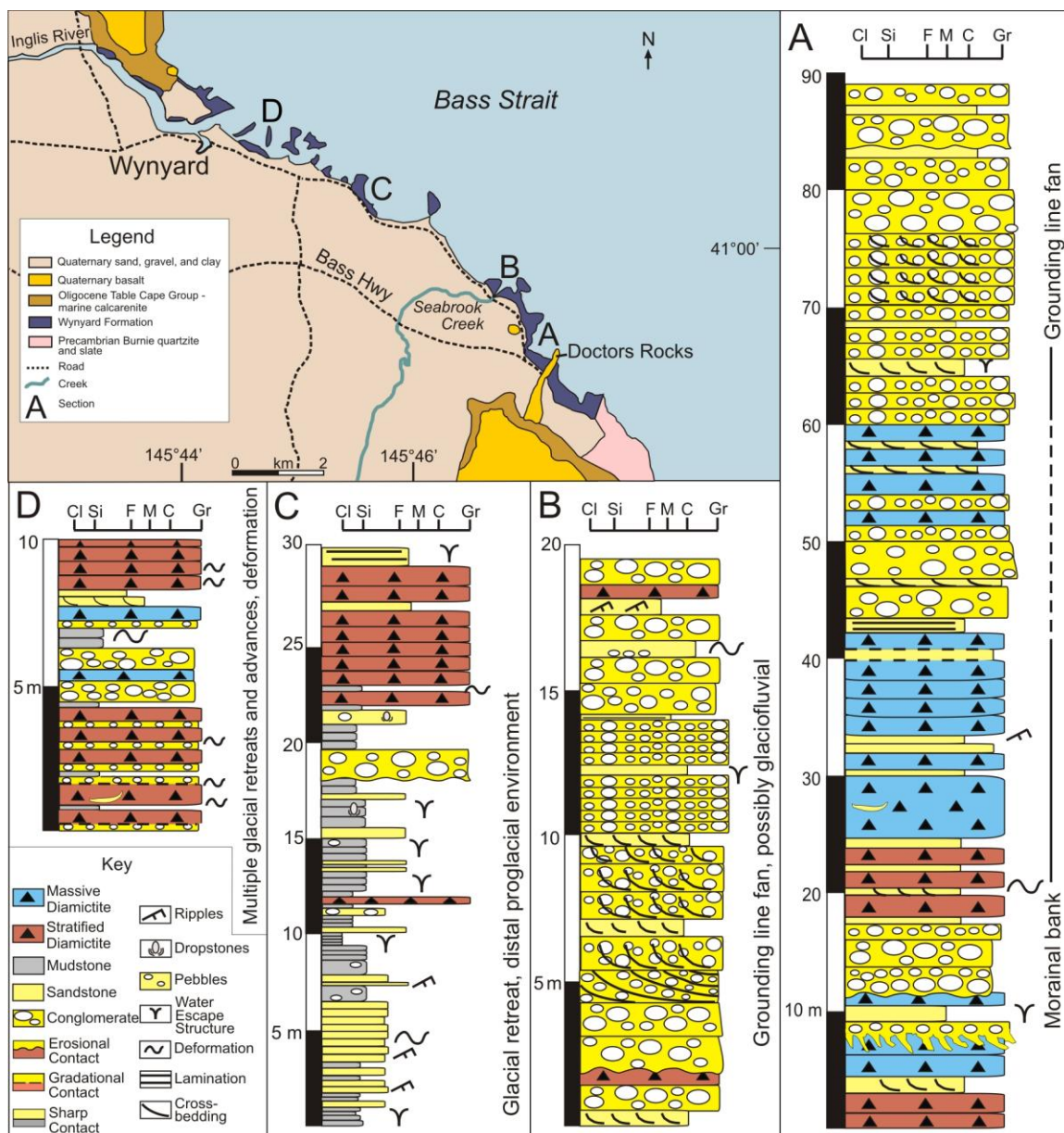


Figure 37. Location map and stratigraphic sections of the Wynyard Formation. Strata young to the west, so section A illustrates the oldest rocks, and section D represents the youngest rocks. The four sections are not continuous due to breaks in the shore platform. Section key also corresponds to Figures 43 and 44.





Figure 38. Massive diamictite facies association. A. Beds of massive diamictite. B. Thin fine-grained sandstone dykes in massive medium-grained sandstone overlying diamictite.



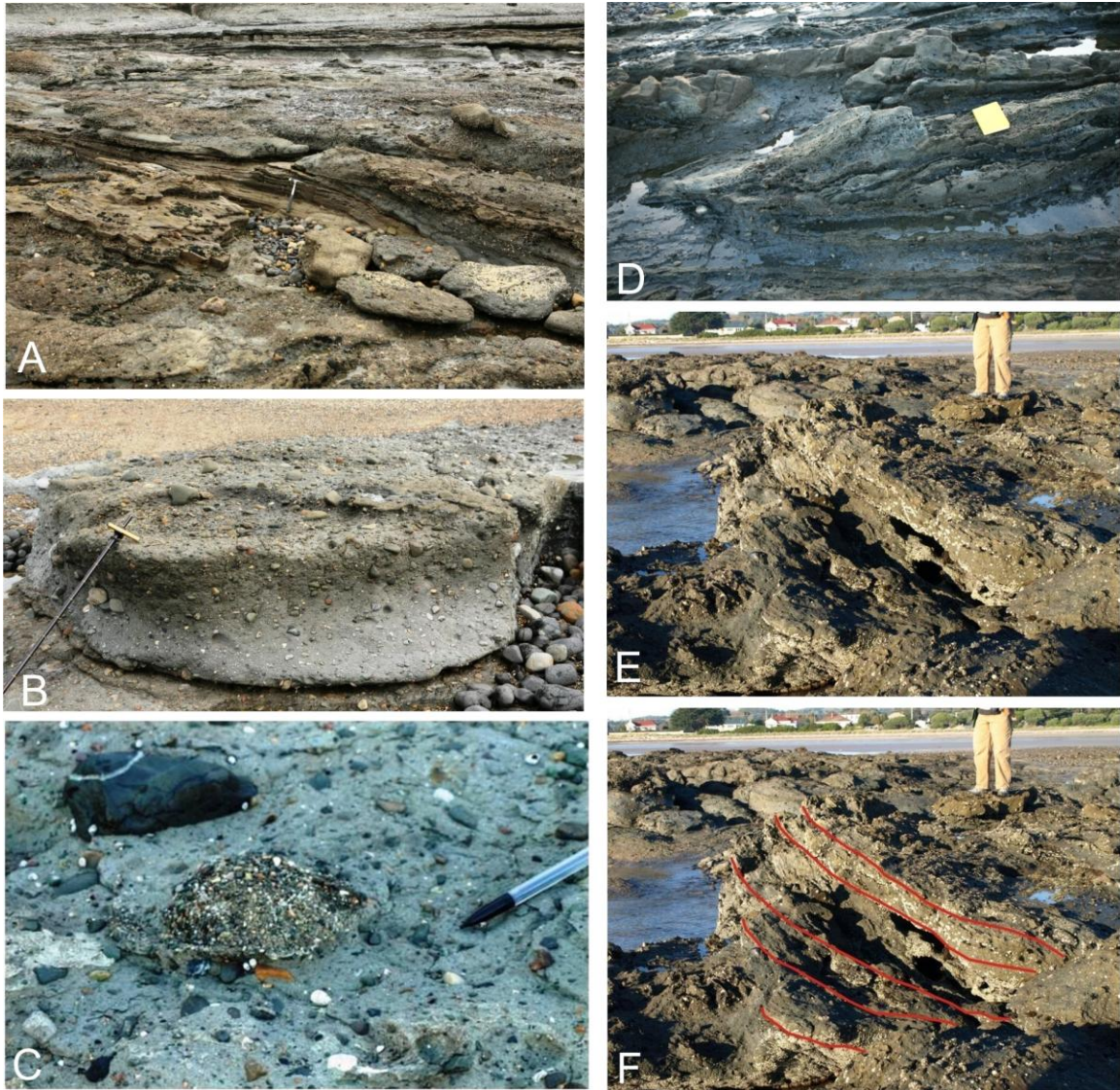


Figure 39. Stratified diamictite facies association. A. Interbedded fine sandstone and stratified diamictite in section A. Hammer for scale rests against cross-bedded sandstone. B. Lensoidal bed of stratified diamictite that shows reverse grading. C. A clump of granules and pebbles within stratified diamictite. D. Sheared interbedded stratified diamictite and sandstone in section A. E. Deformed stratified diamictite in section D. F. Bedding of stratified diamictite is outlined to show that deformation has bent beds into a concave up orientation.

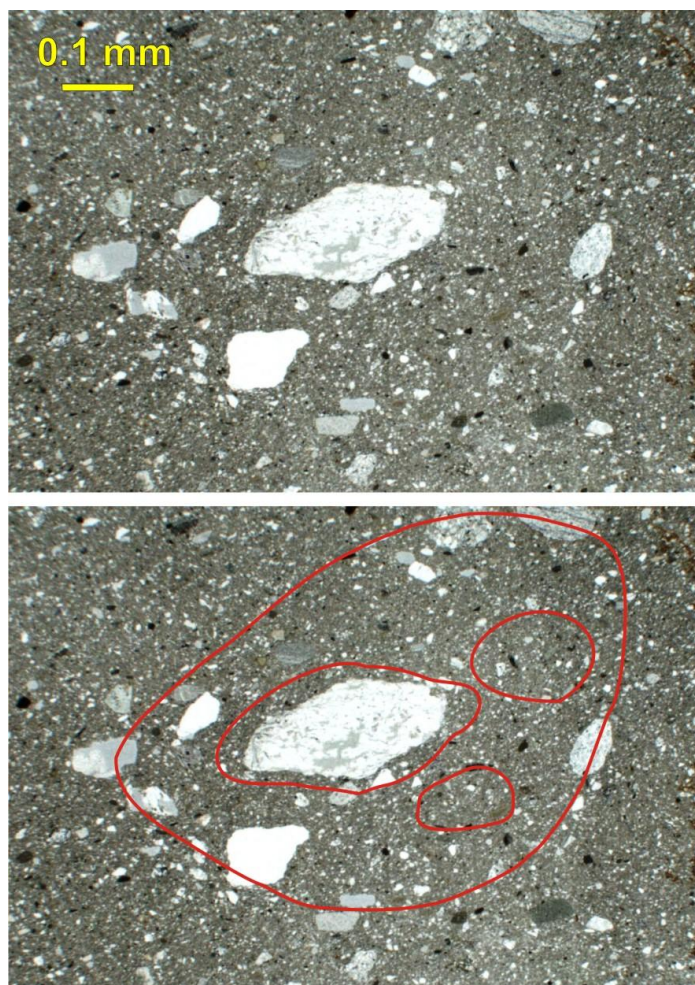


Figure 40. Rotational structures, two around the same core stone, in thin section under plane light from stratified diamictite in the Wynyard Formation.



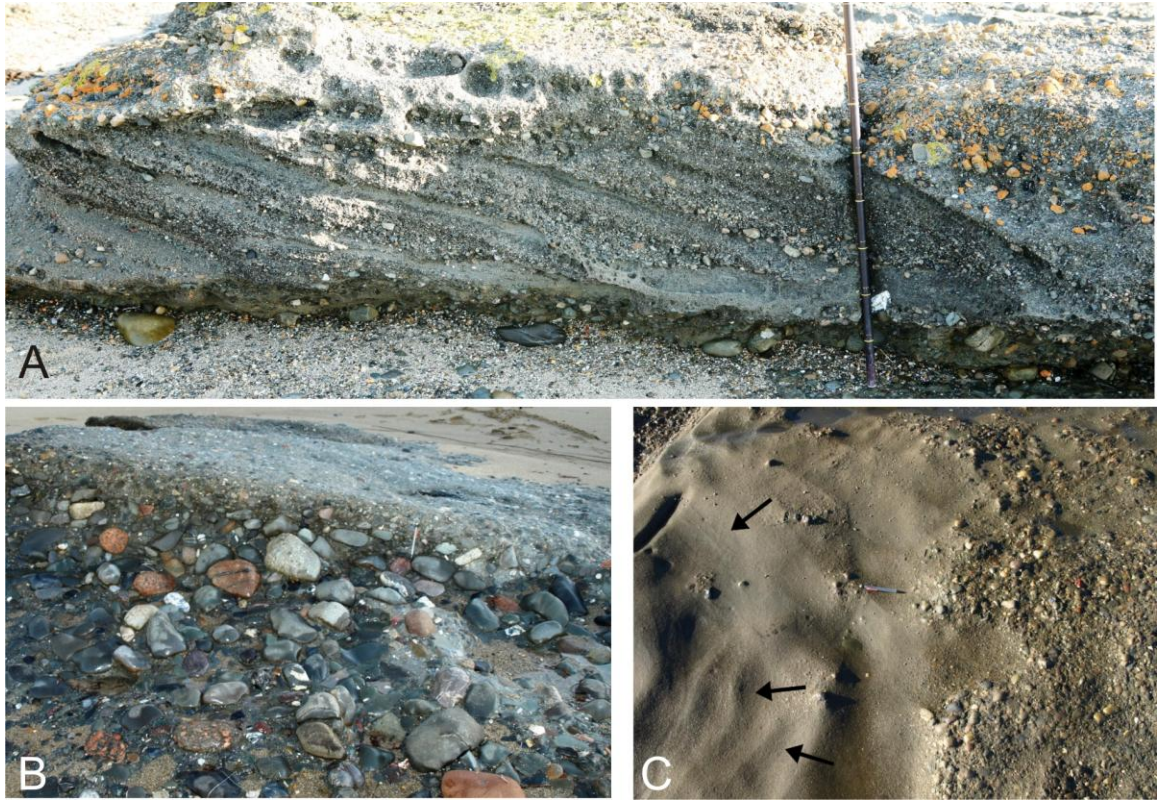


Figure 41. Conglomerate and sandstone facies association. A. Cross-bedding in sandy pebble conglomerate. Grain size fines down foresets, with pebbles grading into medium sand. B. Normally graded cobble conglomerate. Mechanical pencil near the top right of the conglomerate bed for scale. C. Massive fine- to medium-grained sandstone with pebbles that is overlain and grades laterally into sandy pebble conglomerate. Faint fissures in the massive sandstone (pointed out with arrows) are dewatering structures.



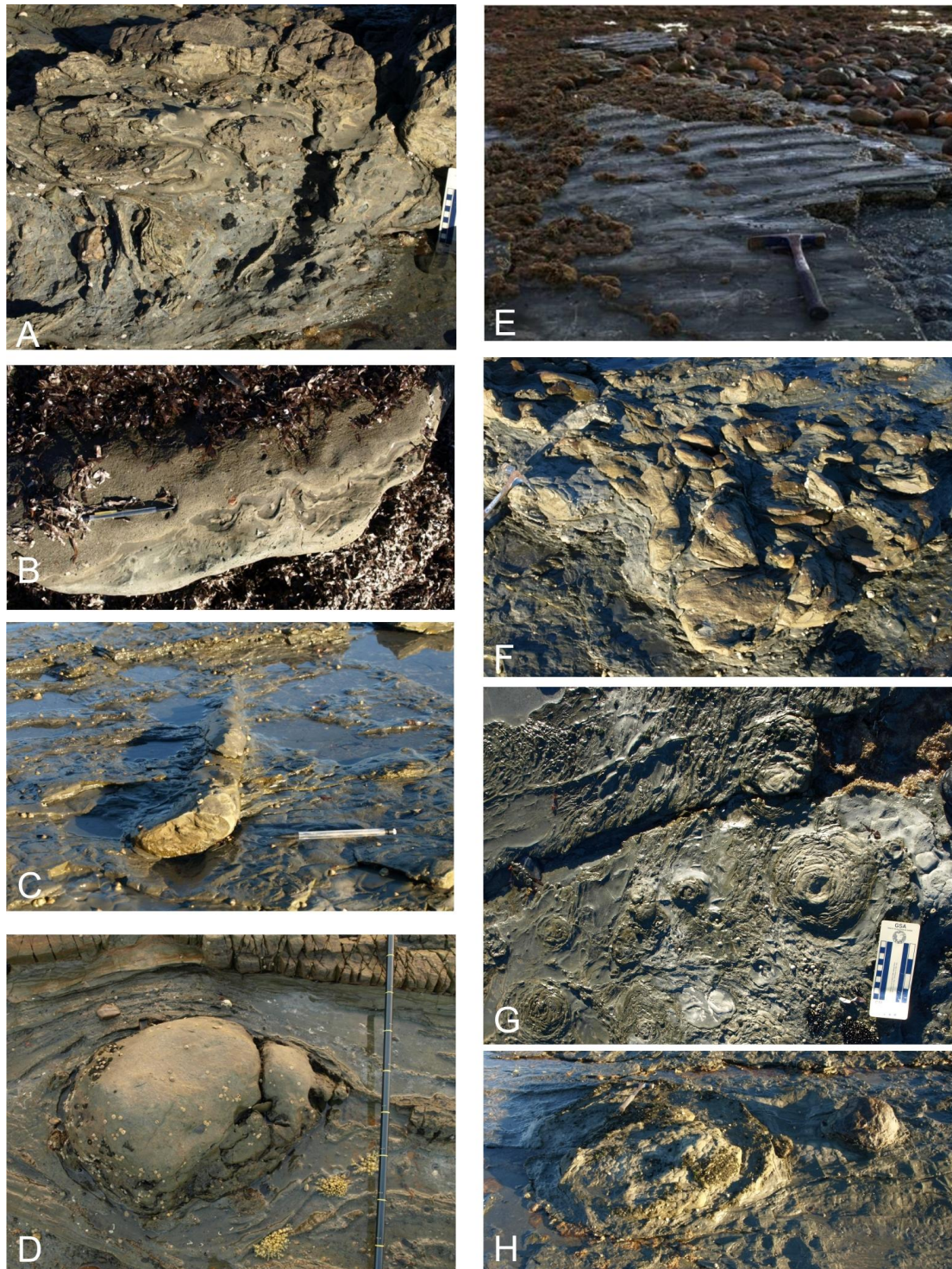


Figure 42. Deformed mudstone and fine sandstone facies association. A. Convoluted mudstone interfingers with underlying muddy diamictite. B. Flame dewatering structures in mudstone. C. A clastic dyke of very fine sand that is internally deformed cuts through mudstone beds. D. Sandstone dropstone in mudstone. The point of view of the photograph is looking down at the top of the bed. E. Rippled fine sand. F. Fine sandstone



load structures within mudstone. G. Mud volcanoes overlying mudstone beds. H. Large sand volcano (80 × 90 cm) and 30 cm dropstone that penetrates substrate occur in the same mudstone bed.

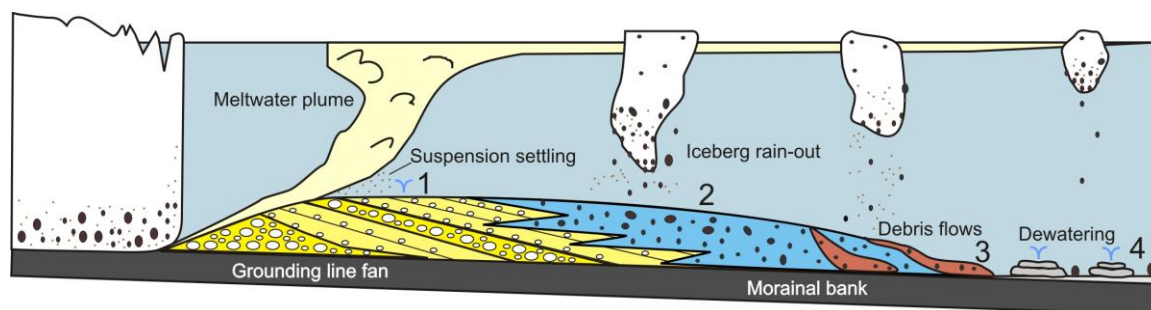


Figure 43. Interpreted depositional processes and environments for the four facies associations of the Wynyard Formation: 1. conglomerate and sandstone, 2. massive diamictite, 3. stratified diamictite, 4. deformed mudstone and fine sandstone. A buoyant meltwater plume carrying fine sand, silt, and clay rises from the glacier terminus. Facies follow the same key as Figure 37. Multiple advance and retreat cycles by the tidewater glacier and efflux variations created the interbedding of these facies as represented in sections in Figure 37.

Age (Ma)	System	International Stage	Microfloral zone	Eastern Australia	Wynyard-Hellyer Gorge	Antarctica	South Africa
280	Early Permian	Cisuralian	4			Buckley	Whitehill
285			3	P2 glaciation	Inglis Formation	Fairchild	Prince Albert
290			3	287.1 ± 2.4 *		Mackellar	290.9 ± 1.7 *
295	Late Carboniferous	Steph.	2	P1 glaciation	Wynyard Formation	Pagoda Formation	Dwyka Group
300			2			?	
305			1				

Figure 44. Correlation diagram for glacial and post-glacial formations in eastern Australia, Tasmania (Wynyard-Hellyer Gorge localities), Antarctica, and South Africa. Ages of formations and palynology stages are from Evans (1969), Truswell (1978), Collinson et al. (1994), Masood et al. (1994), Veevers et al. (1994), Lindström (1995), Price (1997), Askin (1998), Backhouse (1998), Briggs (1998), Claoué-Long and Korsch (2003), Fielding et al. (2008a), and Stollhofen et al. (2008). Dashed lines indicate biostratigraphic age control, and solid lines indicate radiometric age control. Colors of formations reference dominant lithology (see also Fig. 37).

## References

- Allen, J.R.L., 1982. Sedimentary Structures: Their Character and Physical Basis. Developments in Sedimentology, 30. Elsevier, Amsterdam, 2, 663 pp.
- Askin, R.A., 1998. Floral trends in the Gondwana high latitudes: palynological evidence from the Transantarctic Mountains. *Journal of African Earth Sciences* 27, 12–13.
- Backhouse, J., 1998. Palynological correlation of the western Australian Permian. *Proceedings of the Royal Society of Victoria* 110, 107–114.
- Banks, M.R., 1962. The geology of Tasmania: Cambrian System. *Journal of the Geological Society of Australia* 9, 127–145.
- Banks, M.R., 1981. Late Palaeozoic tillites of Tasmania. In: Hambrey, M.J., Harland, W.B. (Eds.), *Earth's Pre-Pleistocene Glacial Record*. Cambridge University Press, Cambridge, pp. 495–501.
- Banks, M.R., Clarke, M.J., 1987. Changes in the geography of the Tasmania Basin in the late Paleozoic. In: McKenzie, G.D. (Ed.), *Gondwana Six: Stratigraphy, Sedimentology, and Paleontology*, 14 pp.
- Benn, D.I., Evans, D.J.A., 1998. *Glaciers and Glaciation*, Arnold, London, 734 pp.
- Biakov, A.S., Vedernikov, I.L., Akinin V.V., 2010. Permian Diamictites in Northeast Asia and their Possible Origins (Permskiye diamiktity Severo-Vostoka Azii i ikh veroyatnoe proiskhozdenie). *Vestnik SVNC DVO RAN*, 14–24.
- Birgenheier, L.P., Fielding, C.R., Rygel, M.C., Frank, T.D., Roberts, J., 2009. Evidence for dynamic climate change on sub-10<sup>6</sup>-year scales from the late Palaeozoic Glacial record, Tamworth Belt, New South Wales, Australia. *Journal of Sedimentary Research* 79, 56–82.
- Blakey, R.C., 2008. Gondwana paleogeography from assembly to breakup – A 500 m.y. odyssey. In: Fielding, C.R., Frank, T.D., Isbell, J.L. (Eds.), *Resolving the Late Paleozoic Ice Age in Time and Space*. Geological Society of America Special Paper, 441, pp. 1–28.
- Boulton, G.S., 1986. Push moraines and glacier contact fans in marine and terrestrial environments. *Sedimentology* 33, 677–698.
- Boulton, G.S., 1990. Sedimentary and sea level changes during glacial cycles and their control on glacimarine architecture. In: Dowdeswell, J.A., Scourse, J.D. (Eds.), *Glacimarine Environments: Processes and Sediments*. Geological Society, Special Publication, 53, pp. 15–52.

- Brezinski, D.K., 1999. The rise and fall of late Paleozoic trilobites of the United States. *Journal of Paleontology* 73, 164–175.
- Briggs, D.J.C., 1998. Permian Productidina and Strophalosiidina from the Sydney-Bowen Basin and New England Orogen; systematics and biostratigraphic significance. *Memoir of the Association of Australasian Palaeontologists*. Association of Australasian Palaeontologists: Sydney, N.S.W., Australia, Australia, 258 pp.
- Burne, R.V., 1970. The origin and significance of sand volcanoes in the Bude Formation (Cornwall). *Sedimentology* 15, 211–228.
- Cai, J., Powell, R.D., Cowan, E.A., Carlson, P.R., 1997. Lithofacies and seismic-reflection interpretation of temperate glacial marine sedimentation in Tarr Inlet, Glacier Bay, Alaska. *Marine Geology* 143, 5–37.
- Caputo, M.V., Gonçalves de Melo, J.H., Streel, M., Isbell, J.L., 2008. Late Devonian and Early Carboniferous glacial records of South America. In: Fielding, C.R., Frank, T.D., Isbell, J.L. (Eds.), *Resolving the Late Paleozoic Ice Age in Time and Space*. Geological Society of America Special Paper, 441, pp. 161–173.
- Chumakov, N.M. 1994. Evidence of Late Permian glaciation in the Kolyma River Basin: a repercussion of the Gondwanan glaciations in Northeast Asia? *Stratigraphy and Geological Correlation* 2, 130–150.
- Claoué-Long, J.C., Korsch, R.J., 2003. Numerical time measurement in the DM Tangorin DDH1 drillcore. In: Facer, R.A., Foster, C.B. (Eds.), *Geology of the Cranky Corner Basin*, pp. 179–205.
- Clapham, M.C., James, N.P., 2008. Paleoecology of Early-Middle Permian marine communities in eastern Australia: response to global climate change in the aftermath of the late Paleozoic ice age. *Palaos* 23, 738–750.
- Clarke, M.J., 1989. Lower Parmeener Supergroup. In: Burrett, C.F. and Martin, E.L. (Eds.), *Geology and Mineral Resources of Tasmania*. Geological Society of Australia Special Publication 15, pp. 295–309.
- Clarke, M.J., Banks, M.R., 1975. The stratigraphy of the lower (Permo-Carboniferous) parts of the Parmeener Supergroup, Tasmania. In: Campbell, K.S.W. (Ed.), *Gondwana Geology, International Gondwana Symposium* 3, pp. 453–467.
- Clarke, M.J., Farmer, N., 1976. Biostratigraphic nomenclature for Late Palaeozoic rocks in Tasmania. *Papers and Proceedings of the Royal Society of Tasmania* 110, 91–109.
- Clarke, M.J., Forsyth, S.M., 1989. Late Carboniferous–Triassic. In: Burrett, C.F., Marten, E.L. (Eds.), *Geology and Mineral Resources of Tasmania: Geological Association*

- of Australia, Special Paper 15, pp. 209–293.
- Collinson, J.D., Thompson, D.B., 1982. *Sedimentary Structures*. London, George Allen and Unwin, 194 pp.
- Collinson, J.W., Isbell, J.L., Elliot, D.H., Miller, M.F., and Miller, J.M.G., 1994. Permian-Triassic Transantarctic Basin. In: Veevers, J.J., and Powell, C.M. (Eds.), *Permian-Triassic Pangean Basins and Fold Belts along the Panthalassan Margin of Gondwanaland: Geological Society of America Memoir 184*, pp. 173–222.
- Collinson, J.W., Hammer, W.R., Askin, R.A., Elliot, D.H., 2006. Permian-Triassic boundary in the central Transantarctic Mountains, Antarctica. *GSA Bulletin* 118, 747–763.
- Cowan, E. A., Powell, R.D., 1990. Suspended sediment transport and deposition of cyclically interlaminated sediment in a temperate glacial fjord, Alaska, U.S.A. In: Dowdeswell, J.A., Scourse, J.D. (Eds.), *Glacimarine Environments: Processes and Sediments*. Geological Society Special Publication 53, pp. 75–89.
- Cowan, E. A., Seramur, K. C., Cai, J., Powell, R.D., 1999. Cyclic sedimentation produced by fluctuations in meltwater discharge, tides and marine productivity in an Alaskan fjord. *Sedimentology* 46, 1109–1126.
- Crowell, J.C., Frakes, L.A., 1970. Ancient Gondwana glaciations. In: Haughton, S.H. (Ed.), *Proceedings and Papers of the Second Gondwana Symposium*, South Africa. Pretoria, CSIR, pp. 469–476.
- Crowell, J.C., Frakes, L.A., 1971. Late Paleozoic glaciation: Part IV, Australia. *Geological Society of America Bulletin* 82, 2515–2540.
- Crowell, J.C., Frakes, L.A., 1975. The Late Palaeozoic glaciation. In: Campbell K.S.W. (Ed.), *Gondwana Geology*. International Gondwana Symposium 3, pp. 313–331.
- DiMichele, W., Montañez, I.P., Poulsen, C.J., Tabor, N.J., 2009. Climate and vegetational regime shifts in the late Paleozoic ice age earth. *Geobiology* 7, 200–226.
- Domack, E.W., Burkley, L.A., Domack, C.R., Banks, M.R., 1993. Facies analysis of glacial marine pebbly mudstones in the Tasmania Basin: Implications for regional paleoclimates during the late Paleozoic. In: Findlay, Unrug, Banks, M.R., Veevers, J.J., *Gondwana Eight*, pp. 471–484.
- Dowdeswell, J. A., Whittington, R.J., Marienfeld, P., 1994. The origin of massive diamicton facies by iceberg rafting and scouring, Scoresby Sound, East Greenland. *Sedimentology* 41, 21–35.

- Dreimanis, A., 1989. Tills, their genetic terminology and classification. In: Goldthwait, R.P., Matsch, C.L. (Eds.), *Genetic Classification of Glacigenic Deposits*. Balkema, Rotterdam, pp. 17–84.
- Downie, C., Sarjeant, W.A.S., 1964. Bibliography and index of fossil dinoflagellates and acritarchs. *Memoirs of the Geological Society of America*, 94, 1–180, figs. 1–3.
- Du Toit, A.L., 1937. *Our wandering continents: an hypothesis of continental drifting*. Oliver and Boyd LTD., Edinburgh, 366 pp.
- Evans, P.R., 1969. Upper Carboniferous and Permian palynological stages and their distributions in eastern Australia. *Gondwana Stratigraphy. IUGS Symposium, Buenos Aires, 1967: Earth Science* 2, 41–54.
- Eyles, C. H., Eyles, N., Miall, A.D., 1985. Models of glacial marine sedimentation and their application to the interpretation of ancient glacial sequences. *Palaeogeography, Palaeoclimatology, Palaeoecology* 57, 15–84.
- Eyles, N., 1993. Earth's glacial record and its tectonic setting. *Earth-Science Reviews* 35, 1–248.
- Faure, K., Cole, D., 1999. Geochemical evidence for lacustrine microbial blooms in the vast Permian Main Karoo, Paraná, Falkland Islands and Huab basins of southwestern Gondwana. *Palaeogeography, Palaeoclimatology, Palaeoecology* 152, 189–213.
- Fielding, C.R., Sliwa, R., Holcombe, R.J., Jones, A.T. 2001. A new palaeogeographic synthesis for the Bowen, Gunnedah and Sydney Basins of eastern Australia. In: Hill, K.C. & Bernecker, T. (Eds.), *Eastern Australasian Basins Symposium*. Petroleum Exploration Society of Australia Special Publication, pp. 269–278.
- Fielding, C.R., Frank, T.D., Birgenheier, L.P., Rygel, M.C., Jones, A.T., Roberts, J., 2008a. Stratigraphic imprint of the Late Paleozoic Ice Age in eastern Australia: a record of alternating glacial and nonglacial climate regime. *Journal of the Geological Society, London* 165, 129–140.
- Fielding, C.R., Frank, T.D., Isbell, J.L., 2008b. The late Paleozoic ice age – A review of current understanding and synthesis of global climate patterns. In: Fielding, C.R., Frank, T.D., Isbell, J.L. (Eds.), *Resolving the late Paleozoic ice age in time and space*. Geological Society of America Special Paper 441, 343–354.
- Fielding, C.R., Frank, T.D., Isbell, J.L., Henry, L.C., Domack, E.W., 2010. Stratigraphic signature of the late Paleozoic Ice Age in the Parmeener Supergroup of Tasmania, SE Australia, and inter-regional comparisons. *Palaeogeography, Palaeoclimatology, Palaeoecology* 298, 70–90.

- Frakes, L.A., Francis, J.E., Syktus, J.I., 1992. *Climate modes of the Phanerozoic*. Cambridge, Cambridge University Press, 274 pp.
- Forsyth, S.M., Farmer, N., Gulline, A.B., Banks, M.R., Williams, E., Clarke, M.J., 1974. Status and subdivision of the Parmeener Super-Group. *Papers and Proceedings of the Royal Society of Tasmania* 108, 107–109.
- Gastaldo, R.A., DiMichele, W.A., Pfefferkorn, H.W., 1996. Out of the icehouse into the greenhouse: a late Paleozoic analogue for modern global vegetational change. *GSA Today* 10, 1–7.
- Gibbs, M.T., Rees, P.M., Kutzbach, J.E., Ziegler, A.M., Behling, P.J., Rowley, D.B., 2002. Simulation of Permian climate and comparison with climate-sensitive sediments. *Journal of Geology* 110, 33–55.
- Gilbert, R., 1990. Rafting in glacimarine environments. In: Dowdeswell, J.A., Scourse, J.D. (Eds.), *Glacimarine environments: processes and sediments*. Geological Society Special Publication 53, pp. 105–120.
- Gould, R.E., 1975. The succession of Australian pre-Tertiary megafossil floras. *Botany Review* 41, 453–483.
- Hand, S.J., 1993. Palaeogeography of Tasmania's Permo-Carboniferous glacial sediments. In: Findlay R.H., Unrug, R., Banks, M.R., Veevers, J.J. (Eds.), *Gondwana Eight: Assembly, Evolution and Dispersal; Proceedings of the 8th Gondwana Symposium*. AA Balkema, Rotterdam, pp. 459–469.
- Herbert, C.T., 1981. Late Paleozoic glacial sediments of the southern Sydney Basin, New South Wales. In: Hambrey, M.J., Harland, W.B. (Eds.), *Earth's Pre-Pleistocene Glacial Record*. Cambridge University Press, pp. 488–491.
- Herbert, C.T., Compton, J.S., 2007. Depositional environments of the lower Permian Dwyka diamictite and Prince Albert shale inferred from the geochemistry of early diagenetic concretions, southwest Karoo Basin, South Africa. *Sedimentary Geology* 194, 263–277.
- Hindmarsh, R.C., Rijdsdijk, K.F., 2000. Use of a viscous model of till rheology to describe gravitational loading instabilities in glacial sediments. In: Maltman, A.J., Hubbard, B., Hambrey, M.J. (Eds.), *Deformation of Glacial Materials*. Geological Society of London, Special Publication, 176, pp. 191–201.
- Hoppe, G., 1959. Glacial morphology and inland ice recession in northern Sweden. *Geografiska Annaler* 35, 105–115.
- Horton, D.E., Poulsen, C.J., 2009. Paradox of late Paleozoic glacioeustasy. *Geology* 37, 717–718.



- Hunter, L.E., Powell, R.D., Smith, G.W., 1996. Facies architecture and grounding-line fan processes of morainal banks during the deglaciation of coastal Maine. *Geological Society of America, Bulletin* 108, 1022–1038.
- Isbell, J.L., 2010. Environmental and paleogeographic implications of glaciotectonic deformation of glaciomarine deposits within Permian strata of the Metschel Tillite, southern Victoria Land, Antarctica. In: López-Gamundí, O.R., Buatois, L.A. (Eds.), *Late Paleozoic Glacial Events and Postglacial Transgressions in Gondwana*. Geological Society of America, Special Publication, 468, pp. 81–100.
- Isbell, J.L., Seegers, G.M., Gelhar, G.A., 1997. Upper Paleozoic glacial and postglacial deposits, central Transantarctic Mountains, Antarctica. In: I.P. Martini (Ed.), *Late Glacial and Postglacial Environmental Changes: Quaternary, Carboniferous-Permian, and Proterozoic*. Oxford University Press, Oxford, U.K., pp. 230–242.
- Isbell, J.L., Lenaker, P.A., Askin, R.A., Miller, M.F. Babcock, L.E., 2003a. Reevaluation of the timing and extent of late Palaeozoic glaciation in Gondwana: Role of the Transantarctic Mountains. *Geology* 31, 977–980.
- Isbell, J.L., Miller, M.F., Wolfe, K.L., Lenaker, P.A., 2003b. Timing of late Paleozoic glaciation in Gondwana: was glaciation responsible for the development of northern hemisphere cyclothems? In: Chan, M.A., Archer, A.W., (Eds.), *Extreme Depositional Environments: Mega End Members in Geologic Time*. Geological Society of America, Special Publication 370, 5–24.
- Isbell, J.L., Koch, Z.J., Szablewski, G.M., Lenaker, P.A., 2008. Permian glacial deposits in the Transantarctic Mountains, Antarctica. In: Fielding, C.R., Frank, T.D., Isbell, J.L. (Eds.), *Resolving the Late Paleozoic Ice Age in Time and Space*. Geological Society of America Special Paper 441, 59–70.
- Jones, A.T., Frank, T.D., Fielding, C.R., 2006. Cold climate in eastern Australian mid to late Permian may reflect cold upwelling waters. *Palaeogeography, Palaeoclimatology, Palaeoecology* 237, 370–377.
- Kneller, B.C., 1995. Beyond the turbidite paradigm: physical models for deposition of turbidites and their implications for reservoir prediction. In: Hartley, A.J., Prosser, D.J. (Eds.), *Characterization of Deep-Marine Clastic Systems*. Geological Society Special Publication 94, 31–49.
- Lawver, L.A., Dalziel, I.W.D., Norton, I.O., Gahagan, L.M., 2008. The Plates 2007 Atlas of Plate Reconstructions (750 Ma to Present Day), Plates Progress Report No. 305–0307, University of Texas Technical Report No. 195, 160 pp.
- Li, Z.X., Powell, C.M., 2001. An outline of the palaeogeographic evolution of the Australian regions since the beginning of the Neoproterozoic. *Earth-Science*

Reviews 53, 237–277.

- Lindsay, J.F., 1997. Permian postglacial environments of the Australian Plate. In: Martini, I.P. (Ed.), *Late Glacial and Postglacial Environmental Changes: Quaternary, Carboniferous – Permian, and Proterozoic*. Oxford, U.K., Oxford University Press, pp. 213–229.
- Lindström, S., 1995. Early Permian palynostratigraphy of the northern Heimefrontfjella mountain-range, Dronning Maud Land, Antarctica. *Review of Palaeobotany and Palynology* 89, 359–415.
- Lønne, I., 2006. Low-velocity glacial surges – Processes unlocked by modern surge on Svalbard. *Geology* 34, 553–556.
- López Gamundí, O. R., 1991. Thin-bedded diamictites in the glacialmarine Hoyada Verde Formation (Carboniferous), Calingasta-Uspallata Basin, western Argentina; a discussion on the emplacement conditions of subaqueous cohesive debris flows. *Sedimentary Geology* 73, 247–255.
- López Gamundí, O. R., 1997. Glacial-postglacial transition in the Late Palaeozoic basins of southern South America. In: I.P. Martini (Ed.), *Late Glacial and Postglacial Environmental Changes: Quaternary, Carboniferous-Permian, and Proterozoic*. Oxford University Press, Oxford, U.K., 147–168.
- Lowe, D.R., 1975. Water escape structures in coarse-grained sediments. *Sedimentology* 22, 157–204.
- Lowe, D.R., 1982. Sediment gravity flows II: depositional models with special references to the deposits of high-density turbidity currents. *Journal of Sedimentary Petrology* 52, 279–297.
- Mantle, D.J., Kelman, A.P., Nicoll, R.S., Laurie, J.R., 2010. *Australian Biozonation Chart*. Geoscience Australia, Canberra, 2 p.
- Marr, J.G., Harff, P.A., Shanmugam, G., Parker, G., 2001. Experiments on subaqueous sandy gravity flows: the role of clay and water in flow dynamics and depositional structures. *Geological Society of America, Bulletin* 113, 1377–1386.
- Masood, K.R., Taylor, T.N., Horner, T., Taylor, E.L., 1994. Palynology of the Mackellar Formation (Beacon Supergroup) of East Antarctica. *Review of Palaeobotany and Palynology* 83, 329–337.
- McDougall, I., Leggo, P.J., 1965. Isotopic age determinations on granitic rocks from Tasmania. *Journal of the Geologic Society of Australia* 12, 295–332.
- Menzies, J.J., van der Meer, J.J.M., 2006. 6<sup>th</sup> international workshop on the

micromorphology of glacial sediments, Hamilton College, June 4-9<sup>th</sup>, National Science Foundation. 71 pp.

- Middleton, G.V., 1970. Experimental studies related to problems of flysch sedimentation. In: Lajoie, J. (Ed.), *Flysch Sedimentology in North America*. Geological Association of Canada Special Paper 7, pp. 253–272.
- Moncrieff, A.C.M., 1989. Classification of poorly sorted sedimentary rocks. *Sedimentary Geology* 65, 191–194.
- Montenat, C., Barrier, P., d'Estevou, P.O. Hibsich, C., 2007. Seismites: an attempt to critical analysis and classification. *Sedimentary Geology* 196, 6–30.
- Montañez, I.P., Tabor, N.J., Niemeier, D., DiMichele, W.A., Frank, T.D., Fielding, C.R., Isbell, J.L., Birgenheier, L.P., Rygel, M.C., 2007. CO<sub>2</sub>-forced climate and vegetation instability during late Paleozoic deglaciation. *Science* 315, 87–91.
- Mulder, T., Alexander, J., 2001. The physical character of subaqueous sedimentary density flows and their deposits. *Sedimentology* 48, 269–299.
- Obermeier, S.F., 1996. Use of liquefaction-induced features for paleoseismic analysis – An overview of how seismic liquefaction features can be distinguished from other features and how their regional distribution and properties of source sediment can be used to infer the location and strength of Holocene paleo-earthquakes. *Engineering Geology* 44, 1–76.
- Obermeier, S.F., Jacobson, R.B., Smott, J.P., Weems, R.E., Gohn, G.S., Monroe, J.E., Powards, D.S., 1989. Earthquake-induced liquefaction features in the coastal setting of south Carolina and the fluvial setting of the New Madrid seismic zone. U. S. Geological Survey Professional Paper 1504, 44 pp.
- Oliveira, C.M.M., Hodgson, D.M., Flint, S.S., 2009. Aseismic controls on *in situ* soft-sediment deformation processes and products in submarine slope deposits of the Karoo Basin, South Africa. *Sedimentology* 56, 1201–1225.
- Owen, G., 1987. Deformation processes in unconsolidated sands. In: Jones, M.E., Preston, R.M.F. (Eds.), *Deformation of Sediments and Sedimentary Rocks*. Geological Society of London, Special Publication, 29, pp. 11–24.
- Parsons, J.D., Whipple, K.X., Simoni, A., 2001. Experimental study of the grain-flow, fluid-mud transition in debris flows. *Journal of Geology* 109, 427–447.
- Peyser, C.E., Poulsen, C.J., 2008. Controls on Permo-Carboniferous precipitation over tropical Pangaea; a GCM sensitivity study. *Palaeogeography, Palaeoclimatology, Palaeoecology* 268, 181–192.

- Poulsen, C.J., Pollard, D., Montañez, I.P., Rowley, D., 2007. Late Paleozoic tropical climate response to Gondwanan deglaciation. *Geology* 35, 771–774.
- Powell, C.M, Li, Z.X., 1994. Reconstruction of the Panthalassan margin of Gondwanaland. In: Veevers, J., Powell, C. (Eds.), *Permian-Triassic Transantarctic Basin, Permian-Triassic Pangea Basins and foldbelts along the Panthalassan margin of Gondwanaland*. *Geologic Society of America Memoir 184*, Geological Society of America Memoir 184, 5–9.
- Powell, R.D., 1981. A model for sedimentation by tidewater glaciers. *Annals of Glaciology* 2, 129–134.
- Powell, R.D., 1983. Glacial-marine sedimentation processes and lithofacies of temperate tidewater glaciers, Glacier Bay, Alaska. In: Molnia, B.F. (Ed.), *Glacial-Marine Sedimentation*. Plenum Press, New York, 185–232.
- Powell, R.D., 1990. Glacimarine processes at grounding-line fans and their growth to ice-contact deltas. In: Dowdeswell, J.A., Scourse, J.D. (Eds.), *Glacimarine Environments: Processes and Sediments*. *Geological Society Special Publication*, 53, 53–73.
- Powell, R.D., 2003. Subaquatic landsystems: fjords. In: Evans, D.J.A. (Ed.), *Glacial Landsystems*. Arnold, London, 313–347.
- Powell, R.D., Cowan, E.A., 1986. Depositional processes at McBride Inlet and Riggs glacier. In: Anderson, P.G., Goldthwait, R.P., McKenzie, G.D. (Eds.), *Observed processes of glacial deposition in Glacier Bay, Alaska*. Ohio State University, Institute of Polar Studies, *Miscellaneous Publications* 256, 140–156.
- Powell, R.D., Domack, E.W., 2002. Modern glacimarine environments. In: Menzies, J. (Ed.) *Modern and past glacial environments*. Oxford, Butterworth-Heinemann Ltd., 361–389.
- Powell, R.D., Molnia, B.F., 1989. Glacimarine sedimentary processes, facies, and morphology of south-southeast Alaska shelf and fjords. *Marine Geology* 85, 359–390.
- Price, P.L., 1997. Permian to Jurassic palynostratigraphic nomenclature of the Bowen and Surat Basins. In: Green, P. (Ed.), *Queensland Minerals and Energy Review Series* 1997, 137–178.
- Price, P.L., Filatoff, J., Williams, A.J., Pickering, S.A., Wood, G.R., 1985. Late Palaeozoic and Mesozoic palynostratigraphic units. CSR Oil and Gas Division Palynology Facility Report 274/25. Queensland Department of Resource Industries Open File Report CR14012.

- Raymond, A., Kelley, P.H., Lutken, C.B., 1989. Polar glaciers and life at the equator: The history of Dinantian and Namurian (Carboniferous) climate. *Geology* 17, 408–411.
- Reid, C.M., Forsyth, S.M., Clarke, M.J., in press. The Parmeener Supergroup – Late Carboniferous to Triassic. In: Quilty, P., Corbett, K., (Eds.), *The Geological Evolution of Tasmania*. Hobart, Tasmania, Geological Society of Australia, Special Publication.
- Rogala, B., James, N.P., Reid, C.M., 2007. Deposition of polar carbonates during interglacial highstands on an Early Permian shelf, Tasmania. *Journal of Sedimentary Research* 77, 587–606.
- Shanmugam, G. 1996. High-density turbidity currents: are they sandy debris flows? *Journal of Sedimentary Research* 66, 2–10.
- Spry, A., 1962. The geology of Tasmania: Cambrian System. *Journal of the Geological Society of Australia* 9, 255–284.
- Stanley, S.M., Powell, M.G., 2003. Depressed rates of origination and extinction during the late Paleozoic ice age: a new state for the global marine ecosystem. *Geology* 31, 877–880.
- Stollhofen, H., Werner, M., Stanistreet, I.G., Armstrong, R.A., 2008. In: Fielding, C.R., Frank, T.D., Isbell, J.L. (Eds.), *Resolving the late Paleozoic ice age in time and space*. Geological Society of America Special Paper 441, 83–96.
- Thomas, G.S.P., Connell, R.J., 1985. Iceberg drop, dump, and grounding structures from Pleistocene glacio-lacustrine sediments, Scotland. *Journal of Sedimentary Petrology* 55, 243–249.
- Truswell, E. M., 1978. Palynology of the Permo-Carboniferous in Tasmania: an interim report. *Bulletin of the Geological Survey of Tasmania* 56, 37 pp.
- van der Meer, J. J. M., 1987. Micromorphology of glacial sediments as a tool in distinguishing genetic varieties of till. *Geological Survey of Finland Special Paper* 3, 77–89.
- van der Meer, J. J. M., Menzies, J., Rose, J., 2003. Subglacial till: the deforming glacier bed. *Quaternary Science Reviews* 22, 1659–1685.
- Veevers, J.J., 2006. Updated Gondwana (Permian-Cretaceous) earth history of Australia. *Gondwana Research* 9, 231–260.
- Veevers, J.J., Conaghan, P.J., Powell, C. McA., Cowan, E.J., McDonnell, K.L., Shaw, S.E., 1994. Eastern Australia. In: Veevers, J.J., and Powell, C.M. (Eds.), *Permian-*

Triassic Pangean Basins and Fold Belts along the Panthalassan Margin of Gondwanaland. Geological Society of America Memoir 184, 11–171.

- Visser, J.N.J., 1994. The interpretation of massive rain-out and debris-flow diamictites from the glacial marine environment. In: Deynoux, M., Miller, J. M. G., Domack, E.W., Eyles, N., Fairchild, I.J., Young, G.M. (Eds.), *Earth's Glacial Record*. Cambridge, Cambridge University Press, 83–94.
- Wadell, H., 1932. Volume, shape and roundness of rock particles. *Journal of Geology* 40, 443–451.
- Willems, B.A., Powell, R.D., Cowan, E.A., Jaeger, J., Trusel, L.D., 2009. A high-resolution record of advance/retreat phase glacimarine sediments: implications in reconstructing glacial dynamics. *Geological Society of America Abstracts with Programs* 41, 71.
- Winguth, A.M.E., Heinze, C., Kutzbach, J.E., Maier-Reimer, E., Mikolajewicz, U., Rowley, D., Rees, A., Ziegler, A.M., 2002. Simulated warm polar currents during the middle Permian. *Paleoceanography* 17, 1057.
- Winsemann, J., Asprion, U., Meyer, T., Schramm, C., 2007. Facies characteristics of Middle Pleistocene (Saalian) ice-margin subaqueous fan and delta deposits, glacial Lake Leine, NW Germany. *Sedimentary Geology* 193, 105–129.
- Woodworth-Lynas, C. M. T., Dowdeswell, J.A., 1994. Soft-sediment striated surfaces and massive diamicton facies produced by floating ice. In: M. Deynoux, J. M. G. Miller, E. W. Domack, N. Eyles, I.J. Fairchild, G.M. Young (Eds.), *Earth's Glacial Record*. Cambridge University Press, Cambridge, 241–259.
- Yassir, N.A., 1990. The undrained shear behaviour of fine grained sediments. In: Knipe, R.J., Rutter, E.H. (Eds.), *Deformation Mechanisms, Rheology and Tectonics*. Geological Society of London, Special Publication, 54, 399–404.

## Chapter 6: Panthalassan margin volcanism: a driver of late Paleozoic deglaciation and extinction?

Lindsey C. Henry<sup>\*a</sup>, Margaret L. Fraiser<sup>a</sup>, Carlos O. Limarino<sup>b</sup>, John L. Isbell<sup>a</sup>

<sup>a</sup>Department of Geosciences, University of Wisconsin-Milwaukee, 3209 N. Maryland Avenue, Milwaukee, WI 53211-0413, USA

<sup>b</sup>Departamento de Ciencias Geológicas, Universidad de Buenos Aires, Pabellón 2, Ciudad Universitaria C1428EHA, Buenos Aires, Argentina

### Abstract

Recent correlation of CO<sub>2</sub> levels with Permian glacial events and biotic crises suggests that increasing CO<sub>2</sub> levels played a role in terminating the late Paleozoic ice age, initiating Late Permian and Mesozoic greenhouse conditions, and facilitating a prolonged interval of biotic stress during the Middle Permian through Early Triassic. Additionally, recent hypotheses promote input of CO<sub>2</sub> into the atmosphere by the Emeishan and Siberian Traps as primary causes of the Middle and Late Permian mass extinctions. It is proposed here that volcanism along the > 12,000 km long Panthalassan margin of Gondwana was a significant contributor of CO<sub>2</sub> into the atmosphere during the Early Permian to Triassic, and thus may represent a previously unrecognized driver of environmental changes during this time. Glacial intervals of the LPIA became progressively limited in ice volume and geographic extent into the Middle and Late Permian, and this decrease in ice volume may have been a response to input of CO<sub>2</sub> from Panthalassan margin volcanism. Further, this input of CO<sub>2</sub> may have stressed biota throughout the Permian, so that organisms were more susceptible to extinction when the

---

\* Corresponding author.

Email addresses: [christi9@uwm.edu](mailto:christi9@uwm.edu) (L.C. Henry), [mfraiser@uwm.edu](mailto:mfraiser@uwm.edu) (M.L. Fraiser), [oscarlimarino@ciudad.com.ar](mailto:oscarlimarino@ciudad.com.ar) (C.O. Limarino), [jisbell@uwm.edu](mailto:jisbell@uwm.edu) (J.L. Isbell).

Emeishan and Siberian Traps were emplaced. Volcanic rocks of the Choiyoi Group, with an estimated volume of 1.5 million km<sup>3</sup>, represent the largest known upper Paleozoic igneous province of the tectonically active Panthalassan margin along which manifold volcanism was occurring. CO<sub>2</sub> output from the Choiyoi group alone is estimated, at a minimum, on the order of 10<sup>22</sup> g. Therefore, it is proposed that the total CO<sub>2</sub> emissions from Panthalassan margin volcanism were ample enough to contribute to Permian-Triassic environmental perturbations and to prime biotic systems for the Middle and Late Permian extinction events. This contribution provides the first linkage of deglaciation of the LPIA and biotic degradation in the Middle Permian - Early Triassic by a common driver, Panthalassan margin volcanism, and further research into the timing and flux of Panthalassan margin volcanism is encouraged.

## **1. Introduction**

The late Paleozoic was an interval of intense environmental restructuring. During this time, Earth transitioned out of the longest and most extensive icehouse episode in the last half billion years into greenhouse conditions that persisted until the start of the present glacial interval in the Oligocene (Frakes et al., 1992; Isbell et al., 2003; Montañez et al., 2007). The late Paleozoic Ice Age (LPIA) consisted of multiple glacial/non-glacial intervals that progressively expanded in ice volume and extent from the Visean (345 – 326 Ma) to the main phase of the LPIA in the Early Permian (Asselian – Sakmarian), after which the glacial intervals were characterized by small ice sheets, ice caps, and alpine glaciers occurring over progressively more limited geographic extent through time (e.g., Fielding et al., 2008a). Later in the Permian, two mass extinctions occurred: first, the Guadalupian crisis in which 58% of marine genera became extinct, and second, the



end-Permian mass extinction, the largest in the Phanerozoic, in which 78% of marine invertebrate genera went extinct (Raup and Sepkoski, 1982; Clapham et al., 2009). The latter event and associated environmental degradation were so severe that a biotic crisis continued into the Triassic for 5 million years (Hallam, 1991; Lehrmann et al., 2006). Furthermore, paleoecological data suggest that these extinction events punctuated a prolonged interval of environmental and biotic stress during the Middle Permian through the Early Triassic (Bottjer et al., 2008).

Evidence indicates that LPIA deglaciation and the extinction events were ultimately linked to atmospheric CO<sub>2</sub> levels (e.g., Kiehl and Shields, 2005; Montañez et al., 2007; Fraiser and Bottjer, 2007). However, for environmental change associated with the LPIA, CO<sub>2</sub> sources are often unaddressed. Herein a contributing driver for environmental degradation is proposed: massive volcanism along the Panthalassan margin of Gondwana (Fig. 45). Volcanism occurred along the Panthalassan margin throughout the Permian and Triassic as a result of subduction and extension between Panthalassa and Gondwana (Veevers et al., 1994c). The suggestion that Panthalassan margin volcanism (primarily in Australia) ‘set the table’ for the end-Permian mass extinction has been made by Veevers and Tewari (1995) and Racki and Wignall (2005), but Panthalassan margin volcanism, which endured from the Pennsylvanian to the Triassic, has not been correlated before with deglaciation of the main phase of the LPIA, the end-Guadalupian extinction, or the gradual decline in biotic diversity throughout the Middle and Late Permian. Further, the timing, magnitude, and CO<sub>2</sub> emissions of Panthalassan margin volcanism have not been explored in depth before this study. The aim of this paper is to present and explore this new hypothesis and to solicit further

research into the magnitude and flux of outgassed CO<sub>2</sub> from the Panthalassan margin and the correlation of volcanic events with deglaciations and extinctions.

## **2. Late Paleozoic Events and $p\text{CO}_2$**

The LPIA persisted for 73 million years from the Middle Mississippian (Visean; 327-342 Ma) to the Middle Permian (Capitanian; ~251 Ma; Fig. 46) with glaciation over Gondwana in the south (glacial deposits are located in South America, Africa, Antarctica, India, Australia, and the Arabian peninsula) and possibly over Siberia in the north (Frakes et al., 1992; Chumakov and Zharkov, 2003). It is hypothesized that glaciation occurred as numerous alpine glaciers, ice caps, and small to moderate-sized ice sheets for 1-10 million year periods, separated by non-glacial intervals of approximately the same duration (Isbell et al., 2003; Fielding et al., 2008b). Early Permian glacial and non-glacial intervals are closely correlated with lower and higher  $p\text{CO}_2$  levels, respectively (Montañez et al., 2007).  $p\text{CO}_2$  was calculated for the Permian from  $^{13}\text{C}:^{12}\text{C}$  ratios in marine invertebrate shells and carbonate and goethite found in paleosols, and it was determined that  $p\text{CO}_2$  increased from ~280 parts per million by volume (ppmv) to up to 3500 ppmv during the Early Permian, when deglaciation ensued in the major part of Gondwana (Royer, 2006; Montañez et al., 2007). Minor glacial episodes persisted in Australia during the Guadalupian with possible regional-scale glaciation occurring in Siberia during the Wuchiapingian-Changhsingian (260-251 Ma; Fig.46; Chumakov and Zharkov, 2003; Fielding et al., 2008a).

Negative correlations between  $p\text{CO}_2$  and late Paleozoic and Cenozoic glaciations suggest that  $p\text{CO}_2$  is a major climate driver (cf., Royer et al., 2004; Montañez et al., 2007). Short term drops in  $p\text{CO}_2$  during the transition from the LPIA to its final

deglaciation coincided with brief glacial events (Fig. 46), reflecting the short-term climatic fluctuations that were superimposed on major climatic shifts and influenced by changing  $p\text{CO}_2$  levels. The Sakmarian-Artinskian Australian glaciation is an example of a regionally limited glacial episode that correlates with a drop in  $p\text{CO}_2$  (Fig. 46; Montañez et al., 2007). Presently the dating for  $p\text{CO}_2$  fluctuations and the glacial/non-glacial cycles is low-resolution, however, the dating of the glaciations in Australia has tighter control than the  $p\text{CO}_2$  curves by at least  $\pm 3$  million years (cf. Montañez et al., 2007; Fielding et al., 2008a, and references within). Therefore, the  $p\text{CO}_2$  drop in the Sakmarian-Artinskian may have endured over a longer time span, correlating with the duration of the Australian glaciation during that time. Drawdown of  $\text{CO}_2$  during glacial intervals has been attributed to  $\text{C}_{\text{org}}$  burial in peat-forming environments and silicate weathering due to tectonic uplift (Gastaldo et al., 1996; Smith and Read, 2000). Coal was deposited at equatorial latitudes during the Carboniferous, whereas coal deposition occurred at high latitudes during the Permian (Collinson et al., 1994; López Gamundí et al., 1994; Veevers et al., 1994a, 1994b; Isbell et al., 1997). Nevertheless, hypotheses on causes of increased  $p\text{CO}_2$  levels in the Sakmarian and late Artinskian (Fig. 46) have not been circulated before this proposal of Panthalassan margin volcanism. Instead, the decline of the LPIA has been attributed to the northward migration of Pangea to warmer latitudes and the early breakup of the supercontinent, altering oceanic and atmospheric circulation patterns (Crowell, 1978, 1999). While biogeochemical shifts at the end of the LPIA have been acknowledged (Crowell, 1999), drivers remain unexplored until now.

Increased  $\text{CO}_2$  levels attributed to volcanic emissions have also been suggested as ultimate causes for both the end-Guadalupian and end-Permian extinctions. The

Emeishan Traps have been suggested as a cause of the end-Guadalupian extinction (Zhou et al., 2002), as the flood basalts may have released between  $1.0 \times 10^{18}$  and  $2.1 \times 10^{18}$  g  $\text{CO}_2$  (using volume estimates from Jin and Shang (2000) and Yin et al. (1992), respectively, and Leavitt's (1982) formula). However, outgassing of ~2000 Gt of methane has been proposed as a proximate cause for the end-Guadalupian mass extinction, perhaps due to the intrusion of the Emeishan Traps into coal deposits (Berner, 2002; Retallack et al., 2006). Methane ultimately oxidizes into  $\text{CO}_2$  and can therefore serve as an additional source of  $\text{CO}_2$ .

Input of  $\text{CO}_2$  into Earth's atmosphere from Siberian Traps continental flood basalt volcanism is considered to be a major driver for the end-Permian mass extinction and its delayed recovery (Payne and Kump, 2007). The Siberian Traps erupted 2-3 million  $\text{km}^3$  of volcanic material, primarily basalt, for 1 million years across the Permian-Triassic boundary (Renne et al., 1995). Using Leavitt's (1982) formula, this volcanism is estimated to have released up to  $1 \times 10^{19}$  g  $\text{CO}_2$  (Wignall, 2001). Further, it has been hypothesized that in addition to volcanic emissions, high levels of  $\text{CO}_2$  were generated at the Permian/Triassic boundary by methane release and oxidation from clathrates (Krull and Retallack, 2000; Berner, 2002). Diminished terrestrial carbon burial and a shift in carbon burial from the continental to marine realm has also been proposed as another driver of the increase in atmospheric  $\text{CO}_2$  (Berner, 2002). However, carbon cycle modeling indicates that volcanic input of  $\text{CO}_2$  at the Permian-Triassic boundary best correlates with the carbon isotope excursions at that time (Payne and Kump, 2007).

Addition of  $\text{CO}_2$  into the atmosphere during the Late Permian is proposed to have caused climate deterioration that ultimately led to reduced thermohaline circulation,

stratification of euxinic oceans, and increased CO<sub>2</sub> in ocean surface waters, and all are proposed kill mechanisms of the end-Permian mass extinction (Wignall and Twitchett, 1996; Grice et al., 2005; Kiehl and Shields, 2005). Therefore, atmospheric CO<sub>2</sub> was likely a significant component to the end-Permian mass extinction and Early Triassic delayed recovery (e.g., Fraiser and Bottjer, 2007).

Herein an additional contributor to increased atmospheric CO<sub>2</sub> from massive volcanism, and therefore a potential driver of Late Paleozoic-Early Mesozoic environmental change and biotic degradation, is proposed: massive volcanism that occurred along the Panthalassan margin of Gondwana (Fig. 45). While the Emeishan and Siberian Traps are frequently cited as CO<sub>2</sub> sources for the end-Guadalupian and end-Permian mass extinctions (respectively), sources of CO<sub>2</sub> linked with deglaciations in the Early Permian have not yet been determined. It is proposed here that CO<sub>2</sub> input from Panthalassan margin volcanism instigated warming that caused final deglaciation of the LPIA. Further, Panthalassan margin volcanism may have stressed the biota throughout the Permian, making organisms more vulnerable to high fluxes of CO<sub>2</sub> during the late Guadalupian and latest Permian.

### **3. Panthalassan Margin Volcanism**

Magmatic arcs developed along the Panthalassan margin from 300-244 Ma (latest Carboniferous-Middle Triassic), forming first in South America, progressing around the southern rim of Gondwana, and ending in present-day eastern Australia (Fig. 45; Veevers et al., 1994c). Evidence for volcanism and intrusive activity along or adjacent to the Panthalassan margin during the Permian includes: 1) in South America, the Choiyoi Group of Argentina and correlative rocks in western Brazil, Chile, Peru, and Bolivia,

dated as Early Permian and Middle Permian – Early Triassic (Groeber, 1946; Coutinho et al., 1991; Sato and Llambías, 1993; López Gamundí et al., 1994; Llambías, 1999; Limarino and Spalletti, 2006); 2) in southern Africa, indirect evidence of distal volcanism is given by tuffs in the Dwyka and Balfour Formations (302 – 288 Ma, Stollhofen et al., 2000; 277 - 254 Ma, Hälbig et al., 1983), tuffs in the Eccra Group ( $289 \pm 3.8$  Ma,  $288 \pm 3$  Ma, Bangert et al., 1999) and volcanoclastic sandstone in the Eccra and Beaufort (Adelaide Subgroup) Groups (Late Permian – Early Triassic, Johnson, 1991; ); 3) in Antarctica, plutonic rocks in Marie Byrd Land (granitoids, 320-110 Ma, Mukasa et al., 2000; Mukasa and Dalziel, 2000; diorite and rhyolite-dacite, 295 Ma, Lopatin et al., 1974; granitoids and granodiorites,  $276 \pm 2$  Ma, Pankhurst et al., 1998) and the Antarctic Peninsula (granites,  $297 \pm 4$  –  $267 \pm 4$ ; Millar et al., 2002), and tuffs and volcanoclastic sandstones in the Ellsworth and central Transantarctic Mountains (277-255 Ma, Collinson, 1994); 4) in New Zealand, volcanic rocks in the Brook Street magmatic arc (250 - 290 Ma, Price et al., 2006); and 5) in Australia, tuffs in Tasmania (265 - 258 Ma, Veevers et al., 1994c) and eastern Australia (265, 256-250 Ma, Bowen Basin; 260 - 250 Ma, Sydney Basin; 259-250 Ma, Gunnedah Basin, Veevers et al., 1994c) and the Taromeo pluton in Queensland (264 Ma, Veevers et al., 1994c; Fig. 46). Moreover, Faure et al. (1995) noted that uplift caused by convergence along the Panthalassan margin uplifted peat deposits, fostering oxidation and release of additional CO<sub>2</sub> into the atmosphere.

In addition to activity on the Panthalassan margin, smaller volcanic events also occurred at the India-Australia rift zone along the Tethyan margin during the Pennsylvanian – Middle Permian and from the Middle Permian to Triassic (Veevers and

Tewari, 1995). Rhyolitic tuff and basalt sills also have been identified from the Pennsylvanian to the Middle Permian in Europe (Veevers et al., 1994a).

#### **4. Choiyoi Group**

The Choiyoi Group (Groeber, 1946; Stipanovic et al., 1965) is the largest known volcanic province to have formed from a magmatic arc along the active margin of Gondwana. In South America, the Choiyoi volcanic province crops out in the Cordillera Frontal, the Cordillera Principal, the Calingasta-Uspallata Basin, the Paganzo Basin, the San Rafael Basin, the Las Matras block, the Chadileuvu block, and the Sierras Pampeanas (Fig. 47), forming an angular unconformity with underlying pre-Carboniferous to earliest Permian strata (López Gamundí et al., 1994; Lambías et al., 2003). Correlative rocks also occur in Brazil, Chile, Peru, and Bolivia. Choiyoi volcanism has been divided into two major volcanic associations: the Early Permian calc-alkaline association (Sato and Lambías, 1993; Lambías et al., 1993; Lambías, 1999) is mainly composed of dacites and andesites which have been interpreted as forming from a large volcanic arc related to the subduction of the paleo-Pacific plate under the western margin of Gondwana; and the Middle Permian – Early Triassic silicic association is comprised of thick sequences of rhyolites, dacites and ignimbrites and formed under extensional tectonics (Nasi and Sepúlveda, 1986; Kay et al., 1989; Sato and Lambías, 1993; Lambías, 1999). Some of these studies used the K-Ar method for dating (e.g., Sato and Lambías, 1993; Lambías, 1999), which is now recognized as a less reliable dating method (McDougall and Harrison, 1988).

Volcanic rocks of the Choiyoi Group are frequently 2 km thick in modern outcrop, but also occur up to 4 km thick (Cortés, 1985; Kay et al., 1989). Presently the

province covers at least 200,000 km<sup>2</sup> and is estimated to have originally covered over 500,000 km<sup>2</sup> (Fig. 47; Groeber, 1946; López Gamundí et al., 1994; Llambías et al., 2003). Using 2 – 4 km as the original thickness of the Choiyoi group, its volume is estimated as  $1 - 2 \times 10^6$  km<sup>3</sup>, with  $1.5 \times 10^6$  km<sup>3</sup> as an intermediate estimate of the predominantly rhyolitic lava (Kay et al., 1989). In order to determine the mass of CO<sub>2</sub> released, Leavitt's (1982) formula can be used:

$$\text{mass of CO}_2 = sf_{\text{dg}}vd$$

where  $s$  is the weight fraction of CO<sub>2</sub> in magma,  $f_{\text{dg}}$  is the fraction of CO<sub>2</sub> gas from the magma,  $v$  is the magma volume, and  $d$  is the solid density of magma. Such parameters of rhyolitic magma are only loosely understood at present. However, for  $s$ , values of 1 - 36 ppm have been determined from studies on the Mono Craters of California (Rust and Cashman, 2007). The actual weight fraction of CO<sub>2</sub> in rhyolitic magma is likely higher than this range, because the examined magma was already partially degassed.  $f_{\text{dg}}$  can be estimated as 0.5 (Leavitt, 1982),  $v$  is  $\sim 1.5 \times 10^6$  km<sup>3</sup> for the Choiyoi Group, and  $d$  is  $2.3 \times 10^{15}$  g/km<sup>3</sup> for rhyolitic magma (Sowerby and Keppler, 1999). Using the range of 1 – 36 ppm CO<sub>2</sub> in magma, the mass of CO<sub>2</sub> emitted from the Choiyoi Group ranges from  $1.7 \times 10^{21}$  to  $6.2 \times 10^{22}$  g. Therefore, the Choiyoi Group, representing just one of the late Paleozoic Panthalassan margin igneous provinces, emitted on the order of  $10^{21}$  -  $10^{22}$  g CO<sub>2</sub> into Earth's atmosphere. Further, this estimate is conservative considering that Permian-Triassic volcanic rocks exposed along the present day Andean Cordillera extends beyond Argentina into Bolivia, Chile, Perú, and Ecuador, forming volcanic successions up to 2000 m thick (Naranjo and Puig, 1984; Kontak et al., 1990; Limarino



and Spalletti, 2006). Therefore,  $10^{21}$ – $10^{22}$  g is a minimum value of CO<sub>2</sub> degassed by the Choiyoi Group due to conservative variable and volume estimates.

## 5. Discussion

This compilation of data presents evidence of manifold volcanism along the Panthalassan margin during the Permian, a period of dramatic environmental and ecological shifts. Volcanism was continuous on the Panthalassan margin during the Permian (Fig. 46) and would have elevated background  $p\text{CO}_2$  levels. Before the onset of volcanism along the Panthalassan margin in the late Carboniferous (~300 Ma), widespread volcanism was absent from the region, because the Panthalassan plate was not subducting beneath Gondwana in the Carboniferous (Veevers et al., 1994c). Once subduction began (~300 Ma), a magmatic arc formed in South America (forming the Choiyoi Group) and continued to propagate around the Panthalassan margin throughout the Permian, reaching the Ellsworth Mountains of Antarctica by 275 Ma and the Bowen Basin of Australia by 265 Ma.

The Choiyoi Group is presented here as a case study of Panthalassan margin volcanism and CO<sub>2</sub> input into the atmosphere. The Early Permian lower cycle of volcanism represented in the Choiyoi Group coincides with the mid-Sakmarian deglaciation (Stollhofen et al., 2000; Isbell et al., 2003), and the Middle Permian-Triassic upper cycle coincides with the Artinskian major deglaciation and ultimate end of the LPIA, the Permian extinctions, and the Early Triassic aftermath (Fig. 46). The output of  $10^{21}$ – $10^{22}$  g CO<sub>2</sub> from the Choiyoi represents only a small fraction of emissions released from volcanism along the Panthalassan margin. More precise dating of the igneous provinces and glacial-interglacial events and a higher-resolution isotope record may

reveal more detailed correlations among volcanism, CO<sub>2</sub> flux, glaciations, and  $p\text{CO}_2$  levels.

Modern outgassing of CO<sub>2</sub> from the mantle occurs at  $2.6 \times 10^{13}$  g/year (Marty and Jambon, 1987), therefore more refined dating is needed to compare this modern rate to the flux of CO<sub>2</sub> from the Choiyoi and other Gondwanan volcanism in the Permian-Early Triassic. Regardless, the multiple deglaciations and overall decline in alpha diversity in the Permian (Fig. 46) require an ultimate driver(s) that cannot be related to outgassing associated with the Emeishan and Siberian Traps.

It may be necessary for large igneous provinces to intrude into carbon-rich sedimentary rocks in order to release enough CO<sub>2</sub> and CH<sub>4</sub> to have major effects on climate (Ganino and Arndt, 2009). Dolomite/limestone, evaporite, coal, and organic-rich shale are the types of bedrock considered to release the most greenhouse gases when metamorphosed by igneous intrusions, and these lithologies occur throughout the Panthlассan margin of Gondwana. In Argentina, over 600 m of Lower Ordovician limestone (La Silla and San Juan Formations) occur in the Precordillera, which was intruded by the Choiyoi Group (López Gamundí et al., 1994; Keller, 1999). In northern Chile and southwest Peru, carbonates from the Pennsylvanian – Lower Permian Machani Formation and the Lower Permian Juan de Morales Formation (~10 m of limestone) were intruded by arc plutons and overlain by volcanic rocks of the Middle Permian – Triassic Peine Group (Díaz-Martínez et al., 2000; Grader et al., 2008). In Antarctica, widespread coal deposition occurred throughout the Transantarctic Basin during the Permian, and interbedded volcanoclastic sandstones occur in the Middle to Upper Permian coal measures (Collinson et al., 1994). Additionally, plutonic rocks were emplaced in Marie

Byrd Land throughout the Permian from the magmatic arc there. Therefore, there may have been contact between the coal measures and volcanic and/or plutonic activity along Antarctica's margin throughout the Permian. In Australia, Permian coal measures occur in the Sydney Basin (Fielding et al., 2008a), where volcanism, such as the Gerringong Volcanics, occurred in the Late Permian (Campbell et al., 2001).

While additional forces, such as the northward migration of Pangea, the early breakup of the supercontinent, and resulting changes in oceanic and atmospheric circulation patterns, were certainly driving deglaciation and biotic crises, the input of CO<sub>2</sub> from the Choiyoi Group and other Panthalassan margin volcanism may have been a contributor to climatic warming that led to deglaciation, sea-level fluctuations, reduced thermohaline circulation, stratification of anoxic bottom waters in the ocean, and mass extinction. Veevers and Tewari (1995) and Racki and Wignall (2005) proposed that Panthalassan margin volcanism assisted the end-Permian environmental degradation, but we recommend expanding the effects of the volcanism to Early - Middle Permian deglaciations, the end-Guadalupian extinction, and the Early Triassic aftermath as well. Also, Kidder and Worsley (2005) proposed that CO<sub>2</sub> input into the atmosphere steadily intensified from the LPIA to the Early Triassic, causing the icehouse-greenhouse shift and later environmental degradation. Panthalassan margin volcanism during the Paleozoic/Mesozoic transition supports this hypothesis.

The combined outgassing of Panthalassan margin magmatism may have progressively raised  $p\text{CO}_2$  levels and thus global temperatures, which contributed to deglaciation and gradually stressed Earth's biota. An increase in the background levels of  $p\text{CO}_2$  due to Panthalassan margin volcanism would increase temperatures, which in turn

would affect ocean circulation, population distributions, and organisms' biocalcification and physiological abilities (Clarke, 1993; Fraiser and Bottjer, 2007). Gradual input of CO<sub>2</sub> by Panthalassan margin volcanism would still have been able to affect environmental degradation, as CO<sub>2</sub> remains in the atmosphere for ~10<sup>5</sup> years following injection (Wignall, 2001). Further, even small changes in the pH of seawater and CaCO<sub>3</sub> saturation wrought by increased *p*CO<sub>2</sub> alter organisms' calcification and physiological abilities (Raven et al., 2005).

This hypothesis is consistent with paleoecological data indicating a prolonged period of decline in diversity and paleoenvironmental shifts among organisms from the Middle Permian to the Early Triassic (Fig. 46; e.g., Bottjer et al., 2008). It is possible that by the time the Emeishan and Siberian Traps flood basalts erupted, organisms were sufficiently strained so that they could not withstand an additional onslaught of *p*CO<sub>2</sub>, and thus catastrophic extinction ensued. Already elevated *p*CO<sub>2</sub> levels in the Permian have been demonstrated by the modeling of Hyde et al. (2006), who propose *p*CO<sub>2</sub> levels greater than 2 – 4 × PAL (present atmospheric level of 280 ppmv CO<sub>2</sub>) in the Late Permian. Moreover, subduction along the Panthalassan margin naturally would have been coupled with divergent tectonism and coincident basalt production (Veevers and Tewari, 1995), which was yet another contributor of CO<sub>2</sub>.

Mounting evidence suggests that late Paleozoic through early Mesozoic environmental change and ecological restructuring were linked to a common Earth-based driver. As massive inputs of CO<sub>2</sub> from large igneous provinces have been shown to restructure the climate and life on Earth (e.g., Courtillot, 1999; Wignall, 2001), an examination of the drivers of environmental change is necessary to foresee environmental

changes in Earth's future, especially considering that anthropogenic input of CO<sub>2</sub> exceeds rates experienced in the ancient record (IPCC, 2007).

### **Acknowledgments**

We thank Barry Cameron, Stephen Dornbos, and Lindsay McHenry for their input. Financial support was provided by the Center of Latin American and Caribbean Studies, the Graduate School (Research Grant Initiative and George A. Boyer Scholarship), and the Department of Geosciences at UWM; the National Science Foundation (ANT-0440919; ANT-0635537; OISE-0825617); the Wisconsin Geological Society; the Geological Society of America (GSA); GSA Coal Division; the American Association of Petroleum Geologists; and UBA.

## Figures

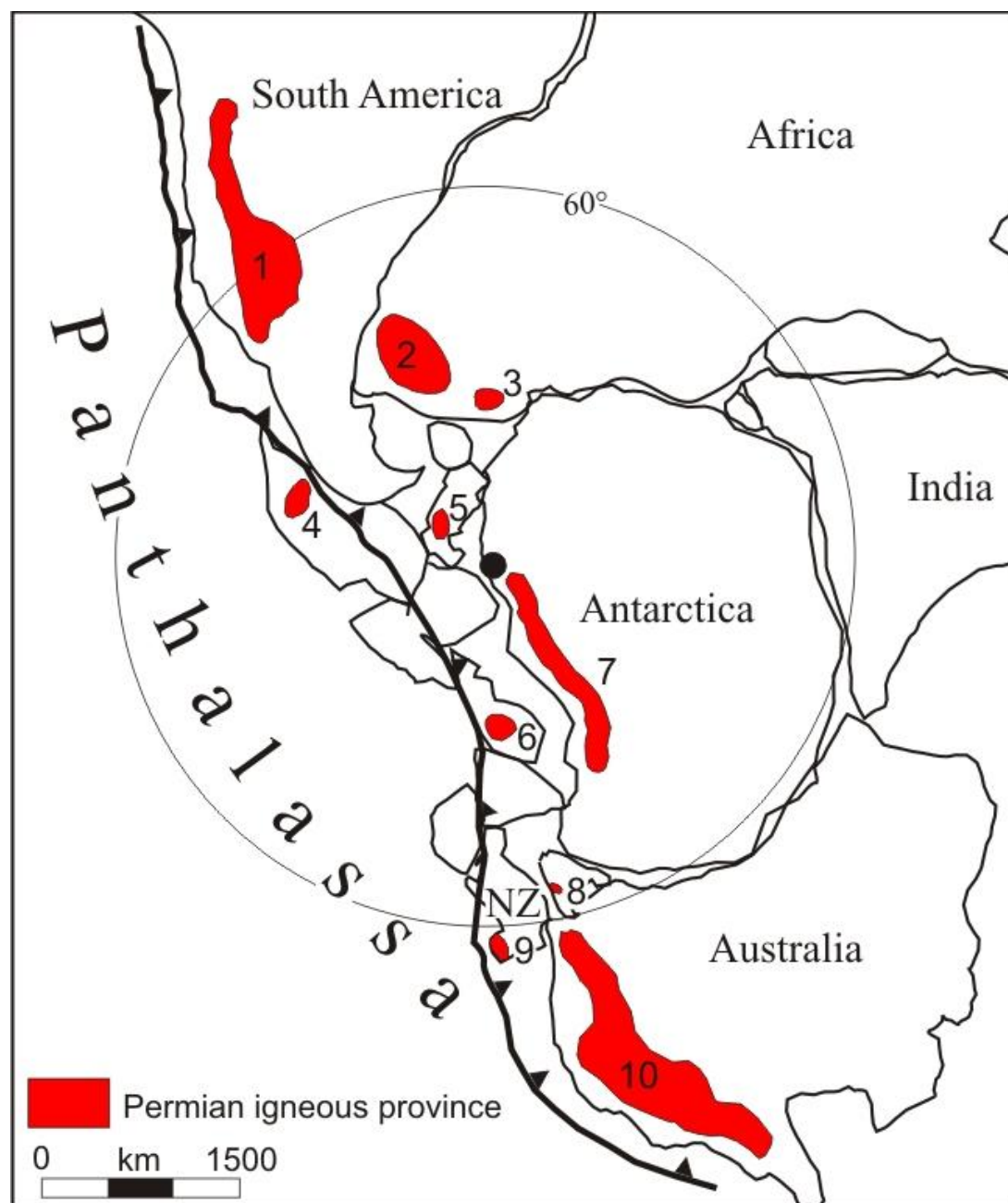


Figure 45. Distribution of igneous provinces associated with the tectonically active Panthalassan margin of Gondwana. 1. Choiyoi Group, 2. Dwyka and Ecca Groups, 3. Beaufort Group, 4. Antarctic Peninsula, 5. Ellsworth Mountains, 6. Marie Byrd Land, 7. Central Transantarctic Mountains, 8. Tasmania, 9. Brook Street Arc, New Zealand, 10. Sydney, Gunnedah, and Bowen Basins and Queensland. References are cited in text. Plates reconstruction is from ~270 Ma, modified from Lawver et al. (2008).

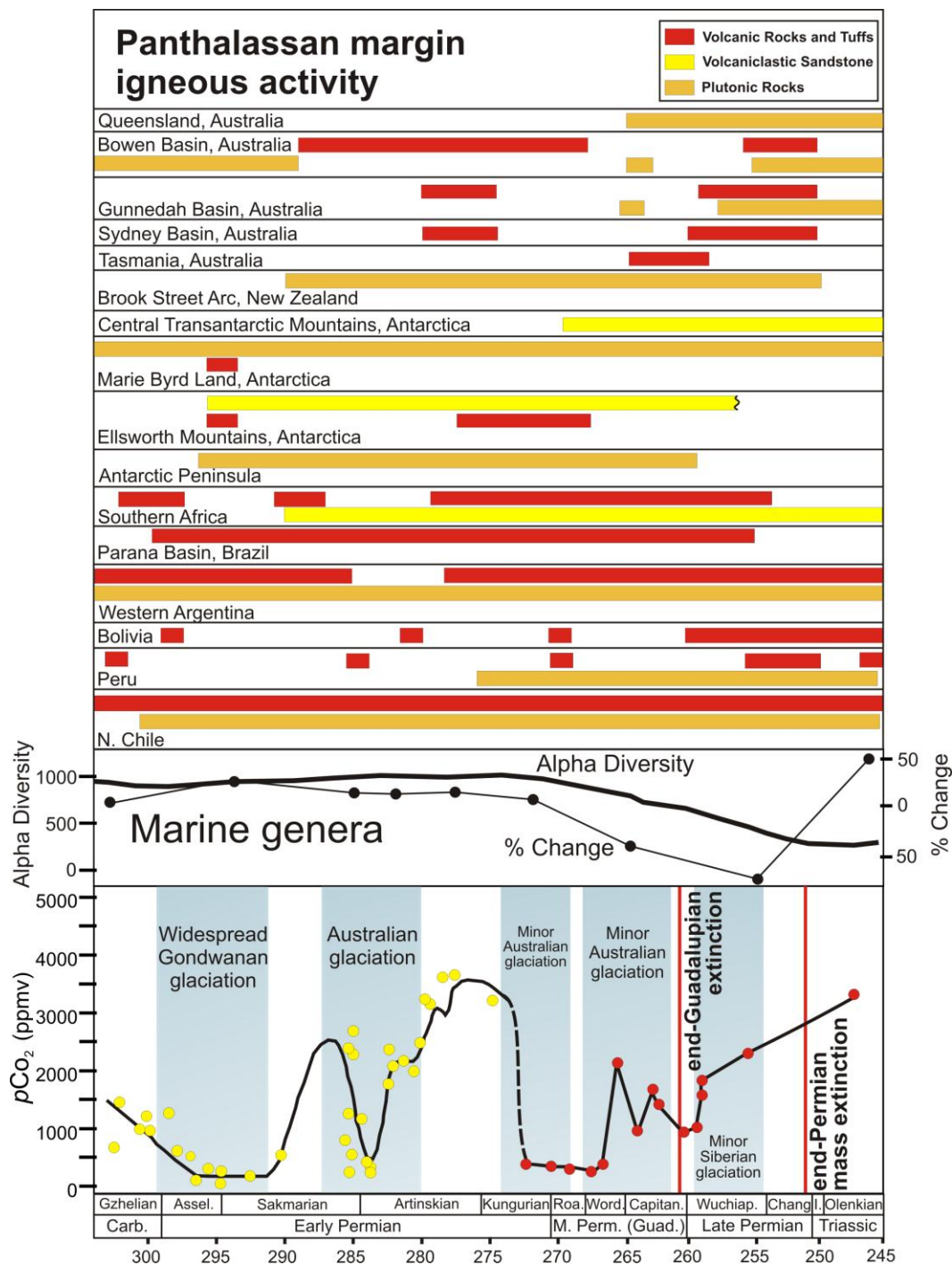


Figure 46. Diagram of climatic, biotic, and igneous events during the Permian. Dates of igneous activity along the Panthalassan margin are from Lopatin et al., 1974; Hålbich et al., 1983; Coutinho et al., 1991; Johnson, 1991; Collinson et al., 1994; Veevers et al., 1994c; Pankhurst et al., 1998; Bangert et al., 1999; Mukasa and Dalziel, 2000; Stollhofen et al., 2000; Campbell et al., 2001; Millar et al., 2002; Price et al., 2006; Grader et al., 2008. Marine genera plots are modified from Bambach et al., 2004. For CO<sub>2</sub> fluctuations,

yellow dots and dotted line are from Montañez et al. (2007), red dots represent data compiled by Royer (2006), and the dashed line links the two data sets.

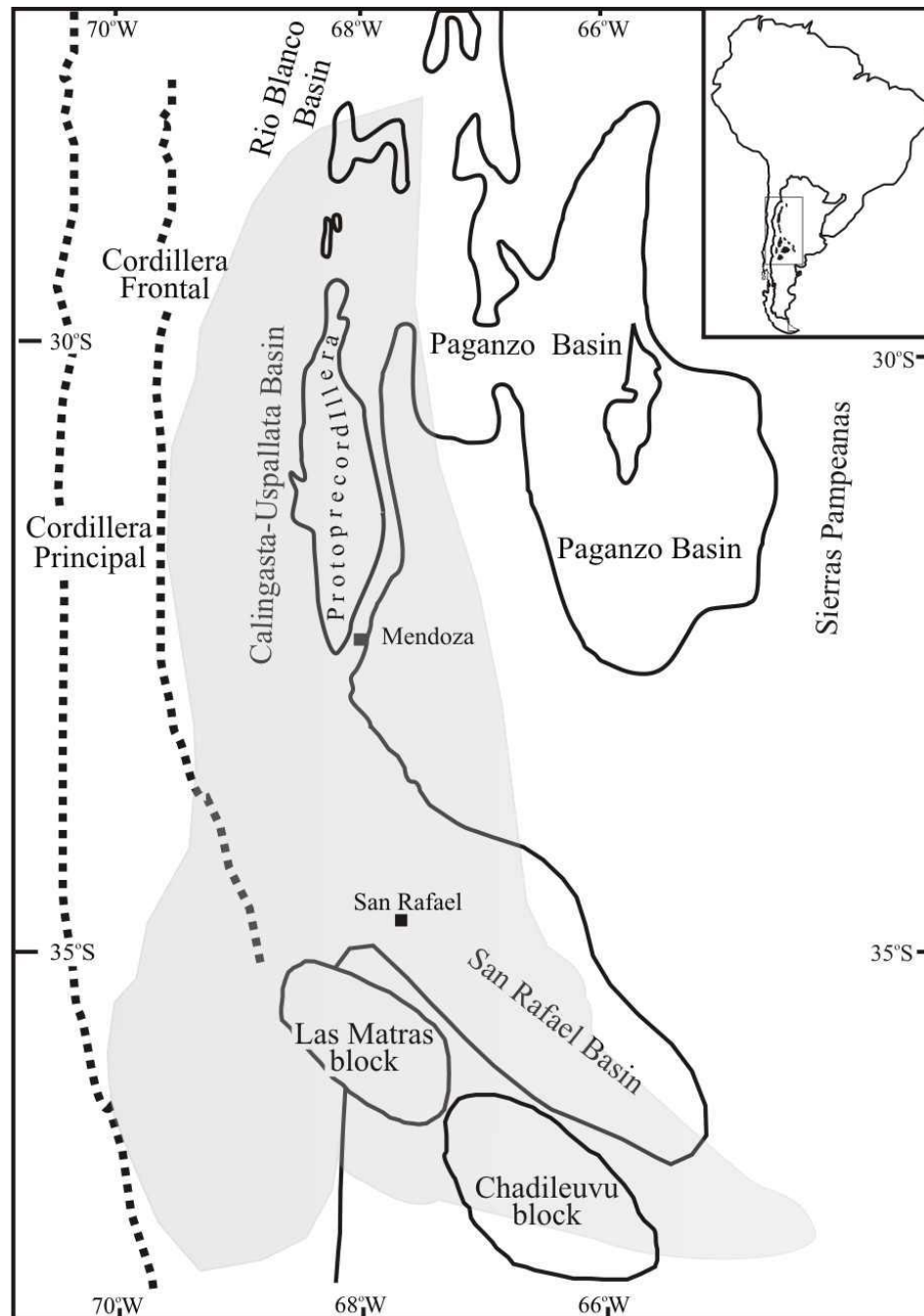


Figure 47. Map showing outcrop locations of the Choiyoi Group and the inferred extent of the Choiyoi volcanism (gray), based on modern outcrops, volcanoclastic sediments, and wells, after Kay et al. (1989), Llambías et al. (1993), and López Gamundí et al. (1994).



## References

- Bambach, R., Knoll, A., Wang, S., 2004. Origination, extinction, and mass depletions of marine diversity. *Paleobiology* 30, 522–542.
- Bangert, B., Stollhofen, H., Lorenz, V., Armstrong, R.L., 1999. The Geochronology and significance of ash-fall tuffs in the glacial, Carboniferous – Permian Dwyka Group of Namibia and South Africa: *Journal of African Earth Sciences* 29, 33–49.
- Berner, R., 2002. Examination of hypotheses for the Permo-Triassic boundary extinction by carbon cycle modeling. *Proceedings of the National Academy of Sciences* 99, 4172–4177.
- Bottjer, D., Clapham, M., Fraiser, M., Powers, C., 2008. Understanding mechanisms for the end-Permian mass extinction and the protracted Early Triassic aftermath/recovery. *GSA Today* 18, 4–10.
- Campbell, L., Conaghan, P., Flood, R., 2001. Flow-field and palaeogeographic reconstruction of volcanic activity in the Permian Gerringong Volcanic Complex, southern Sydney Basin, Australia. *Australian Journal of Earth Sciences* 48, 357–375.
- Chumakov, N., Zharkov, M., 2003. Climate during the Permian-Triassic biosphere reorganizations. Article 2. Climate of the Late Permian and Early Triassic: General Inferences. *Stratigraphy and Geological Correlation* 11, 361–375.
- Clapham, M., Shen, S., Bottjer, D., 2009. The double mass extinction revisited: reassessing the severity, selectivity, and causes of the end-Guadalupian biotic crisis (Late Permian). *Paleobiology* 35, 32–50.
- Clarke, A., 1993. Temperature and extinction in the sea: a physiologist's view. *Paleobiology* 19, 499–518.
- Collinson, J., Isbell, J., Elliot, D., Miller, M., Miller, J., 1994. Permian-Triassic Transantarctic basin. In: Veevers, J., Powell, C. (Eds.), *Permian-Triassic Pangean basins and foldbelts along the Panthalassan Margin of Gondwanaland*. Boulder, Colorado, Geological Society of America Memoir 184, 173–222.
- Courtillot, V., 1999. *Evolutionary catastrophes; the science of mass extinction*. Cambridge University Press, Cambridge, 173 p.
- Coutinho, J., Hachiro, J., Coimbra, A., Santos, P., 1991. Ashfall-derived vitroclastic tuffaceous sediments in the Permian of the Paraná Basin and their provenance. In: Ulbrich, H., Rocha-Campos, A. (Eds.), *Gondwana Seven Proceedings*. São Paulo, Brazil, Instituto de Geociências, Universidade de São Paulo, 147–160.

- Cortés, J., 1985. Vulcanitas y sedimentitas lacustres en la base del Grupo Choiyoi al sur de la estancia Tambillos, provincia de Mendoza, República Argentina. Antofagasta, Congreso Geológico Chileno, IV, Actas1, 89–108.
- Crowell, J., 1978. Continental glaciation, cyclothems, continental positioning, and climate change. *American Journal of Science* 278, 1345–1372.
- Crowell, J., 1999. Pre-Mesozoic ice ages: their bearing on understanding the climate system. *Geological Society of America Memoir* 192, Boulder, 106 p.
- Díaz-Martínez, E., Mamet, B., Isaacson, P., Grader, G., 2000. Permian marine sedimentation in northern Chile: new paleontological evidence from the Juan de Morales Formation, and regional paleogeographic implications. *Journal of South American Earth Sciences* 13, 511–525.
- Faure, K., de Wit, M., Willis, J., 1995. Late Permian global coal hiatus linked to  $^{13}\text{C}$ -depleted  $\text{CO}_2$  flux into the atmosphere during the final consolidation of Pangea. *Geology* 23, 507–210.
- Fielding, C., Frank, T., Birgenheier, L., Rygel, M., Jones, A., Roberts, J., 2008a. Stratigraphic imprint of the Late Palaeozoic Ice Age in eastern Australia: a record of alternating glacial and nonglacial climate regime. *Journal of the Geological Society, London* 165, 129–140.
- Fielding, C., Frank, T., Isbell, J., 2008b. The late Paleozoic ice age – a review of current understanding. In: Fielding, C., Frank, T., and Isbell, J. (Eds.), *Resolving the Late Paleozoic Ice Age in Time and Space: Geological Society of America Special Publication* 441, 343–354.
- Fraiser, M., Bottjer, D., 2007. Elevated atmospheric  $\text{CO}_2$  and the delayed biotic recovery from the end-Permian mass extinction. *Palaeogeography, Palaeoclimatology, Palaeoecology* 252, 164–175.
- Frakes, L., Francis, J., Syktus, J., 1992. *Climate Modes of the Phanerozoic*. Cambridge, Cambridge University Press, 274 p.
- Ganino, C., Arndt, N., 2009. Climate changes caused by degassing of sediments during the emplacement of large igneous provinces. *Geology* 37, 323–326.
- Gastaldo, R., DiMichele, W., Pfefferkorn, H., 1996. Out of the icehouse into the greenhouse: a late Paleozoic analogue for modern global vegetational change. *GSA Today* 10, 1–7.
- Grader, G., Isaacson, P., Díaz-Martínez, E., Pope, M., 2008. Pennsylvanian and Permian sequences in Bolivia: direct responses to Gondwanan glaciation. In: Fielding, C., Frank, T., and Isbell, J. (Eds.), *Resolving the Late Paleozoic Ice Age in Time and*

- Space: Geological Society of America Special Publication 441, 143–159.
- Grice, K., Cao, C., Love, G., Boettcher, M., Twitchett, R., Grosjean, E., Summons, R., Turgeon, S., Dunning, W., Jin, Y., 2005. Photic zone euxinia during the Permian-Triassic superanoxic event. *Science* 307, 706–709.
- Groeber, P., 1946. Observaciones geológicas a lo largo del meridiano 70.1°: 1, Hoja Chos Malal. *Revista de la Asociación Geológica Argentina* 1, 117–208.
- Hälbich, I., Fitch, F., Miller, J., 1983. Dating the Cape orogeny. In: Söhne, A., Hälbich, I. (Eds.), *Geodynamics of the Cape Fold Belt*. Geological Society of South Africa Special Publication 12, 149–164.
- Hallam, A., 1991. Why was there a delayed radiation after the end-Paleozoic extinctions? In: Brasier, M. (Ed.), *Innovations and Revolution in the Biosphere: Historical Biology* 5, 257–262.
- Hyde, W., Grossman, E., Crowley, T., Pollard, D., Scotese, C., 2006. Siberian glaciation as a constraint on Permian-Carboniferous CO<sub>2</sub> levels. *Geology* 34, 421–424.
- IPCC, 2007. Summary for policymakers. In: M.L. Parry, O.F. Canziani, J.P. Palutikof, P.J. van der Linden, and C.E. Hanson (Eds.), *Climate Change 2007: Impacts, Adaptation and Vulnerability. Contribution of Working Group II to the Fourth Assessment Report of the Intergovernmental Panel on Climate Change*. Cambridge University Press, 7–22.
- Isbell, J., Miller, M., Wolfe, K., Lenaker, P., 2003. Timing of late Paleozoic glaciation in Gondwana: was glaciation responsible for the development of northern hemisphere cyclothems? In: Chan, M. and Archer, A. (Eds.), *Extreme depositional environments: mega end members in geologic time*. Geological Society of America Special Paper, Boulder, Colorado, 5–24.
- Jin, Y., Shang, J., 2000. The Permian of China and its interregional correlation. In: Yin, H.; Dickins, J.M.; Shi, G.R.; Tong Jinnan (Eds.), *Permian-Triassic evolution of Tethys and western Circum-Pacific*. *Developments in Palaeontology and Stratigraphy* 18, 71–98.
- Johnson, M., 1991. Sandstone petrography, provenance and plate tectonic setting in Gondwana context of the southeastern Cape-Karoo Basin. *South African Journal of Geology* 94, 137–154.
- Kay, S., Ramos, V., Mpodozis, C., Sruoga, P., 1989. Late Paleozoic to Jurassic silicic magmatism at the Gondwanaland margin: analogy to the Middle Proterozoic in North America? *Geology* 17, 324–328.
- Keller, M., 1999. Argentine Precordillera: sedimentary and plate tectonic history of a

- Laurentian crustal fragment in South America. Geological Society of America Special Paper 941, 131 p.
- Kiehl, J., Shields, C., 2005. Climate simulation of the latest Permian: implications for mass extinction. *Geology* 33, 757–760.
- Kidder, D., Worsley, T., 2004. Causes and consequences of extreme Permo-Triassic warming to equable climate and relation to the Permo-Triassic extinction and recovery. *Palaeogeography, Palaeoclimatology, Palaeoecology* 203, 207–237.
- Kontak, D., Clark, A., Farrar, E., Archibald, D., Baadsgaard, H., 1990. Late Paleozoic – Early Mesozoic magmatism in the Cordillera de Carabaya, Puno, southeastern Peru: Geochronology and petrochemistry. *Journal of South American Earth Sciences* 3, 213–230.
- Krull, E., Retallack, G., 2000.  $\delta^{13}\text{C}$  depth profiles from paleosols across the Permian-Triassic boundary: Evidence for methane release. *GSA Bulletin* 112, 1459–1472.
- Lawver, L., Dalziel, I., Norton, I., Gahagan, L., 2008. The Plates 2007 Atlas of Plate Reconstructions (750 Ma to Present Day), Plates Progress Report No. 305–0307, University of Texas Technical Report No. 195, 160 p.
- Leavitt, S., 1982. Annual volcanic carbon dioxide emission: an estimate from eruption chronologies. *Environmental Geology* 4, 15–21.
- Lehrmann, D., Ramezani, J., Bowring, S., Martin, M., Montgomery, P., Enos, P., Payne, J., Orchard, M., Wang, H., Wei, J., 2006. Timing of recovery from the end-Permian extinction; geochronologic and biostratigraphic constraints from south China. *Geology* 34, 1053–1056.
- Limarino, C. Spalletti, L., 2006. Paleogeography of the upper Paleozoic basins of southern South America: An overview. *Journal of South American Earth Sciences* 22, 134–155.
- Llambías, E., 1999. Las rocas ígneas gondwánicas. *Geología Argentina, Instituto de Geología Recursos Minerales, Anales* 29, 349–376.
- Llambías, E., Kleiman, L., Salvarredi, J., 1993. El Magmatismo Gondwánico. In: Ramos, V.A. (Ed.), *Geología y Recursos Naturales de Mendoza, Relatorio: XII Congreso Geológico Argentino y II Congreso de Exploración de Hidrocarburos (Mendoza)*, 53–64.
- Llambías, E., Quenardelle, S., Montanegro, T., 2003. The Choiyoi Group from central Argentina; a subalkaline transitional to alkaline association in the craton adjacent to the active margin of the Gondwana continent. *Journal of South American Earth Sciences* 16, 243–457.

- Lopatin, B.G., Krylov, A.I., Aliapyshev, O.A., 1974. Osnovnye tektono 403 magmaticcheskie stapy v razvitií zemli Meri Berdi i berega Eitsa (Zapadnaia Antarktida) po radiogennym dannym. *Anarktika Doklady Komissii* 13, 52–60.
- López Gamundí, O., Espejo, I., Conaghan, P., Powell, C., Veevers, J., 1994. Southern South America. In: Veevers, J., Powell, C. (Eds.), *Permian-Triassic Pangean basins and foldbelts along the Panthalassan Margin of Gondwanaland*: Boulder, Colorado, Geological Society of America Memoir 184, 281–329.
- Marty, B., Jambon, A., 1987.  $C/{}^3He$  in volatile fluxes from the solid Earth: implications for carbon geodynamics. *Earth and Planetary Science Letters* 83, 16–26.
- McDougall, I., Harrison, T.M., 1988. *Geochronology and thermochronology by the  ${}^{40}Ar/{}^{39}Ar$  method*. Oxford University Press, New York, 212 p.
- Millar, I., Pankhurst, R., Fanning, C., 2002. Basement chronology of the Antarctic Peninsula: recurrent magmatism and anatexis in the Paleozoic Gondwana Margin. *Journal of the Geological Society, London* 159, 145–157.
- Montañez, I., Tabor, N., Niemeier, D., DiMichele, W., Frank, T., Fielding, C., Isbell, J., Birgenheir, L., Rygel, M., 2007.  $CO_2$ -forced climate and vegetative instability during late Paleozoic deglaciation. *Science* 315, 87–91.
- Mukasa, S.B., Dalziel, I.W.D., 2000. Marie Byrd Land, West Antarctica; evolution of Gondwana's Pacific margin constrained by zircon U-Pb geochronology and feldspar common-Pb isotopic compositions: *Geological Society of America Bulletin* 112, 611–627.
- Naranjo, J., Puig, A., 1984. Hojas Taltal y Chañaral, Carta geológica de Chile. Servicio Nacional de Geología y Minería de Chile, Boletín 62, Santiago de Chile.
- Nasi, C., Sepúlveda, P., 1986. Avances en el conocimiento del Carbonífero en el norte de Chile. Annual Meeting of the Working Group, IUGS-IGCP Project 211, Late Paleozoic of South America, Abstracts, 27–43.
- Pankhurst, R.J., Weaver, S.D., Bradshaw, J.D., Storey, B.C., Ireland, T.R., 1998. Geochronology and geochemistry of pre-Jurassic superterrane in Marie Byrd Land, Antarctica. *Journal of Geophysical Research* 103, 2529–2547.
- Payne, J., Kump, L., 2007. Evidence for recurrent Early Triassic massive volcanism from quantitative interpretation of carbon isotope fluctuations. *Earth and Planetary Science Letters* 256, 264–277.
- Price, R., Ireland, T., Maas, R., Arculus, R., 2006. SHRIMP ion probe zircon geochronology and Sr and Nd isotope geochemistry for southern Longwood

- Range and Bluff Peninsula intrusive rocks of Southland, New Zealand. *New Zealand Journal of Geology & Geophysics* 49, 291–303.
- Racki, G., Wignall, P., 2005. Late Permian double-phased mass extinction and volcanism: an oceanographic perspective. In: Over, D., Morrow, J., Wignall, P. (Eds.), *Understanding Late Devonian and Permian-Triassic Biotic and Climatic Events: Towards an Integrated Approach*. *Developments in Paleontology and Stratigraphy*, 263–297.
- Raup, D.M., Sepkoski, J.J., 1982. Mass extinctions in the marine fossil record. *Science* 215, 1501–1503.
- Raven, J.A., Caldeira, D., Elderfield, H., Hoegh-Guldberg, O., Liss, P., Riebessell, U., Shepherd, J., Turley, C., Watson, A., Heap, R., Banes, R., Quinn, R., 2005. *Ocean Acidification Due to Increasing Atmospheric Carbon Dioxide*. Royal Society, London, U.K. 57 pp.
- Renne, P., Zhang, Z., Richardson, M., Black, M., Basu, A., 1995. Synchrony and causal relations between Permo-Triassic boundary crises and Siberian flood volcanism. *Science* 269, 1413–1416.
- Retallack, G., Metzger, C., Greaver, T., Jahren, A., Smith, R., Sheldon, N., 2006. Mid-Late Permian mass extinction on land. *Geological Society of America Bulletin* 118, 1398–1411.
- Royer, D.L., 2006. CO<sub>2</sub>-forced climate thresholds during the Phanerozoic. *Geochimica et Cosmochimica* 70, 5665–5675.
- Royer, D.L., Berner, R.A., Montañez, I.P., Tabor, N.J., Beerling, D.J., 2004. CO<sub>2</sub> as a primary driver of Phanerozoic climate. *GSA Today* 14, 4010.
- Rust, A., Cashman, K., 2007. Multiple origins of obsidian pyroclasts and implications for changes in the dynamics of the 1300 B.P. eruption of Newberry Volcano, USA. *Bulletin of Volcanology* 69, 825–845.
- Sato A., Llambías, E., 1993. El Grupo Choiyoi, provincia de San Juan, equivalente efusivo del Batolito de Colangüil. XII Congreso Geológico Argentino y 2º Congreso de Exploración de Hidrocarburos 4, 156–165.
- Smith, L., Read, J., 2000. Rapid onset of late Paleozoic glaciation on Gondwana: Evidence from Upper Mississippian strata of the Midcontinent, United States. *Geology* 28, 279–282.
- Sowerby, J., Keppler, H., 1999. Water speciation in rhyolitic melt determined by in situ infrared spectroscopy. *American Mineralogist* 84, 1843–1849.

- Stipanovic, P., Rodrigo F., Baulies, O. Martínez, C., 1968. La formaciones presenonianas en el denominado macizo Nordpatagónico. *Revista de la Asociación Geológica Argentina* 23, 67–88.
- Stollhofen, H., Stanistreet, I.G., Bangert, B., Grill, H., 2000. Tuffs, tectonism and glacially related sea-level changes, Carboniferous-Permian, southern Namibia. *Palaeogeography, Palaeoclimatology, Palaeoecology* 161, 127–150.
- Veevers, J., Clare, A., Wopfner, H., 1994a. Neocratonic magmatic-sedimentary basins of post-Variscan Europe and post-Kanimblan eastern Australia generated by right-lateral transtension of Permo-Carboniferous Pangea. *Basin Research* 6, 141–157.
- Veevers, J., Cole, D., Cowan, E., 1994b. Southern Africa: Karoo Basin and Cape Fold Belt. In: Veevers, J., and Powell, C. (Eds.), *Permian-Triassic Pangean basins and foldbelts along the Panthalassan Margin of Gondwanaland*. Boulder Colorado, Geological Society of America Memoir 184, 223–279.
- Veevers, J., Powell, C., Collinson, J., López Gamundí, O., 1994c. Synthesis. In: Veevers, J., Powell, C. (Eds.), *Permian-Triassic Pangean basins and foldbelts along the Panthalassan Margin of Gondwanaland*. Boulder, Colorado, Geological Society of America Memoir 184, 331–353.
- Veevers, J., Tewari, R., 1995. Permian-Carboniferous and Permian-Triassic magmatism in the rift zone bordering the Tethyan margin of southern Pangea. *Geology* 23, 467–470.
- Wignall, P., 2001. Large igneous provinces and mass extinctions. *Earth-Science Reviews* 53, 1–33.
- Wignall, P., Twitchett, R., 1996. Oceanic anoxia and the end Permian mass Extinction. *Science* 272, 1155–1158.
- Yin, H.-F., Huang, S., Zhang, K., Hansen, H., Yang, F.-Q., Ding, M., Bie, X., 1992. The effects of volcanism on the Permo-Triassic mass extinction in South China. In: Sweet, W.C. (Ed.), *Permo-Triassic events in the eastern Tethys*. Cambridge University Press, Cambridge, 146–157.
- Zhou, M., Malpas, J., Song, X.-Y., Robinson, P., Min, S., Kennedy, A., Leshner, C., Keays, R., 2002. A temporal link between the Emeishan large igneous province (SW China) and the end-Guadalupian mass extinction. *Earth and Planetary Science Letters* 196, 113–122.

## **Chapter 7: A discussion of potential effects of paleotopography on glacial intervals in Argentina and Australia during the late Paleozoic ice age**

### **Abstract**

The stratigraphic, geochemical, and tectonic records of the late Paleozoic ice age (LPIA) continue to improve in resolution, revealing glacial and non-glacial intervals that occurred across Gondwana. To date, these events are roughly correlated with changes in the paleolatitude of Gondwana and fluctuations in greenhouse gases. However, the drivers behind the initiation and collapse of each glacial interval of the LPIA are likely a complex interplay of regional and global conditions and controls, and much work is still necessary to unravel the causes of these climatic perturbations. In this chapter, the role of paleotopography and the equilibrium line altitude (ELA) is examined as a driver of glacial and non-glacial intervals in west central Argentina and eastern Australia. Although local, regional, and global drivers all influenced the waxing and waning of Gondwana glaciers, the ELA and land surface elevation dictated where ice centers developed, and changes in paleotopography due to tectonism were a control on glaciation and deglaciation events. In west central Argentina, the Protoprecordillera, a fold-thrust belt, housed alpine glaciers in the Serpukhovian – Bashkirian (late Mississippian – early Pennsylvanian). The Protoprecordillera collapsed in the early Pennsylvanian, and this loss of altitude coincides with deglaciation in west central Argentina; glaciers did not return to this region for the remainder of the LPIA. In eastern Australia, glacial intervals continued from the late Sakmarian to the Capitanian (Early to Late Permian; P2 to P4 glaciations of Fielding et al., 2008a), well after glaciation had ceased elsewhere in



Gondwana during the mid-Sakmarian. These glacial events occurred during an interval when basins located at higher paleolatitudes went unglaciated. The post- mid-Sakmarian glaciations in eastern Australia were likely fostered by relationships between elevation and the local ELA. Uplifted land area was provided by the Kanimblan highlands in the Tasman Fold Belt, and local climate variability (e.g., possibly driven by ocean circulation patterns) also shifted the ELA to allow for glaciation during P2-P4. Therefore, in addition to the classically cited drivers for LPIA glaciations such as paleolatitude and  $p\text{CO}_2$ , the relationship between the ELA and uplifted regions where glaciers can form and persist should be taken into account when considering the initiation and demise of glacial intervals of the LPIA, as well as other times of glaciation in Earth's history.

## 1. Introduction

The late Paleozoic ice age (LPIA) was a protracted icehouse interval in Earth's history that began in western Gondwana (South America) in the Mississippian, waxed and waned through several glacial intervals of 1-8 Ma duration that alternated with non-glacial conditions of approximately equal length, and ended in eastern Gondwana (eastern Australia) in the Late Permian (Caputo and Crowell, 1985; Dickins, 1997; López Gamundí, 1997; Visser, 1997; Isbell et al., 2003; Fielding et al., 2008a). The LPIA is recognized as a major climatic event in Earth history, and it serves as an analog for Earth's present glaciated state. However, our understanding of the causes for the initiation and termination of glacial intervals throughout the LPIA is rudimentary at present.

Continental drift of Gondwana across the South Pole has long been recognized as a control for the shifting of glacial centers across the supercontinent from west (South

America) to east (Australia) during the LPIA (Du Toit, 1921; Wegener, 1929; Crowell, 1978; Caputo and Crowell, 1985). LPIA glaciations began in western South America during the Visean (Figs. 48 and 49; López Gamundí, 1997; Glacial I of Isbell et al., 2003). During the Namurian (Serpukhovian – Bashkirian), glaciers expanded in western South America (López Gamundí, 1997; Glacial II of Isbell et al., 2003) and first appeared in eastern Australia (Fielding et al., 2008a, 2008b, 2008c). In the Gzhelian - Sakmarian (the latest Pennsylvanian to Early Permian), widespread glaciation occurred across Gondwana (Visser, 1997; Isbell et al., 2008a, 2008b; Fielding et al., 2008a, 2008b; Rocha Campos et al., 2008). This glaciation (Glacial III of Isbell et al., 2003) was centered over Antarctica, with ice centers also occurring in eastern South America, Africa, India, and Australia (Laskar and Mitra, 1976; Collinson et al., 1994; López Gamundí, 1997; Visser, 1997; Mory et al., 2008; Fielding et al., 2008a; Rocha-Campos et al., 2008). Finally, from the late Sakmarian to the Capitanian, glacial centers were located only in Australia (Fielding et al., 2008a, 2008b, 2008c; Mory et al., 2008).

Polar wander paths proposed by Powell and Li (1994) and Lawver et al. (2008) provide hypotheses for the course of Gondwana across the South Pole during the late Paleozoic (Fig. 48). Powell and Li (1994) referenced paleomagnetic poles from eastern and central Australia for their model, in which the pole occurred in southern Argentina in the middle Devonian and shifted to central Africa in the latest Devonian to Mississippian, then migrating into eastern Antarctica in the Pennsylvanian (Fig. 48; Li et al., 1993; Powell and Li, 1994). The pole then shifted to present-day Marie Byrd Land in Antarctica by the middle Permian, and then moved eastward into eastern Australia in the latest Permian. Alternately, the polar wander path by Lawver et al. (2008), developed

from a global model based on the PLATES (University of Texas Institute for Geophysics) paleomagnetic and geophysical database, assigns the pole to a more longitudinal course. In this scheme, the pole occurred in north central Africa in the Late Devonian, migrated to eastern Africa, and then shifted southward through Africa during the Mississippian (Fig. 48). In the Pennsylvanian, the pole moved into Antarctica, then migrated into the Antarctic Peninsula in the Early Permian, shifting along and beyond the Antarctic Peninsula throughout the Late Permian and into the Triassic.

Although glaciation began in western Gondwana and ended in eastern Gondwana during the LPIA, approximating the path of the South Pole proposed by Powell and Li (1994), polar wander can only account for some general trends in glacier occurrence. This mechanism does not explain the vacillation between glacial and non-glacial conditions within the ice age, the timing and variations in the extent of the various glacial events across Gondwana or within a particular region, or the continued mid- to Late Permian glaciations in eastern Australia, when the pole was shifting west (Figs. 48, 49). During these mid- to Late Permian glaciations in eastern Australia, Antarctica remained unglaciated, despite being closer to the pole (cf. Collinson et al., 1994; Isbell et al., 2008b; Henry et al., 2012). Further, glaciation ended in eastern Australia in the late Capitanian-early Wuchiapingian (~260 Ma), at a time when the South Pole may have been migrating towards the region (Fig. 48; cf. Powell and Li, 1994; Fielding et al., 2008a).

Correlation of atmospheric partial pressure of CO<sub>2</sub> ( $p\text{CO}_2$ ; Fig. 50) and carbon and oxygen isotope fluctuations with selected glacial and non-glacial intervals in the Carboniferous and Permian suggests that greenhouse gases were also a major control on

climate fluctuations (Montañez et al., 2007; Frank et al., 2008). However, there are assumptions and incongruities in the geochemical record for the late Paleozoic that should be taken into account. One issue is that geochemical data appear incongruous with certain glacial and non-glacial intervals. For example, during the first half of Glacial II in the Serpukhovian,  $\delta^{13}\text{C}$  and  $\delta^{18}\text{O}$  isotopes actually decrease, which typically occurs during warming (Frank et al., 2008). Later in Glacial II during the Bashkirian and the subsequent C4 glaciation in Australia that extends into the Moscovian, there is a dramatic positive excursion in  $\delta^{13}\text{C}$  and  $\delta^{18}\text{O}$ , but the expected isotopic increase lags behind the occurrence of Glacial II sediments in South America and Australia. Frank et al. (2008) put forward two different explanations for the discrepancies between the isotopic and stratigraphic records: 1) The isotopic data set is too low resolution at present to accurately represent the entirety of Glacial II; or 2) because Glacial II consisted of multiple ice centers waxing and waning at different times in different regions, the paleotropics were not influenced as consistently, creating variable isotopic ratios. Nevertheless, the isotope curves are surprising.

Another issue is that the geochemical record remains undeveloped for polar regions of Gondwana. Data for  $p\text{CO}_2$  levels and  $\delta^{13}\text{C}$  and  $\delta^{18}\text{O}$  are derived from paleotropical carbonates from Laurentia and Eurasia, typically from whole rock analysis or brachiopod calcite (cf. Hayes et al., 1999; Veizer et al. 1999; Frank et al., 2008). This far field data representing isotopic fluctuations in seawater is assumed to record the same climatic fluctuations forcing ice volume changes recorded in near field glacigenic and post-glacial deposits (Frank et al., 2008). This assumption is rarely checked against isotopic signatures of near field regions (with the exception of Scheffler et al., 2003), so a

level of uncertainty remains about the accuracy of using far field chemical proxies to draw conclusions about glacial intervals experienced in polar regions.

Finally, the  $p\text{CO}_2$  curve has only been developed for the latest Carboniferous (Gzhelian) through the Permian (Fig. 50; Glacial III and subsequent Australian glaciations), and does not exist for Glacial I and Glacial II. When this gap in the dataset is filled in, it will be interesting to see if  $p\text{CO}_2$  drawdown occurs during Glacials I and II as it does for P2, a relatively minor glaciation compared to Glacial III.

To summarize, paleolatitude and greenhouse gases were major controls on glaciation, but these drivers alone cannot account for LPIA glaciations and non-glacial intervals. Other factors likely also contributed to the initiation and demise of the glacial intervals (e.g., Jones et al., 2006).

Topography is an obvious control on glaciation, as glaciers are generated at altitudes where snow can accumulate. However, paleotopography is often overlooked in discussions of the drivers of glacial intervals in the LPIA. Instead, data collection and reconstructions have focused on paleolatitude and greenhouse gases. The purpose of this paper is to explore how paleotopography may have contributed to the initiation and collapse of certain glacial intervals during the LPIA, in the regions of west central Argentina and eastern Australia, drawing from published works on the two regions. Glaciation began in west central Argentina and eastern Australia in the Mississippian, before other regions closer to the South Pole were glaciated (Figs. 48 and 49). At the end of the LPIA, glaciation continued in eastern Australia after Glacial III, from the late Sakmarian to the Capitanian, when regions closer to the South Pole were unglaciated (Fielding et al., 2008a; Isbell et al., 2008a; 2008b; 2010; Henry et al., 2012). It has been

proposed that high altitude regions in these areas at these times made these glacial intervals possible, and in west central Argentina, the collapse of a high altitude region contributed to the end of glaciation there.

Powell and Veevers (1987) and Eyles (1993) identify tectonic uplift along the Panthalassan margin of Gondwana, beginning with the collision of the Chilenia terrane against western South America in the late Tournasian-early Viséan (early Mississippian), as an instigating condition for the LPIA. Further, Powell and Veevers (1987) called attention to the latitudinal position of South America and Australia during the onset of LPIA glaciation in those areas. Initiation of glaciation in both of these regions began when these sectors of Gondwana were located at mid-latitudes ( $30^{\circ}$  -  $60^{\circ}$ ), rather than when they were located at high latitudes, and glaciation went on to spread across each respective crustal block. Therefore, rather than polar latitude, onset of glaciation appears to coincide with orogenesis: in South America, convergence and accretion along the Panthalassan margin, and in Australia, uplift along the Tasman Fold Belt (Powell and Veevers 1987). Therefore, this availability of topographic surfaces at high elevations was proposed as a mechanism that allowed glaciers to nucleate and grow in South America and Australia (cf. Powell and Veevers, 1987; Eyles, 1993; Isbell et al., 2010).

Isbell et al. (2010) and Henry et al. (2012) suggested that many of the local variations and problems with the distribution and timing of Gondwana glaciations can be explained by examining the relationship between the equilibrium line altitude (ELA) and the paleo-land surface for a given region through time and space. For glaciation to commence in a region, the land surface must occur above the ELA. The ELA is the elevation in a region above which ice accumulation can occur. The ELA is equivalent to

the snowline, and on a glacier, the ELA is the boundary separating the upper area of accumulation from the lower area of ablation (Fig. 51). Therefore, glaciers cannot form if the ELA resides above the elevation of the land surface in a particular region. Because the relationship between the ELA and land surface changes due to climatic fluctuations and tectonic events, the ELA should be considered a controlling factor on glacier distribution throughout the many phases of the LPIA and other glacial events, as the ELA is the summation of all controlling factors on the development or termination of glaciation in time and space. Paleotopography and the ELA are often overlooked as built-in drivers of glacial intervals, and the purpose of this paper is to explore certain glacial intervals that were influenced by paleotopography, and to recommend that paleotopography be considered when evaluating causes of glaciation and deglaciation.

## **2. The ELA**

The ELA for a given location is controlled by latitude, precipitation, and topography. Glaciers can exist at any latitude on Earth, but at varying altitudes depending on the climate of the region (Broecker and Denton, 1990). Presently glaciers occur in tropical regions at high altitudes (for example, above 4000 m in Irian Jaya, Indonesia; Allison and Peterson, 1989), but in high-latitude regions like Antarctica and Greenland, glaciers can form at sea level (Miller et al., 1975). Therefore the ELA generally rises as latitude decreases, with variations in precipitation creating some fluctuations in this trend (Broecker and Denton, 1990). Moreover, high snowfall will lower an ELA, but in locations with low snowfall, such as arid regions, glaciers will have higher ELAs.

Topography is an important control on the ELA of a glacier, because land surfaces must be available above the ELA for a glacier to form. Further, tectonic movement in a region could impact the ability of glaciers to form: uplift of a region above the ELA would make it possible for glaciers to nucleate, and subsidence of a region below the ELA would cause preexisting glaciers to ablate. The interplay of drivers of glaciation with a focus on paleotopography is explored here for the intervals of Glacial II in the late Mississippian-early Pennsylvanian (Figs. 48 and 49) in west central Argentina and Glacial III/P1 in the latest Pennsylvanian – Early Permian and subsequent glacial intervals in eastern Australia from the late Sakmarian to the Capitanian.

### **3. Glacial II over the Protoprecordillera**

Glaciation began in present-day west central Argentina in the Visean (middle Mississippian; Limarino et al., 2006; Gulbranson et al., 2010; Glacial I of Isbell et al., 2003), with its maximum extent in this region occurring during a second interval of glaciation during the Serpukhovian to early Bashkirian (late Mississippian to early Pennsylvanian; Glacial II of Isbell et al., 2003; López Gamundí, 1997; Limarino et al., 2006; Henry et al., 2008; Gulbranson et al., 2010). The two known glacial intervals in west central Argentina are dated with U-Pb radiometric ages (Gulbranson et al., 2010) and also correlate with biostratigraphically dated glacial deposits in the Tepuel-Genoa Basin in Patagonia of southern Argentina (Fig. 49; Taboada, 2010). In the late Gzhelian – Sakmarian (latest Pennsylvanian-Early Permian), glaciation resumed in Patagonia and commenced in eastern South America in the Paraná Basin in Brazil (Holz et al., 2008; Taboada, 2010) during the glacial maximum across Gondwana (Glacial III of Isbell et al., 2003; P1 of Fielding et al., 2008a). However, glaciers did not return to west central



Argentina after the early Bashkirian. At that time, Patagonia was located in a near polar position while west central Argentina was located in the mid-latitudes (Powell and Li, 1994; Lawver et al., 2008).

The Serpukhovian to early Bashkirian glaciation in west central Argentina was characterized by alpine glaciers that extended off the Protoprecordillera, a fold-thrust belt, into the surrounding basins: the Calingasta-Uspallata, Río Blanco, and Paganzo Basins (Fig. 52; López Gamundí et al., 1994; López Gamundí, 1997; Limarino et al., 2006; Henry et al., 2008). The Protoprecordillera formed during the Middle Devonian to Early Mississippian during the Chañic orogeny along the convergent Panthalassan margin of Gondwana (Ramos, 1988; López Gamundí et al., 1994; Limarino et al., 2006). Initially, the Protoprecordillera formed as an obducted accretionary prism, and then developed into a fold-thrust belt as the Chilenia terrain accreted to western Gondwana (Fig. 53). The alpine glaciers housed there were wet-based, and prior to their retreat, were grounded below sea-level where they entered fjords (López Gamundí, 1997; Henry et al., 2008, 2010). The estimated paleolatitude of the basins surrounding the Protoprecordillera during the mid-Carboniferous ranges from 40° - 60° S (Scotese and Barrett, 1990; Powell and Li, 1994; Torsvik and Cocks, 2004; Lawver et al., 2008; Blakey, 2008).

The Protoprecordillera provided an uplifted land surface on which glaciers could nucleate and grow, with mass balances that allowed them to reach sea level, as indicated by glacimarine deposits contained in paleo-fjords (López Gamundí, 1997; Kneller et al., 2004; Dykstra et al., 2006; Henry et al., 2008, 2010). However, the mountain range collapsed in the early Pennsylvanian – Early Permian (Fig. 53; López Gamundí et al.,

1994; Limarino et al., 2006). Evidence for this collapse includes: 1) provenance changes in sedimentary rocks in the surrounding basins; 2) magmatism indicating a shifting tectonic regime; and 3) marine incursion into the Paganzo Basin.

Late Pennsylvanian to Early Permian sandstones and clasts in the Calingasta-Uspallata Basin suggest provenance from the Sierras Pampeanas, block-faulted uplifts within and adjacent to the Paganzo Basin, and therefore suggesting sediment transport across a collapsed Protoprecordillera that no longer served as a barrier between the Calingasta-Uspallata and Paganzo Basins (Limarino et al., 2003, 2006; Net and Limarino, 2006). A petrofacies study of the Calingasta-Uspallata and Paganzo Basins indicated that in the Carboniferous, the Calingasta-Uspallata Basin was characterized by a lithic petrofacies derived from the Protoprecordillera, and the Paganzo Basin was characterized by a quartzofeldspathic petrofacies influenced by intrusive and metamorphic rocks from the Sierras Pampeanas, a mountain range to the east (López Gamundí et al., 1994). The Carboniferous lithic petrofacies signature in the Calingasta-Uspallata Basin wanes and is replaced by the quartzofeldspathic petrofacies in latest Carboniferous to Early Permian rocks, suggesting that the dividing Protoprecordillera diminished as a barrier between the two basins. Additionally, in the Agua de Jagüel Formation, dropstones consisting of granite and limestone occur within strata at the top of sequence 1 (Henry et al., 2010). The granite clasts were derived from either the Sierras Pampeanas or from granite intrusions into the Protoprecordillera, whereas limestone only occurred on the eastern flank of the Protoprecordillera (cf. Azcuy et al., 1999). If the granite clasts came from the Sierras Pampeanas, the Protoprecordillera was breached and no longer served as a barrier to iceberg drift during late glacial time. The limestone clasts require either

breaching of the highland or long distance transport of icebergs from the eastern flanks of the Protoprecordillera around the range to the western side of the range (cf. Net and Limarino, 1999).

Magmatism began in the Río Blanco Basin and within the Protoprecordillera in the Moscovian (early Pennsylvanian), resulting from a change from compressive tectonics associated with the Chañic orogeny to the establishment of a low-angle eastward-dipping subduction zone and postorogenic extensional conditions (Limarino et al., 2006). This magmatism marks the beginning of the Choiyoi Group, a volcanic province that extended through western Argentina into the Early Triassic (López Gamundí et al., 1994). The magmatism signals a shift to an extensional tectonic regime that caused the collapse of the Protoprecordillera.

Collapse of the Protoprecordillera was likely a major cause of deglaciation of the region, because the loss of altitude would have lowered the land surface below the local ELA and prevented continued growth of ice centers. The collapse of the Protoprecordillera also influenced the post-glacial transgression observed in the surrounding basins (cf. Limarino et al., 2002; Net et al., 2002). The erosion and subsidence of the divide between the more open marine western basins (Calingasta-Uspallata and Río Blanco) and the cratonward eastern basin (Paganzo Basin) allowed for marine ingression into the Paganzo Basin. However, the melting of the alpine glaciers in the Protoprecordillera did not cause the transgression, because the glaciers did not hold sufficient volumes of water to cause a significant eustatic rise and a resulting transgression of the magnitude observed in the Calingasta-Uspallata, Río Blanco, and Paganzo Basins (cf. López Gamundí, 1997; Isbell et al., 2003; Henry et al., 2008, 2010).

Marine incursion into the Paganzo Basin is evidenced by early Pennsylvanian transgressive deposits in the Guandacol, Langares, and Jejenes Formations (Limarino et al., 2002; Net et al., 2002; Pazos, 2002; Kneller et al., 2004; Dykstra et al., 2006). The transgression is also well documented in the Calingasta-Uspallata and Río Blanco Basins, in the Cortaderas, Hoyada Verde, Agua de Jagüel, and Río del Penón Formations (López Gamundí et al., 1994; López Gamundí, 1997; Limarino et al., 2002; Henry et al., 2008, 2010; Gulbranson et al., 2010). Therefore, the collapse of the Protoprecordillera both caused deglaciation in the early Pennsylvanian and induced a regional transgression, allowing for marine incursion into the Paganzo Basin.

There is no record of glaciation in the Calingasta-Uspallata, Río Blanco, and Paganzo Basins following the collapse of the Protoprecordillera; rather, the climate became arid in the Early Permian, evidenced by eolian deposits in the Paganzo Basin (Limarino et al., 2006). Additionally, strata in the Paganzo Basin record a shift from calcic Vertisols to Calcisols during the middle to late Moscovian, indicating the development of an arid climate (Gulbranson et al., 2010). The changing climate of west central Argentina is also probably related to the shifting paleolatitude of the supercontinent at this time; Gondwana migrated northwest throughout the Carboniferous, moving the Andean basins to lower latitudes (Blakey, 2008). However, glaciation occurred in Brazil from the Serpukhovian into the Gzhelian in the Paraná Basin (Fig. 49), which lay at equivalent paleolatitudes as the Andean basins (Holz et al., 2006, 2008; Rocha-Campos et al., 2008). Therefore, an additional driver for deglaciation in the early Bashkirian in the Andean basins is needed other than paleolatitude, so it is here proposed that the end of glaciation in west central Argentina during the LPIA was controlled by a

combination of the collapse of the Protoprecordillera and the migration of that region in Gondwana to lower latitudes.

#### **4. Glacial III and subsequent glaciations in Australia**

The peak of LPIA glaciation occurred in the late Gzhelian – Sakmarian (latest Carboniferous-Early Permian), when ice centers occurred across southern Gondwana in southern and southeastern South America, southern Africa, Antarctica, and Australia (Glacial III of Isbell et al., 2003; Fig. 49; Fielding et al., 2008c). During Glacial III, Antarctica was centered over the South Pole (Fig. 48; Powell and Li, 1994; Lawver et al., 2008), and  $p\text{CO}_2$  levels were low, drawn down to the equivalent of modern atmospheric levels (280 ppmv; Montañez et al., 2007). Deposits in all of these sectors of Gondwana contain glacial marine deposits indicating that mass balances were great enough that the glaciers extended to sea level. In eastern Australia, the latest Carboniferous – Early Permian glaciation is recorded in glacial marine sediments and proglacial continental deposits in multiple formations in the Bowen, Gunnedah, and Sydney Basins (Fig. 54; Fielding et al., 2008a). These basins occurred to the north of the south polar circle during the LPIA.

The latest Carboniferous-Early Permian glacial interval has been classified as the P1 glaciation by Fielding et al. (2008a) for eastern Australia, during which ice sheets, valley glaciers, and ice caps occurred in the region (Jones and Fielding, 2004; Fielding et al., 2008a). Following glaciation, in the mid-Sakmarian (Early Permian), P1 glacial diamictites are sharply overlain by mudstone with rare pebbles and sandstone (Boonderoo Beds) or rhythmically laminated siltstone (Youlambie Conglomerate; Jones and Fielding, 2004). This deglaciation signature of P1/Glacial III glacial diamictites

sharply overlain by mudstone/siltstone with outsized clasts occurs throughout central Gondwana in Early Permian strata: in Tasmania, diamictites of the Wynyard Formation are overlain by the pebbly siltstone of the Inglis Formation (cf. Clarke and Forsyth, 1989), in Antarctica, diamictites of the Pagoda Formation are overlain by laminated mudstone of the Mackellar Formation (cf. Collinson et al., 1994, Isbell et al., 2008b; Isbell, 2010; Miller and Isbell, 2010), and in South Africa, diamictites of the Dwyka Group are overlain by the siltstone and mudstone of the Prince Albert Formation (cf. Visser, 1997; Herbert and Compton, 2007; Stollhofen et al., 2008; Isbell et al., 2008a).

Following Glacial III/P1, there is no sedimentary record of ice contact deposits in polar Gondwana (Patagonia, Brazil, South Africa, Antarctica, and Tasmania), but later glaciation continues in eastern Australia in the P2, P3, and P4 glacial intervals (Fielding et al., 2008a). Polar Gondwana is characterized by non-glacial deposits after the mid-Sakmarian: Antarctic strata are made up of fluvial deposits (Fairchild Formation) and coal-bearing fluvial deposits (Buckley Formation) during P2, P3, and P4 (Collinson et al., 2006), and in South Africa, strata consist of siltstone and mudstone of the Prince Albert Formation (mid-Sakmarian to early Artinskian), which is overlain by black carbonaceous shale of the Whitehill Formation (mid-late Artinskian; Veevers et al., 1994b; Branch et al., 2007). Additionally, the end of Glacial III is correlated with a dramatic rise in atmospheric  $p\text{CO}_2$  in the mid- to late Sakmarian (Montañez et al., 2007). Thus, the P2, P3, and P4 glacial intervals in eastern Australia are identified by glacial marine sediments such as diamictites and outsized clasts, glendonites as cold water indicators, and flooding surfaces interpreted to have been created by isostatic depression in the Bowen, Gunnedah, and/or Sydney Basins (Fielding et al., 2008a). The P2 glacial interval

occurred from 287-280 Ma (late Sakmarian to mid-Artinskian; Fig. 49) and is characterized by outsized clasts and diamictites in the Bowen, Gunnedah, and Sydney Basins, and the base of P2 strata is marked by a flooding surface in the southern Sydney Basin that is attributed to isostatic loading resulting from adjacent ice sheets. Glaciers during P2 are interpreted to have been ice sheets, based on interpreted isostatic loading and broad geographic distribution of glacial sediments. P3 occurred from 273-268 Ma (late Kungurian to latest Roadian) and is identified by outsized clasts in siltstone in the Sydney and Gunnedah Basins and a flooding surface, also attributed to glacial isostatic loading. The glaciers of P3 are hypothesized to be ice sheets, too, because the geographic distribution of glacial sediments is similar to that of P2 (Fielding et al., 2008b). P4 occurred from 267-260 Ma (late Wordian to late Capitanian) and is identified by outsized clasts in mudrock and glendonites in the Bowen and Sydney Basins and a flooding surface in the Bowen Basin (Fielding et al., 2008a, 2008b). Glaciers are interpreted to have been smaller in P4 than P3, possibly smaller ice sheets or ice caps, because dropstones are the only glacial signature for this interval, indicating distal glacial fronts (Fielding et al., 2008b).

Ice cover in eastern Australia is hypothesized to have been most extensive during P2 of the three intervals, depicted as an ice sheet covering most of eastern Australia by Fielding et al. (2008a; Fig. 54). P2 also coincides with an interval of  $p\text{CO}_2$  drawdown in the late Sakmarian – early Artinskian identified by Montañez et al. (2007; Fig. 50), and this correlation raises the question of whether P2 indicates global climate conditions. Glacial indicators correlative with P2 have not been identified elsewhere in Gondwana. Rather, glacial indicators are absent in higher latitude strata in Antarctica and South

Africa at this time. One possible exception of outsized clasts in the Liffey Group and Cascades Group in the nearby Tasmania Basin hypothesized to have been derived from far-traveled icebergs from eastern Australia (Fielding et al., 2010). Therefore, the concomitant non-glacial conditions elsewhere in Gondwana, especially polar Gondwana, suggest that conditions unique to eastern Australia allowed glaciers to form during P2, P3, and P4.

Why would glaciation resume in eastern Australia in the late Sakmarian and continue into the Capitanian (Late Permian), but not return to Gondwanan basins located at higher latitudes? Jones et al. (2006) suggested that cold upwelling waters along eastern Gondwana/eastern Australia allowed anomalously cold conditions to persist into the Late Permian, when the rest of Gondwana experienced warming. This hypothesis of upwelling of cold, nutrient rich, deep ocean water is supported by ikaite formation (cf. also Domack et al., 1993), high total organic carbon contents in offshore Permian strata in eastern Australia, and wind and ocean circulation reconstructions for the region (cf. Gibbs et al., 2002; Winguth et al., 2002). In addition to the possible influence of cold ocean water upwelling, did paleotopography also foster the P2-P4 glacial intervals in eastern Australia?

Continued glaciation in eastern Australia during P2, P3, and P4 was likely fostered by the presence of the Kanimblan highlands (part of the Tasman Fold Belt) to the west of the Bowen, Gunnedah, and Sydney Basins (Fig. 54; cf. Veevers, 2006). The Kanimblan highlands were uplifted by east-west compression in the latest Devonian to early Carboniferous, and subsequent north-south compression during the Serpukhovian-Bashkirian (mid-Carboniferous) related to the collision of Gondwana and Laurasia



further uplifted the Kanimblan highlands (Powell, 1984; Powell and Veevers, 1987; Veevers, 2006).

The tectonic regime later shifted to extension, which occurred from the Asselian to Kungurian (Early Permian, including P1 and P2; Veevers et al., 1994a; Fielding et al., 2001). Then during the Roadian to early Capitanian (following the onset of P3), passive thermal subsidence and associated marine transgression occurred, and paleocurrents show transport from west to east, away from the Kanimblan highlands (Fielding et al., 2001). Foreland loading took place during P4 from the Capitanian to the Wuchiapingian (266-258 Ma; Late Permian), with uplift of the New England Fold Belt to the north and the development of an uplifted volcanic arc to the east. This orogenic activity may have elevated the forebulge of the craton, thereby uplifting the Kanimblan highlands during P4.

Direct paleovalley-infill of the highlands by glacial sediments or similar stratigraphic relationships are not available in the stratigraphic record of eastern Australia, but based on paleogeographic reconstructions, the Kanimblan highlands was the region where the eastern Australian glaciers nucleated from the mid-Carboniferous to the Late Permian (cf. Powell, 1984; Powell and Veevers, 1987; Veevers, 2006; Fielding et al., 2008a, 2008b, 2008c). It has been extensively argued that the highlands provided uplifted land surface where glaciers could nucleate from the Serpukhovian to the Asselian (Powell and Veevers, 1987; Veevers, 2006, 2009), but attention has not been directed towards glacial intervals P2-P4 by these authors. Here it is hypothesized that the Kanimblan highlands and emplaced volcanic formations within the highlands still provided adequately elevated land surface in the Sakmarian – Capitanian, high enough

for glacial ice to accumulate. The combination of the highlands and the ocean circulation patterns that upwelled cold water along the coast of eastern Australia may have resulted in an anomalously cold climate in eastern Australia compared to other regions in Gondwana. Additionally,  $p\text{CO}_2$  levels dropped during P3 and remained low (~300 ppmv) during the initiation of P4 (cf. Royer, 2006; Fig. 50). These conditions allowed the formation of glaciers during P2, P3, and P4.

Therefore, the ELA in the Kanimblan highlands was influenced by tectonic activity that subsided and uplifted the orogen, ocean circulation patterns that influenced the regional temperature, and  $p\text{CO}_2$  levels produced by global climate perturbations. During P3, when the region was subsiding, the ELA was evidently still low enough across the Kanimblan highlands that glaciers persisted. The glacial signature during P3 indicates that the elevation was adequately high and the regional temperature was adequately low for the ELA to fall below the elevation of the highlands. Although  $p\text{CO}_2$  levels were low during P3, glaciation was not occurring elsewhere in Gondwana during P3, even in regions closer to the South Pole, so  $p\text{CO}_2$  levels were not the chief influence driving glacier nucleation during this interval. During P4,  $p\text{CO}_2$  levels rose and fluctuated (cf. Royer, 2006; Fig. 50) and perhaps induced warmer temperatures that resulted in smaller glaciers and a waning glacial signature (cf. Fielding et al., 2008b). Foreland loading occurring during this time may have uplifted the Kanimblan highlands as part of the forebulge, and this uplift may have been sufficient to trigger glaciation due to a relative drop in the ELA. Ultimately, glaciation across eastern Australia was driven by a complex interplay of drivers that shifted the ELA up and down within the Kanimblan highlands, but the glacial signatures of P2-P4 indicate that the ELA fell to

altitudes below the upper elevations of the highlands during those intervals, allowing glaciers to form there.

## 5. Conclusions

The presence of available uplifted land where glaciers could nucleate was a controlling factor for glaciation during the LPIA, as demonstrated by examples from Glacial II in the mid- to Late Carboniferous in Argentina and from P2-P4 in the Early to Late Permian in eastern Australia. In west central Argentina, glaciation occurred over the Protoprecordillera, a fold-thrust belt, in the Serpukhovian-Bashkirian. However, the Protoprecordillera collapsed in the early Pennsylvanian to Early Permian, and glaciation did not resume in that region after the Bashkirian, despite continued glaciation in eastern and southern South America. Therefore, it is reasonable to conclude that the Protoprecordillera provided the necessary elevation for glaciers to maintain positive mass balance ratios and persist during that glacial interval in west central Argentina.

In eastern Australia, glacial intervals continued into the mid- and Late Permian, even though glaciation had ceased in other higher latitude regions in Gondwana in the mid-Sakmarian. The continued glaciation in eastern Australia was likely fostered by elevation provided by the Kanimblan highlands, which provided uplifted land surfaces above the regional ELA. Therefore, in addition to the classically cited drivers of LPIA glaciation such as paleolatitude and  $p\text{CO}_2$ , the presence of uplifted regions where glaciers can form and persist should be taken into account when considering the initiation and demise of glacial intervals of the LPIA. Paleotopography is a built-in ‘driver’ for glaciation: elevation must be high enough for glaciers to form, and this precondition should be remembered when drivers of glaciation and deglaciation are discussed.

# Figures

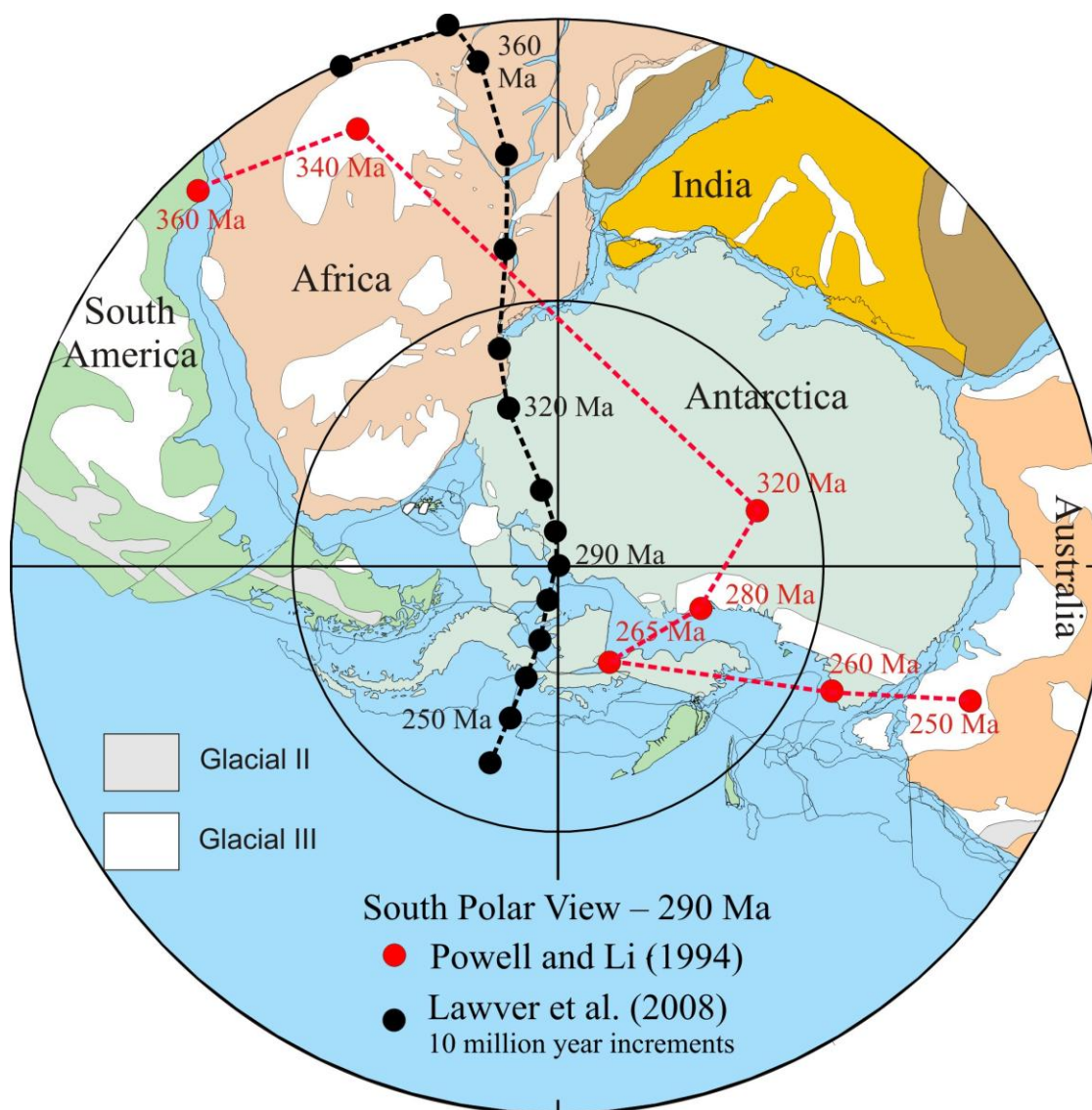


Figure 48. Polar wander paths across Gondwana throughout the Carboniferous and Permian by Powell and Li (1994) and Lawver et al. (2008). Yellow dots in the Lawver et al. (2008) polar wander path represent 10 million year time intervals. Modified from Lawver et al. (2008) PLATES reconstruction and Isbell et al., 2010.

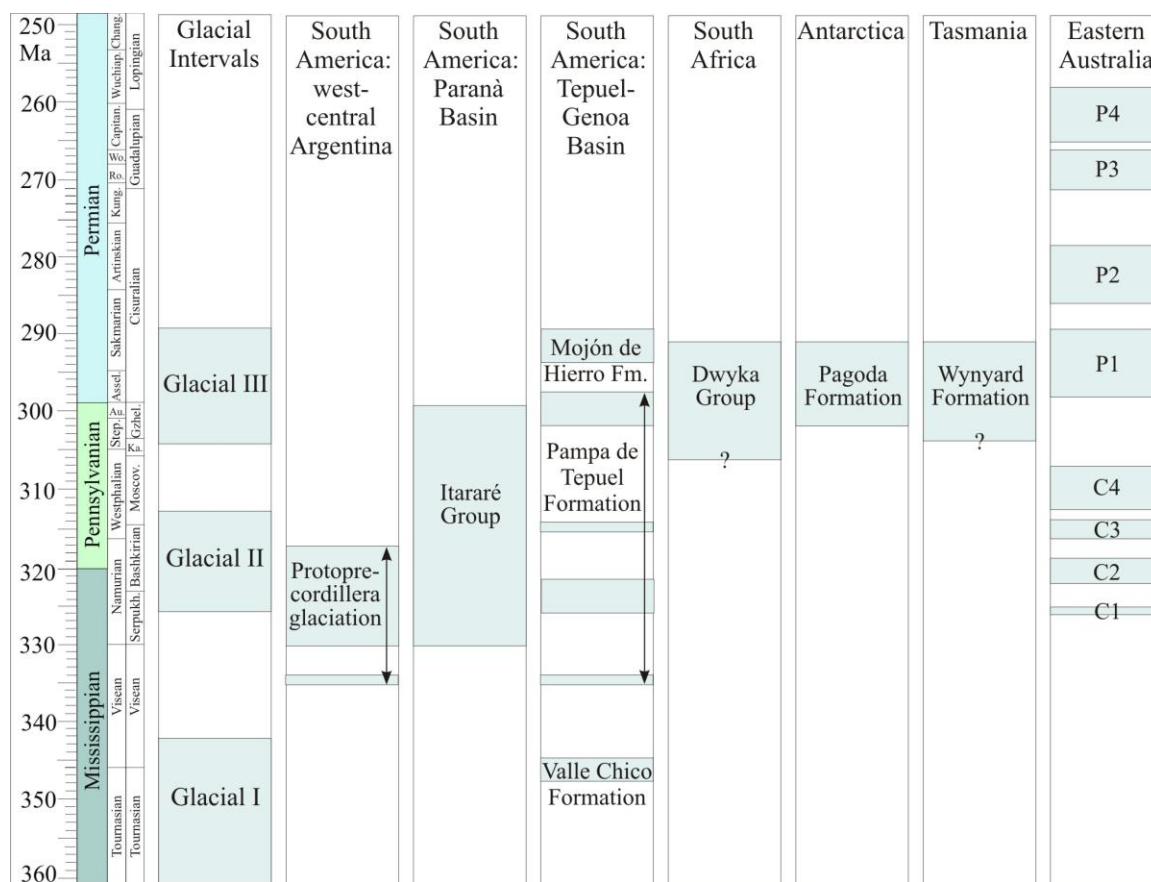


Figure 49. Glacial intervals of the LPIA discussed in the text based on the stratigraphic record. Ages are from Truswell (1978), Collinson et al. (1994), Isbell et al. (2003), Fielding et al. (2008a), Rocha-Campos et al. (2008), Stollhofen et al. (2008), Taboada (2010), and Gulbranson et al. (2010). Carboniferous time scale is from Davydov et al. (2010); Permian time scale is from Gradstein et al. (2004).

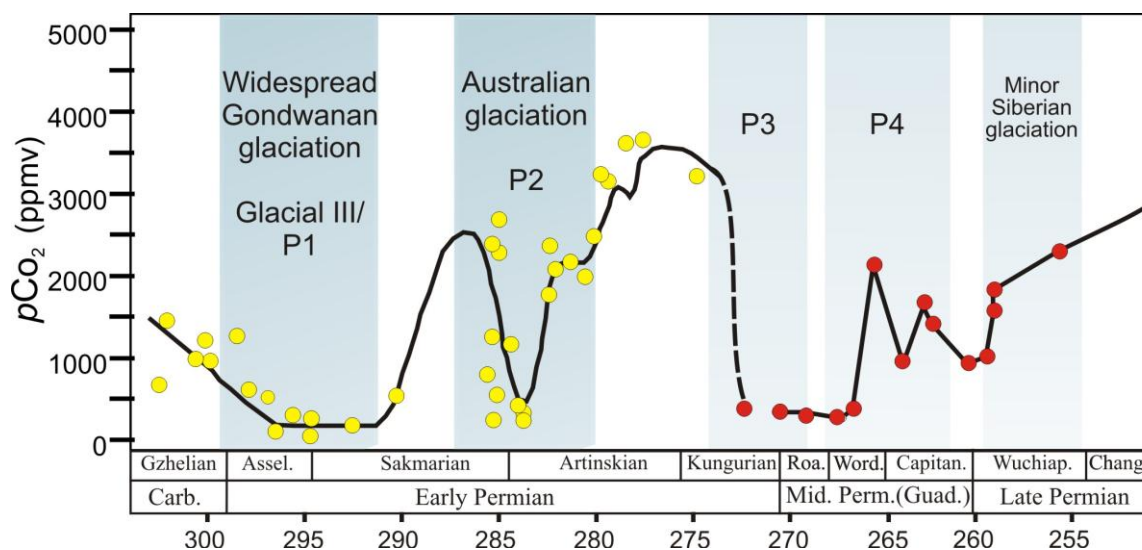


Figure 50.  $p\text{CO}_2$  fluctuations and glacial and non-glacial intervals in the Permian. Yellow dots are from Montañez et al. (2007), red dots represent data compiled by Royer (2006), and the dashed line links the two data sets.

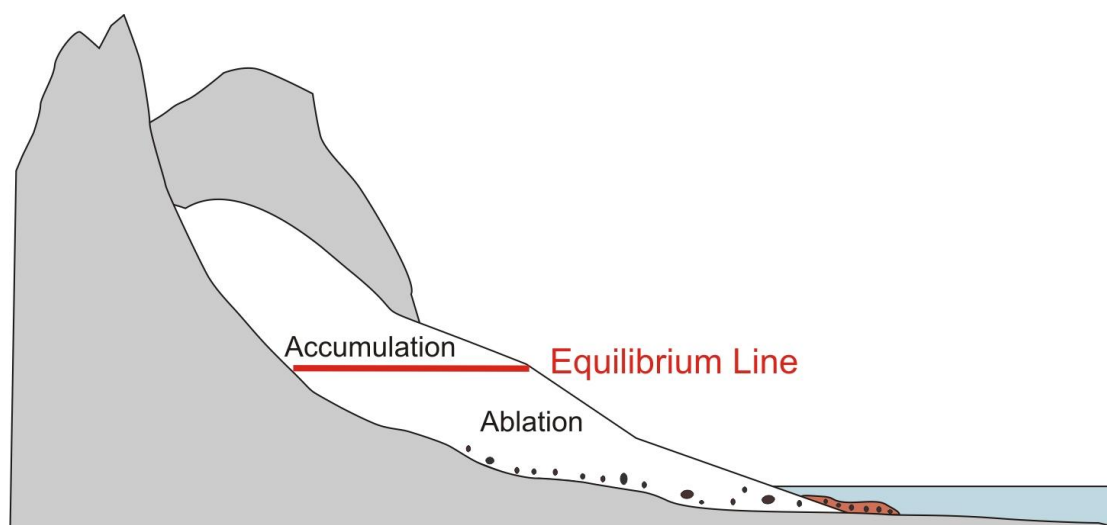


Figure 51. Diagram of the equilibrium line of a glacier, which separates the zone of accumulation above from the zone of ablation below. The altitude of the equilibrium line can shift with tectonic or climatic fluctuations.

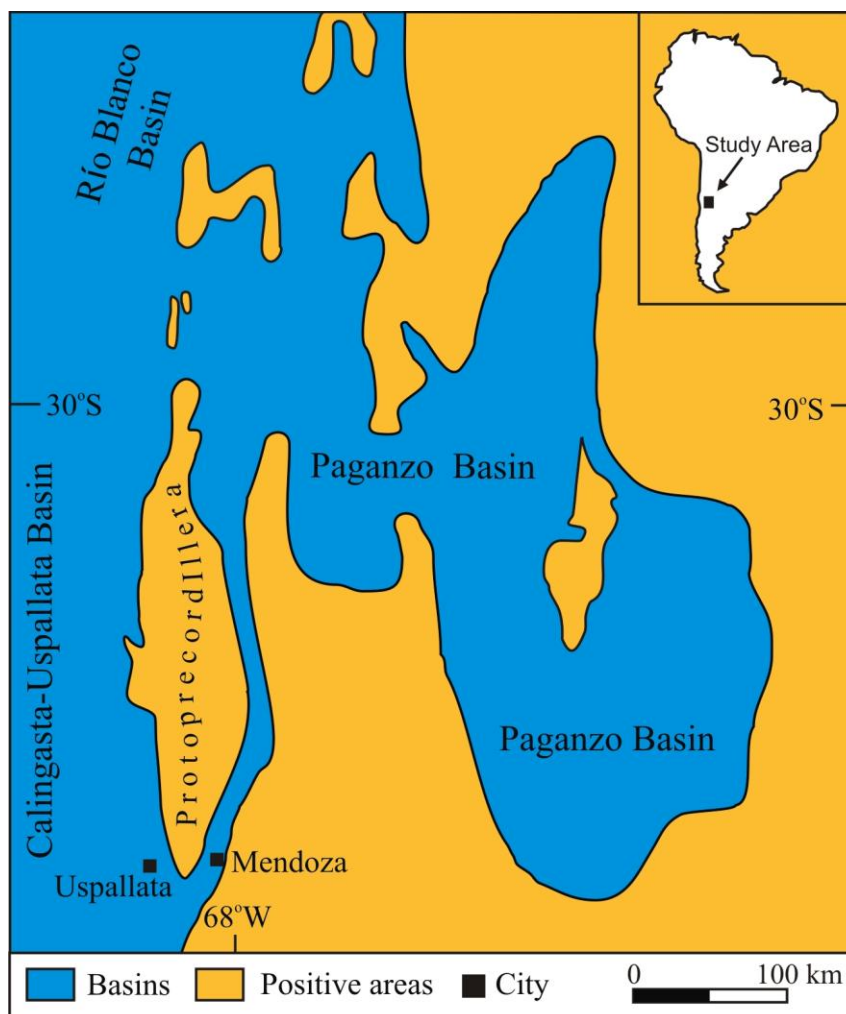
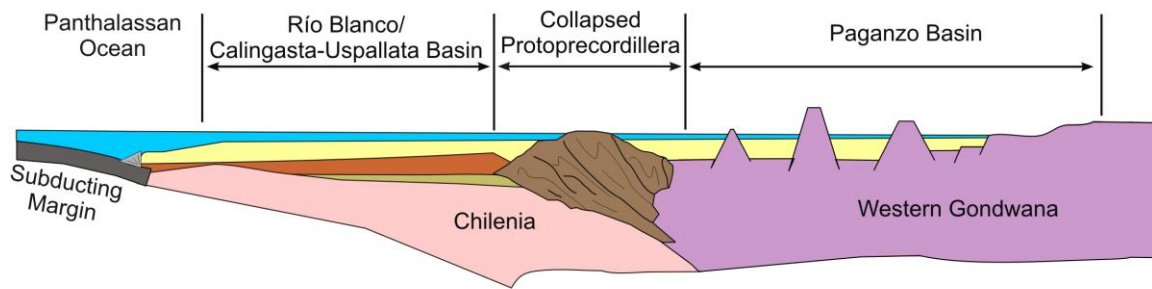


Figure 52. The Protoprecordillera in west central Argentina housed glaciers in the Serpukhovian-Bashkirian (late Mississippian – early Pennsylvanian) and acted as a divide between the Río Blanco and Calingasta-Uspallata Basins to the west and the Paganzo Basin to the east until the collapse of the fold-thrust belt in the Pennsylvanian. Modified from Henry et al., 2010.

## early Pennsylvanian - Early Permian



## late Mississippian - early Pennsylvanian

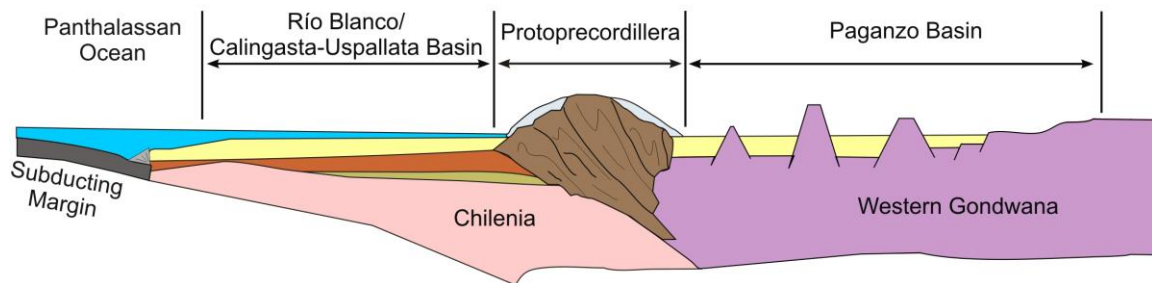


Figure 53. Cross-section showing the collapse of the Protoprecordillera in the Late Carboniferous – Early Permian and resulting loss of alpine glaciers. Modified from Henry et al., 2010.

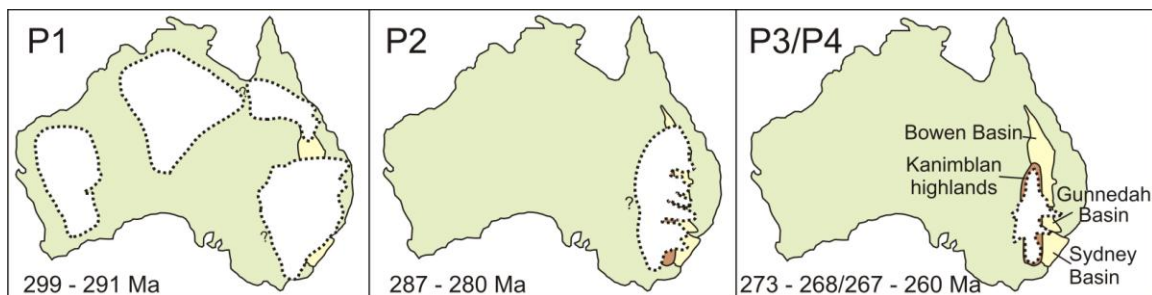


Figure 54. Diagrams of ice extent over Australia during the P1, P2, and P3/P4 glaciations. The Kanimblan highlands provided an uplifted region where glaciers could nucleate through the Late Permian. Deposits from glaciers housed in the Kanimblan highlands were shed into the Bowen, Gunnedah, and Sydney Basins throughout the Carboniferous and Permian. After Veevers (2006), Fielding et al. (2008a, 2008c).



## References

- Allison, I., Peterson, J.A., 1989. Glaciers of Irian Jaya, Indonesia. In: Williams, R.S., Reffigno, J.G. (eds.), *Satellite Image Atlas of the World*. USGS Professional Paper 1386-H, 1–20.
- Azcuy, C.L., Carrizo, H.A., Caminos, R., 1999. Carbonífero y Pérmico de las Sierras Pampeanas, Famatina, Precordillera, Cordillera Frontal y Bloque de San Rafael. *Instituto de Geología y Recursos Minerales, Geología Argentina* 29, 261–318.
- Blakey, R.C., 2008. Gondwana paleogeography from assembly to breakup- a 500 m.y. odyssey In: Fielding, C.R., Frank, T.D., Isbell, J.L. (Eds.), *Resolving the Late Paleozoic Ice Age in Time and Space: Geological Society of America Special Paper* 441, 1–28.
- Branch, T., Ritter, O., Weckmann, U., Sachsenhofer, R.F., Schilling, F., 2007. The Whitehill Formation – a high conductivity marker horizon in the Karoo Basin. *South African Journal of Geology* 110, 465–476.
- Broecker, W.S., Denton, G.H., 1990. What drives glacial cycles? *Scientific American*, January, 43–50.
- Caputo, M.V., Crowell, J.C., 1985. Migration of glacial centers across Gondwana during Paleozoic Era. *Geological Society of America Bulletin* 96, 1020–1036.
- Clarke, M.J., Forsyth, S.M., 1989. Late Carboniferous–Triassic. In: Burrett, C.F., Marten, E.L. (Eds.), *Geology and Mineral Resources of Tasmania: Geological Association of Australia, Special Paper* 15, 209–293.
- Collinson, J.W., Isbell, J.L., Elliot, D.H., Miller, M.F., and Miller, J.M.G., 1994. Permian–Triassic Transantarctic basin. In: Veevers, J.J., Powell, C.M. (Eds.), *Permian–Triassic Pangean Basins and Fold Belts along the Panthalassan Margin of Gondwanaland: Geological Society of America Memoir* 184, 173–222.
- Collinson, J.W., Hammer, W.R., Askin, R.A., Elliot, D.H., 2006. Permian–Triassic boundary in the central Transantarctic Mountains, Antarctica. *GSA Bulletin* 118, 747–763.
- Crowell, J.C., 1978. Gondwanan glaciation, cyclothems, continental positioning, and climate change. *American Journal of Science* 278, 1345–1372.
- Davydov, V.I., Crowley, J.L., Schmitz, M.D., Poletaev, V.I., 2010. High-precision U–Pb zircon age calibration of the global Carboniferous time scale and Milankovitch-band cyclicity in the Donets Basin, eastern Ukraine. *Geochemistry Geophysics Geosystems*, doi:10.1029/2009GC002736.

- Dickins, J.M., 1997. Some problems of the Permian (Asselian) glaciation and the subsequent climate in the Permian. In: Martini, I.P. (Ed.), *Late glacial and postglacial environmental changes: Quaternary, Carboniferous-Permian, and Proterozoic*. Oxford, U.K., Oxford University Press, 243–245.
- Domack, E.W., Burkley, L.A., Domack, C.R., Banks, M.R., 1993. Facies analysis of glacial marine pebbly mudstones in the Tasmania Basin: Implications for regional paleoclimates during the late Paleozoic. In: Findlay, Unrug, Banks, M.R., Veevers, J.J. (Eds.), *Gondwana Eight*, 471–484.
- DuToit, A.L., 1921. The Carboniferous glaciation of South Africa. *Geological Society of South Africa Transactions* 24, 188–277.
- Dykstra, M., Kneller, B., Milana, J.P., 2006. Deglacial and postglacial sedimentary architecture in a deeply incised paleovalley-paleofjord – The Pennsylvanian (late Carboniferous) Jejenes Formation, San Juan, Argentina. *GSA Bulletin* 118, 913–937.
- Eyles, N., 1993. Earth's glacial record and its tectonic setting. *Earth-Science Reviews* 35, 1–248.
- Fielding, C.R., Sliwa, R., Holcombe, R.J., Jones, A.T., 2001. A new palaeogeographic synthesis for the Bowen, Gunnedah and Sydney Basins of Eastern Australia. In: Hill, K.C., Bernecker, T. (Eds.), *Eastern Australasian Basins Symposium*, Petroleum Exploration Society of Australia Special Publication 269–278.
- Fielding, C.R., Frank, T.D., Birgenheier, L.P., Rygel, M.C., Jones, A.T., Roberts, J., 2008a. Stratigraphic imprint of the Late Paleozoic Ice Age in eastern Australia: a record of alternating glacial and nonglacial climate regime. *Journal of the Geological Society, London* 165, 129–140.
- Fielding, C.R., Frank, T.D., Birgenheier, L.P., Rygel, M.C., Jones, A.T., Roberts, J., 2008b. Stratigraphic record and facies associations of the late Paleozoic ice age in Eastern Australia (New South Wales and Queensland). In: Fielding, C.R., Frank, T.D., Isbell, J.L. (Eds.), *Resolving the Late Paleozoic Ice Age in Time and Space*. Geological Society of America Special Paper 441, 41–57.
- Fielding, C.R., Frank, T.D., Isbell, J.L., 2008c. The late Paleozoic ice age—A review of current understanding and synthesis of global climate patterns. In: Fielding, C.R., Frank, T.D., Isbell, J.L. (Eds.), *Resolving the Late Paleozoic Ice Age in Time and Space*. Geological Society of America Special Paper 441, 343–354.
- Fielding, C.R., Frank, T.D., Isbell, J.L., Henry, L.C., Domack, E.W., 2010. Stratigraphic signature of the late Paleozoic ice age in the Parmeener Supergroup of Tasmania, SE Australia, and inter-regional comparisons. *Palaeogeography, Palaeoclimatology, Palaeoecology* 298, 70–90.

- Frank, T.D., Birgenheier, L.P., Montañez, I.P., Fielding, C.R., Rygel, M.C., 2008. Late Paleozoic climate dynamics revealed by comparison of ice-proximal stratigraphic and ice-distal isotopic records. In: Fielding, C.R., Frank, T.D., Isbell, J.L. (Eds.), *Resolving the Late Paleozoic Ice Age in Time and Space: Geological Society of America Special Paper 441*, 331–342.
- Gibbs, M.T., Rees, P.M., Kutzbach, J.E., Ziegler, A.M., Behling, P.J., Rowley, D.B., 2002. Simulation of Permian climate and comparison with climate-sensitive sediments. *Journal of Geology* 110, 33–55.
- Gradstein, F.M., Ogg, J.G., Smith, A.G., 2004. *A Geologic Time Scale 2004*. Cambridge, U.K., Cambridge University Press.
- Gulbranson, E.L., Montañez, I.P., Schmitz, M.D., Limarino, C.O., Isbell, J.L., Marensi, S.A., Crowley, J.L., 2010. High-precision U-Pb calibration of Carboniferous glaciation and climate history, Paganzo Group, NW Argentina. *GSA Bulletin* 122, 1480–1498.
- Hayes, J.M., Strauss, H., Kaufman, A.J., 1999. The abundance of  $^{13}\text{C}$  in marine organic matter and isotopic fractionation in the global biogeochemical cycle of carbon during the past 800 Ma. *Chemical Geology* 161, 103–125.
- Henry, L.C., Isbell, J.L., Limarino, C.O., 2008. Carboniferous glacigenic deposits of the Protoprecordillera of west central Argentina. In: Fielding, C.R., Frank, T.D., Isbell, J.L. (Eds.), *Resolving the Late Paleozoic Ice Age in Time and Space: Geological Society of America Special Paper 441*, 131–142.
- Henry, L.C., Isbell, J.L., Limarino, C.O., McHenry, L.M., Fraiser, M.L., 2010. Mid-Carboniferous deglaciation of the Protoprecordillera, Argentina recorded in the Agua de Jagüel paleovalley. *Palaeogeography, Palaeoclimatology, Palaeoecology* 298, 112–129.
- Henry, L.C., Isbell, J.L., Fielding, C.R., Domack, E.W., Frank, T.D., Fraiser, M.L., 2012. Proglacial deposition and deformation in the Pennsylvanian to Lower Permian Wynyard Formation, Tasmania: a process analysis. Submitted to *Palaeogeography, Palaeoclimatology, Palaeoecology* 315–316, 142–157.
- Herbert, C.T., Compton, J.S., 2007. Depositional environments of the lower Permian Dwyka diamictite and Prince Albert shale inferred from the geochemistry of early diagenetic concretions, southwest Karoo Basin, South Africa. *Sedimentary Geology* 194, 263–277.
- Holz, M., Kuchle, J., Philipp, R.P., Bischoff, A.P., Arima, N., 2006. Hierarchy of tectonic control on stratigraphic signatures: Base-level changes during the Early Permian in the Paraná Basin, southernmost Brazil. *Journal of South American Earth*

Sciences 22, 185–204.

- Holz, M., Souza, P.A., Iannuzzi, R., 2008. Sequence stratigraphy and biostratigraphy of the Late Carboniferous to Early Permian glacial succession (Itararé Subgroup) at the eastern-southeastern margin of the Paraná Basin, Brazil. In: Fielding, C.R., Frank, T.D., Isbell, J.L. (Eds.), *Resolving the Late Paleozoic Ice Age in Time and Space: Geological Society of America Special Paper 441*, 115–129.
- Isbell, J.L., 2010. Environmental and paleogeographic implications of glaciotectonic deformation of glaciomarine deposits within Permian strata of the Metschel Tillite, southern Victoria Land, Antarctica. In: López-Gamundí, O.R., Buatois, L.A. (Eds.), *Late Paleozoic glacial events and postglacial transgressions in Gondwana. Geological Society of America Special Paper 468*, 81–100.
- Isbell, J.L., Miller, M.F., Wolfe, K.L., Lenaker, P.A., 2003. Timing of late Paleozoic glaciation in Gondwana: was glaciation responsible for the development of northern hemisphere cyclothems? In: Chan, M.A., Archer, A.W. (Eds.), *Extreme depositional environments: mega end members in geologic time. Geological Society of America Special Paper 370*, 5–24.
- Isbell, J.L., Cole, D.I., Catunaenu, O., 2008a. Carboniferous-Permian glaciation in the main Karoo Basin, South Africa: stratigraphy, depositional controls, and glacial dynamics. In: Fielding, C.R., Frank, T.D., Isbell, J.L. (Eds.), *Resolving the late Paleozoic ice age in time and space. Geological Society of America Special Paper 441*, 71–82.
- Isbell, J.L., Koch, Z.J., Szablewski, G.M., Lenaker, P.A., 2008b. Permian glacial deposits in the Transantarctic Mountains, Antarctica. In: Fielding, C.R., Frank, T.D., Isbell, J.L. (Eds.), *Resolving the late Paleozoic ice age in time and space. Geological Society of America Special Paper 441*, 59–70.
- Isbell, J.L., Henry, L.C., Limarino, C.O., Koch, Z.J., Fraiser, M.L., Dineen, A.A., 2010. The relationship between equilibrium line altitude and latitude as a control on Gondwana glaciation during the late Paleozoic ice age. *International Sedimentological Congress Abstracts with Programs* 18.
- Jones, A.T., Fielding, C.R., 2004. Sedimentological record of the late Paleozoic glaciation in Queensland, Australia. *Geology* 32, 153–156.
- Jones, A.T., Frank, T.D., Fielding, C.R., 2006. Cold climate in eastern Australian mid to late Permian may reflect cold upwelling waters. *Palaeogeography, Palaeoclimatology, Palaeoecology* 237, 370–377.
- Kneller, B., Milana, J.P., Buckee, C., Al Ja'aidi, O.S., 2004. A depositional record of deglaciation in a paleofjord (Late Carboniferous [Pennsylvanian] of San Juan Province, Argentina): The role of catastrophic sedimentation. *Geological Society*

of America Bulletin 116, 348–367.

- Laskar, B., Mitra, N.D., 1976. Paleoclimatic vicissitudes in India during Lower Gondwana sedimentation. *Geophytology* 6, 162–169.
- Lawver, L.A., Dalziel, I.W.D., Norton, I.O., Gahagan, L.M., 2008. The Plates 2007 Atlas of Plate Reconstructions (750 Ma to Present Day), Plates Progress Report No. 305-0307, University of Texas Technical Report No. 195, 160 pp.
- Limarino, C.O., Césari, S.N., Net, L.I., Marensi, S.A., Gutiérrez, P.R., Tripaldi, A., 2002. The Upper Carboniferous postglacial transgression in the Paganzo and Río Blanco Basins (northwestern Argentina): Facies and stratigraphic significance. *Journal of South American Earth Sciences* 15, 445–460.
- Limarino, C.O., Tripaldi, A., Marensi, S., Fauqué, L., 2006. Tectonic, sea level, and climatic controls on late Paleozoic sedimentation in the western basins of Argentina. *Journal of South American Earth Sciences* 33, 205–226.
- López Gamundí, O. R., 1997. Glacial-postglacial transition in the late Paleozoic basins of Southern South America. In: Martini, I. P. (Ed.), *Late glacial and postglacial environmental changes: Quaternary, Carboniferous-Permian, and Proterozoic*: Oxford, U.K., Oxford University Press, 147–168.
- López Gamundí, O.R., Espejo, I.S., Conaghan, P.J., Powell, C.McA., Veevers, J.J., 1994. Southern South America. In: Veevers, J.J., Powell, C.McA. (Eds.), *Permian-Triassic Pangean basins and foldbelts along the Panthalassan margin of Gondwanaland*. Boulder, Colorado, Geological Society of America Memoir 184, 281–329.
- Miller, G.H., Bradley, R.S., Andrews, J.T., 1975. The glaciations level and lowest equilibrium line altitude in the high Canadian arctic: maps and climatic interpretation. *Arctic and Alpine Research* 7, 155–168.
- Miller, M.F., Isbell, J.L., 2010. Reconstruction of a high-latitude, postglacial lake; Mackellar Formation (Permian), Transantarctic Mountains. In: López-Gamundí, O.R., Buatois, L.A. (Eds.), *Late Paleozoic glacial events and postglacial transgressions in Gondwana*. Geological Society of America Special Paper 468, 193–207.
- Montañez, I.P., Tabor, N.J., Niemeier, D., DiMichele, W.A., Frank, T.D., Fielding, C.R., Isbell, J.L., Birgenheier, L.P., Rygel, M.C., 2007. CO<sub>2</sub>-forced climate and vegetative instability during late Paleozoic deglaciation. *Science* 315, 87–91.
- Mory, A.J., Redfern, J., Martin, J.R., 2008. A review of Permian-Carboniferous glacial deposits in western Australia. In: Fielding, C.R., Frank, T.D., Isbell, J.L. (Eds.), *Resolving the Late Paleozoic Ice Age in Time and Space*: Geological Society of

- America Special Paper 441, 29–40.
- Net, L. I., Alonso, M.S., Limarino, C.O., 2002. Source rock and environmental control on clay mineral associations, lower section of Paganzo group (Carboniferous), northwest Argentina. *Sedimentary Geology* 152, 183–199.
- Net, L.I., Limarino, C.O., 1999. Paleogeografía y correlación estratigráfica del Paleozoico Tardío de la Sierra de Los Llanos, Provincia de La Rioja, Argentina. *Revista de la Asociación Geológica Argentina* 54, 229–239.
- Net, L.I., Limarino, C.O., 2006. Applying sandstone petrofacies to unravel the Upper Carboniferous evolution of the Paganzo Basin, northwest Argentina. *Journal of South American Earth Sciences* 22, 239–254.
- Pazos, P.J., 2002. The Late Carboniferous glacial to postglacial transition: Facies and sequence stratigraphy, western Paganzo Basin, Argentina. *Gondwana Research* 5, 467–487.
- Powell, C.M., 1984. Terminal fold-belt deformation: relationship of mid-Carboniferous megakinks in the Tasman fold belt to coeval thrusts in cratonic Australia. *Geology* 12, 546–549.
- Powell, C.M., Veevers, J.J., 1987. Namurian uplift in Australia and South America triggered the main Gondwanan glaciation. *Nature* 326, 177–179.
- Powell, C. M., Li, Z.X., 1994. Reconstruction of the Panthalassan margin of Gondwanaland. In: Veevers, J., Powell, C. (Eds.), *Permian-Triassic Transantarctic basin, Permian-Triassic Pangea Basins and foldbelts along the Panthalassan margin of Gondwanaland*. *Geologic Society of America Memoir* 184, 5–9.
- Ramos, V.A., 1988. Tectonics of the Late Proterozoic-Early Paleozoic: a collisional history of Southern South America. *Episodes* 11, 168–174.
- Rocha-Campos, A.C., dos Santos, P.R., Canuto, J.R., 2008. Late Paleozoic glacial deposits of Brazil: Paraná Basin. In: Fielding, C.R., Frank, T.D., Isbell, J.L. (Eds.), *Resolving the Late Paleozoic Ice Age in Time and Space: Geological Society of America Special Paper* 441, 97–114.
- Royer, D., 2006. CO<sub>2</sub>-forced climate thresholds during the Phanerozoic. *Geochimica et Cosmochimica* 70, 5665–5675.
- Scheffler, K., Hoernes, S., Schwark, L., 2003. Global changes during Carboniferous – Permian glaciation of Gondwana: linking of polar and equatorial climate evolution by geochemical proxies. *Geology* 31, 605–608.
- Scotese, C.R. Barrett, S.F., 1990. Gondwana's movement over the South Pole during the

- Palaeozoic: evidence from lithological indicators of climate. In: McKerrow, W.S., Scotese, C.R. (Eds.), *Palaeozoic Palaeogeography and Biogeography*, Geological Society, London, Memoirs 12, 75–85.
- Stollhofen, H., Werner, M., Stanistreet, I.G., Armstrong, R.A., 2008. Single-zircon U-Pb dating of Carboniferous-Permian tuffs, Namibia, and the intercontinental deglaciation cycle framework. In: Fielding, C.R., Frank, T.D., Isbell, J.L. (Eds.), *Resolving the late Paleozoic ice age in time and space*. Geological Society of America Special Paper 441, 83–96.
- Taboada, A.C., 2010. Mississippian – Early Permian brachiopods from western Argentina: Tools for middle- to high-latitude correlation, paleobiogeographic and paleoclimatic reconstruction. *Palaeogeography, Palaeoclimatology, Palaeoecology* 298, 152–173.
- Torsvik, T.H., Cocks, L.R.M., 2004. Earth geography from 400 to 250 Ma: a palaeomagnetic, faunal and facies review. *Journal of the Geological Society* 161, 555–572.
- Truswell, E. M., 1978. Palynology of the Permo-Carboniferous in Tasmania: an interim report. *Bulletin of the Geological Survey of Tasmania* 56, 37 p.
- Veevers, J.J., 2006. Updated Gondwana (Permian-Cretaceous) earth history of Australia. *Gondwana Research* 9, 231–260.
- Veevers, J.J., 2009. Mid-Carboniferous Centralian uplift linked by U-Pb zircon chronology to the onset of Australian glaciation and glacio-eustasy. *Australian Journal of Earth Sciences* 56, 711–717.
- Veevers, J.J., Clare, A., Wopfner, H., 1994a. Neocratonic magmatic-sedimentary basins of post-Variscan Europe and post-Kanimblan eastern Australia generated by right-lateral transtension of Permo-Carboniferous Pangaea. *Basin Research* 6, 141–157.
- Veevers, J.J., Conaghan, P.J., Powell, C. McA., Cowan, E.J., McDonnell, K.L., Shaw, S.E., 1994b. Eastern Australia. In: Veevers, J.J., and Powell, C.M. (Eds.), *Permian-Triassic Pangean Basins and Fold Belts along the Panthalassan Margin of Gondwanaland: Geological Society of America Memoir* 184, 11–171.
- Veevers, J., Powell, C., Collinson, J., López Gamundí, O., 1994c. Synthesis. In: Veevers, J., Powell, C. (Eds.), *Permian-Triassic Pangean basins and foldbelts along the Panthalassan Margin of Gondwanaland*. Boulder, Colorado, Geological Society of America Memoir 184, 331–353.
- Veizer, J., Ala, D., Azmy, K., Bruckschen, P., Buhl, D., Bruhn, F., Carden, G.A.F., Diener, A., 1999.  $^{87}\text{Sr}/^{86}\text{Sr}$ ,  $\delta^{13}\text{C}$  and  $\delta^{18}\text{O}$  evolution of Phanerozoic seawater.

Chemical Geology 161, 59–88.

Visser, J.N.J., 1997. Deglaciation sequences in the Permo-Carboniferous Karoo and Kalahari basins of southern Africa: a tool in the analysis of cyclic glaciomarine basin fills: *Sedimentology* 44, 507–521.

Wegener, A., 1929. The origin of continents and oceans (English translation by John Biram of *Die Entstehung der Kontiente und Ozeane*, 4<sup>th</sup> ed.); New York, Dover Publications, Inc., 1966, 246 p.

Winguth, A.M.E., Heinze, C., Kutzbach, J.E., Maier-Reimer, E., Mikolajewicz, U., Rowley, D., Rees, A., Ziegler, A.M., 2002. Simulated warm polar currents during the middle Permian. *Paleoceanography* 17, 1057.



## CURRICULUM VITAE

Lindsey C. Henry

### Education

University of Wisconsin-Milwaukee, Milwaukee, WI

- Ph.D. Geosciences, 2013
- M.S. Geosciences, 2007

Wheaton College, Wheaton, IL

- B.S. Geology, magna cum laude, 2004
- French minor

### Positions Held

Lecturer	University of Miami, 2013, Natural Disasters
Fellow	Advanced Opportunity Program, University of Wisconsin-Milwaukee (UWM), 2010-2013
Intern	BP, Houston, Texas, 2009, 2010, 2012
Graduate School Fellow	UWM, 2008-2009
Graduate Research Assistant	UWM, 2007-2008
Textbook Reviewer	McGraw Hill, 2008
Ad Hoc Lecturer	UWM, 2007, Physical Geology
Graduate Teaching Assistant	UWM, 2005-2010
	Physical Geology, Historical Geology, A History of Life, Oceanography
Intern	Shaw Environmental, Milwaukee, Wisconsin, 2006
Intern	University of Minnesota, 2003, 2004
Teaching Assistant	Wheaton College, 2003

### Dissertation Project

“Late Paleozoic glaciation and ice sheet collapse over western and eastern Gondwana: sedimentology and stratigraphy of glacial to post-glacial strata in western Argentina and Tasmania, Australia”

### Master’s Thesis

“Carboniferous glacigenic deposits of the Hoyada Verde and Tramojo Formations of the Calingasta-Uspallata Basin, west central Argentina.”

### Grants and Awards

- Teaching Assistant of the Year, UWM Geosciences Department, 2010
- 2<sup>nd</sup> place Intern poster, Technofest, BP, 2010
- Graduate Student of the Month, UWM, January 2010
- UWM Chancellor’s Scholarship, 2005-2012
- George Boyer Scholarship, University of Wisconsin-Milwaukee, 2008-2009
- American Association of Petroleum Geologists Student Grants-in-Aid, 2008
- Graduate Student Study Award, Department of Geosciences, UWM, 2006, 2007, 2008, 2009

- Wisconsin Geological Society Scholarship, 2007, 2008
- A.L. Medlin Scholarship for fieldwork, Coal Geology Division of the Geological Society of America (GSA), 2007
- GSA Student Research Grant, 2007
- Center for Latin American and Caribbean Studies Student Travel Award, 2006

#### Field and Specialty Training

- Empowering Capable Climate Communicators Workshop, University of Miami, 2013
- Collaboration in Sedimentary Geology and Paleobiology workshop, Washington, D.C., and in drafting the document TRANSITIONS: The Changing Earth-Life System - Critical Information for Society from the Deep Past, 2011
- Proficiency in SeisWorks, StratWorks, RMS, and GeoGraphix software, BP, 2009, 2010, 2012
- Sedimentology and Paleobiology of San Salvador; UWM Field Trip led by Dr. Steve Dornbos, Dr. Margaret Fraiser, and Dr. John Isbell, 2009
- Fieldwork on late Paleozoic glacigenic rocks in western Argentina, 2006, 2007, 2008
- Fieldwork on late Paleozoic glacigenic and post-glacial rocks in Tasmania, Australia, 2008
- Sequence Stratigraphy of the Mt. Garfield Formation, Colorado; GSA Field Trip led by Dr. Diane Kamola, 2007
- International Workshop on the Micromorphology of Glacial Sediments, facilitated by Dr. Jaap van der Meer and Dr. John Menzies, Hamilton College, 2006
- Sequence Stratigraphy of the Book Cliffs, Utah; UWM Field Trip led by Dr. John Isbell, 2006
- Wheaton College field camp in the Black Hills, South Dakota, 2004
- Fieldwork in the Mojave Desert using GPS and Total Station with Dr. Lesley Perg, University of Minnesota, 2004
- Conducted experiments with AgCl in sediment as a proxy for cosmogenic nuclides for Dr. Lesley Perg, University of Minnesota, 2004
- Fieldwork on marine terraces with GPS and GPR in Northern California with Dr. Lesley Perg, University of Minnesota, 2003
- Built and performed an experiment modeling uplift and erosion at St. Anthony Falls Lab for Engineering and Environmental and Geophysical Fluid Dynamics with Dr. Lesley Perg, University of Minnesota, 2003

#### Publications

##### Manuscripts

- Henry, L.C., Isbell, J.L., Limarino, C.O., in press. The late Paleozoic El Imperial Formation, western Argentina: glacial to post-glacial transition and stratigraphic correlations with arc-related basins in southwestern Gondwana. *Gondwana Research*, <http://dx.doi.org/10.1016/j.gr.2012.08.023>.
- Isbell, J.L., Henry, L.C., Reid, C.M., Fraiser, M.L., 2012. Sedimentology and palaeoecology of limestones-bearing mixed clastic rocks and cold-water carbonates of the Lower Permian Basal Beds at Fossil Cliffs, Maria Island, Tasmania

- (Australia): Insight into the initial decline of the late Palaeozoic ice age. Geological Society, London, Special Publications 376, doi 10.1144/SP376.2.
- Henry, L.C., Isbell, J.L., Fielding, C.R., Domack, E.W., Frank, T.D., Fraiser, M.L., 2012. Proglacial deposition and deformation in the Wynyard Formation, Tasmania: a process analysis. *Palaeogeography, Palaeoclimatology, Palaeoecology* 315–316, 142–157.
  - Isbell, J.L., Henry, L.C., Gulbranson, E.L., Limarino, C.O., Fraiser, M.L., Koch, Z.J., Ciccioli, P.L., Dineen, A.A., 2012. Evaluations of glacial paradoxes during the late Paleozoic Ice Age using the concept of the equilibrium line altitude (ELA) as a control on glaciation. *Gondwana Research* 22, 1–19.
  - Henry, L.C., Isbell, J.L., Limarino, C.O., McHenry, L.J., Fraiser, M.L., 2010. Mid-Carboniferous deglaciation of the Protoprecordillera, Argentina, recorded in the Agua de Jagüel paleovalley. *Palaeogeography, Palaeoclimatology, Palaeoecology* 298, 112–129.
  - Fielding, C.R., Frank, T.D., Isbell, J.L., Henry, L.C., Domack, E.W., 2010. Stratigraphic signature of the late Paleozoic Ice Age in the Parmeener Supergroup of Tasmania, SE Australia, and inter-regional comparisons. *Palaeogeography, Palaeoclimatology, Palaeoecology* 298, 70–90.
  - Henry, L.C., Isbell, J.L., Limarino, C.O., 2008. Carboniferous glacigenic deposits of the Protoprecordillera of west central Argentina *in* Fielding, C.R., Frank, T.D., Isbell, J.L., (eds.), *GSA Special Publication 441: Revising the late Paleozoic ice age in time and space*, 131–142.
  - Isbell, J.L., Fraiser, M.L., Henry, L.C., 2008. Spotlight: Examining the complexity of environmental change during the late Paleozoic and early Mesozoic. *Palaaios* 23, 267–269.

#### Abstracts

- Henry, L.C., Isbell, J.L., Fraiser, M.L., Fielding, C.R., Domack, E.W., Frank, T.D., 2011. Glacial sedimentology and micromorphology of the Wynyard Formation, Tasmania, Australia: implications for climate at the peak of the late Paleozoic ice age. *GSA Abstracts with Programs* 43, 66.
- Isbell, J.L., Henry, L.C., Limarino, C.O., Koch, Z.J., Ciccioli, P.L., Fraiser, M.L., 2011. The equilibrium line altitude as a control on Gondwana glaciation during the late Paleozoic Ice Age. *ICCP 2011 17th international congress on the Carboniferous and Permian*, 74.
- Isbell, J.L., Henry, L.C., Koch, Z.J., Limarino, C.O., Fraiser, M.L., Dineen, A.A., 2010. The relationship between the ELA and latitude as a control on Gondwana glaciation during the late Paleozoic ice age. *International Association of Sedimentology, International Sedimentology Congress*, Sept. 2010, Mendoza, Argentina, Abstracts with Programs.
- Henry, L.C., Limarino, C.O., Fraiser, M.L., Isbell, J.L., 2009. Potential environmental consequences of Panthalassan margin volcanism in the late Paleozoic. *GSA Abstracts with Programs* 41, 360.
- Henry, L.C., Isbell, J.L., Fielding, C.R., Frank, T.D., Fraiser, M.L., 2009. Early Permian glacial advance-retreat cycles recorded in the Wynyard Formation of Tasmania, Australia. *GSA Abstracts with Programs* 41, 72.

- Isbell, J.L., Henry, L.C., Limarino, C.O., Cole, D.I., Gulbranson, E., Montañez, I., Fraiser, M.L., 2009. The late Paleozoic ice age: revision of the western Gondwana record. *GSA Abstracts with Programs* 41, 72.
- Henry, L.C., Isbell, J.L., Limarino, C.O., McHenry, L.M., Fraiser, M.F., 2008. Deglaciation in a Pennsylvanian paleovalley of western Argentina: the Agua de Jagüel Formation. *GSA Abstracts with Programs* 40, Paper 198-4.
- Fraiser, M.L., Henry, L.C., Isbell, J.L., 2008. Examining the Complexity of Environmental and Biotic Change during the Late Paleozoic and Early Mesozoic. *GSA Abstracts with Programs* 40, Paper 266-11.
- Isbell, J.L., Fielding, C.R., Frank, T.D., Henry, L.C., Koch, Z.J., 2008. The late Paleozoic ice age: size and duration of glacial events. *GSA Abstracts with Programs* 40, Paper 266-3.
- Ciccioli P.L., Limarino, C.O., Tedesco, A.M., Henry, L.C., Isbell, J.L., 2008. Paleoenvironmental evolution of the Agua de Jaguel Formation (Late Carboniferous – Early Permian): an example of glacial-postglacial transition in open marine basins. V Simposio Argentino del Paleozoico Superior.
- Henry, L.C., Isbell, J.L., Limarino, C.O., 2007. Revising the late Carboniferous sequence stratigraphy of west-central Argentina: disparate deglaciation successions in the Calingasta-Uspallata Basin. *GSA Abstracts with Programs* 39, 86.
- Henry, L.C., Isbell, J.L., Limarino, C.O., 2007. Short duration glaciation of limited extent in western Gondwana: the Carboniferous glacigenic deposits of the Protoprecordillera of west central Argentina. *GSA Abstracts with Programs* 39, 55.
- Isbell, J.L., Henry, L.C., Limarino, C.O., 2007. Alpine Glaciation in western Gondwana: the Carboniferous glacigenic deposits of the Protoprecordillera of west-central Argentina. *GSA Abstracts with Programs* 39, 85.
- Fielding, C.R., Frank, T.D., Rygel, M.C., Birgenheier, L.P., Isbell, J.L., Koch, Z.J., Henry, L.C., 2007. Reconciling the timing, duration, and character of Late Paleozoic Gondwanan glaciations: relevance to the midcontinent North American stratigraphic records. *GSA Abstracts with Programs* 39, 19.
- Christiansen, L.A., Perg, L.A., Swenson, J.B., 2005. Photosensitive silver chloride; a proxy for cosmogenic nuclides in experimental landscape modeling? *GSA Abstracts with Programs* 37, 83.

#### Collaborators

- Dr. Jennifer Aschoff, BP, Colorado School of Mines
- Dr. Patricia Ciccioli, University of Buenos Aires
- Dr. Eugene Domack, Hamilton College
- Dr. Art Donovan, BP, Texas A&M
- Dr. Gregor Eberli, University of Miami
- Dr. Chris Fielding, University of Nebraska-Lincoln
- Dr. Margaret Fraiser, University of Wisconsin-Milwaukee
- Dr. Tracy Frank, University of Nebraska-Lincoln
- Dr. Erik Gulbranson, University of Wisconsin-Milwaukee
- Dr. John Isbell, University of Wisconsin-Milwaukee

- Dr. Carlos O. Limarino, University of Buenos Aires
- Dr. Lindsay McHenry, University of Wisconsin-Milwaukee
- Dr. Catherine Reid, Canterbury University, N.Z.
- Dr. Ana Tedesco, University of Buenos Aires